GROUNDWATER QUALITY: REPRESENTATIVE AND APPROPRIATE SAMPLING OF LONG-SCREEN WELLS

By

LINDSAY ANTONIA MCMILLAN

A thesis submitted to the University of Birmingham for the degree of DOCTOR OF PHILOSOPHY

Department of Earth Sciences
School of Geography, Earth and Environmental Sciences
College of Life and Environmental Sciences
University of Birmingham
June 2015

Abstract

Groundwater quality sampling guidance typically requires representative samples to be obtained. Such guidance is not always clear what this means and which sampling methods are most appropriate. The situation is complicated by increasing well screen/open interval length. Uncertainty, resulting particularly from observations of vertical flow in wells has led to calls for the use of long-screen (> 3 m) wells to be abandoned for groundwater quality monitoring. Here, four complementary field and modelling studies at various scales are used to examine appropriate groundwater quality sampling in such wells. Numerical modelling demonstrates that literature reported vertical flows in wells < 10 m in length are sufficient to bias pumped groundwater quality sampling. Bias starts for vertical well flow rates less than 50 % of the pumping rate. Vertical flow measurements explain differences and similarities in historical passive sampling between four boreholes and allow vertical aquifer concentration distributions to be quantified. However, such quantification requires per-borehole flow measurement. New technology (Active Distributed Temperature Sensing) provides a versatile alternative to existing borehole flow characterisation methods under ambient and pumping conditions. Data from contrasting field environments demonstrate that even without comprehensive flow investigation long-screen wells can still provide useful information about groundwater concentrations and trends.

Dedication

To my supervisors, Mike Rivett, John Tellam, Peter Dumble and Helen Bray, for all your encouragement and advice over the course of this project.

To my parents for your belief in the importance of education. I wouldn't be here without you.

To Julian for your daily support along the way.

Thank you all.

Acknowledgements

This work forms part of an Open Case Studentship supported by the Natural Environment Research Council [grant number NE/H019170/1] and Case partners Waterra-In-Situ (now In-Situ Europe Ltd) and the Environment Agency (for England). The assistance of In-situ Europe (for providing loan of the Aqua TROLL 200 used during the single borehole tracer tests) and ESI Ltd. (for providing access to their Groundwater Vistas software) are gratefully acknowledged. Thanks also to Stefan Krause for provision of and support with the A-DTS. The Birmingham borehole field site was originally funded by the UK Engineering and Physical Sciences Research Council.

Table of contents

List of Illustrations

List of Tables

CHAPTER 1 INTRODUCTION

1.1 Background

Groundwater quality sampling guidance typically requires a "representative" sample to be obtained. From a statistical perspective, a representative sample is a subset of some population that has characteristics typical of the entire population set. However, from a groundwater quality sampling perspective, it is less clear what this means and indeed how one should go about obtaining such a sample. Commonly in literature, definitions recognise that such a sample should represent in-situ groundwater quality within the aquifer or formation rather than the well where the quality may be potentially compromised (e.g. Barcelona et al., 1985; Barcelona et al., 1994; Thornton and Wilson, 2008; Kozuskanich et al., 2012). Such samples should hence not be unduly biased by borehole/monitoring well design or sampling method (EA, 2003). But should such a sample be an average of aquifer conditions (Huntzinger and Stullken, 1988) and, over what spatial extent is such averaging occurring? Should samples instead be representative of a specific water-bearing zone (ASTM, 2014)? Is it important to assess both spatial (with depth and/or laterally) and temporal influences on sample composition (BSI, 2009)? Is a measure of the mobile load of contaminants (McCarthy and Shevenell, 1998) the defining metric in obtaining a representative sample? At least some authors (Fretwell et al., 2006; Thornton and Wilson, 2008) suggest the definition of representative depends on the sampling objective (for example high-resolution contaminated land assessment using short screen wells (< 3 m) versus a composite sample from long-screen production wells for water resource quality evaluations.

Indeed, any definition of representative may have to be site-specific (Nielsen and Nielsen, 2006). Ultimately, perhaps it is not the origin of the sample *per se* but rather knowledge of the origin that is important (Fretwell et al., 2006). Such knowledge of probable sample origin and the formation groundwater of which it is representative will not only allow appropriate use (or

development) of fit for purpose sampling methods and protocols, but also appropriate use of the groundwater quality data arising. The agenda of this thesis is to understand groundwater quality sample origins, what they are representative of, and to development appropriate methods to determine such origins of groundwater sampled from long screen wells.

1.1.1 Groundwater sampling methods

Irrespective of one's definition of "representative", when it comes to taking a groundwater quality sample from a borehole there are essentially only three methodological options:

- Volume purging (Gibb et al., 1981). This long-standing "traditional" method involves purging multiple well volumes (the volume of the water filled open/screened interval and cased section of the well) prior to sampling. Typically 3-5 well volumes are removed under relatively high pumping rates; water quality parameters (e.g. pH, temperature, electrical conductivity (EC), dissolved oxygen (DO), turbidity) may also be monitored to stability prior to sampling.
- Low-flow sampling (Puls and Barcelona, 1996). Here, pumping rates are low (typically 0.1 – 0.5 l/min) and drawdown is kept to a minimum (typically < 10 cm). Water quality determinants are monitored to stability prior to sampling.
- Passive (zero purge) sampling (Powell and Puls, 1993). In this method no well purging is undertaken prior to sampling. Passive sampling devices include instantaneous grab samplers, equilibrium (diffusion based) samplers, time-integrated (diffusion- or permeation- based) samplers or screening (detect/non-detect) type samplers (Vrana et al., 2005; Verreydt et al., 2010).

The traditional volume purging approach stemmed from recognition that chemical changes may occur in groundwater standing in the well and particularly within the casing (e.g. Pennino, 1988). Such chemical changes mean groundwater standing in the well at the start of sampling

may not be representative of chemical conditions in the adjacent aquifer. Accordingly, such standing water would need to be removed by purging before a representative sample could be obtained. The recommendation to remove 3-5 well volumes prior to sampling came originally from empirical field studies (Gibb et al., 1981; Barcelona et al., 1985). However, later research found some theoretical basis for such a recommendation (e.g. Barber and Davis, 1987). However, concerns regarding the cost/time associated with removing and disposing of 3-5 well volumes (Barcelona et al., 1994; Kearl et al., 1994; Stone, 1997), the excess turbidity and loss of key groundwater contaminants such as volatile organic compounds (VOCs) as a result of the high pumping rates (Puls et al., 1990; Powell and Puls, 1993; Barcelona et al., 1994; Puls and Barcelona, 1996) and recognition that ambient flow in wells may naturally flush wells meaning purging may be unnecessary (Robin and Gillham, 1987; Kearl et al., 1992; Powell and Puls, 1993) lead to the development of low-flow sampling methods. Passive (zero purge) sampling is the ultimate end point of such research designed to address the concerns associated with volume purging. If minimal disturbance is the goal and ambient well flows are such that the screen/open interval is being naturally flushed then why do we purge at all?

1.1.2 The problem with long-screen wells

Much of the research into groundwater sampling methods has focused on short screen monitoring wells (wells with screens ≤ 3 m (10 ft.) in length) (e.g. Gibb et al., 1981; Barber and Davis, 1987; Gibs et al., 1993; Powell and Puls, 1993; Kearl et al., 1994; Gustavson and Harkin, 2000; Annable et al., 2005; Barcelona et al., 2005; Savoie and LeBlanc, 2012). There is ongoing debate as to the use of long-screen wells for groundwater quality monitoring (and indeed whether we should be installing such wells at all) (Elci et al., 2001; Mayo, 2010). Despite somewhat ambiguous UK guidance (BSI, 2009), low-flow and passive sampling methodologies are not generally deemed applicable in long-screen wells (McDonald and Smith, 2009; USEPA, 2010).

Such debate and recommendations are partially a result of concerns over sample origin and sample bias with increasing screen length. For example, the influence of the local permeability field on sample origin (and bias) is widely recognized through the concept that pumped samples are permeability weighted (i.e., higher permeability, more transmissive layers contribute a greater proportion to the sample obtained (Church and Granato, 1996; Puls and Barcelona, 1996; Hutchins and Acree, 2000).

Perhaps of greater concern is the influence of ambient vertical flows that may occur in long-screen wells. Rather than being the exception (Giddings, 1987), ambient vertical flows in wells are expected to be as ubiquitous as vertical flows in aquifers that occur at least to some degree in all aquifers (Elci et al., 2001). Naturally occurring vertical hydraulic head gradients which may induce significant vertical flows in wells are widely reported in a variety of hydrogeological settings (Brassington, 1992; Church and Granato, 1996; Streetly et al., 2002; Dumble et al., 2006; Taylor et al., 2006; Metcalf and Robbins, 2007; Furlong et al., 2011; Ma et al., 2011). Driven by such naturally occurring vertical hydraulic gradients, measurable vertical flows have been reported in wells of a variety of screen lengths (Figure 1.1 collates such reported flows).

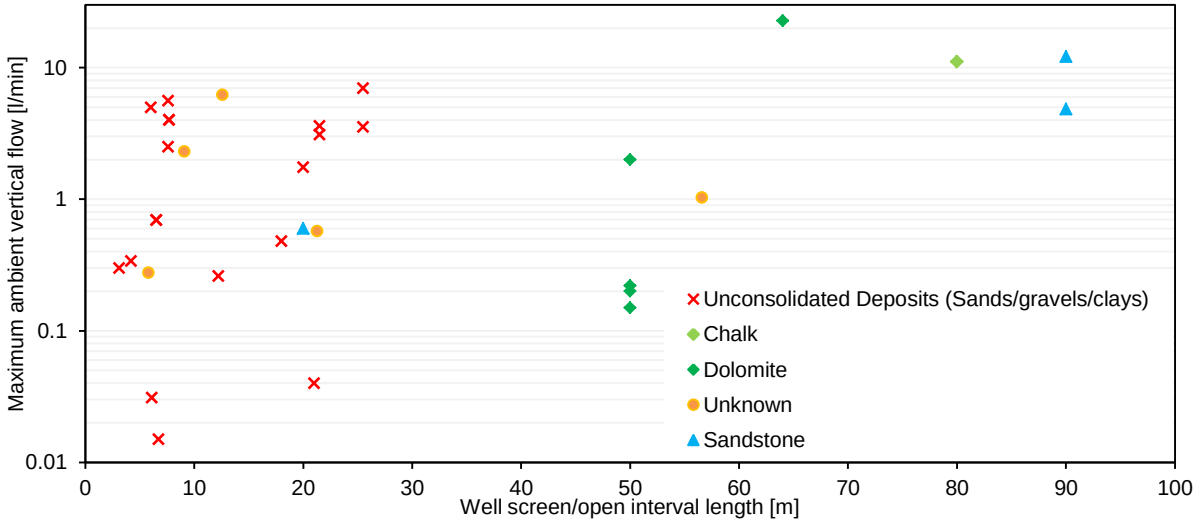

Figure 1.1: Collation of literature reported vertical flows in wells(Molz et al., 1994; Jones and Lerner, 1995; Young and Pearson, 1995; Paillet, 1998; Elci et al., 2001; Newcomer et al., 2010; Vermeul et al., 2010; Ma et al., 2011; Maurice et al., 2011)

The influence of such vertical flows may cause aquifer cross-contamination (Lacombe et al., 1995), passive sampling (Elci et al., 2001; Konikow and Hornberger, 2006; Mayo, 2010) and pumped sampling (Mayo, 2010) bias, errors in hydraulic head and hydraulic conductivity estimation (Kaleris et al., 1995; Elci et al., 2003) and misinterpretation of tracer test results (Riley et al., 2011).

1.1.3 A question of scale

Despite such concerns over sample bias and the influence of vertical flows, recommended monitoring well screen length does depend on the sampling objective. Short screened wells (< 3 m) are usually recommended for contaminated land investigation (Barcelona et al., 1985; Yeskis and Zavala, 2002; BSI, 2009). Screens of < 1 m in length are recommended for high resolution depth-discrete sampling (Puls and Barcelona, 1996). However, while these < 3 m screens are perhaps perceived relatively short (Church and Granato, 1996; Barcelona et al., 2005) they may in fact be long compared to the variation in groundwater quality found over the screen interval (Puls and Barcelona, 1996).

Very long-screen (often production) boreholes may be more appropriate for investigations in large-thickness aquifers where sampling objectives mean an integrative measure of aquifer water quality is required (e.g. Rivett et al., 2012). Such investigations might include those into diffuse pollution (e.g. nitrates), potable water quality or Water Framework Directive status assessment for example (Grath et al., 2007; BSI, 2009). Additionally, the Environment Agency for England has a legacy of hundreds of very long-screen observation wells from which historical groundwater quality data have been collected.

1.2 Overall aims and thesis approach

What is considered too long for a monitoring well depends on the scale of interest, the degree of physical and chemical heterogeneity at that scale, and the sampling objective(s). Whatever the

scale, rather than write off the utility of long-screen wells, there remains a need to critically consider how best to sample from such wells and what such sampling data can (and cannot) tell us about groundwater quality in the adjacent aquifer. Understanding intra-borehole flow and transport before and during sampling is critical to the use of long-screen wells for monitoring. Such knowledge of probable sample origin and the formation groundwater they are representative of will not only allow appropriate use (or development) of informed sampling methods and protocols fit for purpose, but also appropriate use of the groundwater quality data arising.

The hypothesis of the thesis is that: Despite their drawbacks, informed sampling of long-screen wells that realises some indication of the origin of the groundwater sample may provide valuable groundwater quality data that may be appropriate to a range of decision making agenda. The goal of this thesis is hence to critically examine groundwater quality sampling in long-screen monitoring wells at a variety of scales and answer the questions:

- What are appropriate samples from long-screen wells?
- What are such samples representative of?
- How best can such samples be obtained?
- How should data arising be most appropriately used?

The project presents four complementary studies which seek to examine these questions regarding the use of long-screen wells for groundwater quality monitoring. Each of the four studies is presented as a separate data chapter (Chapter 2 – Chapter 5). The studies consider flow logging and groundwater quality sampling in a range of geological formations (layered sandstone, fractured Chalk and unconsolidated sands/gravels). Multiple scales of interest are considered from 3 m screened monitoring wells in a very chemically and physically heterogeneous formation to boreholes open over 50 + m of aquifer in a region of diffuse agricultural pollution.

Chapter 2 presents ambient borehole flow logging method development, associated passive groundwater quality sampling and historical data interpretation in boreholes at two complementary field sites. One site is the nitrate-contaminated East Yorkshire Chalk, the other the Sherwood Sandstone in Birmingham, UK. The aim is to examine the temporal and spatial changes in ambient borehole flows and associated groundwater quality and comment on the implications for appropriate groundwater quality sampling in wells in such aquifers.

Chapter 3 presents a numerical study designed to address systematically the influence of vertical well flows of the magnitude reported in literature (Figure 1.1) on pumped groundwater quality sample origin. The aim is to examine within-well ambient-flow bias to pumped groundwater samples – what are pumped groundwater quality samples representative of?

Chapter 4 presents fieldwork and associated numerical modelling to investigate the use of a technology relatively new to hydrogeology, Active Distributed Temperature Sensing, as a means to quickly characterise a borehole under ambient and pumping conditions. The aim is to develop borehole flow-logging techniques that allow efficient borehole characterisation to inform groundwater quality sampling.

Chapter 5 presents detailed insights into 3 m monitoring well sample origins from proximal multilevel sampler transects in a Dense Non-Aqueous Phase Liquid (DNAPL) source zone. Whilst such wells are typically regarded as being short, the reality at heterogeneously contaminated sites – typified by DNAPL sites – is that such well screens may be comparatively long compared to the scale of variability in contamination present. The aim is to better understand the provenance of samples obtained during conventional sampling (zero purge, low flow, standard volume purging) of typical short screen (3 m) monitoring wells within a spatially heterogeneous (DNAPL) source zone environment. Finally, overall synthesis, concluding remarks of relevance to practitioners on how best to obtain appropriate and representative samples in long-screen wells, and recommendations for further research are presented in Chapter 6.

Each chapter has its own introduction providing an overview of the appropriate literature and the specific aims. Methodology is, in general, chapter specific and as such is presented on a per-chapter basis. Data appendices (summarised on page 149) are provided to supplement the in-thesis discussion.

Chapter 3 has been published as:

- McMillan, L. A., Rivett, M. O., Tellam, J. H., Dumble, P., Sharp, H. (2014). Influence of vertical flows in wells on groundwater sampling. Journal of Contaminant Hydrology 169: 50-61.

Output from the project further formed the basis of:

- McMillan, L. A., Rivett, M. O., Tellam, J. H., Dumble, P. (2015). Groundwater quality sampling at contaminated sites: The long and the short of it. International Environmental Technology 25(2): 50-51.

Both published outputs along with conference abstracts are included in electronic Appendix 1.

CHAPTER 2 RAPID MODEL INTERPRETED SINGLE- BOREHOLE TRACER TESTS TO GUIDE SAMPLING IN LONG-SCREEN WELLS

2.1 Introduction

Anecdotal evidence suggests there is increasing demand from UK practitioners to use (or they are already using) low-flow and passive sampling methods for groundwater quality sampling in long wells. However, without knowledge of the ambient borehole flow regime (and particularly vertical flows) significant uncertainty exists in determining what groundwater quality samples are representative of (Elci et al., 2001; Mayo, 2010).

Flow logging of long boreholes or wells is often used in large-thickness, high resource value, aquifer systems to allow measurement across the vertical aquifer expanse. Comprehensive borehole flow assessment typically aims to detect variation in transmissivities of the geological units penetrated as well as gradients across these units and hence ambient vertical (and horizontal) flow components (e.g. Molz, 1989; Molz et al., 1994). Conventional borehole flow characterization approaches include:

(1) Packer testing (Bliss and Rushton, 1984) which, while comprehensive, can be slow and expensive.

(2) Geophysical flow logging methods such as impeller (Molz, 1989; Le Borgne et al., 2007), electromagnetic (Molz et al., 1994; Young and Pearson, 1995) or heat-pulse (Kerfoot et al., 1991; Paillet et al., 2000) techniques. Due to the need to take many point measurements, these conventional geophysical techniques may be time consuming in long boreholes; impeller and heat-pulse methods are limited in the velocities they can successfully measure.

(3) Borehole fluid conductivity or temperature logging methods (Tsang et al., 1990; Tellam, 1992; Williams and Paillet, 2002). These approaches benefit from straight forward application and potentially allow inflowing and outflowing zones to be quickly discerned. However, these

methods are qualitative in nature and rely on natural contrasts in water temperature or electrical conductivity from the contributing strata with depth.

(4) Where natural contrasts do not exist, single borehole tracer tests (SBTT) can be undertaken (with regulatory permission). These methods infer borehole flows from dilution and dispersal of an introduced tracer. The tracer is emplaced either uniformly throughout the entire borehole column (Hall, 1993) or at discrete points (Tate et al., 1971). Commonly the tracer is detected due to its electrical conductivity contrast with the groundwater (Michalski and Klepp, 1990; Doughty and Tsang, 2005; Maurice et al., 2011). Where regulatory permission to use dissolved tracers may be difficult to obtain, SBTT can use hot water as an alternative tracer (e.g. Leaf et al., 2012; Read et al., 2013). However, the relatively large volumes of hot water required make injection of heated water into the borehole inconvenient in practice. Additionally, the water level in the well and surrounding hydraulic head distribution may be perturbed. An alternative approach has invoked thermal resistance heating of a length of cable to raise the temperature of the borehole water (Pehme et al., 2007; e.g. Banks et al., 2014).

Much of the focus in literature on single borehole tracer tests (SBTT) has been as a means to determine aquifer hydraulic properties. Typically such investigations involve simultaneous pumping either from the borehole into which tracer is emplaced or from an adjacent borehole. Tests are often repeated at different pumping rates. Change in electrical conductivity is monitored with time and from such changes permeability distribution can be inferred (Brainerd and Robbins, 2004; Doughty and Tsang, 2005; West and Odling, 2007). However, Libby and Robbins (2014) instead utilize a post-tracer-emplacement slug test to estimate borehole permeability.

Where monitoring of ambient flows is the objective, vertical flows are often not the focus of the investigation (e.g. Ward et al., 1998; Doughty and Tsang, 2005; Pitrak et al., 2007; Shafer et al., 2010). However, Maurice et al. (2011) do provide detailed exploratory numerical modelling considering the patterns in emplaced tracer profiles that might occur under different horizontal

and vertical ambient flow scenarios. In their associated field application and analysis, the authors do not directly model the uniform emplacement test profiles to estimate borehole velocities. Rather, inflow and outflow points are qualitatively inferred. Multiple point emplacement tests are then carried out adjacent to each inflowing feature identified. Velocities are estimated from movement of these discrete tracer injections.

Doughty and Tsang (2005) do provide direct numerical modelling of uniform emplacement tests albeit under pumping conditions. However, in both the numerical modelling of Doughty and Tsang (2005) and the qualitative analysis of Maurice et al. (2011), a single time is assumed for each vertical profile of the borehole. Such borehole profiles take at least several minutes to collect if not longer. In boreholes with relatively slow rates of ambient vertical flow (Maurice et al., 2011) or under low pumping rates (Doughty and Tsang, 2005) the error introduced from this assumption may be small. However, this may not be the case universally. Higher borehole flow rates (either horizontally or vertically) may result in significant movement of the tracer over the few minutes it takes to profile the entire borehole column.

This study considers direct numerical modelling of uniform emplacement SBTT to:

(1) Provide quantitative estimate of ambient flows in long boreholes. This has the advantage of saving considerable time as subsequent point emplacement tests are not required. The model is made more widely applicable as results are generated for the depth and time of each observed data point; a single time per profile not assumed;

(2) Guide passive sampling in long boreholes and improve subsequent data interpretation;

(3) Improve interpretation of historical passive sampling (and cross-borehole tracer test) data;

(4) Provide advice applicable to groundwater quality sampling practitioners on how often borehole flow measurement should be taken and in how may boreholes at a site.

Method development and subsequent application was undertaken at two complementary field sites. Firstly, the spreadsheet-based numerical SBTT model was developed and applied at a field

site located in the Triassic Sherwood Sandstone in Birmingham, UK where repeat SBTT were carried out in three adjacent boreholes over two consecutive years. The multi-layered sandstone formation at the site is in contrast to much of the SBTT work reported in literature which has primarily focused on fractured rock e.g. Chalks (West and Odling, 2007; Maurice et al., 2011; Sorensen et al., 2015); fractured bedrock (Michalski and Klepp, 1990; Brainerd and Robbins, 2004; Libby and Robbins, 2014); fractured hard rock (Doughty and Tsang, 2005) or fractured shale (Williams and Paillet, 2002). Tracer test interpretation in non-fractured formations such as that at Birmingham may be more challenging as inflow and outflow zones are expected to be non-discrete.

Secondly, SBTT and subsequent passive sampling guided by SBTT results were undertaken in four boreholes located near Kilham in the East Yorkshire Chalk. SBTT and subsequent groundwater sampling were undertaken in two consecutive years under conditions of near historic low and high water levels. Historical passive sampling at the Kilham site by the Environment Agency has found a trend of rising nitrate concentrations. However, variability is observed between wells and between passive sampling taken at different depths in a single well. SBTT flow results are also used to improve interpretation of historical data and provide recommendations for future sampling.

The final aim is to examine the temporal and spatial changes in ambient borehole flows and associated groundwater quality and comment on the implications for appropriate groundwater quality sampling. The model and method development, and results from application at the two complimentary field sites are presented herein.

2.2 Materials and methods

2.2.1 Practicalities of SBTT tracer testing and modelling

2.2.1.1 Principle of uniform SBTT

In a uniform-emplacement SBTT, borehole conductivity is changed by emplacing a tracer of contrasting conductivity (typically higher conductivity saline water although lower conductivity water is sometimes used) uniformly throughout the borehole column. Emplacement is undertaken either using a hose or by recirculation of the tracer in the borehole column (e.g. Doughty and Tsang, 2005; Shafer et al., 2010). Use of a hose offers a lower technology method with the additional advantage that it guarantees distribution of tracer throughout the borehole column. If high ambient flow rates are present in the borehole, the recirculation pumping rate may be insufficient to overcome ambient head gradients and achieve an even distribution of tracer throughout the borehole column.

Emplacement is typically undertaken by means of a hose, secured at the surface, and installed such that its lower end sits just above the bottom of the borehole (Figure 2.1). The volume of tracer required is the volume of the hose pipe within the screened/open section of the borehole. Where water filled casing is present, an additional injection of background-conductivity water is required, equal to the volume of the hose pipe below water in the casing. The background conductivity water is injected after the saline tracer. It acts to displace the saline tracer down the hose pipe to the open/screened interval of the borehole and minimise the entry of saline water into the cased zone.

The saline tracer (and background conductivity water if required) is injected by pouring the water into the top of the hose. After tracer injection, the hosepipe is withdrawn from the borehole leaving a column of raised conductivity water in the open interval of the borehole column. A mixing device (such as an inverted funnel) is usually attached to the bottom of the hose so that

tracer is evenly mixed across the borehole as the hose is removed. Following tracer emplacement, continual depth-conductivity profiles are taken in the open interval of the borehole. The observed changes in conductivity with time in the borehole can be used to infer vertical (and horizontal) borehole flows.

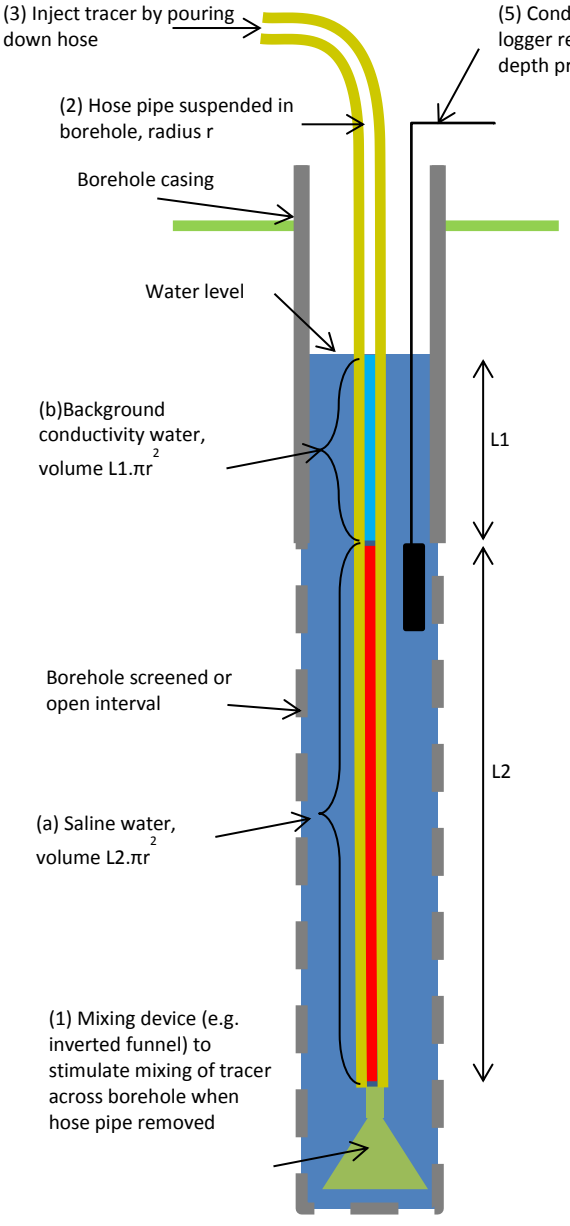

Single borehole tracer testing method:

(1) Attach mixing device (e.g. an inverted funnel) to the bottom of hose).
(2) Hang hose pipe in borehole with end resting just above the bottom of the borehole.
(3) Pour tracer into the top of the hose:
    (a) Saline tracer is added first with volume equal to either (i) the submerged portion of the hose if the water level is below the casing bottom; or (ii) the volume of the hose within the open/screened interval of the borehole.
    (b) If the water level is above the bottom of the borehole casing, then follow the saline tracer injection with an injection of background conductivity water. The volume injected is the volume of the submerged portion of the hose located within the cased section of the borehole.
(4) Pull the hose from the borehole to leave the saline tracer distributed evenly throughout the open/screened interval of the borehole.
(5) Use a conductivity/depth logger to make regular passes up and down the borehole. The logger should be recording at a short time interval (e.g. 2 seconds).

Figure 2.1: Overview of uniform emplacement single borehole tracer test method

2.2.1.2 Measuring conductivity changes in the borehole

Down-hole pressure/conductivity/temperature data loggers (AquaTROLL 200, InSitu Europe Ltd; CTD-Diver, Schlumberger Water Services) provided a quick, portable and relatively inexpensive means of assessing changes in electrical conductivity with depth in the borehole.

SBTT are limited (1) under very low flow conditions, by density effects (typically ignored in analysis); (2) under very high flow conditions, by the time required to profile the borehole. Here, tracer may be flushed from the borehole before sufficient logger profiles can be completed. Where borehole flows are high, swift measurement of changes in conductivity with depth are required. However, as the logger is lowered to a new depth interval it may take time to equilibrate to the new conditions. Such a delay may be due to the time to refresh water over the conductivity cell. Another possible factor in equilibration time is the temperature dependence of electrical conductivity measurements; for example the minimum response time given for a change in temperature for the CTD-Diver is 3 minutes (SWS, 2014).

Exploratory laboratory testing in beakers of varying NaCl concentration (and hence conductivity) suggests conductivity equilibration, while not as slow as quoted temperature equilibration times, is not instantaneous (Figure 2.2a). Within 5 seconds, the diver has responded to the change in conductivity. However, it takes several minutes to reach true stability. For beakers of both descending and ascending NaCl concentration, conductivity stabilises after 5 minutes; a linear relationship is found between beaker conductivity and NaCl concentration (Figure 2.2b, c).

(a)

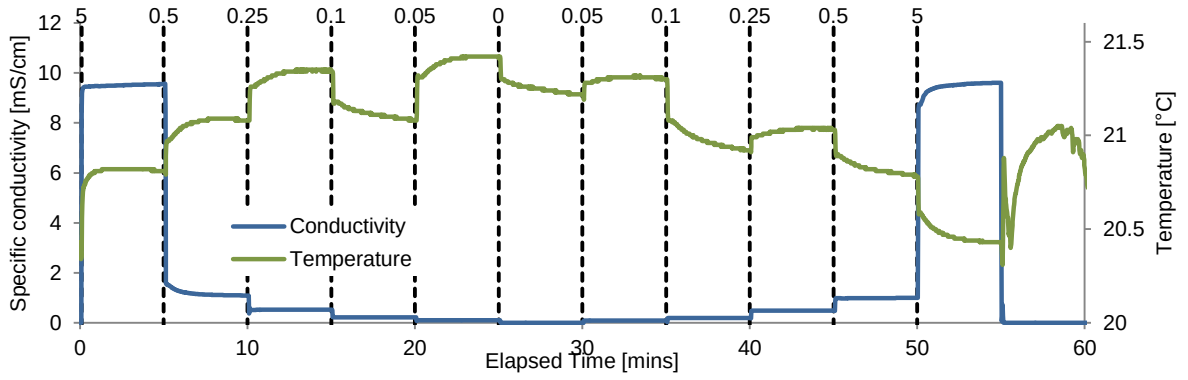

(b) (c)

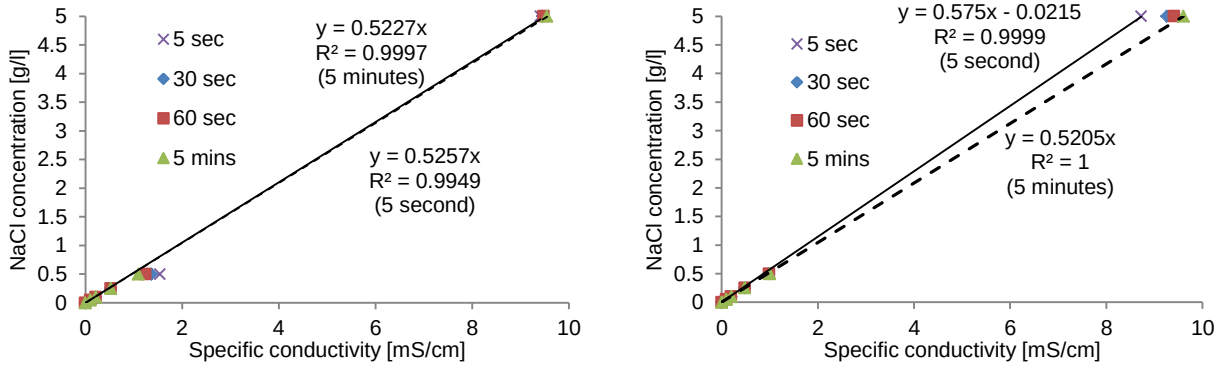

Figure 2.2: CTD-Diver conductivity (and temperature) equilibration time (a) diver conductivity and temperature profiles as the diver is placed in beakers of descending (0 – 30 minutes) and ascending (30-55 minutes) conductivity. Black dashed lines indicate change of beaker, the labels at the top of each line indicate the NaCl concentration [g/l] in that beaker; beakers were 500 ml in volume (b) conductivity vs. NaCl concentration calibration for beakers of decreasing NaCl concentration; (c) conductivity vs. NaCl concentration calibration for beakers of increasing NaCl concentration.

The delay in stabilisation is most significant when moving between waters of very different conductivity (e.g. from 5 g/l to 0.5 g/l NaCl beakers). If in-borehole dispersion is relatively low a relatively sharp interface will result between the emplaced tracer and the inflowing background conductivity water. In such a scenario, with a large contrast in conductivity over a small distance, a swiftly moving logger may not accurately represent the conductivity profile in the borehole. The conductivity bias (and potential offset in measured interface location) will depend on whether the logger is moving from high to low conductivity water or *vice versa* (Figure 2.2 b, c), and hence whether the logger is being lowered down or being raised upwards in the borehole. To

assess the potential impact of diver equilibration on SBTT results, initial SBTT modelling was undertaken using the downward profiles for calibration. Upward profiles were reserved to validate modelling results.

2.2.1.3 SBTT tracer test numerical modelling

Numerical modelling was simplified by assuming concentration mixing across the borehole is instantaneous. Hence, the numerical model was formulated using the standard 1D advective-dispersion equation (e.g. Appelo and Postma, 2009):

$$\frac{\delta c(z,t)}{\delta t} = D(z)\frac{\delta^2 c(z,t)}{\delta z^2} - v(z)\frac{\delta c(z,t)}{\delta z} + R(z) \qquad \text{Eq. [2.1]}$$

where c is concentration as a function of time (t) and depth (z) in the borehole; v(z) is the depth-dependent vertical fluid velocity in the borehole; $R(z)$ represents concentration sources and sinks as a function of depth, in this case inflows and outflows to/from the adjacent formation; and $D(z)$ is hydrodynamic dispersion, which depends on the borehole velocity:

$$D(z) = \alpha v(z) \qquad \text{Eq. [2.2]}$$

The 1D advection-dispersion equation was solved by centrally-weighted explicit finite difference formulation. However, as in the approach of Maurice et al. (2011), inflows and outflows were not solved numerically, rather they were piecewise specified over the borehole length (L). From the specified inflows and outflows, the vertical distribution in borehole velocity at each depth interval z is:

$$v_z = \frac{Q'_{in,z}\Delta z - Q'_{out,z}\Delta z}{\pi r^2} + v_{z-1} \qquad \text{Eq. [2.3]}$$

where Q' is the volumetric inflow/outflow per unit length of the borehole; v_{z-1} is the vertical velocity in the previous depth interval; Δz is the grid discretisation; and r the borehole radius. v_0 and v_L are 0. Inflowing and outflowing contributions were hence:

$$R(z) = \frac{Q'_{in}(z)}{\pi r^2} c_{in}(z) - \frac{Q'_{out}(z)}{\pi r^2} c(z) \qquad \text{Eq. [2.4]}$$

To ensure numerical stability and accuracy, a check was made to ensure stability, Courant and Peclet criterion were met; that is:

$$\frac{D\Delta t}{(\Delta x)^2} < \frac{1}{2} \qquad \text{Eq. [2.5]} \qquad \frac{v\Delta t}{\Delta x} < 1 \qquad \text{Eq. [2.6]} \qquad |v|\frac{\Delta z}{D(z)} < 1 \qquad \text{Eq. [2.7]}$$

A Dirichlet (constant concentration) boundary condition was used at the top of the model (representing dispersive exchanges with the casing water). At the bottom of the borehole, where a zone of stagnation exists, a zero-flux boundary condition was used. In fact, initial sensitivity testing showed the advection-dominated model results were relatively insensitive to these boundaries.

Implicit in the use of the 1D advection dispersion equation (Eq. [2.1) is that laminar flow prevails in the borehole. A Reynolds number < 1700 (Avila et al., 2011) represents laminar flow conditions in pipes. At the end of modelling the Reynolds number resulting from the predicted maximum borehole flow was calculated to ensure the assumption of laminar flow was not violated.

Model time and grid discretisation were customisable to allow for refinement in cases where borehole velocities were high. Calibration parameters specified as a function of depth in the open interval of the borehole were: (1) volumetric inflows and outflows (with model check to ensure they are equal); (2) starting specific conductivity distribution in the borehole; (3) background specific conductivity (the specific conductivity of the inflowing water). The only additional calibration parameter was the dispersivity, α.

The spreadsheet model output was a graph of modelled versus observed SBTT tracer profiles with model run times typically less than a minute on a modern laptop. Time averaging of each observed profile was not undertaken; rather the model generated a simulated equivalent for the depth and time of each individual conductivity observation. The model makes no assumptions regarding the initial conductivity distribution, the direction of flow or the location of inflow and outflow points. As such, the numerical model could equally well be used to interpret the results of point dilution tests (Maurice et al., 2011), horizontal borehole dilution tests (Pitrak et al., 2007) or emplacement tests under pumping conditions (West and Odling, 2007).

The model has good agreement with the Ogata-Banks analytical solution (Ogata and Banks, 1961) for the 1D advective-dispersion equation (Figure 2.3).

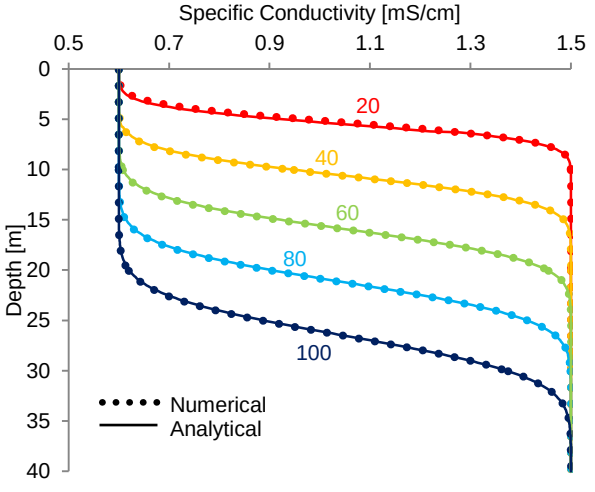

Figure 2.3: 1D numerical vs. 1D analytical (Ogata-Banks) solution comparison . Q is 0.5 m^3/h, borehole diameter is 0.2 m, and α is 0.2. Inflow is at the top of the borehole and outflow at the bottom. Hence, in the numerical model, 0.5 m^3/h inflow is assigned to the first cell and 0.5 m^3/h outflow assigned to the last. Coloured labels indicate profile time, dots are the numerical solution result and solid line the analytical solution

2.2.2 Field sites and experiments

2.2.2.1 Triassic sandstone

The experiment site for the initial SBTT method testing is located at the University of Birmingham, UK (Figure 2.4). The site consists of three 50 m deep, 0.15 m diameter boreholes

(Bouch et al., 2006). Two of the boreholes (BH2 and BH3) are in close proximity (*c.*7 m) with a third borehole (BH1) approximately 20 m away. BH1 is cased to 12.35 metres below ground level (m bgl); BH2 to 15.65 m bgl and BH3 to 12.30 m bgl. Below the casing, all there boreholes are open to 50 m bgl. The site provided an ideal location for preliminary method testing and model verification; it has been extensively investigated including geophysical logging (Bouch et al., 2006), lithological logging and core permeability testing (Bee, 2003; Bouch et al., 2006), cross-hole packer testing (Joyce et al., 2007) and forced gradient tracer tests (Joyce et al., 2007; Riley et al., 2011; Greswell et al., 2014).

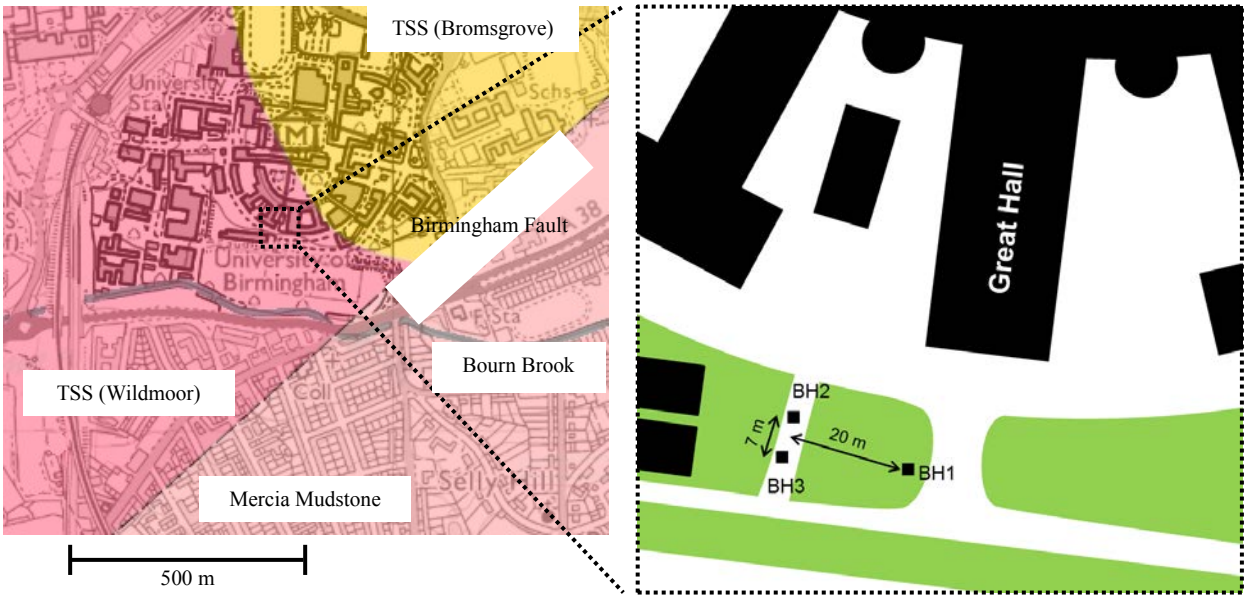

Figure 2.4: University of Birmingham field site : (a) Geology of the local area showing the Birmingham Fault boundary of the Triassic Sherwood Sandstone Group (TSS) with downthrown Mercia Mudstone. Groundwater in the TSS is forced upwards by the presence of the Birmingham Fault, discharging to the Bourn Brook; (b) Schematic of field site showing location of BH1, Bh2 and BH3. Geology map courtesy of Edina.ac.uk

The local geology is dominated by the Wildmoor Sandstone Formation of the Triassic Sherwood Sandstone (TSS) Group, which forms one of the UK's major groundwater aquifers (Tellam and Barker, 2006). The continental red-bed TSS is overlain by Quaternary deposits and made-ground of variable depth and hydraulic conductivity. The boreholes penetrate a series of poorly cemented fluvial sandstones interspersed with well-cemented fluvial and aeolian sandstones. The sandstone deposits are separated by low-permeability mudstone and paleosol

units which may extend laterally over tens of metres or more (Bouch et al., 2006). The subsurface can be considered as a multi-layered aquifer, with measured sandstone matrix hydraulic conductivities ranging from approximately 8×10^{-3} to 5 m d^{-1} (Bee, 2003), while double packer testing suggests a range of 0.07 to 2.0 m d^{-1} (Ferguson, 2006). The site is characterized by a large upward vertical head gradient attributed to the Birmingham Fault (Riley et al., 2011) approximately 200m away that forces flow upwards to discharge in a local stream. Vertical hydraulic gradients have been observed previously at the site (Ferguson, 2006). The flow system has high temporal variability and since 2006 the upflow is thought to have reduced (Riley et al., 2011).

Initial SBTT were carried out in BH2 and BH3 during June 2011 with further SBTT carried out in BH1 and BH3 in August 2012. Water quality sampling was not undertaken as previous (unpublished) groundwater quality sampling data have suggested little variation in water chemistry with depth. Pursuant to EA (2011), permission was gained from the local Environment Agency office prior to undertaking the SBTT.

2.2.2.2 East Yorkshire Chalk

The experiment site is located north-west of Kilham in the Chalk wolds of East Yorkshire (Figure 2.5). The site comprises four 0.2 m diameter boreholes (Bartondale, Tancred Pit, Henpit Hole and Middledale) located in two converging dry valleys (Langtoft to the south; Broachdale to the north) which form part of a larger network of dry valleys across the area.

The Yorkshire Chalk is the most northerly outcrop of the English Chalk Group, which collectively forms the most important aquifer in the UK, accounting for over 50 % of total groundwater abstractions (Allen et al., 1997). The distribution of often solution enlarged fractures provides the principal permeability (and storage) in the aquifer with negligible matrix permeability and low matrix storage occurring as a result of the small pore throats (typically

between 0.1-1μm, Price et al., 1976). Solution enhanced fractures important to flow are most prevalent in the zone of water table fluctuation (typically < 50 m bgl, Allen et al. (1997)). Increasing overburden pressure and decreased groundwater circulation result in a reduction in fracture frequency, fracture aperture, and hence permeability below 50 m bgl (Allen et al., 1997).

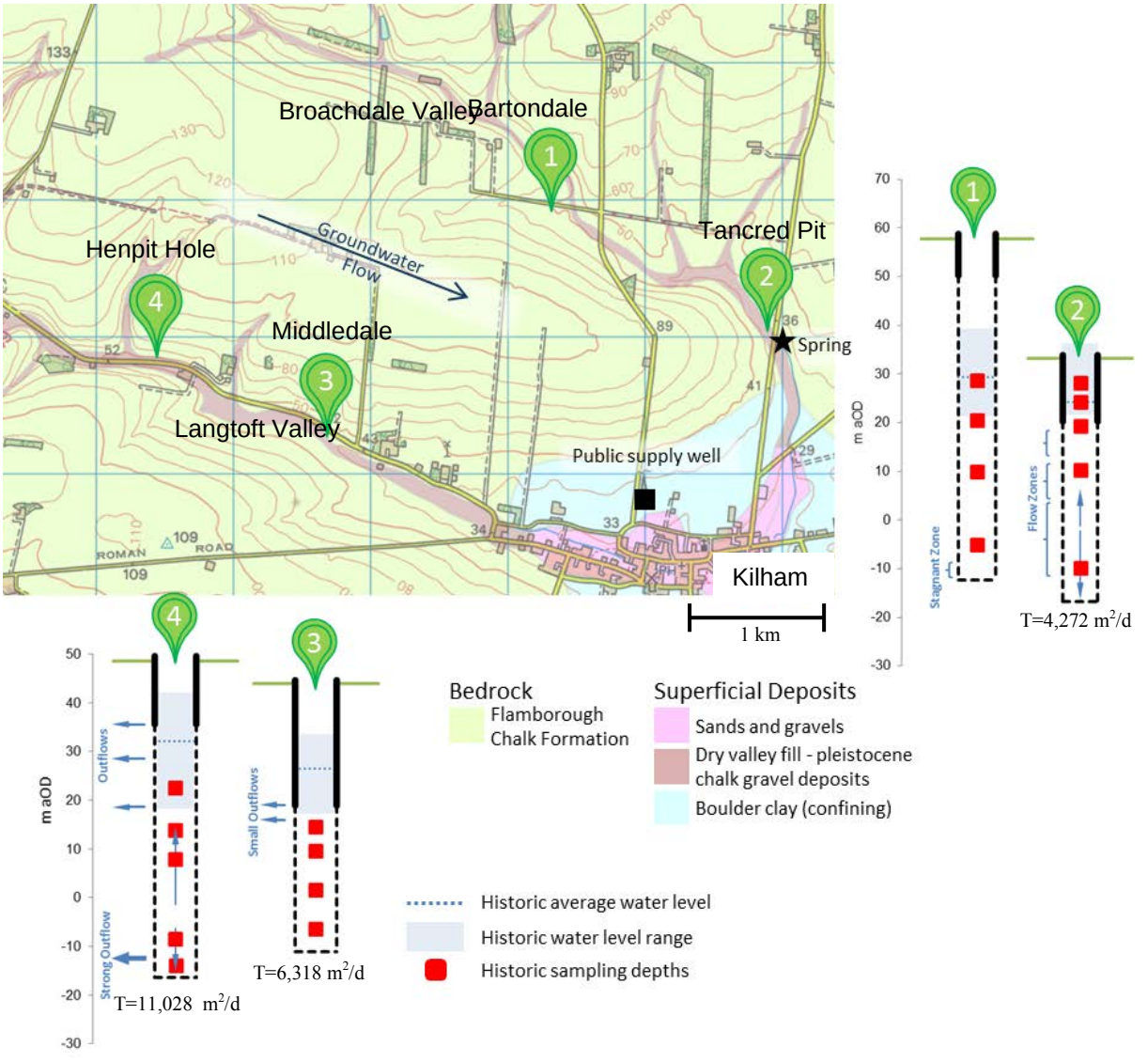

Figure 2.5: Overview of Kilham field site . Main map shows location of boreholes and geological setting. Borehole schematics show borehole casing and open interval depths in metres above Ordnance Datum, m aOD to allow comparison of the depth of the open interval between the four boreholes. In text discussion presents results in metres below casing top (m bct). Historical and average water level variation and historical sampling depths are shown for each borehole; comments on the location of inflows and outflow are as inferred from 1994 CCTV. Geology map courtesy of Edina.ac.uk.

The English Chalk Group is divided as a result of lithological and faunal differences into Northern (including Yorkshire) and Southern provinces. The generally higher permeability of the

thin-bedded Northern province Chalk is ascribed to its hardness when compared with the softer, more massive Chalk of the southern province. However, even within the Yorkshire Chalk permeability values vary significantly; they tend to be highest immediately to the west of a buried paleo cliff line marking the edge of confining quaternary cover present in much of the east of the area (Gale and Rutter, 2006). The confined region of the Yorkshire Chalk is associated with significantly lower permeability and storage values resulting from reduced flow and hence little solution-driven fracture enhancement (Gale and Rutter, 2006).

The boreholes at the field site are located in the unconfined Chalk. However, quaternary drift becomes confining immediately to the south-east with springs (and indeed artesian overflow) occurring at the intersection with the confinement (Figure 2.5). The outcropping Flamborough Chalk Formation is the youngest in the area with the 300 – 350 m thick beds dipping at about 2.2° towards the south east (Ward et al., 1998). Despite being a member of the northern province, the Flamborough Formation is lithologically more similar to the softer Chalk of southern England than the harder underlying chalk formations (Gale and Rutter, 2006).

The absence of drift deposits and thin soils mean groundwater is susceptible to nitrate pollution in the predominantly arable agricultural region. Attenuation of nitrates as a result of denitrification is not significant in the unconfined area of the aquifer due to the prevailing aerobic conditions (Rivett et al., 2007). Linear increases in nitrate concentrations have commonly been observed across the unconfined aquifer (Smedley et al., 2004). Indeed, nitrate concentrations at the Kilham public water supply well (located just north of Kilham, Figure 2.5) have been increasing since the 1970s with the 50 mg/l (11.3 mg/l NO_3 as N) drinking water standard for nitrate in potable water (EU Drinking Water Directive, 98/83/EC) exceeded since the mid-90s (Gale and Rutter, 2006).

Previous hydrogeological characterisation in the area has included borehole geophysical logging (Buckley and Talbot, 1994), hydraulic testing (Ward et al., 1998), and a variety of single

borehole and cross-borehole tracer testing (Ward and Williams, 1995; Ward et al., 1998). Hydraulic gradients in the Broachdale valley ($2\times10^{-3} – 2\times10^{-4}$) are lower than those observed in the Langtoft valley (7×10^{-3}-2×10^{-3}), with transmissivity measured in the 0.2 m diameter boreholes varying from > 11,000 m^2/d at Henpit Hole to less than 5000 m^2/d at Tancred Pit (Ward et al., 1998). Transmissivity values are not reported for the 0.2 m diameter Bartondale borehole.

Cross-borehole tracer testing by Ward and Williams (1995) found maximum groundwater velocities of 440 m/d in the Broachdale valley and 480 m/d in the Langtoft Valley. However, the tracer testing indicated considerable flow path complexity. For example, a connection was not found from Henpit Hole to Middledale borehole but connections from Henpit Hole to boreholes further downgradient were observed. Bartondale borehole was found to be isolated from the main fracture network in the Broachdale valley.

CCTV logging, carried out in 1994, indicated variable flows in the four boreholes (Figure 2.5) with diverging flows observed in Henpit Hole and Tancred Pit, some small outflow observed directly below the casing of the Middledale borehole and no flow observed in Bartondale. However, fluid logging (temperature and conductivity) profiles showed insufficient contrast with depth to identify flowing features (Ward and Williams, 1995).

The Environment Agency for England (unpublished data) has carried out a schedule of intermittent water quality sampling and more frequent water level measurements in the boreholes located around Kilham. Water quality sampling was undertaken from the early 1990s to 2010. Analyses reported include major ions, water quality parameters (alkalinity, temperature, EC, pH) and infrequently metals (total and dissolved iron and manganese). The passive groundwater quality samples (grab sampling) were taken at varied depths within the four boreholes (Figure 2.5) with not all depths sampled during each sampling round.

During this project, SBTTs were carried out in January 2012 (following a prolonged UK drought with very low water levels) and in March 2013 (where heavy rain during the 2012/2013

winter had meant water levels were high). Permission was gained from the local Environment Agency office and the local water company (Yorkshire Water) was notified prior to undertaking the tracer tests.

Guided by the SBTT results, passive sampling rounds were undertaken in March 2012 (allowing for a return to background conditions post-SBTT) and March 2013. S650 Hydrasleeves (InSitu Europe, Figure 2.6) tethered to a single line were used to take four concurrent passive samples per borehole. Hydrasleeves have a check valve at their top end which seals on submergence. The sealed valve prevents ingress of well water as the device is lowered into position. The valve only opens once the Hydrasleeve is pulled upwards at a rate greater than 0.3 to 0.6 m/s (GeoInsight, 2006). Once the valve opens, the hydrasleeve fills with groundwater over 1-2 times its hydrasleeve. Once the device is full the check valve reseals preventing further mixing with borehole water as the hydrasleeves are removed from the well.


Figure 2.6: Hydrasleeve

Hydrasleeve sample depths were determined from the inflowing and outflowing zones identified from the SBTT. The deployment depth of the top of each hydrasleeve was calculated as:

$$H_{depth} = S_{depth} - \frac{(1.5H_l)}{2} \qquad \text{Eq. [2.8]}$$

where $H_{depth}$is the attachment depth of the top of the hydrasleeve, S_{depth} is the desired sample depth and H_l is the Hydrasleeve length.

On-site field parameter measurement included alkalinity to pH 4.5 (measured by a Hach digital titrator) and temperature, turbidity, pH, Oxidation Reduction Potential (ORP), Dissolved Oxygen (DO) and Electrical Conductivity (EC) (measured by AquaTROLL 9500, InSitu Europe Ltd). Two 50 ml water quality samples were collected for later major cation (Na^+, K^+,

Mg^{2+}, Ca^{2+}, NH_4^+) and anion (NO_2^-, NO_3^-, Br^-,Cl^-,SO_4^{2-},PO_4^{3-}) analysis. Samples were filtered using 0.45 μm disposable filters. They were transported in a cool box and refrigerated prior to chemical analyses. Sample preservation was as per BSI (2012); Cation samples were acidified to below pH 2 using HNO_3; no preservation was used for anion samples.

Ion analysis was via ion chromatography (Anions, Dionex ICS-90; Cations, Dionex ICS-1100). Sample analysis was as soon as possible (given Dionex instrument availability) but within 1 month. 7 point calibration was used at the beginning and end of each ion chromatography analysis run; QA/QC measures included rinse blanks, laboratory blanks, duplicates and ion mass balance checks.

2.3 Results and discussion

2.3.1 Birmingham SBTT

The purpose of the Birmingham SBTT carried out during 2011 and 2012 was twofold. Firstly the tests provided a means to assess SBTT method and model development; secondly the tests allowed investigation of the spatial and temporal variation in ambient borehole flows in three closely located boreholes in a multi-layered sandstone aquifer.

Saline water, emplaced at a concentration of 100 mg/l NaCl in the open intervals of BH2 and BH3 during the 2011 SBTT, resulted in an initial electrical conductivity value in the open intervals of the boreholes of 3.5 mS/cm (Figure 2.7 b and c). Initial conductivity was higher (4 mS/cm) in BH1 and BH3 in 2012 (Figure 2.7 a and d) as a result of the slightly higher (120 mg/l NaCl) emplaced tracer concentration. In the 2011 tests (Figure 2.7 b and c), the early-time conductivity peak recorded at *c.* 45 m bgl is probably the result of too much salt water being poured into the hose; in such a scenario excess tracer overshoots the bottom of the hose and collects in the bottom of the borehole. The volume of salt water emplaced in 2012 was accordingly reduced. Small variations in EC with depth were seen in the early time profiles (red

profiles) in all four borehole tests (Figure 2.7). Such small early time variations are a result of incomplete mixing of the tracer with the borehole water. However, dispersion and mixing, particularly due to the repeated movement of the logger up and down the borehole, acted to smooth these variations.

In all four SBTT conductivity levels had significantly decreased below 35 m bgl by the completion of the first downward pass of the logger. Such a reduction is indicative of background conductivity groundwater entering the boreholes in this region. With time, this lower conductivity inflowing water moved up the borehole, displacing the higher conductivity water ahead of it. In the 2011 SBTT (Figure 2.7 b and c) it took 3 hours and less than 1.5 hours (BH2 and BH3 respectively) for conductivity to return to background (0.5 mS/cm). In the 2012 SBTT (Figure 2.7 a and d) it took approximately 1.5 hours for both boreholes (BH1 and BH3) to return to background conditions.

The most noticeable differences between borehole tests are: (1) the much slower movement of the tracer front in BH2 (indicative of slower ambient flows) compared with either BH1 or BH3; (2) the slowing of the later time (> 54 minutes) tracer/fresh water front between 12 and 17 m bgl in BH1 (Figure 2.7 a). Such a slowing suggests an intermediary outflowing zone immediately below this region reducing upward flow in the borehole. A similar slowing in the tracer front was not observed in BH2 and BH3 (Figure 2.7 b, c and d) suggesting no intermediary outflowing zone but rather a single outflow zone immediately below the casing.

2.3.1.1 SBTT Modelling

Flow directions and approximate rates of flow can be inferred from direct observation of the SBTT profile. However, numerical modelling of the uniform-emplacement SBTT can confirm and quantify such inferences. Such an approach is presented here.

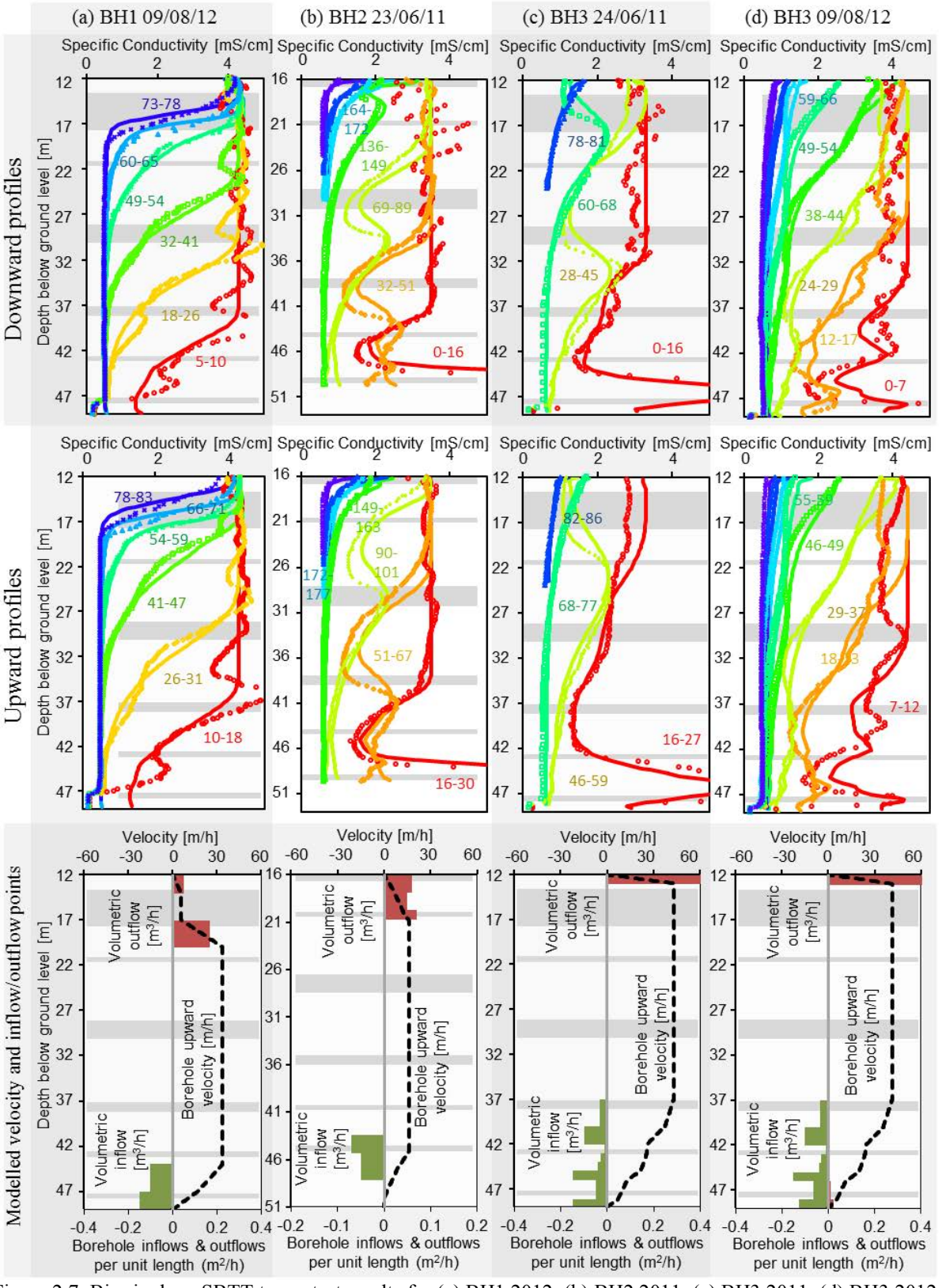

Figure 2.7: Birmingham SBTT tracer test results for (a) BH1 2012; (b) BH2 2011; (c) BH3 2011; (d) BH3 2012. Figure rows are (1) measured (data points) vs. modelled (solid lines) downward SBTT profiles; (2) modelled vs. measured upward SBTT profiles; (3) Calibrated borehole vertical velocity profile, inflow/outflow locations and magnitudes. Colour shows elapsed time. Grey shading shows the presence of low permeability layers identified from previous work at the site (Riley et al., 2011). Water levels for a - d were 4.3, 7.8, 6.8 and 4 m bgl respectively.

A reasonable model calibration was achieved against the observed downward conductivity profiles for all four Birmingham SBTT (Figure 2.7, first row). Use of the calibrated model parameters to model the upward conductivity profiles (Figure 2.7, second row) provided validation of the model calibration. Here, downward-profile calibrated inflows and outflows provided an equally good match to upward profile observations. Logger equilibration time (Section 2.2.1.2) did not add a large source of error to the recorded conductivity profiles.

For all BHs, numerical simulations confirmed the previous inferences on borehole inflow and outflow points and flow direction. Predicted ambient borehole flows were upwards, with inflows located towards the bottom of the boreholes and outflows at the top (Figure 2.7, third row). Predicted maximum upward velocities in the boreholes were 16.4 m/h, 34 m/h, 41 m/h and 43 m/h (BH2, BH1, BH3 2012 and BH3 2011 respectively). Such velocities are much below that required to invalidate the assumption of laminar flow in the 15 cm diameter boreholes (1336 m/h for Re = 1700).

Numerical simulations were done without reference to the location of low permeability horizons inferred from packer testing (Riley et al., 2011) (grey shading in Figure 2.7). The shorter casing in BH1 and BH3 means the open interval of these boreholes intersects with an additional permeable layer above the uppermost low-permeability horizon observed in BH2. Modelling of the SBTT was clearly able to distinguish the difference in the location of the higher and lower permeable horizons located at the outflows zones in BH1, BH2 and BH3 (Figure 2.7, third row). However, the thinner low permeability horizons in the inflow regions of the boreholes (below 37 m bgl) were not detected; such resolution is beyond the SBTT method.

The gradient of the observed tracer/fresh water front in BH3 (Figure 2.7 c and d) was shallower than that observed in either BH1 or BH2. This shallower gradient is indicative of a more diffuse inflow region with inflows predicted over the bottom 13 m of BH3. The inflowing

regions in BH1 and BH2 are more distinct with inflows predicted in the bottom 5 metres of both boreholes.

Cross flows (inflow and outflow at the same location in the borehole) are identified in SBTT profiles as nick-points of reducing conductivity without an accompanying change in upward (or downward) tracer front speed that would result if just inflows were present. The SBTT modelling suggested the possibility of cross flow at the bottom of BH3 during 2012 (Figure 2.7 d). Cross-flow nick points can only be identified before the tracer is displaced and conductivity returns to background. In the main inflow region at the bottom of BH3, tracer was quickly displaced due to the upwards flow of water. Cross-flow identification therefore relied on the use of very early time profiles only. However, the lack of repeat profiles for analysis and the conductivity variation that resulted from early-time incomplete mixing made firm identification of cross-flows difficult. However, the implication for water quality variation in the borehole are small; whether cross flows are present or not, water quality in the borehole is dominated by the inflows from the bottom of the borehole.

2.3.2 Kilham

SBTT method testing and associated model development, undertaken at the Birmingham boreholes, was able to quantify ambient borehole inflows and outflows and discriminate between low and high permeability layers in the multi-layered sandstone. Following on from such method development, SBTT testing and subsequent passive groundwater sampling were undertaken in four open boreholes located in the East Yorkshire Chalk where rising nitrate concentration had been observed at a nearby public water supply (PWS) well. The purpose of the fieldwork was three fold: (1) to improve interpretation of historical data; (2) to investigate spatial and temporal trends in flows in the four similarly sited boreholes and (3) to provide recommendations for appropriate sampling at the site and more generally.

2.3.2.1 Historical data overview

A rising trend in nitrate concentration is observed in all four study boreholes (Figure 2.8). Such a rising trend is consistent with that observed at the PWS well located downgradient (Gale and Rutter, 2006). Drinking Water Standards exceedance is observed from the late 1990s in Henpit Hole and Middledale (Figure 2.8 c and d) with marginal exceedances from some samples observed from the late 2000s in Bartondale and Tancred Pit (Figure 2.8 a and b).

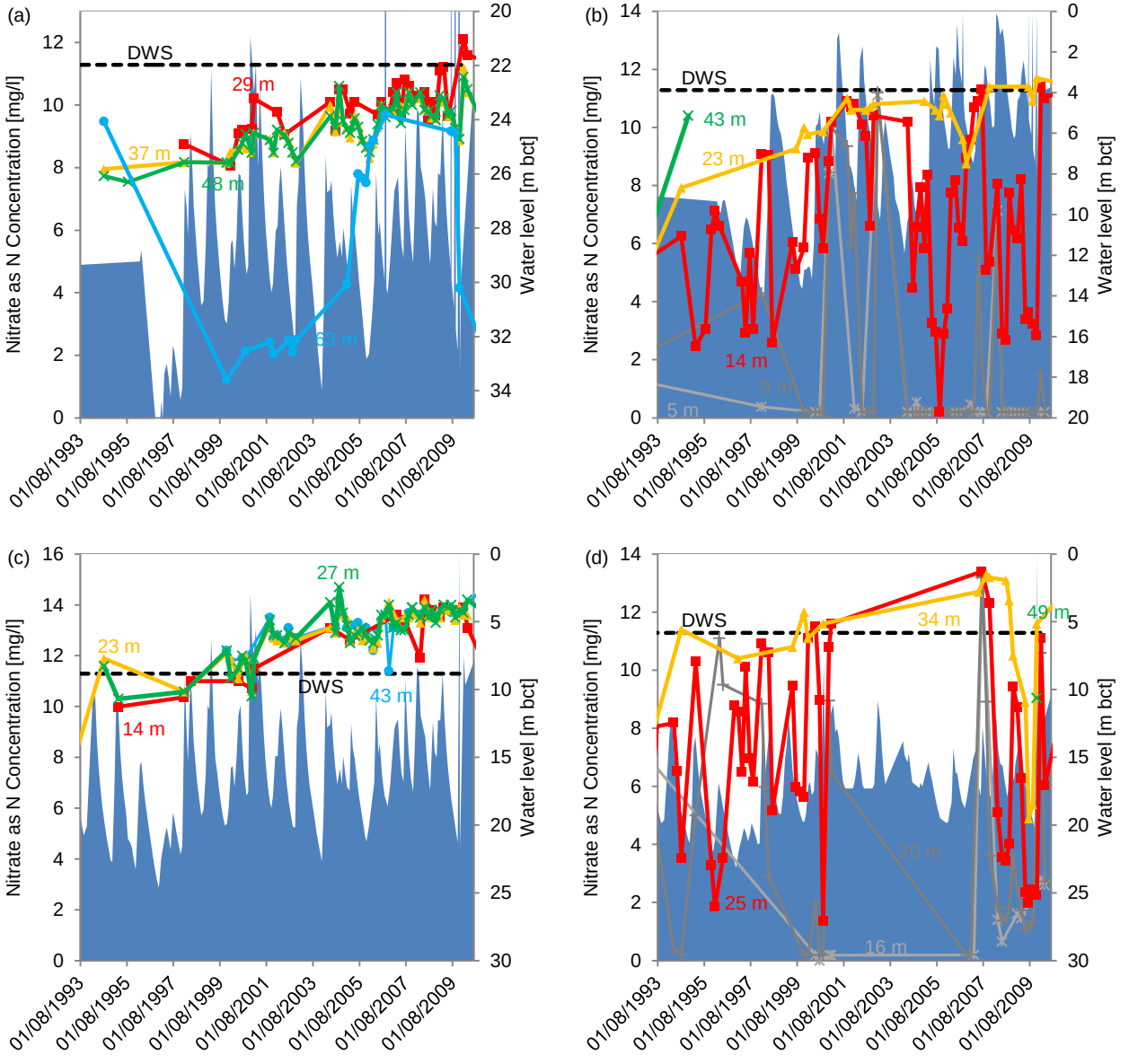

Figure 2.8: Temporal variation in nitrate concentration as a function of sample depth below casing top in (a) Bartondale; (b) Tancred Pit; (c) Henpit; (d) Middledale. Grey lines are samples taken within the casing; blue shading indicates water level variation; the black dashed line indicates the 11.3 mg/l NO_3 as N drinking water standard (DWS).

Observed NO_3 concentration at all depths in Henpit Hole (Figure 2.8 c), and at all but the lowest depth (63 m bct) in Bartondale (Figure 2.8 a) show very similar concentration values and trends. In these two boreholes, sample concentration is broadly independent of sampling depth. However, for Tancred Pit and Middledale (Figure 2.8 b and d) NO_3 concentration is much more variable with depth. Samples taken in and immediately below the bottom of the casing (red lines in Figure 2.8 b and d) show significant variability. At some times, these concentrations are equal to the higher nitrate values observed deeper in the borehole (e.g. 2001, 2007). At other times, NO_3 as N concentrations observed in or immediately below the casing are much lower (< 3 mg/l NO_3 as N) than those observed at depth in the boreholes. There is some suggestion (Figure 2.9) that higher nitrate values in or immediately below the casing are associated with a rising water table; lower nitrate values are associated with a falling water table. However, the relationship between water level and nitrate concentration is not clear.

Some authors have observed depletion of Nitrate in stagnant borehole casing water relative to aquifer concentrations (Humenick et al., 1980). However, at Kilham the time between nitrate highs and lows (typically months at most) is not sufficiently long for observed variation in nitrates immediately below the casing to be explained by stagnation and nitrate loss. It may be that low nitrate concentrations are a result of infiltration of rain water into the casing as a result of leaks in the borehole head works. As water levels fall this low nitrate water mixes with aquifer water immediately below the casing resulting in a decrease in nitrate relative to samples drawn from deeper in the open interval of the borehole.

Nitrate concentrations observed from samples taken deeper in both boreholes (23 m bct and 34 m bct for Tancred Pit and Middledale respectively, Figure 2.8 b and d) show a rising trend with much reduced temporal variability compared with those samples taken in or immediately below the casing. This rising trend at depth is similar in gradient to those observed in Bartondale or Henpit Hole. Post-2007 Middledale samples taken at 34 m bct exhibit a sharp drop in nitrate

concentration. Such a drop is at odds with the historical upward rising trend in Middledale, in the other three boreholes considered and that at the Kilham PWS and is unexplained.

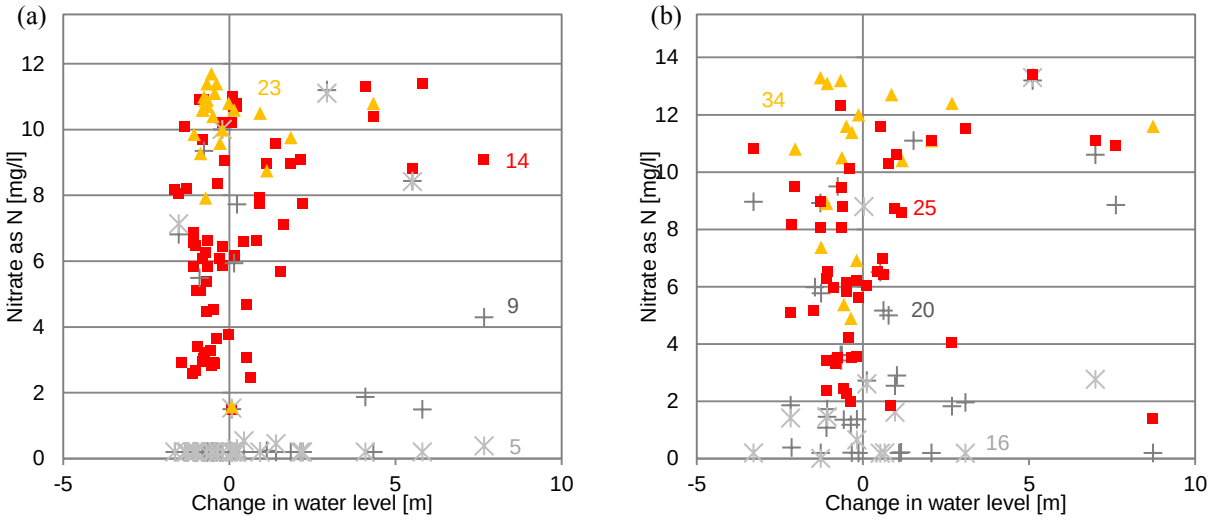

Figure 2.9: Nitrate concentration as a function of change in water level for (a) Tancred Pit and (b) Middledale. Numbers indicate the depth at which the samples were taken. Grey data points are from within the casing, red data points are from immediately below the bottom of the casing and orange data points from deeper in the open interval of the borehole.

Tracer testing by Ward et al. (1998) attempted to identify the source protection zone around the Kilham public water supply well. However, the results were complex with direct connections not found between the four upgradient boreholes considered in this study and the PWS. Connections were, however, found between the upgradient study boreholes and with springs down-gradient of the PWS. Given this lack of direct connection to the PWS it is not unsurprising that, even when selecting the depth at which samples match most closely, nitrate concentrations observed in the four upgradient boreholes are not wholly representative of those at the PWS (Figure 2.10). While the rising trend in nitrates is broadly consistent, absolute concentration values are several mg/l lower in the upgradient boreholes than those observed in the PWS.

Tracer testing (Ward and Williams, 1995; Ward et al., 1998) also found no connections between Bartondale and Tancred Pit in the Broachdale valley or between Henpit and Middledale in the Langtoft valley. However, despite such inferred lack of connections, boreholes located in

the same valley appear to have related nitrate concentrations.. Nitrate concentrations are consistently lower in the Broachdale valley (Figure 2.10, Bartondale and Tancred) than those observed in the Langtoft valley (Figure 2.10, Middledale and Henpit).

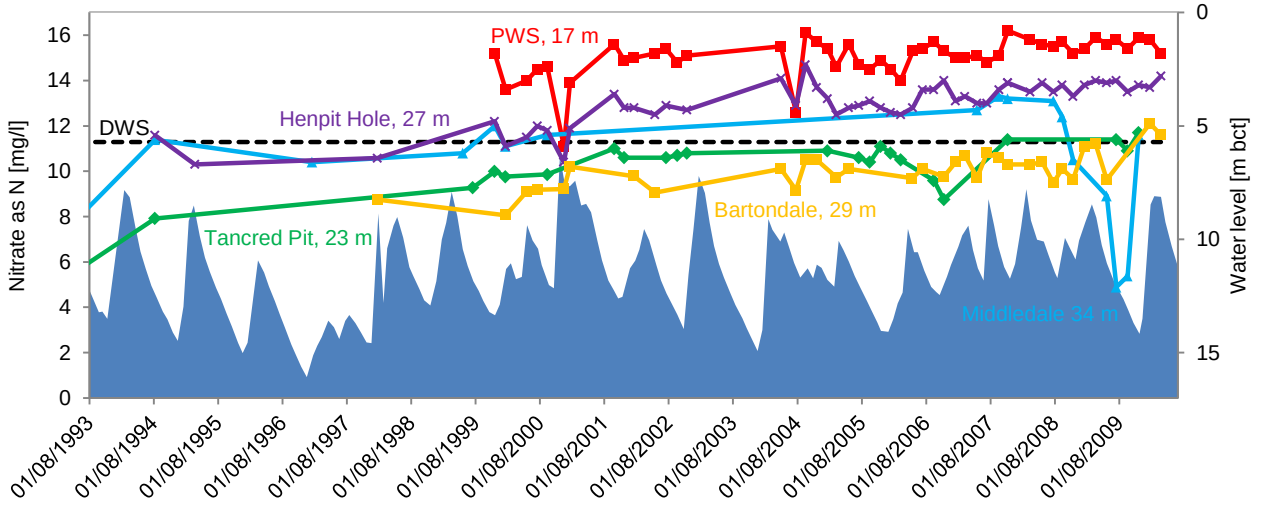

Figure 2.10: Historical trend in Nitrates in Bartondale, Tancred Pit, Middledale and Henpit Hole compared with Kilham Public Water Supply well. The depths given in the figure indicate the depth (m bct) from which the samples were taken. Bartondale, Tancred Pit, Middledale, Henpit Hole sample depths were selected as those that give the best match to the PWS data. PWS sampling data were only available from 17 m bct. The water level data are taken from the PWS.

2.3.2.2 2012/2013 SBTT flow logging

SBTT flow logging and subsequent passive sampling were undertaken during 2012 and repeated during 2013 in Bartondale, Tancred Pit and Middledale. The exception was Henpit Hole where an obstruction located approximately at the bottom of the casing prevented installation of the tracer-emplacement hose during the 2013 SBTT. Consequently only 2012 data are presented for Henpit. However, hydrasleeve sampling from Henpit was possible in 2012. During 2012, a period of drought meant water levels were towards historic lows (Figure 2.11); by contrast March 2013 water levels were towards the top of the historical range.

Compared with the Birmingham boreholes (Figure 2.7), Kilham boreholes (Figure 2.12, Figure 2.13) show much more variability in the SBTT conductivity profiles, both between boreholes and in the same borehole over different years. For example, tracer emplaced in Bartondale in 2012

(Figure 2.12 a) had not moved 30 hours after emplacement with no ambient borehole flow observable. By contrast, in 2012, tracer emplaced in Henpit Hole (Figure 2.13 a) had all but disappeared within 10 minutes. However, a raised conductivity signal remained slightly longer at the top and bottom of the Henpit borehole. It can be inferred (with some caution given the scarcity of data) that strong inflows were present in the middle of the borehole which diverged displacing tracer both upward and downwards. Outflows appear to be located towards both the bottom and top of the borehole. The SBTT modelling suggests the discharge of water through Henpit Hole under ambient conditions was at least 10 m^3/h in 2012. By means of a comparison, such a discharge is significantly more the 20 m^3/d threshold above which borehole abstractors would need to seek a licence from the Environment Agency (EA, 2013). Transmissivity may provide a clue to anticipated rate of flow; the very high transmissivity Henpit Hole exhibited the highest ambient flow of the four boreholes considered.

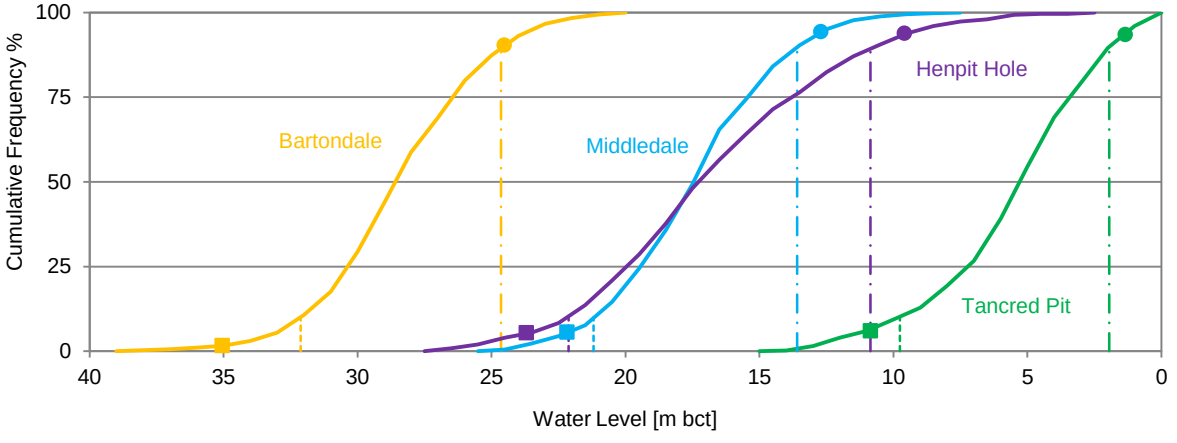

Figure 2.11: 2012/2013 water levels compared with historical (1979-2010) cumulative frequency ; dash and dash-dot lines show 10th and 90th percentiles respectively; squares are water levels during 2012 SBTT, circles are water levels during 2013 SBTT.

Tracer emplaced in Tancred Pit (Figure 2.12b) during 2012 and 2013 was displaced upwards in the borehole. This upward displacement is likely to be the result of inflows at the bottom of the borehole. An increase in the speed of movement of the tracer/freshwater interface at approximately 35 m bct suggests a further inflow was located at this depth with borehole outflow

inferred to be directly below the casing. However, the relative slowing of the tracer/freshwater interface in this region suggests that outflows were distributed over a vertical zone rather discharging a single discrete fracture.

Like Henpit, interpretation of the Middledale SBTT (Figure 2.13 b) suggests diverging flow in 2012. However, as in the case of Henpit, swift disappearance of the tracer below 45 m bct means any such interpretation must be treated with caution. Above 45 m bct, tracer was displaced upwards in the borehole as a result of upward flow with the SBTT modelling suggesting outflows were located directly below the casing. The observed slowing in the rate of movement of the tracer front and the decrease in conductivity between 30 and 35 m bct suggests a relatively complex pattern of cross flow and outflow existed in this zone during the 2012 SBTT. The lack of change in conductivity with time below 53 m bct in Middledale is indicative of a zone of stagnation.

2013 Tancred (Figure 2.12 b) and Middledale (Figure 2.13 b) SBTT profiles (and simulated inflow and outflow locations) were generally consistent with the 2012 SBTT. Modelling suggests there was change in inflow or outflow location or flow direction with the increased water levels. However, as might be expected given the much higher water levels, predicted flows velocities are greatly increased. The modelling suggests the maximum upward velocity in Middledale had more than doubled from 51 m/h in 2012 to 121 m/h in 2013. The change in upward velocity is even greater in Tancred with modelled velocity increasing from 30 m/h in 2012 to nearly 200 m/h in 2013. As a result of the increased flow in Middledale in 2013, the emplaced tracer disappeared very swiftly. Such swift disappearance means the location of the multiple outflow zones and cross flow inferred during the 2012 SBTT cannot be verified.

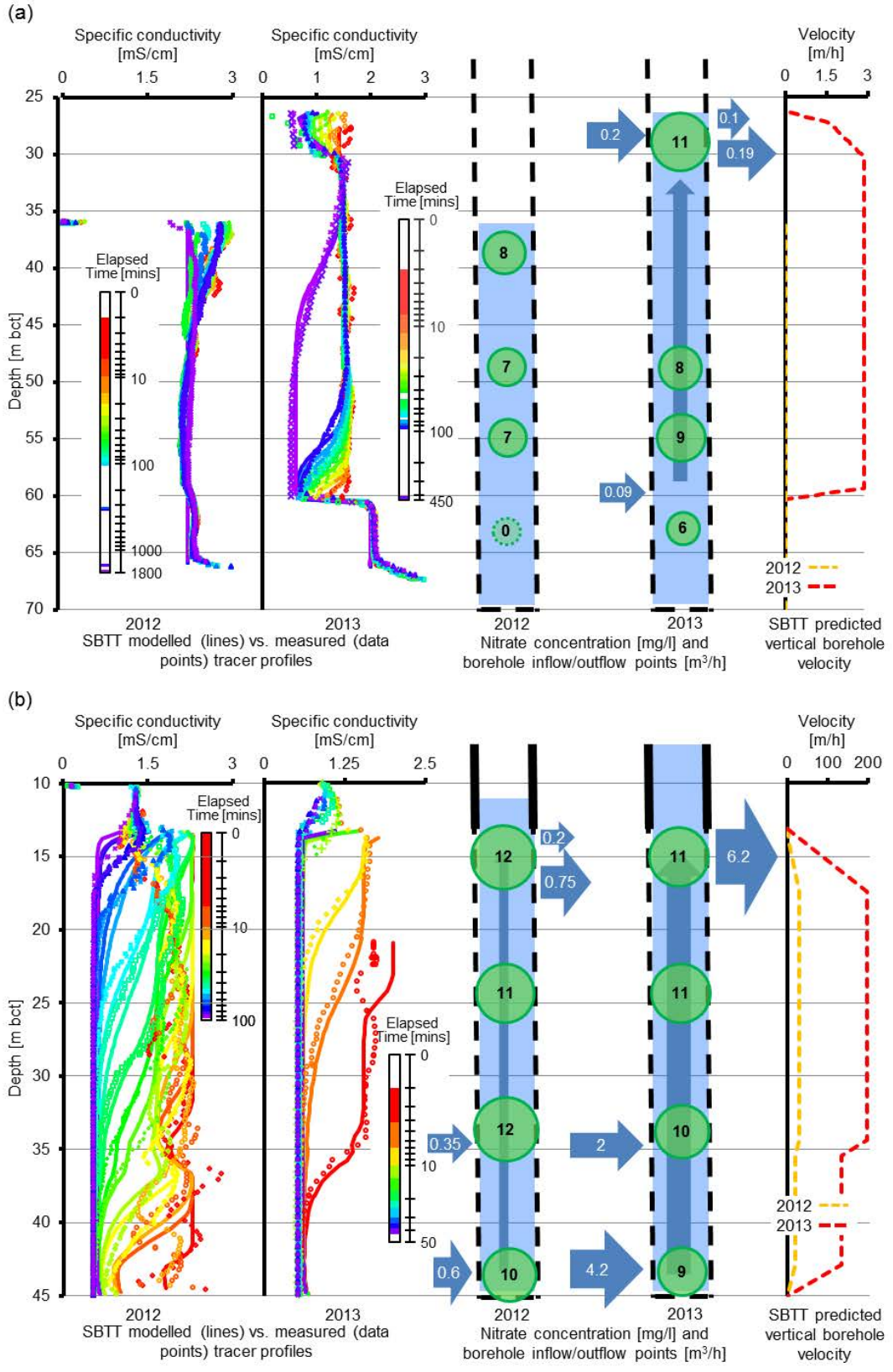

Figure 2.12: Summary of 2012 and 2013 fieldwork (SBTT and associated modelling and hydrasleeve depth sampling) results for Broachdale valley : (a) Bartondale; (b) Tancred Pit. Blue arrows indicate SBTT-predicted inflow and outflow locations and magnitude of flow (m^3/h). Green circles are nitrate concentration (NO_3 as N, rounded to nearest mg/l); the positioning of the circles indicates the depth of the hydrasleeve from which the sample came.

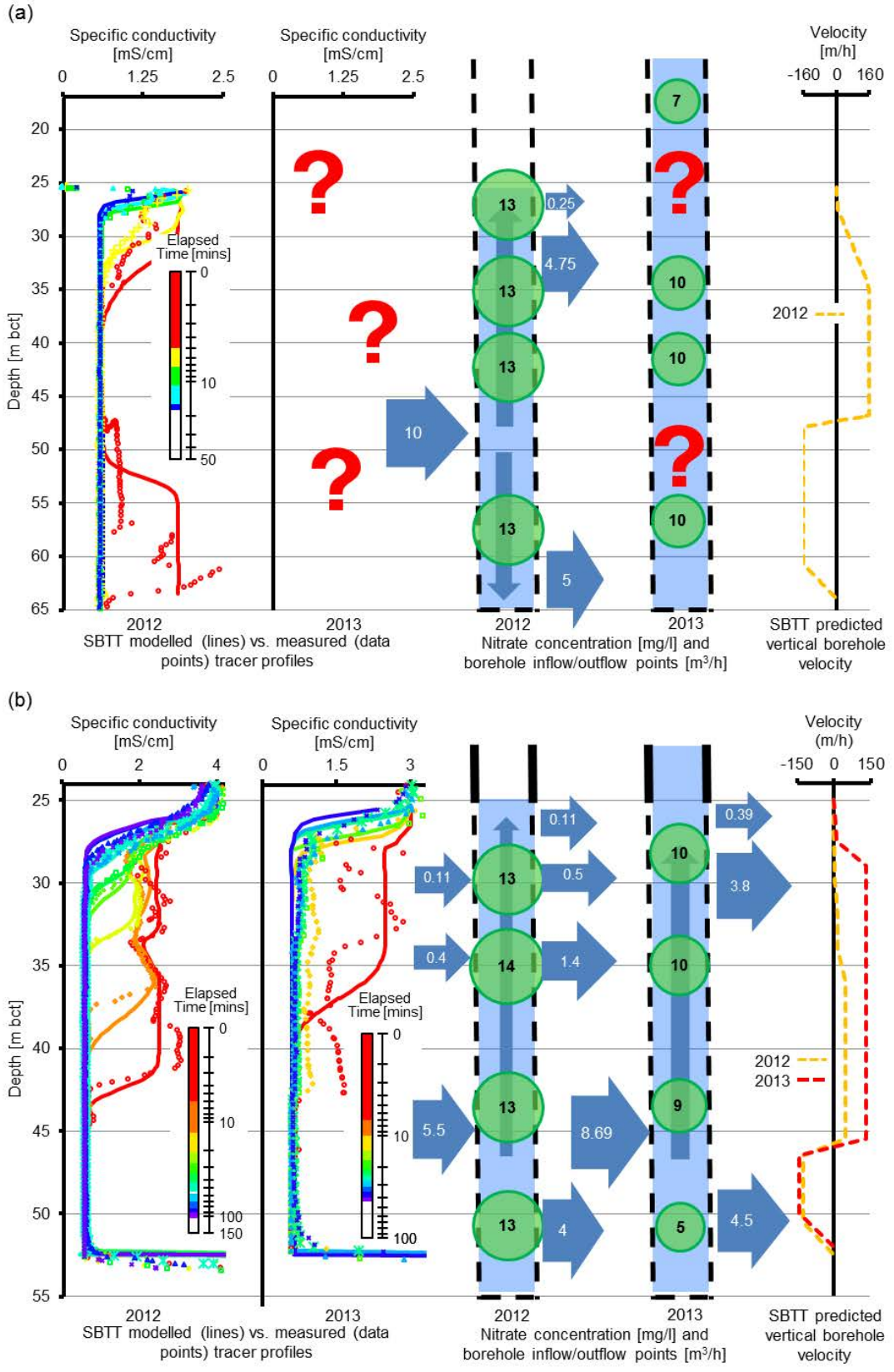

Figure 2.13: Summary of 2012 and 2013 fieldwork (SBTT and associated modelling and hydrasleeve depth sampling) results for Langtoft valley : (a) Henpit; (b) Middledale. Blue arrows indicate SBTT-predicted inflow and outflow locations and magnitude of flow (m^3/h). Green circles are nitrate concentration (NO_3 as N, rounded to nearest mg/l); the positioning of the circles indicates the depth of the hydrasleeve from which the sample came.

Bartondale shows a different result (Figure 2.12a) with significant differences in 2012 and 2013 SBTT profiles. The decrease in tracer between 26 and 30 m bct during 2013 suggests that rising water levels in the open section of the borehole had activated a zone of fracturing through which cross flow was occurring. In addition to this cross flow immediately below the water table, tracer displacement up the borehole from 59 m bct is evidence of upward flow from this point. Outflow points cannot be categorically identified until the tail of the tracer arrives. This was not quite the case by the time of the last profile (450 minutes) taken at Bartondale in 2013. However, the position of this profile means that the outflow point for the upward flowing water was either the same zone of fracturing through which cross-flow was occurring or immediately below the cross-flow zone. Borehole vertical flows were very slow relative to the other three boreholes considered; maximum simulated upward velocity is only 2.9 m/h.

SBTT measured flows (Figure 2.12, Figure 2.13) are broadly comparable with those observed from geophysics (Figure 2.5), however key differences exist: (1) Bartondale geophysics identified a stagnant zone below 68 m bct; SBTT modelling suggested a zone of little to no flow extends from 61 m bct to the bottom of the borehole. The existence of such a zone explains the low nitrate concentrations observed at 63 m bct compared with samples taken higher in the borehole where ambient flows are intermittently present under high water levels. (2) Tancred geophysics suggested diverging flow in the borehole with inflows around 35 m bct. SBTT testing identified 35 m bct as an inflow point however flow is upwards, rather than diverging. (3) Middledale geophysics identified outflows immediately below the casing as per the SBTT; inflow zones and the relatively strong flows compared with Tancred were not identified.

However, analysis of the previous SBTT undertaken at the site assumed no vertical flows were present (Ward et al., 1998). As a result, for the Middledale SBTT, the inflow zone between 42 and 49 m bct was identified however outflow zones located between 25 and 35 m bct were not identified. Ward et al. (1998) ascribe borehole transmissivity and lateral connectivity to the

inflowing horizons alone. Cross-borehole tracer tests (Ward and Williams, 1995) indicated a connection exists between Middledale and Little Kilham Farm (a borehole located several hundred metres down-gradient of Middledale in the Langtoft valley). However, using the average dip (2.2°) and dip (150°) direction Ward et al. (1998) found that the high transmissivity zones at 42 – 49 m bct in Middledale (the only flow zone they observed) would not intersect with the open interval of the Little Kilham Farm borehole. Hence, the authors inferred that inter-borehole connection is a result of cross-bed fracture development. However, using the same dip and dip direction values, the outflowing feature identified by 2012/2013 SBTT at 25-35 m bct in Middledale would intersect with the bottom of the Little Kilham Farm borehole. Perhaps, rather than cross-bedding fractures providing the inter-borehole connection, the Middledale borehole acts as the connecting path. Given the rate of upflow observed in Middledale, the borehole column is clearly acting as a path to transfer groundwater between the two fracture zones.

2.3.2.3 Hydrasleeve sampling

Hydrasleeve sampling, informed by SBTT results, was carried out during 2012 and 2013. 2012 hydrasleeve depths (Table 2.1) were selected, in order of importance, to: (1) target inflow/outflow zones identified from the SBTT; (2) provide good coverage over the length of the borehole; (3) match historical EA sampling depths. To provide a direct comparison, 2013 sampling depths were as per 2012. The exceptions were the shallowest hydrasleeves in Henpit and Bartondale which were both raised by 10 m to account for the much higher water table.

Groundwater composition as observed in both 2012 and 2013 (Figure 2.14) was typical of the Ca-HCO_3 type observed in the unconfined region of the Yorkshire Chalk (Smedley et al., 2004). In general, nitrate concentrations were higher during 2012 (10 – 14 mg/l NO_3 as N) than during 2013 (5 – 11 mg/l NO_3 as N) (Table 2.2, Figure 2.12, Figure 2.13). The exception was Bartondale where, in 2012, NO_3 as N concentrations were below detection limit at the bottom of the borehole

(63 m bct) and only 7 - 8 mg/l above (< 60 m bct). During 2013, at equivalent depths in the Bartondale borehole, NO_3 as N concentrations were 6 mg/l and 8 – 11 mg/l respectively (Figure 2.12a). In 2012, NO_3 as N concentrations observed in the Langtoft valley (Figure 2.13) were noticeably higher (13 – 14 mg/l) than in the Broachdale valley (0 – 12 mg/l, Figure 2.12). During 2013, this trend is reversed; maximum concentrations in the Broachdale valley (11 mg/l) were fractionally higher than those observed in the Langtoft valley (10 mg/l).

Borehole	BH depth [m bct]	Casing bottom [m bct]	Year	Water level [m bct]	Inflow locations [m bct]	Outflow locations [m bct]	Historical EA sampling depths [m bct]	Hydrasleeve depths [m bct]
Bartondale	70	7.5	2012	35.035	NA	NA	29,37.3,47.8,62.8	38,48,55,63
			2013	26.77	26.77-30.77, 59.77-60.77	26.77-30.77		28,48,55,63
Tancred Pit	50	13	2012	10.855	33-35, 41-43	13-17	5,9,14,23	14,25,32,38
			2013	1.32	33-35, 41-43	13-17		14,25,32,38
Henpit	65	13	2012	23.70	43.7-44.7	23.7-31.7, 56.7-59.7	14,23,27,43	27, 36, 42,58
			2013	9.515	?	?		17, 36, 42,58
Middledale	55	25	2012	22.18	45.5-46	25-31, 34.5-35, 50-52	19.75,25,33.75,49	30,35,43,51
			2013	12.70	45.5-46	25-31, 50-52		28,35,43,51

Table 2.1: 2012/2013 Hydrasleeve depths

Middledale and Henpit (Figure 2.13) showed little variation in NO_3 as N concentration with depth. Such a result is expected given SBTT flow simulations suggested water chemistry in the boreholes is dominated by a single inflow horizon. The exceptions were two samples taken in 2013, the shallowest hydrasleeve sample from Henpit and the deepest hydrasleeve sample from Middledale. DO concentration for the deepest Middledale hydrasleeve sample (56 % saturation) was significantly lower than the 100 % saturation observed in the Middledale hydrasleeve samples taken at shallower depths. Such data suggest that in 2013 the deepest hydrasleeve sample, targeted at 51 m bct may have been drawn from the stagnant zone immediately below (identified from SBTT as located at 52 m bct). Similarly decreased DO (77 % saturation) and decreased NO_3-N concentrations were observed in the 2013 Bartondale hydrasleeve sample taken at 63 m bct. SBTT modelling suggests this sample was also drawn from a stagnant zone in the

Bartondale borehole. The decrease in NO_3-N and DO in both boreholes may be the result of slow bacterially mediated reduction in the stagnating water due to the partially reducing conditions and only a limited supply of dissolved organic carbon.

Water quality samples taken at 17 m bct in Henpit were also lower in nitrate than samples from deeper in the borehole. It may be that this decreased nitrate concentration was the result of stagnation in this zone. However, 1994 geophysics (Figure 2.5) suggests outflow zones are present in the top third of the open interval of the Henpit borehole. Perhaps, like Bartondale, these outflow zones have an element of cross-flow. Bypass flow of recharge through the unsaturated zone can result in decreased nitrate concentration input at the water table (e.g. Sorensen et al., 2015) and hence may explain the lower concentrations observed directly below the water table in Henpit. The combined ammonium and nitrate observed in the shallowest Henpit samples is further evidence of mixing of two different waters (Table 2.2). However, without directly supporting flow data (and with a crashed water quality meter meaning the DO result was lost) any conclusions can only be speculation.

Limited data from the Yorkshire Chalk (Gale and Rutter, 2006) suggest that pore water and fracture nitrate concentrations are much higher in the unsaturated zone than in the zone of water table fluctuation or below. Decreased concentrations with depth are interpreted as dilution of nitrate load from the unsaturated zone with less contaminated groundwater from deeper in the aquifer. Such a pattern of decreasing nitrate concentration with depth was observed from hydrasleeve samples taken in boreholes with multiple inflow points with depth (Tancred Pit and Bartondale 2013, Figure 2.12). A simple mass balance approach (assuming perfect mixing) cwas used to predict inflowing fracture concentrations (and hence upgradient aquifer concentration distribution) in these multiple-inflow boreholes (Figure 2.15).

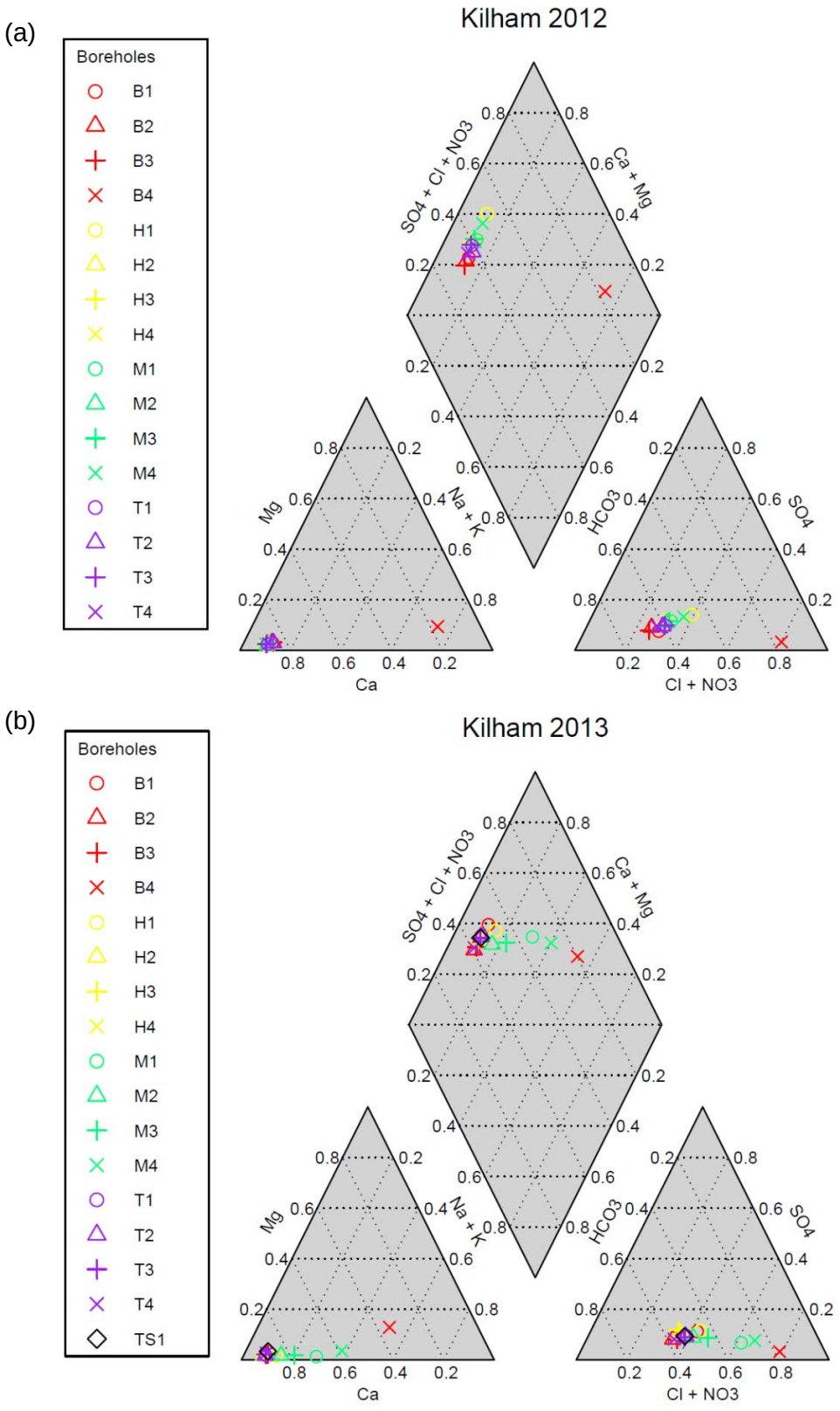

Figure 2.14: Piper diagrams for (a) 2012 and (b) 2013 hydrasleeve sampling . TS1 is a sample from the spring located by Tancred Pit borehole.

	Name	Depth	NH_4^+	Na^+	K^+	Mg^{2+}	Ca^{2+}	NO_2^-	Br^-	Cl^-	NO_3^-	SO_4^{2-}	PO_4^{3-}	T	Turbi-dity	ORP	pH	DO	EC	Mass Balance
		m bct	mg/l	mg/l	mg/l	mg/l	mg/l	mg/l	mg/l	mg/l	mg/l	mg/l	mg/l	°C	NTU	mV		% sat.	µS/cm	-
2013	H1	17	3.9	12.8	b.d.l	0.9	73.7	b.d.l.	b.d.l	52.5	31.8	25.7	b.d.l.	-	-	-	-	-	-	-0.008
	H2	35.5	b.d.l	10.4	b.d.l	1.1	102.5	b.d.l.	b.d.l	53.3	44.6	30.2	b.d.l.	8.3	1554	0.16	7.6	103	558	-0.04
	H3	41.5	b.d.l	11.2	b.d.l	1.1	103.6	b.d.l.	b.d.l	51.9	45.0	35.6	b.d.l.	7.9	34	0.19	7.6	103	566	-0.05
	H4	58	1.70	10.9	b.d.l	1.1	99.0	b.d.l.	b.d.l	56.4	46.5	28.6	b.d.l.	7.9	13.66	0.22	7.6	103	555	-0.04
	T1	14	b.d.l	10.8	b.d.l	1.4	98.7	b.d.l.	b.d.l	55.6	47.3	28.2	b.d.l.	7.7	101	0.29	7.7	100	532	-0.05
	T2	25	b.d.l	10.8	b.d.l	1.1	98.0	b.d.l.	b.d.l	55.8	47.3	26.9	b.d.l.	7.9	45	0.27	7.6	100	534	-0.03
	T3	32	b.d.l	10.8	b.d.l	1.4	98.2	b.d.l.	b.d.l	53.4	44.6	24.8	b.d.l.	8.5	244	0.26	7.6	100	427	-0.01
	T4	38	b.d.l	10.9	b.d.l	1.8	98.9	b.d.l.	b.d.l	46.7	40.5	22.3	b.d.l.	8.2	10	0.25	7.6	95	532	-0.03
	B1	38	b.d.l	10.7	b.d.l	1.3	95.1	b.d.l.	b.d.l	56.4	48.1	30.9	b.d.l.	8.3	24	0.32	7.7	101	528	-0.02
	B2	48	b.d.l	10.5	b.d.l	1.3	91.0	0.02	b.d.l	44.2	35.2	20.9	b.d.l.	8.7	39	0.32	7.6	101	509	-0.05
	B3	55	b.d.l	10.9	b.d.l	1.4	91.7	b.d.l.	b.d.l	50.0	38.9	21.8	b.d.l.	7.9	96	0.33	7.6	99	402	-0.2
	B4	63	b.d.l	129	b.d.l	16.8	75.6	b.d.l.	b.d.l	461.2	26.0	26.6	b.d.l.	8.5	26	0.33	7.7	78	1071	-0.13
	M1	30	b.d.l	48.9	b.d.l	1.4	102.8	b.d.l.	b.d.l	186.8	44.1	31.1	b.d.l.	9.5	7	0.39	7.6	103	725	-0.06
	M2	35	b.d.l	21.4	b.d.l	1.3	104.9	b.d.l.	b.d.l	80.3	44.2	30.0	b.d.l.	9.0	1839	0.39	7.5	106	584	-0.06
	M3	43	b.d.l	30.1	b.d.l	1.5	102.6	b.d.l.	b.d.l	102.2	41.9	30.9	b.d.l.	9.2	7	0.39	7.5	105	640	-0.1
	M4	51	b.d.l	55.0	b.d.l	2.7	73.9	0.1	b.d.l	206.1	23.9	33.9	b.d.l.	9.3	39	0.37	7.6	57	637	-0.03
2012	H1	27	-	10.5	1.0	1.7	101.9	-	-	29.3	57.2	30.7	b.d.l.	-	-	-	-	-	-	0.12
	H2	35.5	-	11.4	1.0	1.7	99.0	-	-	28.9	56.4	30.2	b.d.l.	-	-	-	-	-	-	-0.008
	H3	41.5	-	11.4	1.0	1.7	103.0	-	-	29.2	57.8	31.3	b.d.l.	-	-	-	-	-	-	-0.004
	H4	58	-	10.4	0.8	1.4	82.5	-	-	28.4	56.1	30.5	b.d.l.	-	-	-	-	-	-	-0.08
	T1	14	-	11.8	0.8	1.7	97.1	-	-	27.9	52.3	25.0	b.d.l.	-	-	-	-	-	-	0.02
	T2	25	-	13.8	1.3	2.0	92.5	-	-	27.0	49.9	24.0	b.d.l.	-	-	-	-	-	-	0.02
	T3	32	-	11.1	0.7	1.6	95.4	-	-	26.3	52.0	24.4	b.d.l.	-	-	-	-	-	-	0.02
	T4	38	-	11.2	0.8	1.6	89.5	-	-	25.5	45.6	23.2	b.d.l.	-	-	-	-	-	-	-0.009
	B1	38	-	11.6	0.9	1.8	80.6	-	-	23.6	33.9	15.3	b.d.l.	-	-	-	-	-	-	0.06
	B2	48	-	11.7	0.9	1.8	81.7	-	-	25.0	32.0	20.5	b.d.l.	-	-	-	-	-	-	0.003
	B3	55	-	12.6	0.9	1.9	84.1	-	-	25.0	32.0	18.2	b.d.l.	-	-	-	-	-	-	0.01
	B4	63	-	340	2.2	23.1	69.4	-	-	522.3	0.7	29.3	b.d.l.	-	-	-	-	-	-	0.05
	M1	30	-	12.5	0.9	1.7	96.7	-	-	29.0	57.6	29.9	b.d.l.	-	-	-	-	-	-	0.01
	M2	35	-	12.90	1.0	1.7	100.0	-	-	31.4	60.7	31.4	b.d.l.	-	-	-	-	-	-	-0.03
	M3	43	-	12.2	1.2	2.0	106.0	-	-	29.6	59.2	31.3	b.d.l.	-	-	-	-	-	-	0.03
	M4	51	-	11.2	1.0	1.7	101.7	-	-	28.7	56.4	30.0	b.d.l.	-	-	-	-	-	-	0.08

Table 2.2: Summary of Kilham hydrasleeve sampling; mass balance column gives the ion mass balance error

Applying this mass-balance approach to the Tancred and Bartondale hydrasleeve (Table 2.2) and SBTT flow (Figure 2.12) data gave predicted inflowing NO^3-N concentrations 1 - 3 mg/l higher than those observed in the borehole (Table 2.3). Such concentrations exceed the 11.3 mg/l NO_3 as N water quality standard while in-borehole concentrations generally did not.

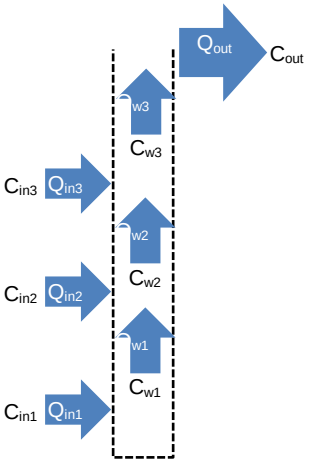

$$Q_{out} = Q_{w3} \qquad C_{out} = C_{w3}$$

$$Q_{w3} = Q_{in1} + Q_{in2} + Q_{in3} \qquad C_{in3} = \frac{C_{w3}Q_{w3} - C_{w2}Q_{w2}}{Q_{in3}}$$

$$Q_{w2} = Q_{in1} + Q_{in2} \qquad C_{in2} = \frac{C_{w2}Q_{w2} - C_{w1}Q_{w1}}{Q_{in2}}$$

$$Q_{w1} = Q_{in1} \qquad C_{in1} = C_{w1}$$

Figure 2.15: Mass balance approach to predicting inflowing fracture concentrations. C indicates concentration, Q is volumetric flow and the subscripts *in*, *w*, and *out* indicate inflowing fracture measurements, in-well measurements and outflowing fracture measurements respectively.

	Fracture	Depth [m bct]	Q [m^3/h]	Q [l/min]	Nitrate as N [mg/l]
Bartondale 2013	Inflow 1	59	0.09	1.50	8.37
	Inflow 2	28	0.2	3.33	11.99
	Outflow	28	0.29	4.83	10.87
Tancred 2013	Inflow 1	43	4.2	70.00	9.13
	Inflow 2	35	2	33.33	13.29
	Outflow	15	6.2	103.33	10.48
Tancred 2012	Inflow 1	43	0.6	10.00	10.29
	Inflow 2	35	0.35	5.83	13.86
	Outflow	15	0.95	15.83	11.60

Table 2.3: Mass balance calculated inflow/outflow fracture concentrations for Bartondale and Tancred Pit . Inflow/outflows are as calculated from the 2012/2013 SBTT (Figure 2.12, Figure 2.13). Nitrate concentrations for Inflow 1 and Outflow are as observed from hydrasleeve sampling. Inflow 2 nitrate concentrations (high-lighted in yellow) are calculated

2.3.2.4 Mechanisms for variation in saturated zone nitrate concentration in the unconfined chalk

Mechanisms for variation in saturated zone nitrate concentration include (Allen et al., 1997; Gale and Rutter, 2006; Allshorn et al., 2007; Rivett et al., 2007; Stuart et al., 2008; Sorensen et al., 2015): (1) nitrate input to the water table by piston flow through the unsaturated zone; nitrate transfer by such mechanisms can be slow meaning nitrate inputs to the water table may continue to rise despite changes in agricultural practice; (2) diffusion of nitrate from unsaturated zone pore waters (loaded with nitrate due to piston flow) into the rising water table; (3) transport of nitrate from the soil zone directly to the water table by bypass flow during recharge events. If high nitrates are not present in the soil zone, such a mechanism can alternatively result in dilution of nitrate at the water table; and (4) activation/deactivation of additional fractures as the water table rises and falls allowing lateral movement of nitrate loaded groundwater. Bypass flow transport has been previously observed in the East Yorkshire chalk (Zaidman et al., 1999).

There are insufficient data to investigate in detail the relationship between nitrate concentration and water level in the Kilham boreholes as for example Lawrence et al. (1983) or Stuart et al. (2008). Nevertheless if the upward rising trend is removed (Figure 2.16 a) and just the seasonal variation considered (Figure 2.16 b), there is some suggestion that Bartondale samples taken from 29 m bct exhibit a positive relationship between water level and nitrate concentration. The SBTT and hydrasleeve sampling presented here provide a possible explanation – with rising water levels a fracture is activated between 25 and 30 m bct in Bartondale. Such fracture activation results in cross flow of higher nitrate concentration water. The high nitrate input from the activated fracture is a result of either bypass flow from the surface or flushing of nitrate previously held in the unsaturated zone (Stuart et al., 2008). For Henpit, there is some suggestion that when water levels rise above 15 m bct the reverse is true; an inverse

relationship exists between water level and nitrate concentration. It may be that as water levels in Henpit Hole rise above 15 m bct a fracture is activated. During high water levels, bypass flow contribution from this fracture dilutes nitrate concentrations in the borehole. Downward flow from the fracture at 15 m bct in Henpit Hole to the outflow zone identified by the SBTT at 25 – 35 m bct explains the dilution in nitrate concentrations observed historically in Henpit at 27 m bct when water levels are high. The lower nitrate concentrations observed at 17 m bct in Henpit during 2013 hydrasleeve sampling are also explained. Dilution following high rain fall events has been suggested as a mechanism to explain mid-winter nitrate lows observed from previous groundwater quality monitoring in the Yorkshire Chalk (Lawrence et al., 1983).

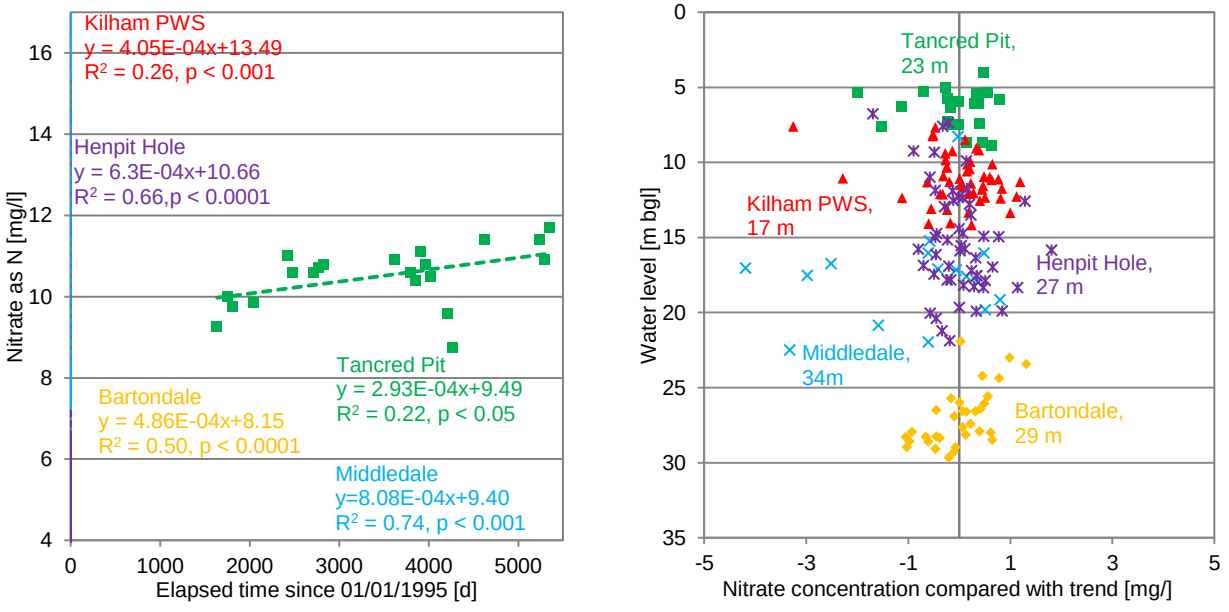

Figure 2.16: Nitrate concentration vs. water level at Kilham : (a) Detrending Nitrate sampling data (blue cross outliers at 5000+ elapsed days (post 2008) excluded from Middledale trend line fitting); (b) Nitrate concentration as a function of water level in the boreholes. Data are from the same depths as those in Figure 2.10.

By contrast, Middledale and Tancred Pit, show little seasonal variation in nitrate concentration. In these boreholes, the zone of water table fluctuation is above the bottom of the casing. Hence, increases (or decreases) in nitrates as a result of the rising and falling water table do not have an immediate impact on borehole water quality. Rather, the SBTT analysis suggested that water quality in these boreholes is dominated by inflows at depth. Nitrate variation in such

inflows is expected to be less strongly related to water level due to the delay in the arrival of the water from upgradient and possible mixing with cleaner water from deeper in the aquifer.

2.3.3 Repeatability of flow measurements and implications for water quality sampling

Flow direction and inflow/outflow location were very similar across the three sandstone boreholes considered in this study. Such a result may be anticipated given the very close proximity of the three boreholes. However, subtle differences in inflow and outflow location did exist and the magnitude of flows varied between boreholes and with time. Such subtle variations may not be important to water quality sampling; here samples taken at any depth in the borehole would be dominated by inflows from the bottom of the borehole.

There were greater dissimilarities between the chalk boreholes due both to their greater spatial separation and to the inherently more variable nature of fractured chalk. Flow direction, which may depend on the positioning and number of flowing features intersecting the borehole, was not consistent between boreholes. Within each borehole, flow direction was generally consistent with time with no flow reversals observed. The exception was Bartondale where measurable borehole flows only occurred under high water levels. In boreholes with open interval spanning the zone of water table fluctuation fractures potentially important to flow and transport can be activated/deactivated seasonally. Even for boreholes cased over the zone of water table fluctuation, the percentage contribution from different inflow zones varied with time. Such variation is important if a mass balance approach is to be used for calculating inflowing concentration with depth. Whether located in sandstone or chalk, and whether cased in the zone of water table fluctuation or not, previous flow measurements in a borehole may at best be a guide to future borehole flows. Additionally, flow measurements at nearby boreholes may not be indicative of flow patterns in other boreholes in the area.

In the two field sites reported here a reversal in borehole flow was not observed. However, this is not the case universally. For example, further (unpublished) work undertaken during this project at an additional field site located in the Triassic sandstone near Ormskirk found a reversal in head gradient (from a downward head gradient to an upward head gradient) as a result of a rebounding water table due to reduced water company abstractions in the area. Such reversals in flow in boreholes have also been reported in literature; for example daily reversals in flow in long-screen wells were reported by Vermeul et al. (2011). These daily reversals were due to fluctuations in water level at a nearby river.

2.3.4 Appropriate groundwater quality sampling

In boreholes with very high flows such as those observed at Kilham it is uncertain if pumping could fully overcome vertical head gradients and whether a permeability-weighted sample could ever be obtained. Indeed, even if vertical head gradients can be overcome, cross-contamination means it is uncertain if groundwater pulled back during pumping from the ambient outflowing zones in the well is representative of upgradient aquifer concentrations in that fracture or represents cross-contamination from the fracture of highest head intersecting the screen. In such cases it might be better to accept vertical flows are present and target such flow streams as are occurring naturally. If a flow stream sample is the objective, then which of the groundwater quality metrics such a sample can return is most appropriate? Is it the maximum concentration observed in the borehole? The maximum (mass-balance inferred) concentration in the aquifer? The outflowing concentration? An average of samples taken at different depths in the borehole?

For the purposes of WFD assessment, groundwater quality status testing is triggered if a threshold screening value (37.5 mg/l NO_3) is exceeded (UKTAG, 2012). Groundwater quality status testing then requires taking a 6-year mean from each "representative" sample point and then aggregating such samples across the region. Often such sampling points are pumping

boreholes where it is assumed that the sample provides an integrated sample representative of a greater spatial extent of the aquifer. If an integrated sample is the goal then perhaps the most appropriate sample from the boreholes considered in this study is the outflowing concentration (which like a pumped sample tends to be an aggregate of inflows from across the open interval of the borehole). If threshold exceedance is the most important criteria then aiming to sample the maximum (most conservative) value in the borehole may be more appropriate. In either case such samples can be obtained using passive sampling. Ambient well flows are such that there is no need to purge "unrepresentative" stagnant water from with the open section of the borehole.

So how many and where should such passive sampler(s) be located? If the maximum inflowing concentration is required, then passive samples must be taken adjacent to each inflow point. Where multiple inflow points exist, regular SBTT may be required to allow accurate mass balance calculations of the maximum concentrations in the adjacent aquifer.

However, if the maximum in-borehole concentration is required then only one sample is necessary. For the boreholes considered the position of highest (and lowest) concentration did not change with time. It might be appropriate therefore to initially take a number of passive samples from across the borehole column (but avoiding taking a sample from immediately below the casing) and subsequently target sampling at the depth of highest concentration. For such a method SBTT (or other flow measurement techniques) are not required. However, subsequent analysis must recognise that the maximum sampled concentrations may not represent maximum in-aquifer concentrations.

If only the outflowing (integrated) concentration is required then a single passive sample is all that is required for the boreholes in this study. For boreholes with small variation in water level or with water levels consistently within the casing, then a single SBTT per borehole may be all that is necessary to inform passive sampler placement. For boreholes with large water level

fluctuations within the open interval, then SBTT are required under both high and low water levels.

2.4 Conclusions

Uniform emplacement single borehole tracer tests were undertaken at two contrasting field sites located in two of the most important aquifers in the UK. Direct numerical modelling of the uniform emplacement SBTT allowed quantitative estimates of ambient flows in long boreholes to be obtained. The model was made applicable to boreholes with high flow rates as results are generated for the depth and time of each observed data point; a single time per profile is not assumed. SBTT tests were used to inform optimal placement and interpretation of passive sampling in long boreholes and improve understanding of historical data.

The uniform emplacement tests allowed a wide range of ambient borehole flows to be identified. The tests were successful in both the fractured East Yorkshire Chalk and in the multi-layered Triassic sandstone underlying Birmingham where inflow and outflow zones were non-discrete. Flows identified were generally complementary with previously carried out geophysical investigations. Direct modelling of the uniform emplacement tests meant it was not necessary to carry out subsequent point emplacement tests to estimate borehole velocities. The field method and associated modelling were quick and easy to undertake. However, the method is limited by high flows where tracer may disappear from the borehole before logger profiling can be completed.

Flow regimes were generally comparable in the closely sited boreholes in the Triassic Sherwood Sandstone although differences in outflow location resulted from small differences in casing length. However, in the East Yorkshire Chalk flow regimes exhibited significant differences both between boreholes and within the same borehole over different years. In boreholes where the zone of water table fluctuation is within the open interval, borehole flow

regimes may differ seasonally as fractures are activated and deactivated with rising and falling water levels.

At both sites, ambient borehole flows were sufficiently high to make purging unnecessary. Targeting particular flow zones using low-flow or passive sampling (flow-stream sampling) is most appropriate in these settings. Knowledge of the flow regime explained both uniformity and variations in current and historical passive sample concentrations within each boreholes. Such knowledge can provide justification for a reduction in number of passive samples taken (and hence a reduction in associated sampling and analysis costs).

Combining SBTT-inferred volumetric inflows with multiple-depth passive sampling, a simple mass balance approach allows quantification of concentration variation in the aquifer with depth. However, such quantification ideally requires flow measurements to be carried out at the time of every sampling event. From a WFD perspective it may be more appropriate (and easier) to target concentrations in the borehole which provide the most integrated sample or the maximum in-borehole concentration. For the boreholes considered here, the location in the open interval of this maximum concentration sample did not change with time.

As long as passive samples are not drawn from within or immediately below the casing, then the groundwater quality trends observed in the boreholes considered here are comparable with that of a nearby public water supply well. Identification of trends did not require detailed flow knowledge. Judicious use of sampling data from long-screen wells can complement data collected from pumping wells for the purposes of WFD groundwater status assessment for example.

CHAPTER 3 INFLUENCE OF VERTICAL FLOWS IN WELLS ON GROUNDWATER SAMPLING

3.1 Introduction

Groundwater quality observed from the sampling of monitoring wells (or boreholes) is fundamentally controlled by the origin of the groundwater extracted. Sample provenance may depend upon a complex interplay of the scale (e.g. screen length) of the monitoring well, the sampling method and protocol employed and the prevailing local hydrogeological conditions. As has been shown (Chapter 2), the latter influence may prove significant between wells even where similar sampling protocols are adopted that are designed to promote consistency in approaches.

Ambient vertical flows in wells are likely to be greater where well screens are longer, and/or geological layering or fracturing promotes increased vertical head gradients. Use of shorter screens may reduce ambient vertical flows, however, ambient vertical flows of 0.015 – 2.3 l/min have been reported in wells with screens between 3 m and 10 m in length (Figure 1.1).

Implicit to many groundwater sampling evaluations, particularly in wells < 10 m in length, is the (perhaps unrecognized) assumption that pumping overcomes any ambient vertical gradients and a permeability-weighted sample (also referred to as a flow-weighted average sample or a screen-weighted sample (Church and Granato, 1996; Hutchins and Acree, 2000; Martin-Hayden, 2000a) was eventually obtained.

Research exists as to the provenance of pumped samples from wells under non-vertical flow conditions. At long pumping times, pump intake position may not be important and the sample origin is directly related to the permeability distribution over the well screen interval (Varljen et al., 2006). However, it may take a significant time, often longer than the typical sampling time, before this permeability-weighted sample concentration is attained due to the later arrival of groundwater entering the distant ends of the screen farthest from the pump intake (Reilly and

Gibs, 1993; Martin-Hayden, 2000a; Martin-Hayden, 2000b; Martin-Hayden et al., 2014). Well casing storage (Barber and Davis, 1987), well screen and sand pack design (Kozuskanich et al., 2012), the partial mixing of inflowing water with water within the well screen during pumping (Martin-Hayden and Wolfe, 2000) and even the purging method (Robbins and Martin-Hayden, 1991) may additionally affect the stabilization time. With increasing screen length in particular, chemical stability may take a very long time to occur, even if pumping rates are increased (Rivett et al., 1990; Mayo, 2010). However, the sensitivity of pumped sample provenance to ambient vertical flows has not been systematically mapped out.

The aim is hence to examine the phenomenon of ambient-flow biased samples and investigate what such samples are representative of. Can the literature-reported range of vertical flows in wells bias sampling results and lead to samples that are weighted by ambient head gradients in addition to other hydraulic influences? Presented herein is the numerical modelling study designed to address this question.

3.2 Materials and Methods

3.2.1 Numerical Modelling Overview

Numerical flow modelling with particle tracking was used to investigate pumped sample provenance under ambient horizontal head gradients and for increasing vertical gradients for 14 different model scenarios with varying screen length, well diameter, pumping rate, aquifer depth, permeability distribution and boundary conditions (Table 3.1). For each scenario the relative influence of vertical head gradients was varied by varying the position of the monitoring well in the aquifer. Each vertical flow simulation was compared with a corresponding baseline case with the same scenario parameters but no ambient vertical head gradients.

Scenario	Screen Length (m)	Well Diameter (cm)	$K_{x,y}$ (m/d)	Anisotropy Ratio (K_v:K_h)	$K_{x,y,z}$ (m/d) (Low K Layer)	Screen K (m/d)	Aquifer Depth (m)	Boundary	Pump Rate (L/min)
1	6	5	5	1:10	N/A	N/A	30	C.H.	0.3
2	6	5	5	1:1	N/A	N/A	30	C.H.	0.3
3	6	5	0.5	1:10	N/A	N/A	30	C.H.	0.3
4	6	5	0.5 (top 50%) 5 (bottom 50%)	1:10	N/A	N/A	30	C.H.	0.3
5	6	10	5	1:10	N/A	N/A	30	C.H.	0.3
6	6	5	5	1:10	N/A	0.5	30	C.H.	0.3
7	6	5	5	1:10	N/A	0.05	30	C.H.	0.3
8	3	5	5	1:10	N/A	N/A	30	C.H.	0.3
9	10	5	5	1:10	N/A	N/A	30	C.H.	0.3
10	6	5	5	1:10	N/A	N/A	60	C.H.	0.3
11	6	5	5	1:1	0.05 (Middle)	N/A	30	C.H.	0.3
12	6	5	5	1:1	0.05 (Top)	N/A	30	C.H.	0.3
13	6	5	5	1:10	N/A	N/A	30	Recharge	0.3
14	6	5	5	1:10	N/A	N/A	30	C.H.	0.5

Table 3.1: Summary of model parameters for 14 scenarios.

Well screen lengths of 3 – 10 m are considered with pumping rates that vary from those recommended for low-flow sampling through to higher pumping rates perhaps adopted in purging. While the lower end of the above screen range is typically recommended for low-flow sampling (e.g. US EPA, 2010), some authors have suggested such sampling can be used with screen lengths > 3 m (Barcelona et al., 2005; Varljen et al., 2006; Metcalf and Robbins, 2007). Indeed, low-flow or zero-purge sampling options are doubtless attractive in longer screen wells as the removal of fixed purge volumes becomes increasingly onerous. From a UK perspective, whilst well screens < 3 m are advocated for monitoring wells (BSI, 2010), other guidance suggests low-flow sampling is most applicable in wells with long-screen lengths (BSI, 2009). It is recognized that well screen lengths < 3 m are becoming more prevalent in contaminated site investigations and that a 10 m well screen may perhaps be perceived to be unreasonably long. However, the use of 10 m, or even longer, well screens still remains significant internationally. For example, within the UK context, they can be used in the monitoring of thick (> c. 100 m) aquifer resource units and low storage aquifers with high amplitude dynamic water tables. Also long well screens may be found in older wells/boreholes inherited from long-term monitoring of

aquifer resources or, for example, sentinel monitoring at landfill sites where a reasonable thickness of a potentially impacted aquifer may be monitored.

Vertical flow simulations for each scenario were run initially without pumping to assess the induced ambient vertical flows in the well. Pumping at low-flow rates was then simulated to investigate the sampling bias induced by the aquifer vertical gradients. Finally for each scenario, the pumping rate was increased to see if vertical gradients could be overcome and permeability-weighted sampling conditions achieved. Several transient simulations were used to investigate the possible variation in flux distribution as drawdown proceeds; in particular, the arrival at the pump intake of water initially in the casing.

The scope of the modelling excluded direct assessment of the implications of water quality variations within a monitored aquifer. The modelling results will assume more importance where concentration variations are significant between different geological (permeability) horizons sampled by the well. The flow-based assessment presented here underpins such future work.

3.2.2 Model Setup

MODFLOW 2000 (Harbaugh et al., 2000) was used to model the sampling scenarios simulated (Figure 3.1). The model finite difference grid was 400 m wide and either 30 or 60 m deep. Variable horizontal grid spacing was used ranging from a minimum as dictated by the borehole diameter to a maximum of 30 m at the inflow boundary. Uniform vertical discretisation was used. The existence of a vertical plane of symmetry through the borehole and parallel to groundwater flow allowed half the domain of interest to be simulated.

Head boundaries were specified at the left- and right-hand side of the model. The remaining boundaries were no flow. For baseline no ambient vertical flow simulations the head gradient between left and right boundaries was uniform with depth in the aquifer. In these simulations, the well was centered both vertically and horizontally in the aquifer. For vertical flow cases, the

conceptual model was one of predominantly horizontal regional flow from an aquifer discharging at a surface-water body with vertical gradients increasing as discharging water converges at the outflow point. For these scenarios, the right constant head boundary was specified in the top layer of the model only.

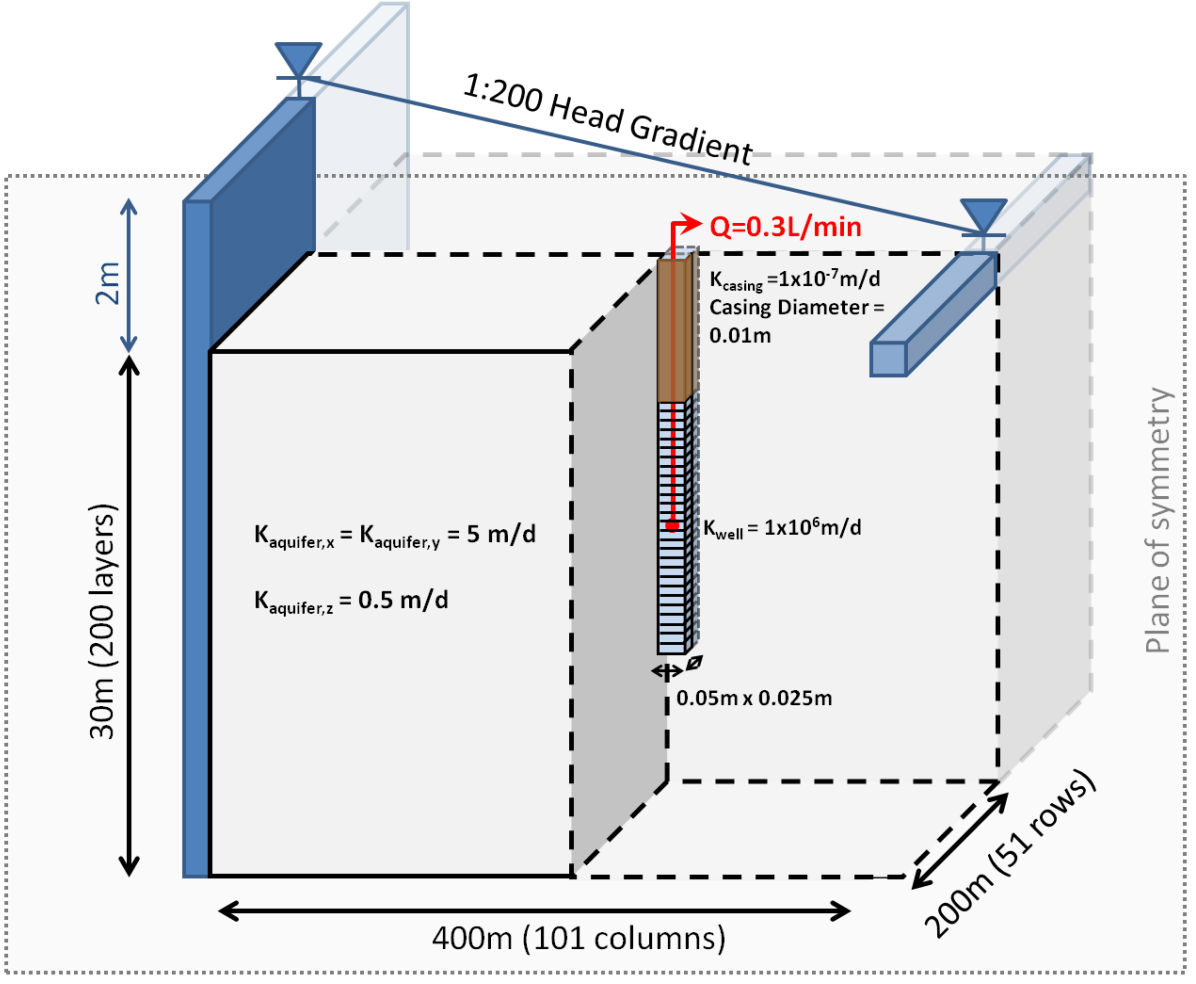

Figure 3.1: Summary of model domain and parameters for Scenario 1 with vertical head gradients (not to scale).

Rather than fixing well inflows/outflows or near well hydraulic gradients, for vertical flow simulations model boundary conditions were specified at a distance from the well. This allowed pumping simulations to affect (and possibly overcome) near well vertical head gradients. For each scenario the influence of vertical gradients on the well was varied by varying the horizontal distance of the well from the outflow boundary.

Initial sensitivity testing demonstrated that increasing the horizontal head gradient between the inflow and outflow boundaries lead to increased vertical head gradients due to the larger volume of water converging on the outflow point. Therefore, the horizontal gradient acted as a control on the magnitude of any in-well vertical flows. A final horizontal hydraulic head gradient of 1:200 was chosen as being both a realistic value, and one able to generate ambient vertical well flow rates that were comparable to those reported in literature.

While possibly important during groundwater sampling at some sites, variation in sample origin due to well dewatering effects was outside the scope of this investigation. To prevent well dewatering effects in the unconfined simulations, the model head gradients were specified such that they were above the top boundary of the model. The only exception to this was Scenario 13 where model inflows were derived from recharge alone with no left-hand constant head boundary. In this scenario, recharge was uniformly distributed at a rate of 1.41 mm/d. The recharge value was selected to give model inflows comparable to Scenario 1.

It was hypothesized that any impedance to vertical flow in the aquifer was likely to be important in driving ambient vertical well flows. For this reason, the starting vertical scenario (Scenario 1) was that of a permeable (5 m/d) aquifer with a 1:10 vertical to horizontal anisotropy ratio. Aquifer hydraulic properties in subsequent scenarios were chosen to represent a non-exhaustive range of alternatives: an isotropic aquifer (Scenario 2); a lower permeability aquifer (Scenario 3); a two-layer aquifer (Scenario 4); and an isotropic aquifer with a single 1.5 m low-K layer intersecting the middle (Scenario 11) or top of the well (Scenario 12).

For all scenarios, a single column of high-conductivity cells was used to simulate the water column both in the screened and cased sections of the well. During initial sensitivity testing with the MT3D code (Zheng and Wang, 1999) for transport simulation using MODFLOW velocity data, the influence of the in-well hydraulic conductivity (K_{well}) on transport to the pump intake was investigated in an aquifer with hydraulic conductivity of 5 m/d. Simulations of flow and

transport to the pump intake were performed for various K_{well} values and compared against an analytical solution (Martin-Hayden, 2000a). The analytical solution described the temporal variation in pumped sample concentration given a formation concentration that varied linearly from high concentration adjacent to the screen near the pump intake to low concentration at the far end of the screen. A K_{well} value of at least 10^6 m/d was required to provide a close match to both early and late time analytical data (Figure 3.2) and account for the delayed arrival of stream lines originating at a distance from the pump intake. A K_{well} value of 10^6 m/d was used for all further scenarios. This value is comparable with K_{well} estimates using Poiseuille's law (e.g. (Martin-Hayden, 2000a; Reilly and Gibs, 1993)); assuming fresh water at 12 °C, equivalent conductivities for 5 cm and 10 cm diameter wells are calculated as 5.4×10^7 m/d and 2.1×10^8 m/d respectively.

Well casing above the open interval was simulated using MODFLOW's wall boundary condition with a very low K value (1×10^{-7} m/d) to simulate the impermeable casing with a thickness of 0.01 m. This value was found to be sufficiently low to provide an effectively impermeable barrier with negligible flow observed through the casing relative to the screened interval of the well.

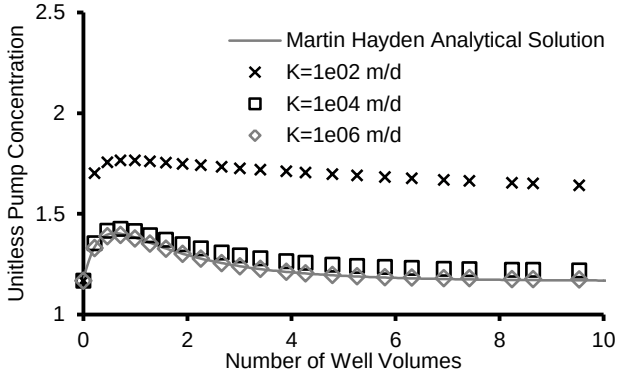

Figure 3.2: Comparison of MT3D transport results with Martin-Hayden's (2000a) analytical solution for increasing K_{well} values.

Lower conductivity screens have been shown to have a homogenizing effect on well inflows in a heterogeneous aquifer under pumping conditions (Houben and Hauschild, 2011). Scenarios 6

and 7 were used to investigate the effect of a low K well screen on well inflows under ambient vertical gradients. Screen conductivity values were chosen arbitrarily to be lower than the surrounding aquifer and were explicitly modelled using MODFLOW's wall boundary condition. Values of 0.5 and 0.05 m/d were chosen for Scenarios 6 and 7 respectively. In all other cases head loss across the screen was assumed negligible and the screen was not modelled.

A single cell within the well screen interval was specified as a well boundary condition to represent the pump intake. The initial pumping rates were either 0.3 or 0.5 l/min (within the range of 0.1-0.5 l/min recommended for low-flow pumping (Puls and Barcelona, 1996)). Unless otherwise specified, the pump was located in the centre of the well screen. During vertical flow simulations, pumping rates were incrementally increased until ambient vertical flows were overcome. The maximum pumping rate used was 36 l/min. Actual modelled pumping rates were half of those stated above due to simulation of half of the model domain.

3.2.3 Flow Simulation

The groundwater flow equations were solved using the PCG2 package of MODFLOW. To minimize mass balance errors and artificial oscillations due to very high-*K* well cells, head-change and residual-convergence-criteria values were set to $1x10^{-6}$ m and 0.001 m^3/d respectively. Cell-by-cell well in-flows and outflows were obtained directly from the MODFLOW CBB files. Constant-head and volumetric fluxes across the right, front and lower faces of each well grid cell were recorded for each timestep. These flows, in addition to the flows from the right face of the cell immediately to the left of the well cell, allowed the total inflows/outflows in the well to be calculated for each vertical layer. The inflows/outflows were multiplied by two as only half the well was modelled.

Steady-state flows were simulated when comparing well inflows and outflows under unpumped and pumped conditions. Limited transient flow simulations were used to investigate

the possible variation in flux distribution as drawdown proceeds and particularly the arrival at the pump intake of water initially in the casing. The 12-hour duration of the transient flow simulations was chosen to be significantly longer than the completion of groundwater sampling using well pumping methods (low-flow, or traditional 3-5 well volumes). During the transient simulations, the specific yield was set to 0.1 in the aquifer and 1 in the well. Specific storage was specified as $1x10^{-4}$ 1/m.

3.2.4 Particle Tracking

Particle tracking using the MODPATH 5 (Pollock, 1994) code in time series mode and transient MODFLOW velocity data were used to investigate the temporal variation in the well's capture zone. The relatively low pumping rates and the partially penetrating screens form capture zones that extended only a few metres from the screen. Consequently, particles did not need to be distributed throughout all layers of the model. Particles were placed in, up-gradient and down-gradient of the well in layers 10-145 (layers numbered top to bottom). Particles were placed in row 1 on the cell face at the top edge of the model along the plane of symmetry. Particles were released at the onset of pumping and were removed from the model upon arrival at the pump intake. Six particles were placed in each cell (evenly distributed in two rows) to provided sufficient resolution for early time (<1 hour) capture zones. During particle tracking, porosity within the well was 1 and outside the well 0.25.

3.2.5 Quantifying the bias to sampling

To allow comparison between vertical flow scenarios it was necessary to quantify the vertical flow induced sample bias. For a particular vertical flow scenario, the bias was calculated by finding the percentage inflow from each layer and then summing the difference between this and the percentage inflow from each layer under baseline horizontal gradient conditions:

$$\% \, Bias = \sum_{i=1}^{n} \left| \frac{Q_{in,i}^{v}}{Q_{T}^{v}} - \frac{Q_{in,i}^{h}}{Q_{T}^{h}} \right| \times 100 \qquad \text{Eq. [3.1]}$$

where $Q_{in,i}$ is the volumetric inflow for the well cell in layer i, Q_T is the total volumetric inflow to the well over all layers, n is the number of layers intersected by the well and the superscripts v and h indicate vertical flow and ideal horizontal flow conditions respectively.

3.3 Results and Discussion

3.3.1 Origin of pumped sample water from wells with no ambient vertical flows

Under horizontal head gradients, flow converges vertically to the well screen since the well is partially penetrating in these scenarios (Figure 3.3 g - i). This explains the higher influxes at the top and bottom of the well screen during pumping (Figure 3.3 a - c). However, while the long-time pumping capture zone encapsulates the entire well screen (Figure 3.3 g - i), the time to reach this state depends on the volume of water to within the well screen (Figure 3.3 d - f). For Scenario 1 it takes 2 hours to purge all well screen and casing water (Figure 3.3 d) and achieve a sample comprising 100 % formation water. In Scenario 5 it takes over 3 hours (Figure 3.3 e). Even for a well with a 3m screen, for the low-flow pumping rate used, it takes just over one hour (Figure 3.3 f) to purge all non-formation water. In all three cases, to achieve a sample comprising 100 % formation water requires purging the equivalent of several well volumes. However, stabilization of drawdown to within 95 % of steady-state drawdown was achieved within 10 minutes.

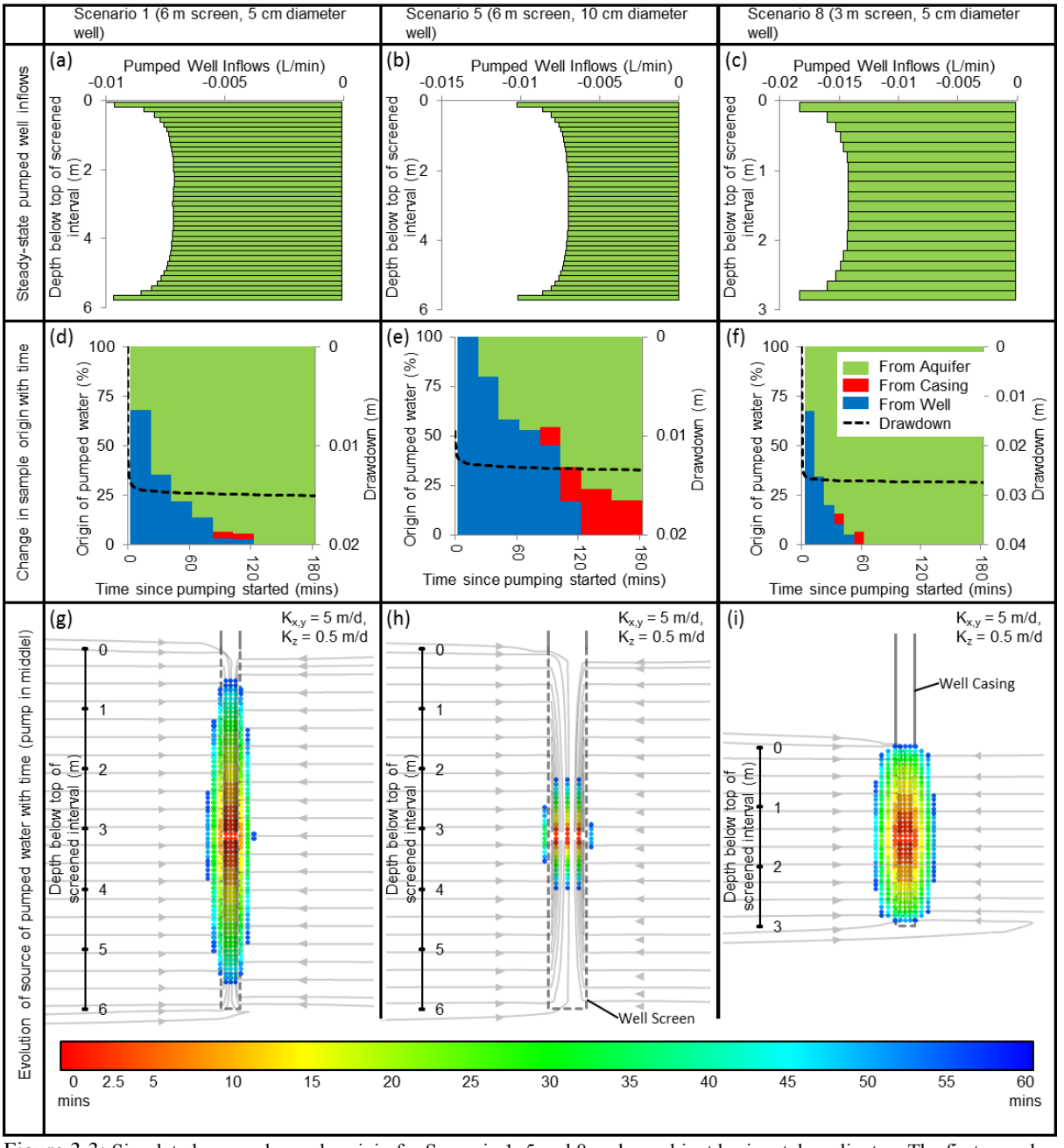

Figure 3.3: Simulated pumped sample origin for Scenario 1, 5 and 8 under ambient horizontal gradients . The first row shows the steady-state pumped well inflows. The second row shows the variation in pumped water origin with time compared with the simulated drawdown. The third row shows the temporal evolution of sample origin with the pump intake located at the middle of the screen. In all cases the pumping rate is 0.3 l/min. Particle colour indicates time, arrowed lines indicate long-time pumping capture zone.

After groundwater from the entire screen has reached the pump intake, the pump intake location may not affect the zone of the screen sampled. However, the time to reach this position depends on the well screen volume. In wells with longer screens it can be inferred that prolonged pumping may be required to collect water from the entire screen interval. Until then, pump intake position, pumping rate and pumping duration will play an important role in determining the origin

of the water sampled and therefore the sample concentration, even without vertical flows. This result compares well to the modelling of Martin-Hayden et al. (2014) who found that purging of at least two screen volumes was required to obtain a sample consisting of 94 % formation water. For the cases considered, well drawdown was not a good indicator of pumping capture zone stabilization across the screen interval.

Some casing water will always be purged due to the drawdown induced by pumping (Figure 3.3 d-f). The location of the pump intake determines the arrival time of the casing water at the pump intake. The farther the pump intake is located from the top of the screen, the later the casing water will arrive at the pump intake. While the volume of casing water is small and possibly well mixed with other water flowing towards the pump intake, the influence of the casing water may be an additional consideration when siting the pump intake for various types of sampling with a pump.

3.3.2 Ambient vertical-flow simulations

3.3.2.1 Sensitivity of ambient vertical flows in unpumped wells to aquifer and well properties

The following observations are made on the vertical flow simulations (and therefore the likelihood of vertical flows occurring in wells) during unpumped conditions (Figure 3.4):

(1) The farther the well is from the outflow boundary, the smaller the induced vertical flow in the well. In the main body of the aquifer, groundwater flow is predominantly horizontal; upward flows are only seen near the outflow boundary due to convergence of groundwater flow from deeper in the aquifer. A flow reversal is seen at a distance from the outflow boundary in Scenario 13 where recharge drives downward flow in the well.

(2) In the discharge zone, simulated ambient vertical flows are within the observed range reported in the literature for well screens between 3 m and 10 m in length; in fact in the 3

m well the flows are much less than the maximum reported (a simulated value of 0.05 l/min compared with 0.3 l/min observed).

(3) Anisotropy/heterogeneities provide a strong control on the degree of vertical flow simulated within the well. Under isotropic conditions, significant vertical flows are not seen until very close to the outflow boundary.

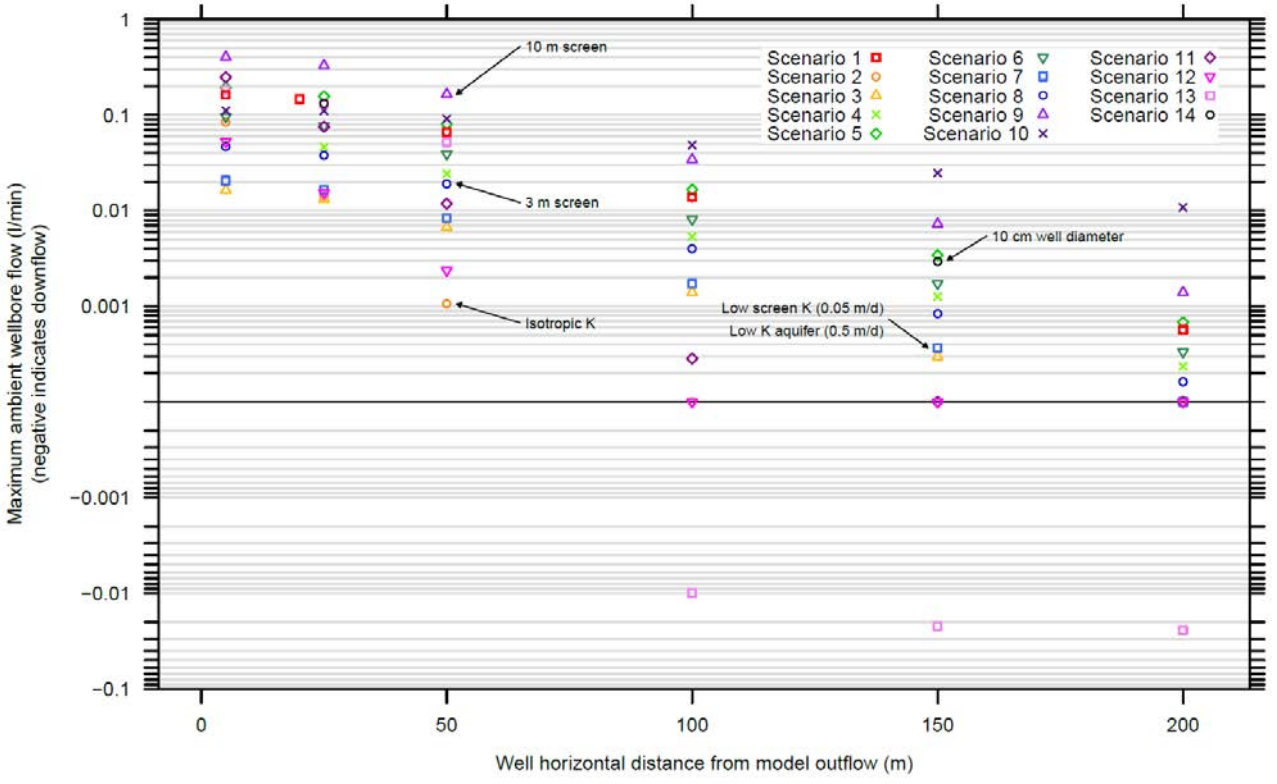

Figure 3.4: Change in simulated maximum ambient upflow flow in the well with distance from the model specified head outflow boundary for all vertical flow scenarios.

(4) Increasing well volume (length or diameter) increases the magnitude of vertical flows, with screen length having a greater effect as the head difference between opposite ends of the screen is greater.

(5) Lower aquifer K values reduce flows into and out of the well and hence decrease vertical flows in the well. Reducing screen K has a similar effect. However, care should be taken to prevent excessive drawdown if undertaking pumped sampling in low permeability settings or with a low K screen.

Typical ambient vertical flow patterns in the well were similar to those noted by others (Konikow and Hornberger, 2006; Reilly et al., 1989; Segar, 1993), with inflows biased towards the region of highest head intersected by the well screen (the bottom of the well in this case) and outflows towards that of lowest head (the top of the well screen) (Figure 3.5 a). A gradual reduction of inflows and increase of outflows is observed between these two points. If the hydraulic conductivity distribution is not homogenous, inflows and outflows may still be biased towards zones of higher conductivity intersected by the well screen (Figure 3.5 b).

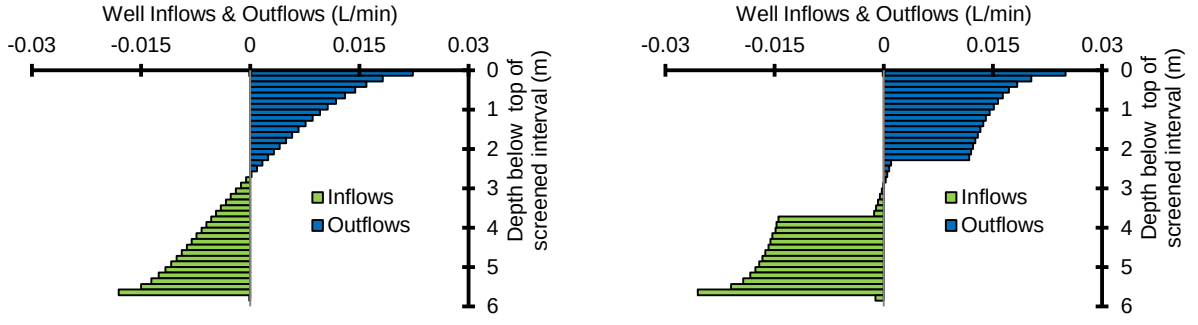

Figure 3.5: Simulated ambient well inflows/outflows under vertical head gradients for: (a) Scenario 1 (6 m well screen, 1:10 anisotropy) and, (b) Scenario 11 (6 m well, 1.5 m thick low *K* layer intersecting the middle of the well) with the well located 5m from the outflow boundary.

3.3.2.2 Origin of pumped sample water from wells with ambient vertical flows

With increasing vertical flows, pumping may not be able to counteract the vertical head gradients that generate ambient upflow in the well. The sample origin becomes biased towards the ambient inflowing zones in the well (e.g., results from Scenario 1, 5 and 8, Figure 3.6).

For Scenario 8 (3 m screen) pumping at 0.3 l/min is sufficient to partially overcome the ambient vertical head gradients generating a maximum ambient upflow in the well of 0.05 l/min (Figure 3.6 c, f). Like the baseline case (Figure 3.3 i), at long pumping times the sample is drawn from the entire screen interval and is independent of the pump intake position. However, it requires over 60 minutes of pumping to reach this position. Unlike the baseline case, the sample origin does not depend only on the formation hydraulic conductivity distribution. The sample

remains partially biased toward the zone of highest head intersected by the screen with a greater portion of the sample being drawn from the bottom of the screen interval.

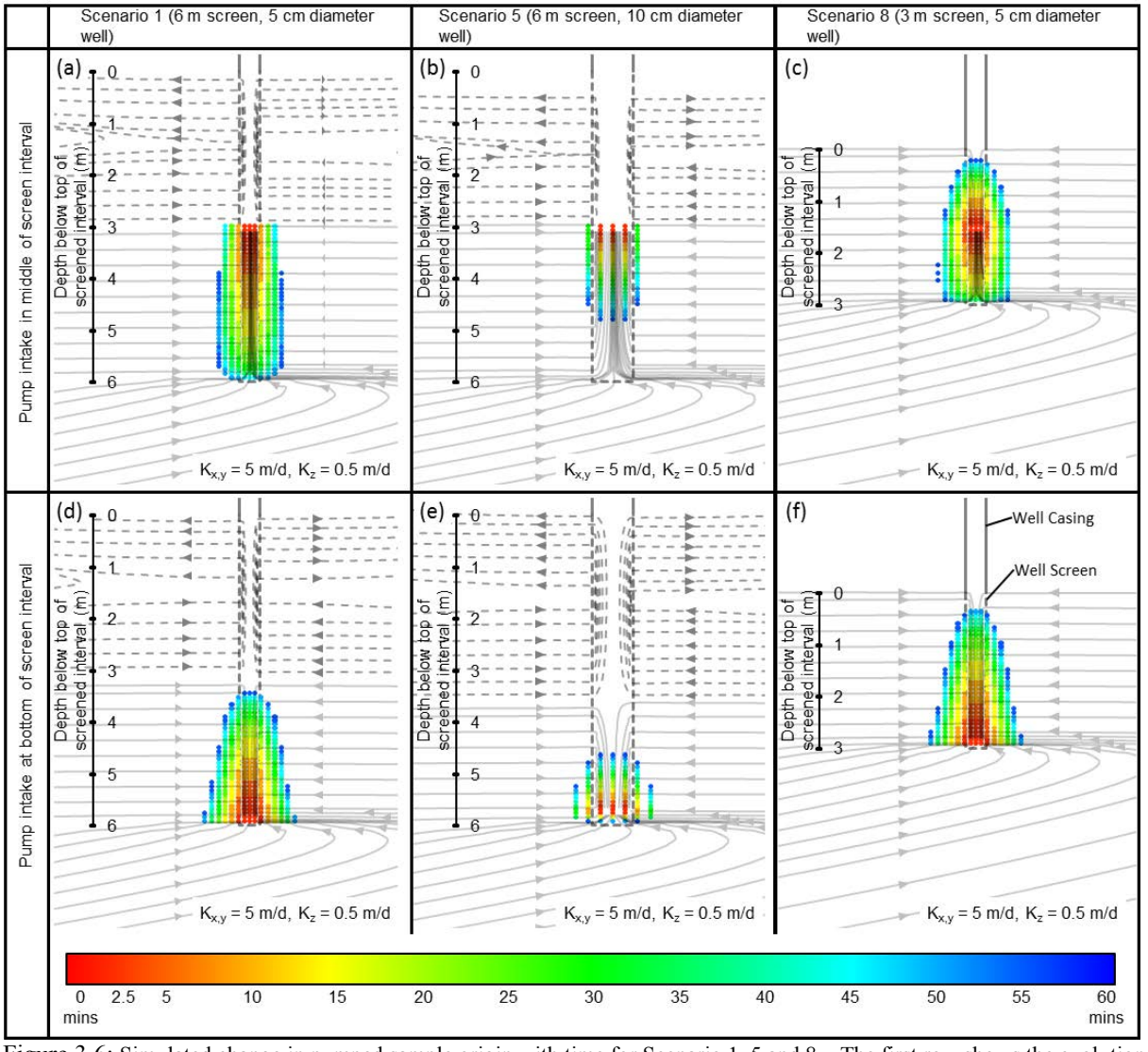

Figure 3.6: Simulated change in pumped sample origin with time for Scenario 1, 5 and 8 . The first row shows the evolution in sample origin with the pump intake located in the middle of the screen interval. The second row shows the evolution in sample origin with the pump intake located at the bottom of the screen interval. In all cases the pumping rate is 0.3 l/min. Maximum ambient upflow in the well is 0.16, 0.19 and 0.05 l/min for scenarios 1, 5 and 8 respectively. Particle colour indicates time, solid arrowed lines indicate long-time pumping capture zone, and dashed lines indicate flows in the well that bypass the pump intake.

In Scenario 1, with maximum ambient upflow in the well of 0.16 l/min, pumping at 0.3 l/min is insufficient to overcome the ambient vertical head gradients (Figure 3.6 a, d). Even after extended pumping, the pumped sample is drawn entirely from the bottom half of the screen interval. Like Scenario 8 (Figure 3.6 c, f), at long times the origin of the sample in the screen interval is independent of the pump intake position. During pumped sampling, ambient upflow,

driven by the ambient vertical head gradient, continues in the upper portion of the screened interval of the well. This water bypasses the pump intake entirely; even if mixing with casing water were to occur, there will be no bias to the sample in this case.

Unlike the two previous cases, for Scenario 5, with ambient upflow in the well of 0.19 l/min, pump intake position is important even after extended pumping. Different portions of the aquifer are sampled when the pump intake is positioned in the middle (Figure 3.6 b) or the bottom of the screen interval (Figure 3.6 e). With the pump intake located at the bottom of the screen interval (the zone of the screen with highest inflow), the pumped sample is drawn from only the bottom third of the well. Any ambient flows entering farther up the well screen bypass the pump intake entirely (Figure 3.6 e). Moving the pump intake to the middle of the well screen (Figure 3.6 b), the zone of the well with highest flow, allows a mixture of the entire inflowing zone of the screen to be sampled. This maximizes the portion of the aquifer sampled but gives a more mixed sample.

The pump intake position has very little effect on the well inflows and outflows during pumping (Figure 3.7 a). The difference in sample composition due to the pump intake location is clearer when considering the patterns of vertical flows in the well during pumping (Figure 3.7 b). When the pump intake is located in the middle of the screened interval, 0.045 l/min of groundwater entering the well through the lower half of the screen interval flows past the pump intake during pumping. The volume of water not captured by the pump depends on the rate of ambient vertical flows in the well.

As suggested by Greswell et al. (2014), in wells with high ambient vertical flows, pumped sampling at low rates can be thought of as almost analogous with taking a passive sample when compared with the volumes of groundwater flowing past the pump intake. Groundwater not captured by pumping will exit the well higher up in the screen interval. The pumped sample composition will depend on the degree of in-well mixing between streamlines originating from different screen intake points. If lateral dispersion and mixing between streamlines in the well are

low, sampling may only draw from a subset of upward flowing streamlines. If the pumped sample does not represent a fully mixed snapshot then horizontal position of the pump intake in the well becomes important in sample origin and sample repeatability. It can be inferred that dispersion and mixing are also important if the pump intake is located at the top of the well. The sample origin will depend on what water is carried to the pump intake, what water exits the well screen lower down, and the degree of mixing between waters of different origin moving upwards in the screen interval. If full mixing between streamlines can be assured, taking multiple samples at different depths in the screened portion of the well may be a way of assessing vertical changes in water quality from different screen inflow points.

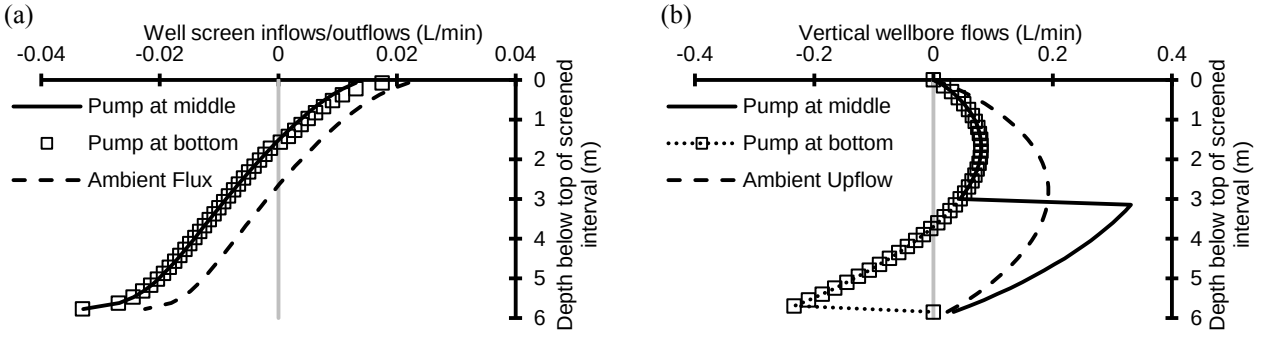

Figure 3.7: Comparison of well flows for Scenario 5 under ambient vertical head gradients with pump intake located at the bottom and middle of the screen . (a) Inflows and outflows in the well screen under ambient and pumping conditions (negative indicates inflow), (b) Vertical flows in the well under ambient and pumping conditions (negative indicates downwards flow). Maximum ambient upflow in the well is 0.19 l/min.

3.3.2.3 The transition from baseline conditions to vertical ambient head gradient biased samples

As ambient upflow increases, a transition from permeability-weighted sampling conditions to vertical head gradient biased conditions (flow stream sampling) occurs. The sample becomes increasingly biased towards the zone of the screen intersecting the region of highest head (Figure 3.8 a). For a fixed pumping rate, sample origin depends on the rate of ambient upflow in the well. However, sample bias does not occur only when ambient vertical flows in the well are much greater than the pumping rate. For example, considering Scenario 1 (Figure 3.8 a), the sample

origin begins to become biased towards the zone of highest head intersecting the screen for ambient vertical flows in the well of only 0.01 l/min. Once the maximum ambient flow in the well reaches 0.07 l/min the inflow to the well is zero at the top of the screen during pumping. As the maximum ambient upflow increases to 0.15 l/min (50 % of the pumping rate) the sample origin is dominated by the ambient vertical hydraulic gradient and the sample is drawn from the bottom half of the screen interval only.

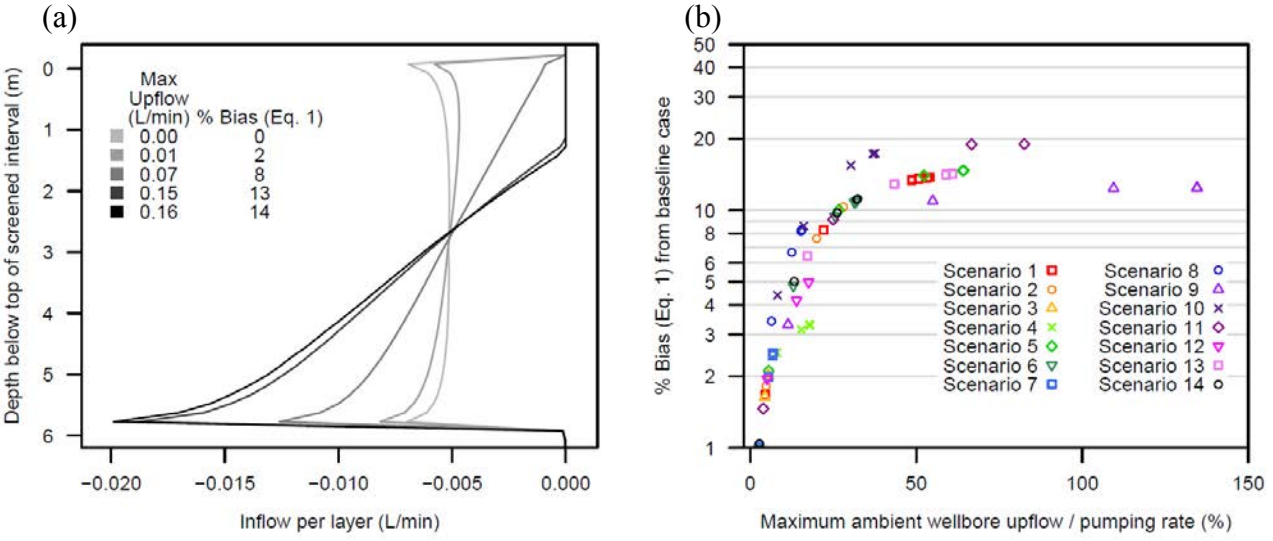

Figure 3.8: Departure from no vertical flow baseline as a function of ambient upflow in the well : (a) Deviation from baseline (Eq. 1) and variation in pumped influxes for scenario 1 (Q = 0.3 l/min), (b) deviation from baseline conditions for all scenarios.

Comparing the percentage bias to the pumped sample due to ambient vertical flows (Eq. 1) against the maximum ambient upflow in the well, a similar pattern is observed for all scenarios (Figure 3.8 b). As the maximum ambient upflow in the well increases from 0 % to 50 % of the pumping rate the percentage bias increases. A transition between baseline sampling conditions and vertical head gradient biased conditions occurs. Within this transition zone sample origin is very sensitive to ambient upflow rates. If ambient vertical flows in the well vary (e.g. seasonally), sample origin during pumped sampling will differ even if fixed sampling procedures are used. A similar conclusion is drawn by Riley et al. (2011) for tracer testing in the presence of vertical flows.

As the maximum ambient upflow in the well increase beyond 50 % of the pumping rate, the percentage bias to sampling levels off. In this zone, well inflows are determined by the ambient vertical head gradients with pumping having little ability to counteract vertical flows in the well. Changes in ambient vertical flow rates become less important to the sample origin, pump position becomes important even at long times and pumped sampling becomes increasingly analogous to a passive sample.

3.3.2.4 Overcoming ambient vertical flows bias via increased pumping

If a well sampling is undertaken at higher pumping rates, vertical gradients can be overcome and the sample can be drawn from the entire screen interval. For scenario 1, with maximum ambient upflow in the well of 0.16 l/min, pumping at 0.3 l/min results in vertical flow bias of 14 % (Figure 3.9). Increasing the pumping rate to 2 l/min reduces the ambient vertical flow induced bias to < 10 %. However, achieving a 10 % bias does not provide a sample drawn from the entire screen interval (Figure 3.8 a). The pumping rate has to be increased to tens l/min to approach 0 % bias and achieve a permeability-weighted sample unbiased by ambient vertical head gradients. The pumping rate required to fully overcome vertical head gradients is many tens of times the vertical head gradient driven ambient upflow in the well.

Using the simulated maximum ambient upflow in the well to compare all scenarios, a linear relationship exists between the maximum ambient upflow simulated in the well and the pumping rate required to overcome the vertical gradient induced bias. For example, to reduce the ambient vertical flow induced sampling bias to 3 % (Eq. 3.1) it is necessary to pump at 11.5 times the maximum ambient upflow rate in the well (Figure 3.10 a). Similar linear relationships exist for other percentage biases Figure 3.10 b). As observed for Scenario 1 (Figure 3.9), it is necessary to use a pumping rate of tens of times the ambient vertical flow rate in the well to fully overcome ambient vertical head gradients and achieve a bias approaching zero. Hence, for the modelling

scenarios considered, knowledge of the maximum ambient upflow in the well is enough to estimate the pumping rate required to overcome the in-well vertical flows. Detailed knowledge of the flow distribution was not required.

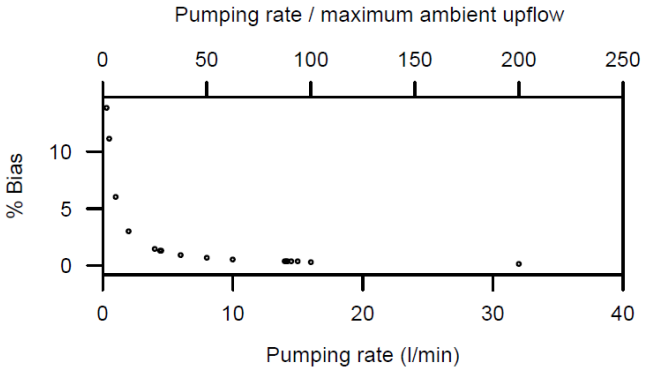

Figure 3.9: Variation in sample bias (Eq. 1) with increasing pumping rate under ambient vertical head gradients (Scenario 1, maximum ambient vertical flow in the well =0.16 l/min).

The implication for groundwater sampling in wells with maximum ambient upflow in the range observed in literature (Figure 1.1, 0.015 – 2.3 l/min) is that low-flow sampling will be biased towards the zones of highest head intersecting the screen. Increasing the pumping rates to several litres per minute may not fully overcome the ambient vertical head gradients observed. To obtain a permeability-weighted sample from across the screen interval during pumped sampling in these wells the pumping rate may need to be tens of litres per minute or higher.

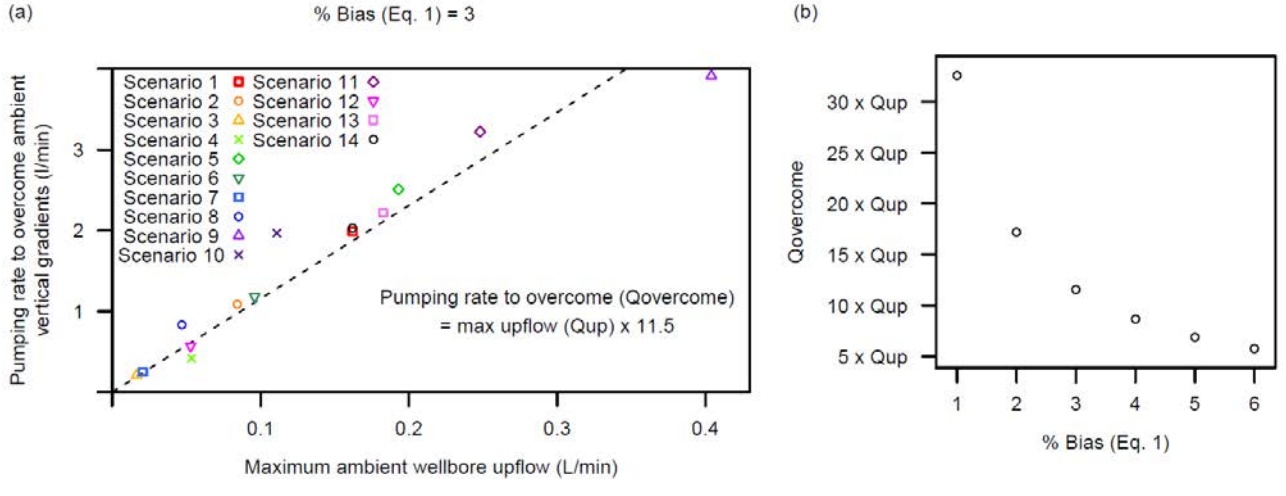

Figure 3.10: Pumping rate required to overcome ambient vertical head gradients as a function of ambient well upflow (a) Maximum ambient well upflow versus pumping rate required to reduce sample bias (Eq. 3.1) to 3 % (all scenarios), (b) pumping rate to overcome vertical head gradients versus % bias (all scenarios).

3.4 Conclusions

Numerical modelling to evaluate the effect of ambient vertical flows on groundwater sampling using pumps has demonstrated that naturally occurring vertical flows of the magnitude reported in literature (Figure 1.1) may be a key control on groundwater quality sample origin even in wells with screens < 10 m in length. If permeability-weighted sampling from across the screen interval is the goal it may be necessary to pump at rates many times the ambient vertical flow rate in the well. Purging at low pumping rates such as those recommended for low-flow sampling would not be sufficient. Ambient vertical flows in the wellbore are increased by:

(1) greater aquifer hydraulic conductivity and greater aquifer depth;

(2) greater proximity to discharge (or recharge) zones;

(3) greater well volume (well diameter and length), screen hydraulic conductivity;

(4) greater vertical/horizontal hydraulic conductivity anisotropy (including the presence of discrete layers of low permeability).

For situations where the maximum ambient upflow in the well is < 5 % of the pumping rate the numerical modelling undertaken here has demonstrated that:

(1) it is possible to overcome ambient vertical gradients, even with low-flow pumping, and achieve a sample drawn from the entire screen interval;

(2) pumping rate and time (which can be significant in sampling terms) are important controls on sample origin (this is the case even without vertical flows);

(3) during early pumping the sample origin will depend on pump intake position but at long times may be pump independent.

As ambient upflow in the well increase towards 50 % of the pumping rate, a transition occurs. The sample becomes increasingly biased towards the zone of highest head intersecting the screen. In these cases:

(1) water may not be drawn from the entire saturated screen interval even with extended pumping times;

(2) if ambient vertical flow rates vary (e.g. seasonally), the sample origin may vary even if pump intake position, pumping rate and pumping time are fixed;

(3) pump intake position is important in determining the sample origin, this may be the case even after an extended pumping period;

(4) targeting the zone of the well with maximum vertical flow maximizes the vertical extent of aquifer sampled (the most integrated sample is obtained).

For wells with ambient upflow rates much greater than the pumping rate the sample is entirely biased towards the zone of highest head (a flow-stream sample). The pumped sample becomes analogous to a passive sample. In these cases:

(1) pumping rate and time are not important

(2) pump intake position is the key control on the sample origin

(3) sampling from the base of a borehole provides a more discrete sample from that inflow zone, and through appropriate choice of sampling location might enable level-determined sampling

(4) however, quantitative predictions of water quality variation with depth may depend on assessing the degree of dispersion and mixing as water of different origins enters and exits the well screen

Vertical flows can introduce considerable uncertainty when attempting to relate sample concentration to in-aquifer conditions, even in wells with screens < 10m in length. Knowledge of the ambient vertical flow rate in the well can be used, in conjunction with sampling objectives, to guide decisions on pumping rate, pumping duration and pump intake location. From a practitioner community viewpoint, sampling objectives will determine if a detailed knowledge of

sample origin is required. If this detailed knowledge is required then supporting vertical flow investigations such as the single borehole tracer tests carried out in Chapter 2 are recommended.

CHAPTER 4 ACTIVELY HEATED FIBRE OPTIC DISTRIBUTED TEMPERATURE SENSING FOR RESOLVING IN-BOREHOLE FLOWS AND AQUIFER HYDRAULIC CHARACTERISTICS

4.1 Introduction

Chapters 2 and 3 have shown that vertical hydraulic gradients (and temporal variation in such gradients) may be a significant factor affecting groundwater quality sample provenance in long-screen wells. Measuring the effect of such gradients in boreholes under non-pumping and pumping conditions may be critical to underpinning groundwater quality sample interpretation. Flow logging using impellers is more likely to be successful under pumping conditions or in fracture-flow dominant aquifers where there are focused flows entering and leaving a borehole and high vertical flows induced within the borehole. More sensitive techniques (e.g. tracer tests, heat-pulse flow logging) may, however, be necessary to detect the more dispersed inflows and gentler vertical borehole flows where the aquifer permeability is porous medium (matrix) dominated. In such aquifers the geological units may gradationally change, the aquifers may have less obvious transmissivity contrasts and have weaker, but potentially still important, vertical hydraulic gradients.

Single borehole tracer tests have been shown (Chapter 2) to provide a quick and inexpensive means of assessing flows in boreholes. However, such tests are relatively time consuming if full borehole assessment under pumping and non-pumping conditions is required. It may be that Fibre Optic Distributed Temperature Sensing (DTS) offers a convenient alternative by which to assess borehole flows under a wide range of pumping and non-pumping conditions.

Use of DTS in earth sciences and hydrology has provided significant improvements in the temporal and spatial resolution of temperature measurements (Selker et al., 2006a; Selker et al., 2006b; Selker, 2008; Tyler et al., 2008). DTS has been used to monitor natural temperature

contrasts, for example to detect the mixing of groundwater and surface water (Krause et al., 2012; Krause and Blume, 2013; Rose et al., 2013). Where natural temperature contrasts do not exist, DTS can also be used in a so called "active" configuration (A-DTS) where thermal resistance heating of the armoured cable sheath or of an integrated heating cable is used to induce artificial heating along the cable length. The relative rates of cooling along the cable can provide information on the nature of the surrounding environment, for example soil moisture content (Sayde et al., 2010; e.g. Gil-Rodríguez et al., 2013).

DTS has received some limited use as a methodology to detect borehole flows. For example, DTS has been used during SBTT for monitoring the cooling from an injection of hot water (Leaf et al., 2012; Read et al., 2013) or after the borehole water temperature has been raised by heated cables installed alongside the DTS cable (Liu et al., 2013; Banks et al., 2014). A-DTS has been used to detect the location of flowing fractures intersecting a borehole and the flow contribution from these fractures during high rate pumping (Read et al., 2014).

Here, A-DTS is applied in a borehole located at the University of Birmingham. The site, discussed in detail in Chapter 2, is a well-characterized multi-layer sandstone aquifer where inflowing and outflowing zones are expected to generally be non-discrete, in contrast to the example of Read et al. (2014) cited above, and hence more difficult to detect. As demonstrated in Chapter 3, the location and rate of inflows and outflows from such zones are expected to vary between ambient and pumping conditions and with pumping rate. Knowledge of the inflows and outflows under these different conditions are hence used to help resolve the flow regime in the test borehole and the hydraulic characteristics of the adjacent aquifer. In doing this greater use is made of the post-heating data. These data become available if DTS monitoring is continued after a conventional A-DTS measurement period; the advantage is that such measurements extend the range of flow velocities that can be interpreted.

The aim is to develop new borehole flow-logging techniques that allow efficient borehole characterisation to inform groundwater quality sampling. Such an aim is demonstrated through field testing and the development of supporting modelling interpretation methods. Innovative use of the A-DTS system may indeed provide the versatility needed for application in a wide range of hydrogeological conditions and offer complementarity and advantage over conventional techniques.

4.2 Materials and Methods

4.2.1 Experiment Overview

The field site at the University of Birmingham is discussed in detail in Chapter 2. A-DTS measurements were undertaken in BH2 (Figure 2.4). The experimental setup is summarised in Figure 4.1. A-DTS was used to investigate borehole flows under ambient (non-pumping) and pumping conditions. The experimental design can be summarized as (1) passive DTS monitoring of the ambient borehole temperature, (2) an 80 minute A-DTS heating phase during non-pumping conditions, (3) cooling phase, monitoring the return to background temperature conditions (120 minutes), and (4) pumping flow investigations at rates between 9 and 156 l min^{-1}. During pumping investigations, the pump intake was located just above the bottom of the casing in BH2 (~ 15 m bgl). For each pumping rate, A-DTS temperature measurements were taken until temperatures along the cable had stabilized (at least 10 minutes).

Heating and cooling data taken under ambient flow conditions were used to calibrate a numerical model of the A-DTS cable in the borehole. Temperature data taken during pumping conditions provided model validation data. Single-borehole tracer test and impeller flow meter data (Riley et al., 2011) provide comparative data to validate the A-DTS model results.

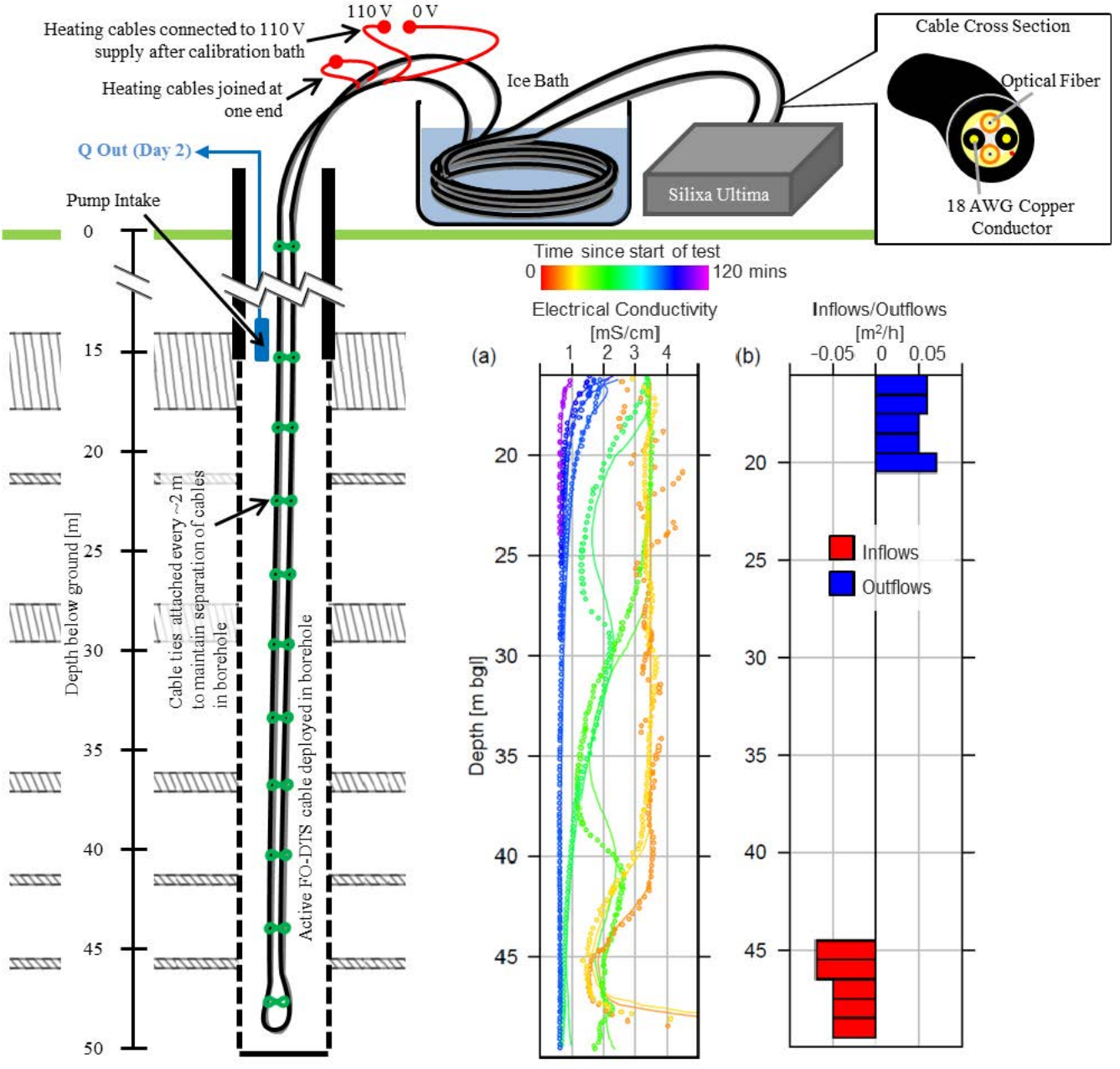

Figure 4.1. Experiment design with details of DTS cable deployment in BH2 (not to scale) (cable cross-section amended from image from http://www.nexans.us/). Sub-figures show results of previous single borehole tracer tests: (a) Simulated vs. measured electrical conductivity profiles (data points are measured data; solid lines are simulated). (b) Model predicted ambient inflows/outflow locations and rate. Grey hatched lines indicate the location of low permeability layers identified previously in the borehole from geological logging and cross-hole testing (Ferguson, 2006; Riley et al., 2011).

4.2.2 Distributed Temperature Sensing

DTS analyses the properties of a laser pulse applied to a fibre optic (FO) cable that is placed within the observed medium (i.e. groundwater in a borehole). It measures the temperature dependent backscatter of the pulsed laser signal propagating through the fibre optic cable (Selker

et al., 2006a; Selker et al., 2006b; Tyler et al., 2009). In this study, the instrument (*Silixa Ultima-S*) measures the intensity of the backscatter of Raman Stokes (temperature independent) and anti-Stokes (temperature dependent) signals from a 1×10^{-8} s light pulse emitted into the FO cable. The DTS system used here is capable of measuring temperature at high precision (0.05 °C) and with a sampling resolution of 0.125 m. For the DTS surveys in this study, single-ended measurements were conducted (Hausner et al., 2011) with the laser application and sampling occurring in one direction along the fibre optic cable. Measurements were averaged for 30-second intervals.

The FO cable (Berk-Tek CL3R-OF OM2+ Composite 2 Fibre Cable) applied in this study had a length of 337 metres and contained two buffered optical fibres and two 18 American Wire Gauge 1.024 mm diameter stranded copper conductors (Figure 4.1). These copper conductors were joined at one end of the cable to a 16 A waterproof connector and at the other end to an IP44 16 A 110 V plug via an in-line residual current device. The total measured resistance along the joined loop of copper conductors was 12.4 Ω. Connected to a 110 V supply, the power input along the cable is calculated as 2.9 W m^{-1}.

A 100 m loop of the FO cable was suspended in borehole BH2 (Figure 4.1). The cable was weighted at the bottom and with cable ties approximately every 2 m securing the cables while ensuring they were separated both from each other and the borehole wall. During cable heating, special care must be taken to ensure that the undeployed section of the cable (outside the borehole) does not overheat, potentially causing damage to the plastic cable sheath. Accordingly, to minimise potential induction, the remainder of the FO cable was reeled out on the ground in large loops of >20m diameter.

To correct for temperature offset and differential loss along the cable (Tyler et al., 2009; Hausner et al., 2011; van de Giesen et al., 2012), sections > 10 times the spatial sampling interval at both cable ends were calibrated in a temperature controlled ice bath. These sections were

isolated from the active heating to provide an independent temperature measurement, unaffected by the cable heating. Temperatures in the ice bath (~0°C) were monitored continuously by independent reference thermistors throughout the experiment. DTS monitored temperatures observed at the start and end cable sections exposed to the control ice bath were matched during the calibration procedure in order to account for potential differential attenuation of signal and set to equal independent thermistor measurements to account for signal offset.

4.2.3 Additional Instrumentation

In addition to DTS measurements, groundwater temperature in the borehole was monitored independently using thermistors deployed at 15, 20, 25 and 45 m bgl. The thermistors were connected to data loggers (HOBO U12-006) logging at 10 second intervals. Calibration (precision ± 0.1 °C) of the thermistors was based on the use of water of baths of known temperature. At each deployment depth, cable ties were used to position the thermistors at approximately 0.01 m distant from the DTS cable.

4.2.4 Single Borehole Tracer Test (SBTT)

The SBTT carried out in BH2 during 2011 provided flow characterisation data for comparison with A-DTS observations (Chapter 2). The 1-D numerical modelling suggested groundwater entered BH2 in the bottom 5 m of the open section at a rate of 4.83 l min^{-1} (Figure 4.1 b). The simulations confirmed previous observations of upward flow in the borehole; groundwater was estimated to flow up the length of the borehole (maximum upward velocity of 4.56×10^{-3} m s^{-1}) and discharge into the upper most permeable unit in the borehole (Figure 4.1 b). This unit is located just below the bottom of the casing.

4.3 Numerical Simulations

4.3.1 Model Description

Numerical modelling of a simplified cable design was carried out using COMSOL Multiphysics (v.4.4) to calculate the flow rates that reproduce the observed DTS cable temperature responses. A simplified cable design was simulated in a radially symmetric model domain (Figure 4.2). The model domain was discretized using a free-triangular mesh refined in the cable region to ensure numerical stability.

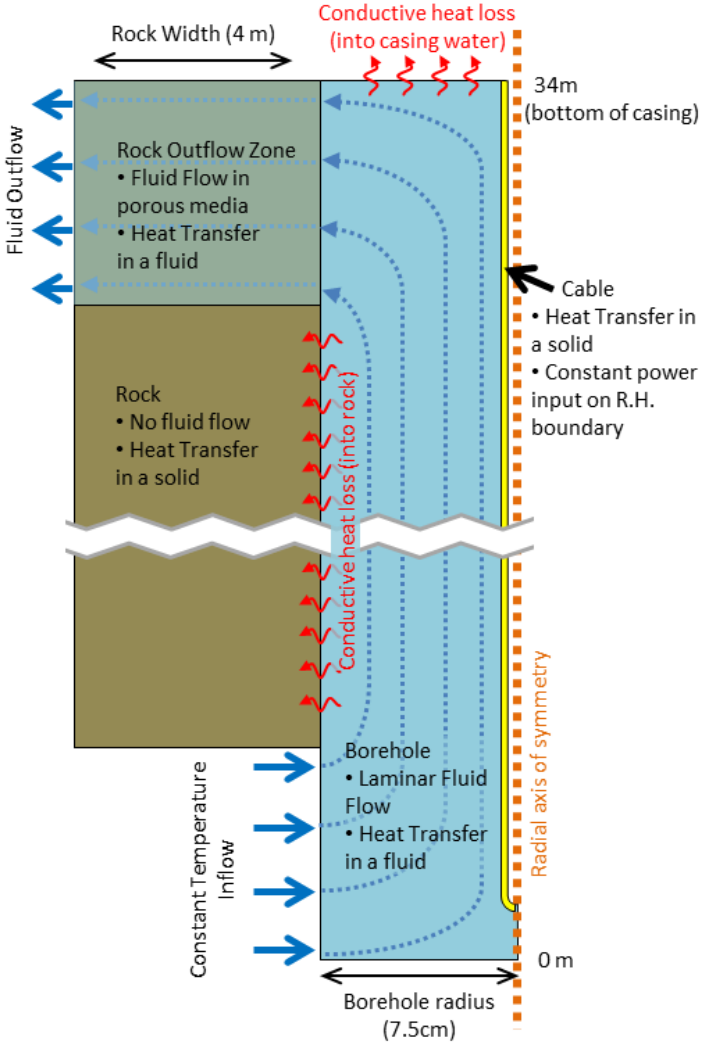

Figure 4.2: Model schematic comprising a radially symmetric model domain (not to scale).

The maximum observed rise in borehole water temperature over the heating period was less than 0.5 °C. Over that range, the effect on fluid flow due to variable density and viscosity will be

very small. Therefore, steady-state flow in the open borehole and transient heat transfer between the A-DTS cable and the surrounding borehole fluid were simulated independently.

4.3.2 Fluid Flow

COMSOL's laminar flow interface was used to simulate incompressible, Newtonian fluid flow in the open section of the borehole. The transition from laminar to sustained turbulent flow in pipes is characterized by Reynolds' Number values between 1700 and 2300 (e.g. Avila et al., 2011). Taking the Reynolds' Number characteristic distance as the diameter of the borehole, simulated ambient flow rates were checked to ensure that the assumption of laminar flow was not invalidated. It was found that vertical fluxes in BH2 would need to exceed 1.39×10^{-2} m s^{-1} for this to be the case.

Borehole flow was described by a reduced version of the Navier-Stokes equation (Douglas et al., 2011):

$$\rho_w \frac{d\mathbf{u}}{dt} + \rho_w(\mathbf{u} \cdot \nabla)\mathbf{u} = -\nabla \cdot p + \mu_w \nabla^2 \mathbf{u} + \mathbf{F} \qquad \text{Eq. [4.1]}$$

where ρ and μ are density and dynamic viscosity and the subscript w indicates the borehole fluid. $\mathbf{u}$ is the velocity vector, p is pressure, and $\mathbf{F}$ represents other body forces. During initial sensitivity testing, the simulated cable temperature was found to be relatively insensitive to the fluid velocity at the borehole wall. Hence, fluid was assumed stationary at the boundary between the rock and the borehole (a no slip boundary was specified). However, cable temperature was sensitive to the fluid velocity at the fluid/cable boundary. The properties of this boundary were a calibration parameter.

To minimize boundary effects, the region of simulation was extended to include fluid flow (and heat transport) into the rock immediately adjacent to the borehole. In the fluid outflow region of the borehole, borehole fluid flow was coupled with constant-density, steady-state fluid

flow in porous media. The location and magnitude of inflows to the rock (outflows from the borehole) were a calibration parameter and were piecewise specified along the boundary between the rock and fluid domains. Constant heads were fixed at the outflow boundary of the rock. In the rock, hydraulic conductivity was isotropic and homogeneous. Fluid velocities were calculated from the simulated head distribution assuming a porosity of 0.25.

4.3.3 Heat Transport

COMSOL's Heat Transfer module was used to simulated time-dependent heat transfer from the boundary with the heating cable through the cable sheath, transfer in the flowing borehole fluid and conduction into the surrounding rock. A constant power boundary (2.9 W m^{-1}) was used to simulate heat inflows from the heating cable.

Advection/conduction of heat in the fluid flowing through the borehole and rock was described by (Bejan, 2013):

$$\rho C_p \frac{dT}{dt} = \nabla \cdot \left(\rho C_p \boldsymbol{u} T + k \nabla T\right) + R \qquad \text{Eq. [4.2]}$$

where $\boldsymbol{u}$ is the fluid velocity vector (Section 3.2), and C_p and k are the heat capacity and thermal conductivity in the relevant region respectively. T is temperature and R represents sources/sinks of thermal energy.

Heat transport through the sheath and the main body of the rock between the inflow and outflow sections of the borehole is purely conductive and was described by (Bejan, 2013):

$$\rho C_p \frac{dT}{dt} = \nabla \cdot (k \nabla T) + R \qquad \text{Eq. [4.3]}$$

Heat was allowed to leave the system by advection at model outflow points, via conduction into the rock adjacent to the borehole and into the constant temperature boundary at the boundary with the bottom of the casing.

Inflowing groundwater and initial model temperature was 11^{o}C. An exact match to the A-DTS measured temperatures was not attempted as the model was calibrated by comparing the relative change in cable temperature rather than the absolute values.

4.3.4 Model parameters and calibration

A-DTS temperature profiles taken at the end of active heating and during cooling and return to background conditions were used for calibration of the numerical model. The model was calibrated manually by adjusting model parameters to minimize the root-mean-square error (RMSE) between measured and simulated change in FO cable temperature. Model calibration parameters were (1) the thermal conductivity of the plastic sheath and the borehole fluid, (2) the heat capacity of the plastic sheath, (3) the location and magnitude of ambient fluid inflows and outflows, and (4) the fluid velocity (stationary or moving) at the fluid/cable boundary. The heat capacity of the borehole water, the cable power and the thermal properties of the surrounding rock were fixed. As DTS measurements are susceptible to spatial-temporal noise (e.g. Voigt et al., 2011), model calibration was undertaken using profiles smoothed in space using a centrally aligned rolling mean with a window size of six.

4.4 Results and Discussion

4.4.1 Fibre Optic Distributed Temperature Sensing under ambient (non-pumping) conditions

Three phases can be distinguished in the evolution of the observed temperature-depth profiles (Figure 4.3): (1) A sudden increase in temperature in the cable after starting active heating; (2) a

"steady-state" active-heating phase where cable temperatures remained generally stable; and (3) a cooling period where cable temperature falls quickly immediately after heating was stopped, before a slow tailing as cable temperature returned to background

DTS cable temperatures at the end of the experiment were on average approximately 0.09°C lower than those of the ambient temperature profile (Figure 4.3 a, Background versus Phase 3h profiles). There are no data to suggest this change is due to in-borehole processes; it is not supported by the thermistor data (Figure 4.4) and was possibly the result of calibration issues. To calculate the change from background conditions during the heating phase (Figure 4.3 b) the profiles were corrected by linear interpolation between 0 °C at the start and 0.09 °C at the end (Figure 4.3 a, Background corrected) in order to align with final temperature profiles along the cable.

Heating of the cable resulted in a temperature increase of ~ 2.5 °C in the FO cable that appears to stabilize after 10 minutes of heating (Figure 4.3 a, Phase 2a). However, closer examination (Figure 4.3 c) reveals that temperatures did not completely stabilize but continued to rise at a much slower rate. However, this temperature increase during the remainder of the heating phase was not uniform along the FO cable. Rather, the temperature gradient along the FO cable increased with a measured FO cable temperature increase of 0.2 °C near the top of the open section of the borehole compared with < 0.05°C at the bottom of the borehole (Figure 4.3 c). Based on previously observed upward head gradients in the borehole (Riley et al., 2011), this observation can be interpreted as the movement of water that had entered the borehole column at the bottom of the borehole, moved upwards and then exited at the top. As the water moved upwards in the borehole, it gained heat through contact with the heated cable. Water (and hence FO cable) temperature is therefore expected to be warmer near the outflow point where the water would have been in contact with the heated cable for the longest time. If a cable heating period

exceeds the residence time of water in the borehole, true steady-state conditions may be reached. The small but continuous increase in cable temperature observed throughout Phase 2 suggests this stage was not reached during the experiment and implies that water residence time in the borehole was greater than the cable heating time (80 minutes).

Within 15 minutes of the end of cable heating, temperatures recorded at the FO cable within the open section of the borehole declined to between 0.1 and 0.3°C above background temperature (Figure 4.3 d, Phase 3b). This can be interpreted as the FO cable temperature equilibrating with that of the surrounding water once cable heating stopped. The return to background temperatures took significantly longer than the initial decline in temperatures (~2 hours) with the cable cooling more quickly at depth in the borehole (Figure 4.3 d). This evolution in cable temperature can again be explained by upward borehole flow; a front of cooler background temperature water entered at the bottom of the borehole and moved upwards, progressively displacing the higher temperature heated water in the borehole as it went.

The thermistors were lower accuracy and sensitive to electrical interference (observed particularly as increased noise during heating; Figure 4.4). However, the thermistor measurements (taken approximately 1 cm from the cable) corroborated the qualitative interpretation of the DTS profiles. A rise in water temperature of a few tenths of a degree was observed during the heating phase before a gradual return to background temperature (Figure 4.4). The change in thermistor temperature during heating declined with greater depth in the borehole. After the end of the active heating the return to background was quickest at depth. DTS measurements from the same depths as the thermistors showed a similar pattern (Figure 4.4). Post-heating, measured cable temperatures quickly returned to values comparable to thermistor measured water temperatures. Time to return to background conditions was again quickest at depth.

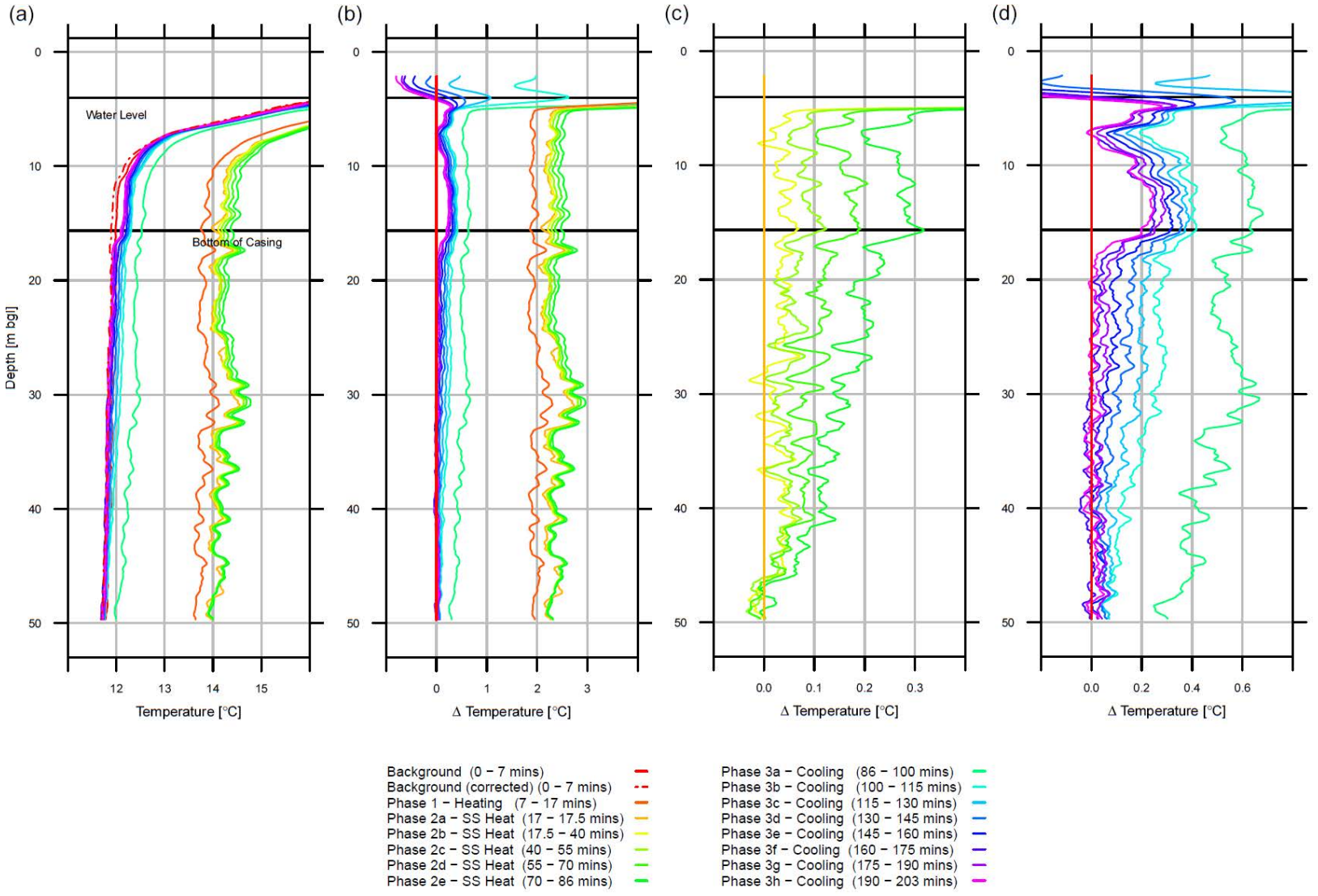

Figure 4.3: DTS cable profiles (a) Time series of measured DTS cable profiles in BH2, (b) Time series of change in DTS profile temperature (from corrected background), temperature, (c) change in DTS cable temperature during steady-state heating (difference in temperature is from Phase 2a profile), (d) change in DTS cable temperature (corrected) from background with time during cooling (Phase 3).

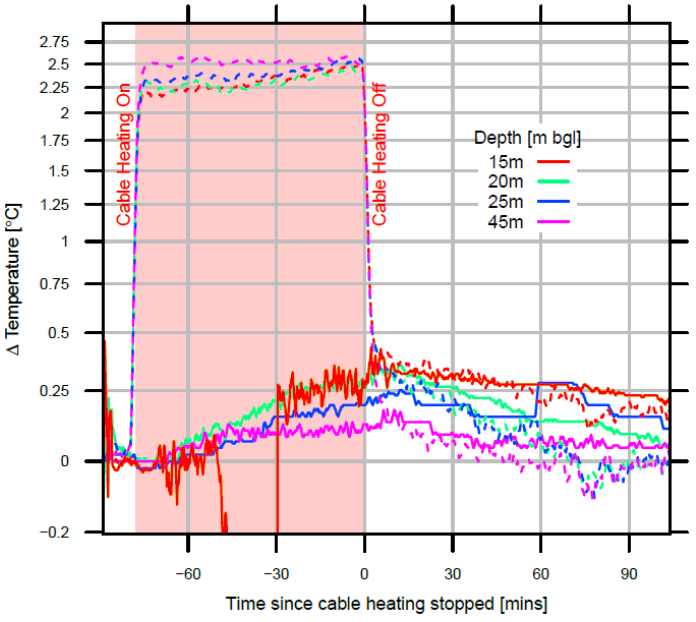

Figure 4.4: Change in thermistor temperature and DTS cable temperature (corrected) from background with time . Thermistors suspended at 15, 20, 25 and 45 m bgl; corresponding FO cable temperatures are those observed at the same depth in the borehole. Dashed lines are FO cable temperature measurements, solid lines are thermistor temperature measurements.

4.4.2 Iterative Forward Modelling

Numerical simulation (Figure 4.5, Figure 4.6, parameters summarized in Table 4.1) confirmed the qualitative interpretation of field data (Section 4.1). Simulated flows (Figure 4.5 c) enter the borehole over the bottom 5 m, flow up the borehole and exit below the casing. The average root-mean-square error (RMSE) for all measured versus simulated profile residuals (Figure 4.5 b) was 0.048 °C. Overall model bias (the mean of residuals) was (-0.016 °C).

The simulated cable temperature during, and post-, heating was strongly influenced by the thermal conductivity of the surrounding water. The calibrated water thermal conductivity value was 0.912 W m^{-1} K^{-1}, 1.6 times that expected from consideration of the material properties of water alone. To obtain a good match to observed data, it was also necessary to assume moving fluid (a slip boundary condition) at the cable/fluid boundary. The maximum simulated ambient flow velocity in the borehole (3.06×10^{-3} m s^{-1}, Figure 4.5 c) does not invalidate the assumption of laminar flow. Therefore, to explain the greater than expected cooling rate (high k_w, presence

of slip), another process must be invoked: one candidate is the presence of increased mixing brought about by the presence of the cable ties and the changing position with depth of the cable relative to the centre of the borehole.

Parameter	Symbol	Value	Units	Notes
Specific heat capacity of cable	C_{ps}	900	J kg^{-1} K^{-1}	Calibrated
Specific heat capacity of water	C_{pw}	4196	J kg^{-1} K^{-1}	Fixed
Specific heat capacity of rock	C_{pr}	1243	J kg^{-1} K^{-1}	Fixed
Thermal conductivity of cable	k_s	0.2	W m^{-1} K^{-1}	Calibrated
Thermal conductivity of water	k_w	0.912	W m^{-1} K^{-1}	Calibrated
Thermal conductivity of rock	k_r	2.5	W m^{-1} K^{-1}	Fixed
Cable power	-	2.9	W m^{-1}	Fixed
Total ambient borehole flow	-	3.25	l min^{-1}	Calibrated
Fluid/cable boundary condition	-	Slip	-	Calibrated

Table 4.1: Final model parameters (subscripts s, w, r indicate the cable sheath, borehole fluid and surrounding rock respectively)

Relative to the thermal conductivity of the water, the thermal conductivity of the plastic sheath had a small impact on the cable temperature during heating. For example, increasing the cable thermal conductivity by 10 % (0.2 – 0.22 W m^{-1} K^{-1}) resulted in a 6 % (0.15 °C) decrease in the simulated cable temperature at the end of heating. Post-heating simulated cable temperature was insensitive to the cable thermal conductivity. The final calibrated value for this parameter was 0.2 W m^{-1} K^{-1}. Simulated cable temperatures were insensitive to the plastic sheath heat capacity. This was left as the starting value (900 J kg^{-1} K^{-1}, a typical value for PVC).

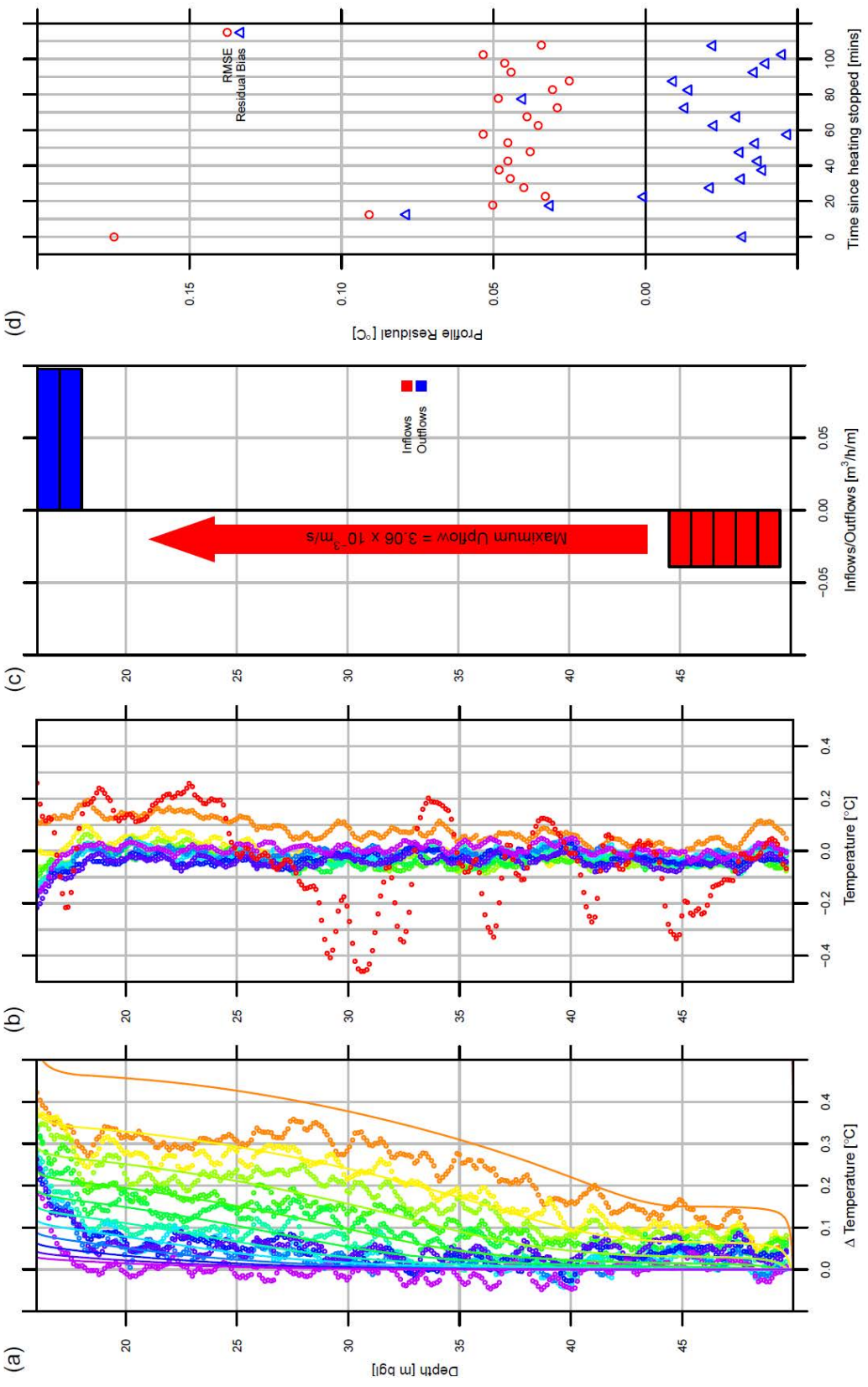

Figure 4.5: Numerical modelling results for non-pumping conditions (a) Simulated versus measured data; solid lines are simulated), (b) Simulation residuals as a function of depth and time, (c) model pr residual biases per profile.

The location and magnitude of model inflows were relatively well constrained by the quick cooling in the bottom 5 m of the borehole and by variation in cooling rates with depth in the borehole. Model outflows were less well constrained. Outflows can only be unambiguously determined by observing the arrival of the inflowing background temperature water at the outflow point. However, conductive cooling of the pulse of heated water meant there was little temperature contrast by the time its tail end had arrived at the outflow zone. Similar model fits were obtained if outflows were distributed in the top 2 m or the top 5 m below the borehole casing. The relatively quick dispersal of heat through conductive cooling provides a lower limit on the flows heat tracing can detect when compared with dissolved tracers.

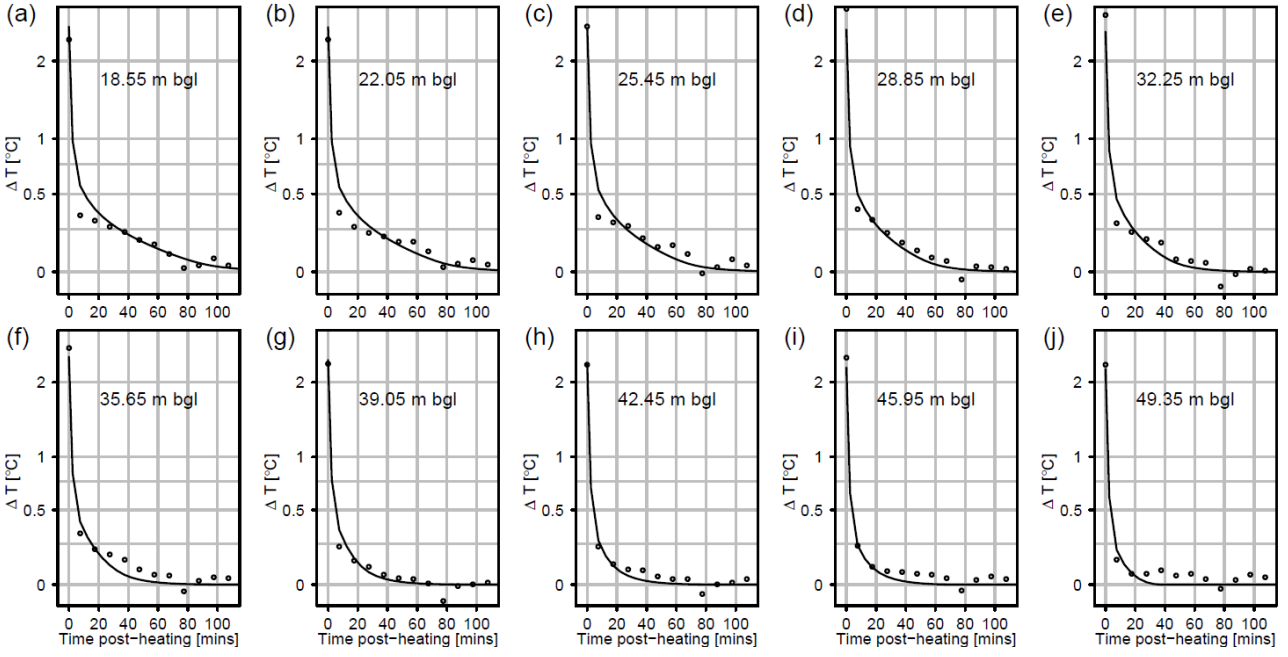

Figure 4.6: Numerical modelling results for non-pumping conditions. Simulated versus measured DTS temperature (data points are measured data; solid lines are simulated) with time from the end of heating for ten different depths in the borehole (depth (m bgl) is indicated by the individual labels for each figure).

Individual profile root-mean-square errors and residual biases are shown in Figure 4.5 d. The largest residual errors occurred (1) for the first two profiles post-heating, where in the upper portion of the outflow zone (16 – 25 m bgl) the model predicted higher temperatures compared with observed results (Figure 4.6 a-c); the later cooling data suggest this was not the result of additional inflows at this point (a quicker return to background conditions would be anticipated if

this were the case); (2) for the first profile (the cable temperature at the end of the heating phase) (Figure 4.5 b). Even with moving average smoothing applied, large-scale peaks and troughs were observed along this profile. The origin of these deviations could not be conclusively verified during the experiment. Such deviations may be due to variation in the cable position in the borehole. Alternatively, given the amplitude of these oscillations was less in the parts of the cable in the non-flowing casing water (Figure 4.5 a, b), they may be the result of increased cooling due to turbulence around the cable ties (as observed by Read et al. (2014)).

Observation of the change in gradient of A-DTS heating profiles with time is enough to infer an upward head gradient (Figure 4.5 c). Such inference is consistent with previously observed upward head gradients (Riley et al., 2011). Extension of the A-DTS method to include analysis and modelling of post-heating data validated the prediction of an upward head gradient. Such modelling also allowed the location and magnitude of the inflowing and outflowing zones to be quantified. These locations corresponded well with those predicted from the SBTT in 2011 (Figure 4.1). However, the DTS measurements suggest ambient groundwater fluxes have decreased in BH2 between 2011 and 2013.

4.4.3 Fibre Optic Distributed Temperature Sensing under pumping conditions

As observed during the ambient flow test (Figure 4.3 b) an increase in the spatial variance in cable temperature was seen during heating under pumping conditions (Figure 4.7 a). The location and magnitude of peaks and troughs remain after temporal averaging. They are in the same spatial location as those observed during the ambient flow test (Figure 4.7 a). Their location is independent of pumping rate. This corroborates the previous assumption that, rather than being related to the flow system, they were artefacts of the cable deployment. It may be that, as observed by Read et al. (2014), these peaks and troughs were due to cooling induced by turbulence around the cable ties.

In addition to the observed peaks and troughs, a persistent high-temperature region is observed in each profile between 28 and 33 m bgl (Figure 4.7 a). If FO cable temperature is inversely correlated with borehole flow velocity then such a high temperature region would imply a decrease in borehole flows at this location. Such a decrease in flow velocities (suggesting outflows from the borehole) would be highly unlikely under the high pumping rates considered. The magnitude of this high-temperature zone relative to temperatures in the same profile observed immediately below decreases for high pumping rates (80–150 l min^{-1}, *c.* 0.15°C change) and increases for low pumping rates (9-25 l $min^{-1,}$ *c.* 0.3 °C change). For Day 1 (3.25 l min^{-1} upflow) *c.* 0.2°C change is observed.

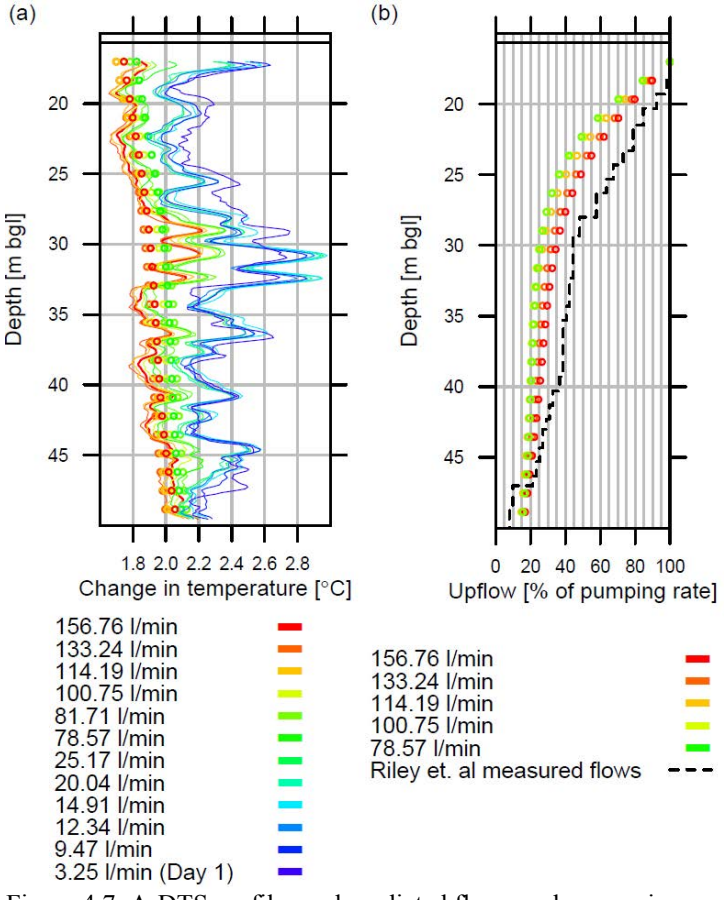

Figure 4.7: A-DTS profiles and predicted flows under pumping conditions. (a) A-DTS profiles of change in cable temperature from background under varying pumping rates and under ambient flow conditions (Day 1) (dots are "smoothed" profiles). (b) Previously measured (using impeller flow meter (Riley et al., 2011)) vs. DTS predicted borehole vertical flows under high rate pumping conditions (calculated using smoothed profiles in Figure 4.7 a and calibration curve from Figure 4.9 a).

Exploratory simulations using the calibrated COMSOL model (Figure 4.9 b) suggested that cable temperature variation of up to 0.3 °C can result if the cable is located at the edge of the borehole compared with the centre of the borehole. The simulated change in cable temperature was only significant when the cable was very close to or touching the borehole wall. The variation in cable temperature as a function of position in the borehole depended on the rate of flow past the cable (Figure 4.9 b). For a cable resting against the borehole wall, a change in temperature of nearly 0.3°C was observed at flow rates between 10 and 50 l min^{-1}. The change in temperature was reduced to 0.15 °C as upward flow increased to 80 l min^{-1}. The change in temperature was also less for low upflows; for 5 l min^{-1} the change in temperature was reduced to approximately 0.25°C. These temperature changes were very similar to those observed under comparable pumping rates in the region between 28 and 33 m bgl. It may be that despite efforts to prevent it using cable ties, the observed temperature high was due to the cable lying near to or against the borehole wall in this region. The change in cable centralization may be the result of changes in the borehole deviation in this region; the borehole deviation becomes less vertical at this point (Figure 4.8).

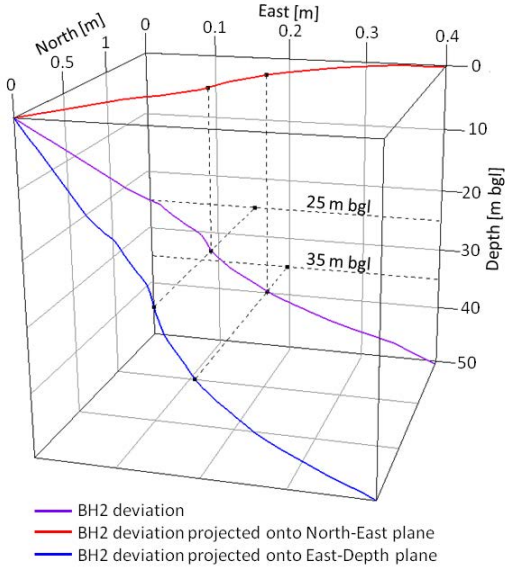

Figure 4.8: BH2 deviation

Despite the various temperature artefacts, average cable temperatures directly below the pump intake (16-20 m bgl) showed a strong correlation with pumping rate (Figure 4.9 a). The numerical model calibration was also validated; using non-pumping model calibration parameters (Table 1), simulated heated cable temperature compared well with observed DTS temperatures (Figure 4.9 a).

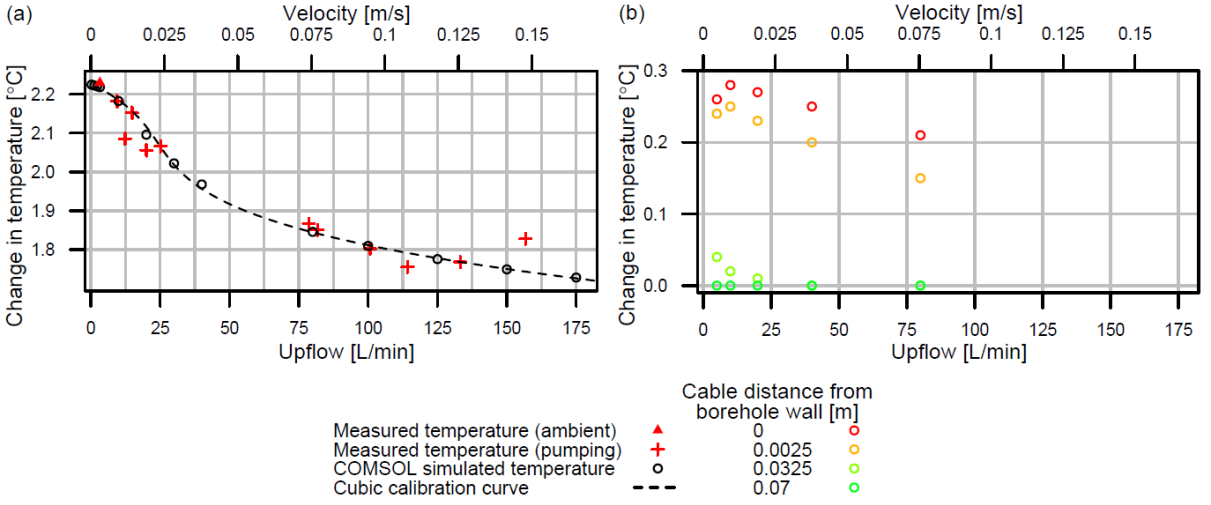

Figure 4.9: Sensitivity of A-DTS to flow conditions and cable position (a) Simulated vs. measured change in A-DTS cable temperature from background as a function of vertical flow past the cable (measured temperature is an average taken directly below pump intake). (b) The dependence of simulated A-DTS cable temperature on the cable distance from the edge of the borehole (borehole radius is 0.075 m).

A linear relationship was not observed between upward velocity and cable temperature. At high velocities (> 0.17 m s^{-1}) the rate of conductive heat transfer through the cable and into the water becomes increasingly limiting. The cable temperature was most sensitive to velocities between 0.01 and 0.04 m s^{-1} where advective heat transport is the dominant factor affecting cable temperature. At velocities below 0.01 m s^{-1} (Q = 10 l min^{-1} in this borehole) the dominant mechanism for heat transport away from the cable is heat conduction (along with possible density mixing effects). Changes in pumping rate are not easily discernible from A-DTS heating profiles alone. At flow rates below 0.01 m s^{-1}, interpretation of post-heating data, such as that carried out during the non-pumping interpretation (Section 4.2) would allow inflowing and outflowing zones and flow rates to be more accurately determined.

For the lower pumping rates considered (9-25 l min^{-1}), a significant difference in cable temperature was not observed below 30 m bgl when compared with non-pumping (Day 1) measurements (Figure 4.7 a). Above 30 m bgl, the cable temperature was reduced relative to the non-pumping temperature observations (Figure 4.7 a). As pumping rates increase a gradual transition from ambient-hydraulic-head weighted to hydraulic-conductivity weighted inflows is expected (Chapter 3). During the lower pumping rates considered (9-25 l min^{-1}), the data suggest ambient head gradients were not fully overcome, and inflows from bottom of the borehole remained relatively consistent with those under ambient flow conditions. Additional inflows were drawn from above 30 m bgl in order to meet the pumping demand.

For the high pumping rates considered (80 – 150 l min^{-1}), a noticeable reduction in cable temperature was observed along the whole cable length compared with non-pumping cable temperatures (Figure 4.7 a). Applying the modelled temperature/flow calibration curve (Figure 4.9 a) to smoothed profiles (Figure 4.7 a) of cable temperature allowed the change in flow rate with depth in the borehole to be estimated (Figure 4.7b). Despite the loss of spatial resolution due to smoothing, the predicted flows were comparable with flow measurements taken using an impeller flow meter (Riley et al., 2011) during high-rate (164 l min^{-1}) pumping. The data suggest the pumped water was drawn from the entire open interval of the borehole. However, inflows were not constant with depth; inflowing zones above 30 m bgl contributed *c.* 70% of the abstracted water. Use of these A-DTS inferred variation in inflow rates in combination with effective K estimates from traditional pumping test interpretation (e.g. Kruseman and De Ridder, 1990) would allow the vertical hydraulic conductivity distribution across the open interval of the borehole to be estimated (Parker et al., 2010).

4.5 Conclusions

Active DTS has been shown to present an efficient method for investigating flows in a borehole in a multi-layered sandstone aquifer. Analysis of A-DTS profiles taken under pumping conditions after 10 minutes of heating was sufficient to detect variation in inflows with depth and pumping rate. In combination with an estimate of effective aquifer hydraulic conductivity such data can provide an efficient way to estimate the adjacent vertical permeability distribution. Making use of post-heating data analysis, in addition to providing validation of A-DTS inferred flows, allowed lower flow rates and directions to be quantified. Such analysis allowed ambient aquifer hydraulic gradient effects to be explored. Observed flow patterns and rates compared well with those obtained using more traditional methods of flow measurement.

The data obtained provided comprehensive assessment of borehole hydraulic properties under non-pumping and a range of pumping conditions. They would be useful in informing water well design, for highlighting contaminant origin and potential redistribution or for informing optimal groundwater quality sampling method and subsequent water quality data interpretation. Similarly comprehensive flow investigations using traditional flow-measuring techniques would require substantially longer time and potentially require multiple instruments/methods to span the range of flows considered.

Preliminary exploratory modelling using the calibrated numerical model helped explain temperature anomalies in the data arising as artefacts of the deployment of the cable in the borehole. To aid DTS cable data interpretation it is recommend that effort is made to ensure the DTS cable is kept away from the borehole wall and centralizers are regularly spaced in order to clearly identify temperature artefacts arising from these items.

CHAPTER 5 INSIGHTS FROM PROXIMAL MULTILEVEL SAMPLER TRANSECTS ON MONITORING WELL SAMPLE ORIGINS IN A DNAPL SOURCE ZONE

5.1 Introduction

The focus of the field study presented in Chapter 2 was on very long (50 m +) open boreholes. However, monitoring of groundwater quality at contaminated sites has in general involved the widespread use of much shorter monitoring wells. Typically these wells are screened over intervals of 3 m (10 feet), or more recently perhaps 1.5 m (5 feet) (e.g. Barber and Davis, 1987; Puls and Paul, 1997; Basu et al., 2006; Fretwell et al., 2006; FDEP, 2008). The variation in groundwater quality over the well screen interval may be of importance particularly in or down-gradient of contaminant source zone areas where sampling data from monitoring wells may underpin source assessment and the increasingly surgical targeted remediation of DNAPL source zone mass.

Dense non-aqueous phase liquid (DNAPL) source zones may contain discrete layers (cm's) of DNAPL, particularly as the source ages. This marked spatial variation arises from not only the initial control of the geological permeability field on DNAPL distribution (e.g. pooling on low permeability layers) but also preferential dissolution due to flow bypass around parts of the source zone due to the presence of the DNAPL itself (Parker et al., 2003; Rivett and Feenstra, 2005). Discrete dissolved-phase plumes may also be maintained downgradient as vertical and horizontal transverse dispersion may be limited (Rivett et al., 2001). The spatial variation in DNAPL occurrence and dissolved-phase plumes generated from that DNAPL source may hence be significant over a 1.5 to 3 m interval nominally monitored by standard monitoring wells in the near vicinity of source zones. While a sample drawn from such a monitoring well may indicate relatively high contamination indicative of high aquifer concentrations, the origins of the sample

likely remain a mystery and heterogeneity of the source or plume unresolved (Basu et al., 2008). Source and dissolved-phase plume heterogeneity of significance to standard monitoring wells is indeed the case at the site selected for study herein and has provided opportunity to examine this issue in detail (Rivett et al., 2014).

Techniques are available to allow high resolution characterization of the spatial variability in contaminant concentration and mass flux in or down-gradient of DNAPL source zones (e.g. high-resolution core sampling (Parker et al., 2003), direct-push (Guilbeault et al., 2005), multi-level transects (Basu et al., 2006), interwell partitioning tracer tests (Annable et al., 1998) or passive flux meters (Annable et al., 2005)). Traditional monitoring wells may also be used to provide high resolution characterization. For example, analytical (Zeru and Schäfer, 2005; Bayer-Raich et al., 2007) or numerical (Bauer et al., 2004) inversion of time-series of long-term pumping concentrations from monitoring wells can be used to estimate the spatial variance in mass flux downgradient from DNAPL source zones. However, the abstraction volumes required for this method are not only onerous in terms of timeframes and potentially water disposal issues, but also mean it is not applicable in lower permeability formations; the analytical and numerical analysis assumptions are such that highly physically or chemically heterogeneous formations are also excluded. Despite the existence of these various high resolution characterization techniques the constraints, both technically and financially, mean it is highly probable that "traditional" sampling of 1.5 or 3 m screen monitoring wells will remain a prominent feature of practitioner site assessment.

Previous modelling work (Chapter 3, Varljen et al., 2006) has suggested that pumped sampling from 3 m monitoring wells will provide an integrated, permeability-weighted, sample from across the screen interval. At long times the origin of such samples over the screen interval may be independent of pump intake position and pumping rate. However, observed vertical flows in wells of 3 m may be sufficient to bias sampling results (Chapter 3); a permeability weighted

sample is by no means guaranteed even after prolonged pumping. Laboratory studies have demonstrated that in-well mixing processes may mean in-well water quality is analogous to an integrated sample even without pumping (Britt, 2005). However, the result of such mixing means it can be difficult assess the vertical distribution in contamination over the screen interval even with multiple passive samples taken from discrete depths in a monitoring well.

Limited field studies have aimed to investigate in detail the provenance of groundwater samples in monitoring wells at contaminated sites (e.g. Puls and Paul, 1997; Reilly and LeBlanc, 1998; Hutchins and Acree, 2000; Sukop, 2000; Metcalf and Robbins, 2007; McDonald and Smith, 2009). These studies have provided possible explanations for the provenance of samples (and sample bias) in monitoring wells. Aquifer concentrations and permeability distributions are inferred although detailed data (for example from adjacent multi-level transects) to confirm such inferences are often lacking. Often the focus of such studies is on monitoring wells > 3 m in length with the conclusion being that use of such wells should be abandoned for groundwater quality monitoring. There remains a lack of quantitative field-scale assessment considering what 3 m monitoring wells can (and cannot) tell us about temporal and spatial variation in groundwater quality and contributing sources (particularly NAPL) at complex contaminated sites. Do such wells eventually provide permeability-weighted average concentrations? How sensitive are they to sampling method? What is an appropriate sample from such wells and what is it representative of? Are such wells appropriate for monitoring of (DNAPL) source zone areas or their near vicinity?

An opportunity has arisen at the SABRE (Source Area BioREmediation, Buss et al., 2010) field site where a trichloroethene (TCE) DNAPL source area has been intensively characterized prior to and during a pilot-scale research study to evaluate bioremediation of a DNAPL source zone (Buss et al., 2010). The site is highly instrumented and has provided opportunity to compare traditional monitoring well samples with data from multi-level transects (ML) in the close

vicinity. The varied field data allow the provenance of groundwater samples from monitoring wells in a complex, chemically and physically heterogeneous environment to be investigated in detail. The aim is to use evidence from proximal ML monitoring to better understand the provenance of samples obtained during conventional sampling (zero purge, low flow, standard volume purging) of typical short screen (3 m) monitoring wells in spatially heterogeneous (DNAPL) source zone environments. A key outcome of the study is to be able to recommend on the utility of such standard monitoring well approaches in monitoring complex, but not untypical, contaminated environments. The approaches to this aim are:

(1) to evaluate the existing SABRE research study (baseline monitoring and bioremediation phases) data obtained primarily from monitoring wells and nearby ML transects alongside other site data that assist meeting this specific study goal;

(2) to collect new field data from the SABRE site using bespoke designed field experiments to understand concentration variations within monitoring wells during sampling;

(3) to use numerical flow and transport modelling to inform data interpretation and to explore sensitivities to monitoring well sample origins; and

(4) to consider the implications of the study for practitioners more generally (i.e. beyond the study site).

5.2 Materials and methods

5.2.1 Field site and historical field data overview

The data used were drawn largely from project SABRE (Buss et al., 2010) supplemented by a phase of fieldwork initiated under the remit of this PhD agenda several years after the SABRE research project. The objective of the SABRE project was to provide detailed field observations to improve process understanding during in-situ bioremediation in the vicinity of an aged TCE source zone. The TCE contamination is the result of operations at a large chemical manufacturing

plant previously active at the Midlands UK located field site. Down-gradient of the source area a chlorinated solvent plume containing varying proportions of both TCE and its biodegradation daughter products (cis-dichloroethene (DCE) , vinyl chloride (VC) and ethene (Ee)) has been observed in the shallow (6 m) sand and gravel aquifer underlying the site. The source contamination is the result of TCE leakage from subsurface effluent pipes during the 25 year operational period of the chemical plant. The source architecture was expected to be complex reflecting the source age with site operation having ceased 20 years prior to the SABRE field investigations.

The shallow aquifer underlying the site consists of *c.* 1 m of made ground overlying *c.* 5 m of superficial Quaternary alluvium and river terrace gravels (Chambers et al., 2010; Dearden et al., 2013). Below this lies *c.* 50 m of relatively impermeable Triassic mudstone (Mercian Mudstone Group) which may be weathered in the top 0.5 to 1.25 m (Chambers et al., 2010). The Quaternary deposits are heterogeneous; they are generally finer in the upper *c.* 1-2 m and comprise a sequence of alluvial sands, silts and clays with mm scale laminations (Lelliot et al., 2008; Chambers et al., 2010). These finer deposits grade into *c.* 4 m of poorly sorted river terrace deposits. The river terrace deposits comprise coarser sands and gravels formed from river channel deposition. Groundwater at the site flows to a discharge point at a local river (Chambers et al., 2010) with natural groundwater heads typically 1 - 2 m bgl (below ground level) and natural hydraulic gradients of 0.001-0.002 (Dearden et al., 2013).

During the SABRE project a 3-sided U-shaped test cell (Figure 1) was installed parallel with the prevailing groundwater flow direction and intersecting the TCE source zone (located during previous investigations at *c.* 7 - 10 m down the cell). The cell is open upgradient of the source zone to allow groundwater inflow. At the far end of the cell an abstraction pump was in operation during SABRE field investigations. The cell is covered at the surface to prevent direct recharge

and has plastic sheet pile walls. Together, these barriers prevent additional inflows along the length of the cell allowing accurate assessment of DNAPL mass removal during cell operation to be made. The cell abstraction rate during cell operation (1.4 – 1.6 l/min) was selected to give groundwater velocities comparable with those occurring naturally (Rivett et al., 2014). Cell water levels as measured at SW70 and SW75 (and T2a and T3a) were highly variable during cell operation; typically values were between. 2 and 4 m bgl with decreasing water levels in the cell ascribed to cell dewatering due to clogging in the inflow area of the cell reducing cell inflow rates.

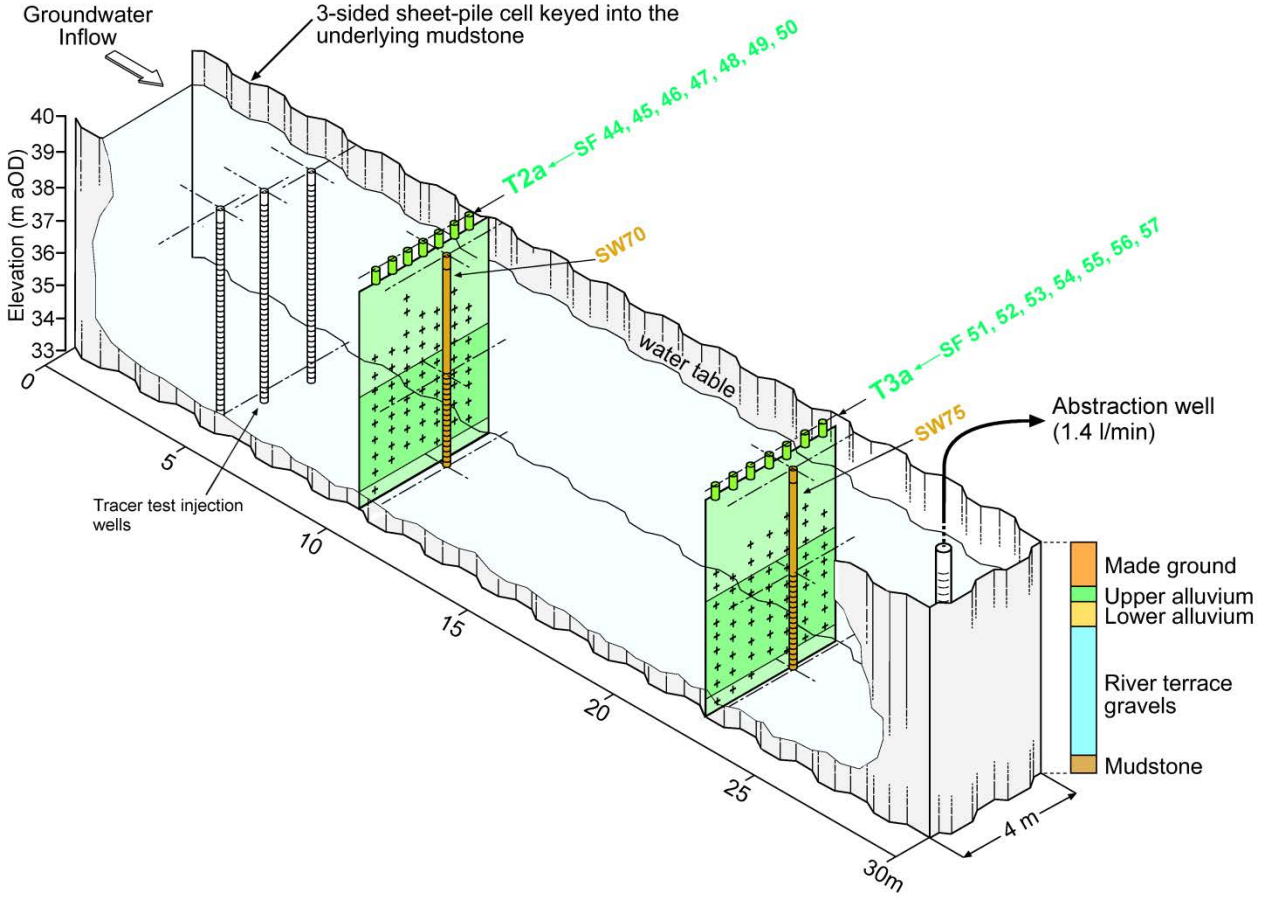

Figure 5.1: Schematic of SABRE cell (after Rivett et al., 2014) showing location of monitoring wells (SW70 and SW75), upgradient multi-level transects (T2a and T3a), abstraction well and tracer test injection wells. Crosses in the multi-level transects indicate the location of multi-level transect ports; monitoring well screen intervals are indicated by the segmented sections in the lower half of each well.

Seven sampling operations (Table 5.1) were undertaken taken over the 2-year operational period of the cell (Buss et al., 2010). The first three sampling operations were used to assess

baseline (pre-bioremediation) conditions in the cell. The following four operations were during active bioremediation in the cell when electron donor injection and subsequent bioaugmentation was undertaken in the source zone over a two week period (Mack et al., 2010; Cai et al., 2012).

During SABRE field investigations, high-resolution groundwater monitoring was undertaken in the source zone and in the down-gradient dissolved phase plume using multilevel transects installed both perpendicular to and parallel with groundwater flow. In addition to the multi-level transects a number of 3 m screen monitoring wells were installed down-gradient of the source zone. Two such monitoring wells are the focus of this study: monitoring well SW70 (Figure 5.1) is located at or immediately downgradient of the DNAPL source zone; monitoring well SW75 is located in the dissolved plume, down-gradient of the source zone. Multi-level transects T2a and T3a provide complementary depth-discrete contaminant concentration distribution; these transects lie immediately upgradient of SW70 and SW75 respectively. The transects were selected as their multi-level port locations provide good spatial coverage at the depth of the 3 m monitoring well screen intervals (Figure 5.1).

Operation	1	2	3	4	5	6	7
Day	-64	-37	-20	149	257	511	588

Table 5.1: SABRE Sampling Operations . Day 0 is the start of the electron donor injection. Negative days indicate the baseline period and positive days indicate the active remediation phase. Cell abstraction started at Day -90. Mean cell residence time is estimated at c. 42 d (Cai et al., 2012; Rivett et al., 2014)

During SABRE project sampling SW70 and SW75 were sampled using a 12 V submersible pump (WaSP) placed near the bottom of the screen interval of the well. Pumping was undertaken at rates of 1 - 5 l/min with the motivation that traditional purged monitoring well water quality samples would result. Purged water was monitored for stabilization of water quality parameters with a minimum of 3 well volumes (24 l assuming rest water levels at 2 m bgl) of water removed prior to sampling. T2a and T3a multi-level transects were sampled at 200 ml/min using a peristaltic pump. Transect port samples were taken following chemical stabilization with a

minimum of 3 tube volumes removed prior to sampling. Formation dewatering meant it was not always possible to sample all transect ports.

In addition to the transect and monitoring well sampling data, other data drawn on include: (1) chlorinated ethene (TCE, cDCE, VC and Ee) concentrations measured at the abstraction well (used to constrain mass flow estimates through cell); (2) hydraulic conductivity (K) estimates from Hvorslev (Hvorslev, 1951) analysis of falling-head tests on T2a and T3a (used to provide initial estimates of hydraulic conductivity distribution at SW70 and SW75); (3) conservative tracer test breakthrough times at T2a (used to provide additional evidence of cell transport pathways away from the source zone). The conservative tracer test was undertaken from injection wells located 5 m upgradient of T2a (Dearden et al., 2010). Monitoring at T2a was undertaken 14 times over the 25 day period of the test.

5.2.2 Additional data collection

To supplement the historical sampling data, additional sampling at the site was carried out in July 2013 and April 2014. The aim of the additional sampling rounds was to assess current cell conditions and to provide additional information on the provenance of SW70 and SW75 monitoring well samples. Such an aim was achieved by carrying out Reverse Flow Tests (RFT, Tellam, 1992) in both SW70 and SW75. RFT provide a method to estimate both vertical variation in aquifer water quality and inflow rates (permeability distribution) across the screen interval (or open section) of a well. RFT are particularly applicable in 3 m, monitoring wells where space issues mean alternatives methods such as packer interval sampling are not practical (Jones and Lerner, 1995). Additionally, packer testing may not be appropriate in screened well with gravel pack such as those at the SABRE site due to the possibility of flow bypass in the gravel pack. RFT provide a more comprehensive method (without the danger of false negatives) of determining aquifer chemical heterogeneity when compared with qualitative methods such as

pumped sample chemical disequilibrium (Ayotte et al., 2011) or depth sampling for example. However, the RFT method is relatively expensive and time-consuming by comparison.

5.2.2.1 Reverse flow test field method

In a reverse flow test the well is pumped in turn from the top and then the bottom (or *vice versa*) of the screen interval with vertical variation in electrical conductivity (EC) in the well monitored for stability in each instance. However, EC at the SABRE site is primarily controlled by chloride and bicarbonate ion concentration (Chambers et al., 2010) and not directly related to chlorinated ethene concentrations. Hence, rather than monitoring EC, the field method involved taking repeated water quality samples from five intermediary depth intervals (non-main stem samples) in the well in addition to sampling from the main pump intake (main stem sample) (Figure 5.2, Table 5.2).

The two main stems were pumped in turn using a peristaltic pump with pumping rates of 0.38 l/min. Non-main stem intervals (narrow diameter Teflon tubing) were sampled simultaneously using a peristaltic pumping at very low flow rates (<0.04 l/min). The non-main stem samples were taken once at least one tubing volume had been removed. Non-main stem interval 1 (the shallowest) allowed casing water quality to be assessed; the remaining four intervals allowed well water quality variation with depth (under pumping conditions) to be assessed. The schedule of sampling is found in Table 2.

Water quality samples were sent to an accredited UK laboratory for chlorinated ethene (TCE, cDCE, VC) and limited inorganic (chloride (Cl) and sulphate (SO_4) analysis with additional onsite recording of inline water quality parameter (temperature, turbidity, oxidation-reduction potential (ORP), pH, EC, dissolved oxygen (DO)) variation during purging undertaken using an AquaTROLL 9500 (InSitu Europe). QA/QC controls included field rinse blanks, field blanks and duplicate samples.

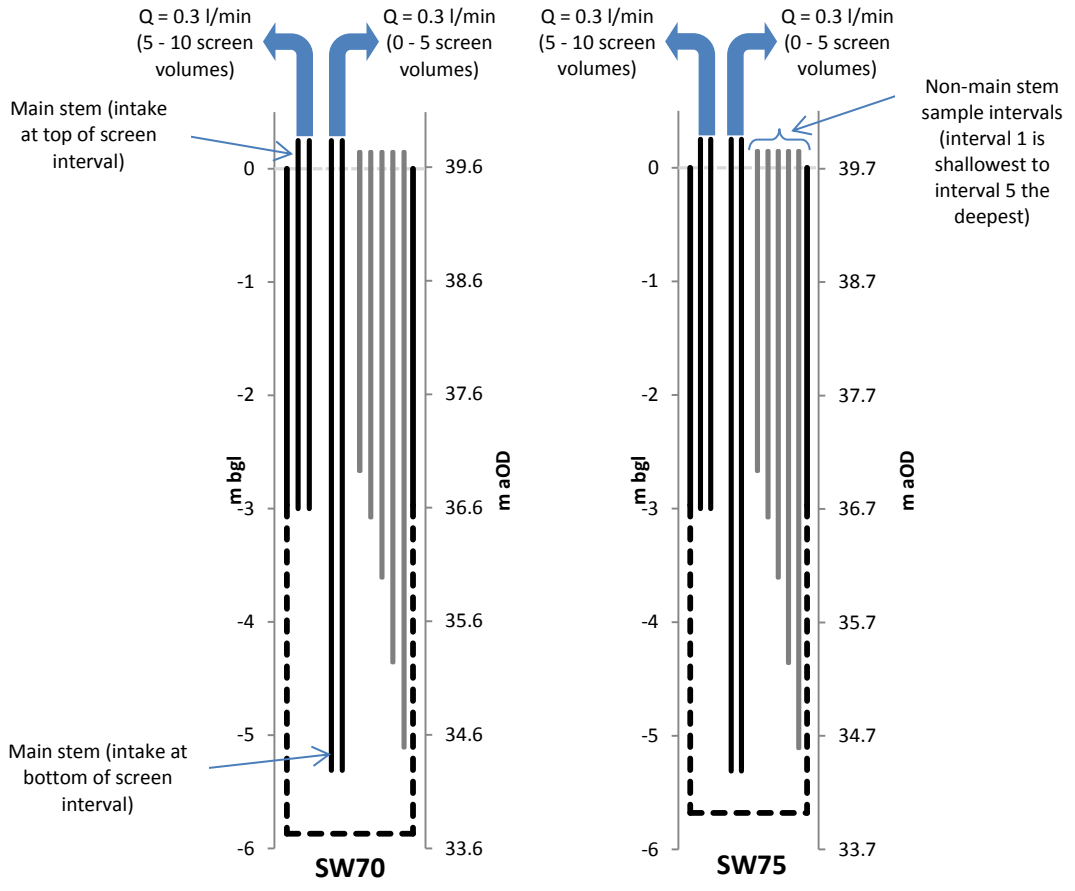

Figure 5.2: Reverse flow experimental setup in SW70 and SW75.

The RFT method allows an estimate of aquifer vertical groundwater quality distribution to be obtained by iterative solution of a set of simultaneous equations (Tellam, 1992). The equations relate aquifer concentration and permeability distributions to in-well concentration observations. However, an assumption of the method is that water quality stability is reached by the end of each pumping phase. Here, simultaneous equations were formulated using both chlorinated ethene and chloride water quality data. The RFT model was fitted by minimizing the Root Mean Square Error (RMSE) between observed well concentrations and RFT-predicted well concentrations.

		Sampled?						
		Main Stem	Non-main stem intervals					
Cumulative screen volumes removed	Pump intake location		Interval 1	Interval 2	Interval 3	Interval 4	Interval 5	Notes
0	Bottom	Y	Y	Y	Y	Y	Y	Baseline (pre-purge conditions)
1.5	Bottom	Y						
3	Bottom	Y	Y	Y	Y	Y	Y	
5	Bottom	Y	Y	Y	Y	Y	Y	Final concentrations with pump at the bottom
5	Top	Y						Baseline conditions with pump at top (should be broadly equivalent to non-main stem interval 2 concentrations)
10	Top	Y	Y	Y	Y	Y	Y	Final concentrations with pump at the top

Table 5.2: Reverse flow sampling schedule

The disadvantage of using determinants (e.g. chlorinated ethenes) which are not readily detectable inline is that it is difficult to assess chemical stability on site. Instead the monitoring wells were pumped from the bottom and then the top for 5 screen volumes each. Such purge times were guided by previous modelling (Chapter 3, Martin-Hayden, 2014) that suggested the removal of at least 3 screen volumes is required for stability. Interim samples were taken as per the schedule in Table 2 to allow for later assessment of stability. Pumping rates were low (*c*. 0.38 l/min) to avoid excessive drawdown and hence minimize the influence of mixing with casing water on well water samples.

In the interim period between the seven historical sampling operations (Table 1) and the 2013/2014 sampling undertaken during this project, the cell has experienced periods of stagnation interspersed with consultant-led cell remediation activities. However, the cell was last operational in 2010 and consequently had been in a long period of stagnation prior to 2013/2014 sampling visits. Without cell abstraction in operation, continuity of chlorinated ethene

concentrations between the (no-longer upgradient) transect ports and the monitoring wells can no longer be assumed. Nevertheless, sampling from the transects provides the only independent verification of chlorinated ethene distribution in the adjacent formation. Accordingly, in addition to SW70/SW75 monitoring well sampling, a subset of T2a/T3a transect ports were sampled. Time and cost constraints meant the full range of ports were not be sampled. However, significant build up of undetermined organic matter, ascribed to lack of cell operations, meant sampling the transects (and to a lesser extent the monitoring wells) was problematic. Difficulties with clogging (observed as black 'slime' fragments in pumped water which may be remnants of bioremediation activity and bio-clogging) were such that insufficient data were collected during 2013. Accordingly, only the 2014 data are presented here.

5.2.3 Numerical modelling overview

During historical SABRE operations SW70 and SW75 monitoring well groundwater quality samples were taken using the "traditional" volume purge approach. The aim of numerical modelling was twofold: (1) to examine quantitatively inferences on monitoring well sample origin drawn from observations on historical field data; (2) to examine the groundwater quality samples which might have resulted had different sampling approaches been undertaken and hence to comment on how best to sample such monitoring wells.

Numerical modelling of the cell during the SABRE sampling operations (Table 1) was undertaken using MODPATH 5 (Pollock, 1994) and MT3DMS (Zheng and Wang, 1999) in conjunction with MODFLOW (Harbaugh et al., 2000) calculated specific discharges. The scope of modelling excluded direct simulation of the evolution of chemical concentrations in the cell between sampling operations. Rather, individual simulations of transient flow and transport during monitoring well sampling were undertaken separately for each SABRE sampling operation. TCE, cDCE and VC were all included in the numerical modelling; however Ee was

omitted due to the infrequent sampling for this product compared with the other species considered. Particle tracking using MODPATH was used to assess advective well capture zones and compare simulated tracer test transport velocities to those observed in the conservative tracer test (Dearden et al., 2010).

5.2.3.1 Model setup

The unconfined model domain (Figure 5.3) is a simplified representation of the SABRE cell: the model domain is 29 m long, 4 m wide and 6 m deep and comprises 101 columns, 51 rows and 200 layers. The monitoring and abstraction wells are represented explicitly using a single column of very high hydraulic conductivity (10^6 m/d) cells (Chapter 3). The high-K cells extend from the top of the model to the bottom of the screen interval of each well. The well casing is represented by MODFLOW's Wall boundary condition with a K value of 10^{-7} m/d and thickness of 0.01 m. The model grid is refined in the vicinity of the wells such that model well cross-sectional areas are equivalent to the real-world well dimensions. Grid refinement is reduced away from the wells up to a maximum row/column width of 0.13 m. Uniform layer spacing of 3 cm is used between 1.5 and 6 m bgl. Above this, which for the majority of the model is above the water table, the layer heights incrementally increase up to a maximum of 40 cm in the top layer.

The pump intake, located at the bottom of the screen interval of the monitoring wells during sampling, is explicitly represented using MODFLOW's Well boundary condition. Pumping rates used during SW monitoring well sampling were between 1 and 5 l/min. Accordingly, simulated pumping rates were initially set to 1 l/min; sensitivity to increased (and decreased) pumping rate was later investigated. Similarly, to simulate the abstraction pump, a Well boundary condition abstracting at a rate of 1.4 l/min is placed in the middle of the screen interval of the abstraction well.

Transient sampling simulations were of 60 minute duration, this being significantly longer than the time to remove 3 well volumes (24 l) from the monitoring wells while pumping at 1 l/min. Relative to this short simulation time, changes in wider groundwater heads are assumed negligible. For this reason, the only model inflows are via a steady-state general head boundary (GHB) at the left-hand side of the model. Recharge is zero and boundaries with the underlying clay and sheet pile walls are assumed impermeable; these are no flow boundaries in the model.

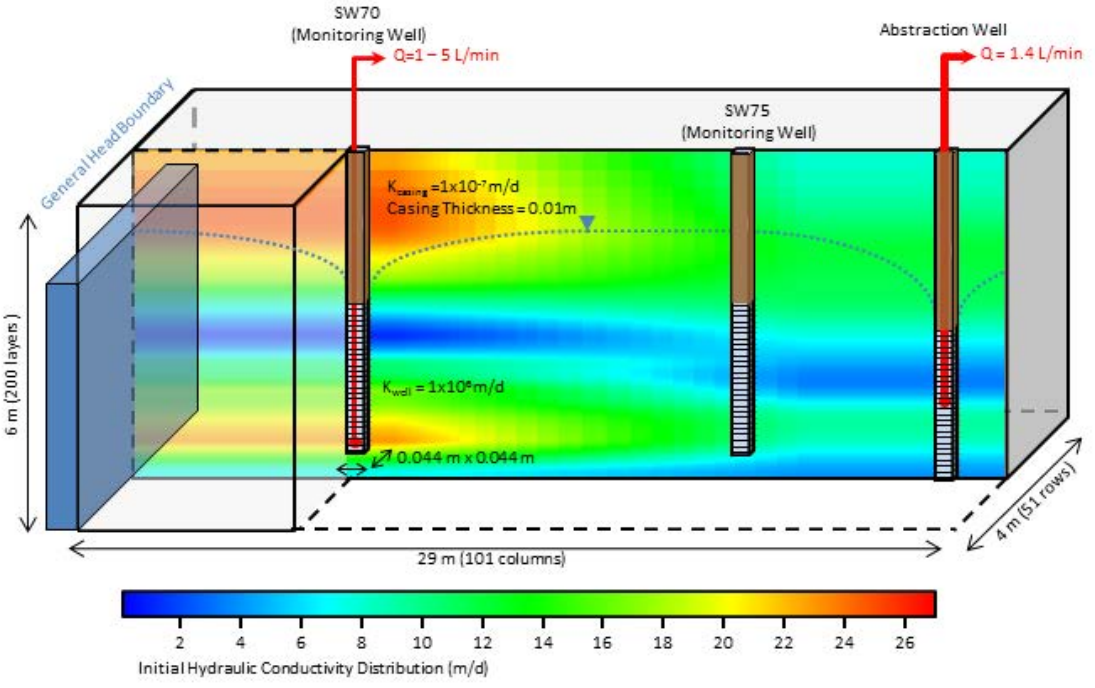

Figure 5.3: Summary of model domain and parameters (not to scale)

Observed heads in wells located immediately outside the cell remained roughly constant at *c.* 1.2 m bgl during SABRE cell operation. The right-hand GHB head is 1.2 m bgl with conductance configured (distance = 100 m, hydraulic conductivity = 0.5 m/d) such that initial heads at T2a and T3a matched those observed (*c.* 2 m bgl for T2a, *c.* 2.5 m bgl for T3a). The exception was during operations 5 and 7 when cell dewatering had resulted in decreased heads. For these simulations, the GHB was lowered to 2.2 m bgl such that the water table was *c.* 3 m bgl at T2a and *c.* 4 m bgl at T3a.

Extrapolation/interpolation of data (falling head test derived permeabilities and sampled concentrations for each operation) drawn from T2a and T3a provided the means by which initial model permeability and chlorinated ethene concentration distributions were calculated. Ordinary kriging was used to interpolate laterally across the cell at T2a and T3a. Linear interpolation was then used to assign values between the kriged permeability distributions at T2a and T3a. Upgradient of T2a and downgradient of T3a permeability and concentration distributions were extrapolated – these were assumed to be the same as T2a and T3a respectively. For concentration kriging non-detects were set to the detection limit and non-sampled ports were not included. Model porosity was set to the suggested cell average (25 %, Cai et al. (2012)). Specific yield and specific storage were chosen to be 0.1 and 0.0001 respectively. The heterogeneous permeability distribution in the model was assumed to account for large-scale (macro) dispersion. To simulate small-scale dispersive processes local to the monitoring wells, and to ensure model stability, model longitudinal dispersivity was set to 0.04 m and the transverse dispersivity to $1/10^{th}$ that (0.004 m). Retardation factors for TCE and its daughter products are relatively low (typically 1-10) but depend on the fraction of organic carbon (foc) (Wiedemeier, 1999). In the case of the SABRE site, calculation of a retardation factor is complicated by changes in organic carbon content between sampling operations due to the electron donor injection (Cai et al., 2012). However, timescales considered here are very short (< 60 minutes) and hydrodynamic distances small so in this case the retardation of the chlorinated ethenes during transport to the pump was omitted.

5.2.3.2 Model calibration

Model performance was assessed by comparing simulated monitoring well sample concentrations against those observed. However, simulated monitoring well concentrations are highly likely to be sensitive to the physical heterogeneity of the formation adjacent to the well

screen interval, to the chlorinated ethene distributions local to the well and even to porosity variation and non-equilibrium sorption effects. Despite the good spatial coverage provided by T2a/T3a ports at the depth interval of SW70 and SW75 the highly heterogeneous nature of the cell (both chemically and physically) means interpolation between these points may not fully represent in-cell conditions. Additionally, given the biostimulation during active remediation, porosity and hydraulic conductivity may vary with time. For these reasons, it is highly likely that any calibrated model of the cell will be non-unique. However, the approach taken assumed that hydraulic properties were constant with time and that porosity was uniform in space and time. Chemical concentrations interpolated from T2a/T3a were fixed. Therefore, (non-exhaustive) calibration was undertaken by manual calibration of permeability distributions across T2a and T3a alone.

However, such calibration was informed/constrained by data in addition to observed monitoring well concentration. Given the location down-gradient of the source, and with the sheet pile cell walls preventing lateral inflows total molar chlorinated ethene mass flux through T3a should be consistent with abstraction well mass flux observations. Hence, T3a K estimates were additionally constrained by comparing calibrated K-weighted estimates of chlorinated ethene mass flux though T3a with observed abstraction well mass flux. Observed peak arrival times during the tracer tests to T2a were compared with model simulated values to additionally constrain T2a changes in permeability.

Summary residual statistics (root mean square error (RMSE) and residual bias) represented the overall model fit. These statistics were calculated using results from both monitoring wells, for all chemical components (TCE, cDCE and VC) and for all operations:

$$RMSE = \sqrt{\frac{\sum_{o=1}^{7}(\sum_{c=1}^{3}(\sum_{w=1}^{2}(\hat{y}_{ocw} - y_{ocw})^2))}{42}} \qquad \text{Eq. [5.1]}$$

$$Bias = \frac{\sum_{o=1}^{7}(\sum_{c=1}^{3}(\sum_{w=1}^{2}(\hat{y}_{ocw} - y_{ocw})))}{42} \qquad \text{Eq. [5.2]}$$

where o is the operation (1-7), c is the chlorinated ethene component (TCE, cDCE or VC), w is the monitoring well (SW70 or SW75), $\hat{y}_{ocw}$ is the modelled sample value for a particular operation, chemical and monitoring well and y_{ocw} the observed sample value.

The purging times used during SW70 and SW75 sampling are uncertain and, depending on the time for inline water quality parameters to reach stability, may have varied between SABRE sampling rounds. Model residual statistic results may have been improved by varying simulated pumping rate and purging time between SW70 and SW75 and between sampling operations. However, there are insufficient data to support such an approach. Instead a single, unknown purging time, greater than the time to remove 3 well volumes (24 minutes) was assumed. For each set of model parameters, calibration results were reported at five minutes intervals assuming purging times between 25 and 60 minutes. The final purging time selected was that which minimized the overall residual summary statistics.

5.2.3.3 Predictive modelling

Predictive modelling using a non-exhaustive range of scenarios (Table 5.3) was undertaken with the aim to investigate the effect pumping rate, pumping time and pump intake position might have on monitoring well sample concentrations in the SABRE cell. Predictive modelling was undertaken using the final calibrated hydraulic conductivity distribution.

Scenario	1	2	3	4
Pumping rate (l/min)	2.5	1	0.3	0.3
Pump intake location (in screen interval)	bottom	bottom	bottom	top

Table 5.3: Predictive modelling scenarios

5.3 Results and discussion

5.3.1 Initial comments on ML transect data and monitoring wells samples

Observed TCE, cDCE and VC distributions were very heterogeneous spatially with orders of magnitude variation in concentration seen across the multi-level transects during the seven sampling operations (Figure 5.4 and Figure 5.5, columns 2 - 8). Such variation is reflective of proximity to the heterogeneous DNAPL source. In general, for T3a, the pattern of chlorinated ethene distribution was consistent with higher concentrations observed below 4 m bgl (Figure 5.5) and lower concentrations above. T2a presented a more complex picture, with low concentrations of TCE above 4 m bgl contrasting with high cDCE values (Figure 5.4). The opposite is observed below 4 m bgl.

Chlorinated ethene concentrations remained relatively stable during the baseline (pre-active remediation) period in both T2a and T3a. Dechlorination daughter products (cDCE and VC), which are not thought to have been present in the initial DNAPL release, were observed in both ML transects. However, degradation daughter product enrichment was variable across the cell. For example, there was a relative absence of TCE above 4 m bgl (Figure 5.4 b, c, d) in T2a with high cDCE molar concentrations (Figure 5.4 j, k, l). By contrast, below 4 m bgl, relatively high TCE concentrations remained with daughter products making up a much smaller contribution to total chlorinated ethene mass.

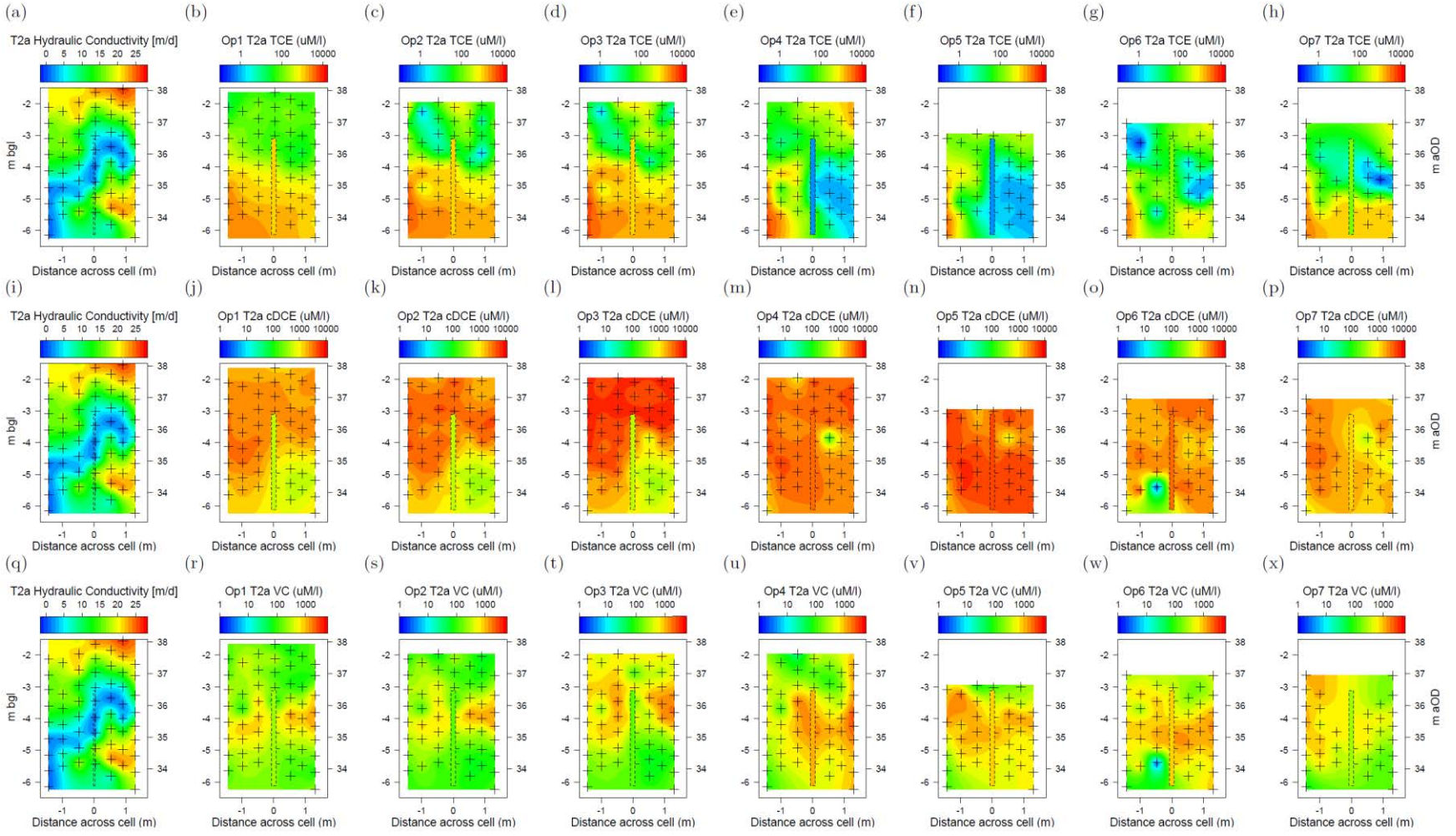

Figure 5.4: Kriged T2a chlorinated ethene concentration (uM/l, log colour scale) compared with SW70 monitoring concentrations (data drawn from historical SABRE sampling operations). Row 1 is TCE, row 2 cDCE and row 3 V transect permeability (from falling head tests). Dashed line indicates location of SW70 screen interval; radius is in chlorinated ethene plots to make SW70 monitoring well concentrations more visible. Crosses indicate location of p later plots (operations 5, 6 and 7) ports above c. 3 m bgl were not sampled as cell water levels were too low.

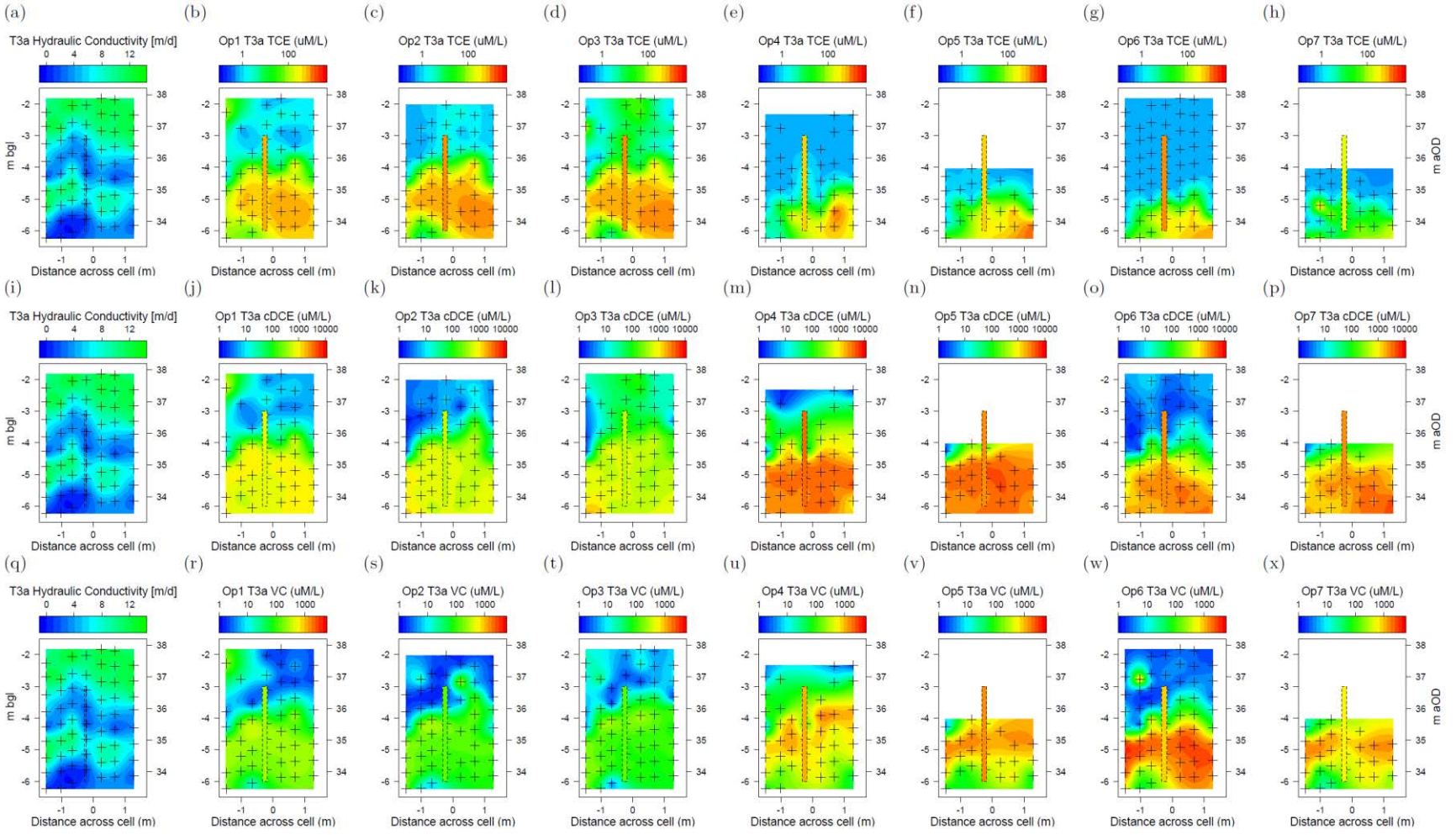

Figure 5.5: Kriged T3a chlorinated ethene concentration (uM/l, log colour scale) compared with SW75 monitoring concentrations (data drawn from historical SABRE sampling operations). Row 1 is TCE, row 2 cDCE and row 3 V transect permeability (from falling head tests). Dashed line indicates location of SW75 screen interval; radius is in chlorinated ethene plots to make SW75 monitoring well concentrations more visible. Crosses indicate location of p later plots (operations 5 and 7) ports above c. 4 m bgl were not sampled as cell water levels were too low.

Unsurprisingly, monitoring well samples did not fully reflect the complexities gained from the ML transect sampling. For example, during baseline conditions molar concentrations of TCE (1765 - 1826 uM/l) recorded in SW70 were high with cDCE and VC concentrations (649 - 835 uM/l and 176 - 320 uM/l respectively) accounting for less than a third of the total mass of chlorinated ethenes observed. The relative enrichment in daughter products observed in T2a in the upper half of the cell during baseline conditions was not reflected in SW70 monitoring well samples. SW75 baseline samples were similarly reflective of the higher chlorinated ethene concentrations observed in the lower half of T3a rather than the low concentrations observed above 4 m bgl.

Literature values for the TCE solubility limit (S^{TCE}) range from 1100 mg/l to 1400 mg/l (8.4 and 10.7 mM/). The 1 -10% solubility rule of thumb (US EPA, Feenstra and Cherry, 1988; 1992; Pankow and Cherry, 1996) can be used to assess the possible presence of DNAPL upgradient of a sampling point. The low percentage concentrations relative to S^{TCE} required to indicate the possible presence of DNAPL reflect concentration dilution in the dissolved phase plume. Such dilution can result from, for example, hydrodynamic dispersion, the offset of the sampling point relative to the plume centre line, mixing with non-contaminated water outwith the plume, or in-well mixing processes. During baseline sampling operations (Figure 5.4 & Figure 5.5, Op1 – Op3), total molar chlorinated ethene concentrations in both SW70 and SW75 (and indeed such concentration values observed from the lower half of both ML transects) were > 10 % of even the upper limit for S^{TCE}. Such high percentage concentration values provide clear indication of the presence of upgradient DNAPL from both monitoring wells and ML transects.

During active remediation, enrichment in dechlorination daughter products and depletion of TCE were observed in both monitoring wells and ML transects (Figure 5.4 & Figure 5.5, Op4 –

Op7). Total chlorinated ethene molar concentrations observed in monitoring wells samples approached or were above the lower literature value for S^{TCE} (1100 mg/l).

Hydraulic conductivity distributions measured at T2a and T3a were also heterogeneous (Figure 5.4 & Figure 5.5, column 1). Permeability was higher across T2a, ranging from < 1 to 28 m/d, while at T3a values were lower (< 0.1 to 14 m/d). Values were generally high in the upper alluvium (above 2 m bgl) with greater variation in permeability observed in the poorly-sorted river terrace gravels below. An area of higher permeability in the river terrace gravels was observed in both transects at 5 m bgl; this area is confined to the right-hand-side of the cell at T2a but is cell wide at T3a.

5.3.2 Clues to the provenance of the monitoring well samples

Given pumped monitoring well samples are expected to provide some sort of permeability-weighted average of adjacent aquifer concentrations, it is not surprising that, with a few exceptions (e.g. Figure 5.4 e, f, j, k, l; Figure 5.5 b, c, d, m, o), observed monitoring well concentrations did not reflect minimum or maximum concentrations observed in the adjacent transects. However, such exceptions can be extremely useful in providing evidence as to the provenance of monitoring well samples. In such cases in can be inferred that monitoring well sample provenance must be strongly biased towards similarly high or low concentration zones in the adjacent aquifer with little contribution to sample concentration being made from other parts of the cell. Consideration of such exceptions suggest that SW70 sample provenance was strongly biased towards the lower right-hand side of the cell (Figure 5.4 e, f, j, k, l). The picture is slightly less clear for SW75 however in general the data suggest that sample provenance was from the lower half of the cell but perhaps less strongly biased towards the right hand side than for SW70

(Figure 5.5 b, c, d, m, o). For both T2a and T3a, these zones identified as important to monitoring well sample provenance coincided with areas of high permeability in the cell.

Indeed, permeability-weighted means of chlorinated ethene concentrations as observed in these high-K zones in both T2a and T3a (dashed circles in Figure 5.6 b, g) provided a good prediction of observed SW monitoring well concentrations (Figure 5.6 d, i). By contrast, permeability-weighting by ports from across the screen interval (black circles in Figure 5.6 b, g) provided a much poorer fit to SW70 sample concentrations and to a lesser extent to SW75. Inorganics data from a limited set of the sampling operations provided a consistent picture - an improved fit is seen using the high-K ports (Figure 5.6 e, j) over that predicted from the upgradient ports (not shown, RMSE values were 2 mM/l and 2 mM/l for SW70 and SW75 respectively; biases were 2 mM/l and 1 mM/l).

Numerical modelling (Chapter 3) suggested at long times (> 3 SV) pumped sample from such 3 m monitoring wells will provide a permeability-weighted sample drawn from across the screen interval (assuming significant vertical hydraulic gradients are not present). Rather than suggesting that such permeability weighting is not the case for the monitoring wells considered here it is more likely that well inflows were more complex than can be inferred from simplistic consideration of the permeability distribution observed in the upgradient transect. The sample is likely to have contributions from across the screen interval, however K contrasts are such that such contributions may be largely drowned out by inflows from the high K zone.

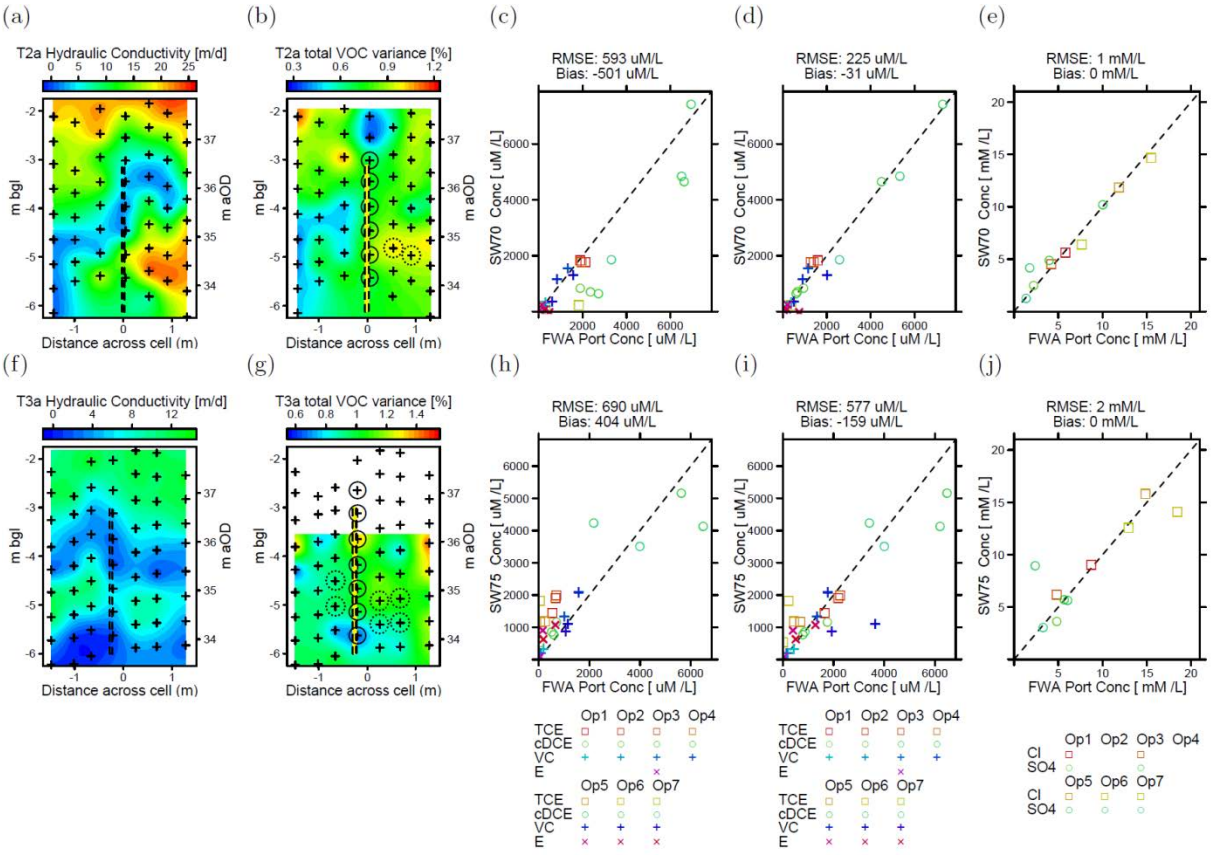

Figure 5.6: Clues to provenance of monitoring well samples. (a) and (f) show T2a and T3a K distribution (from falling head tests); (b) and (g) show the percentage temporal variance in total chlorinated ethene (TCE, cDCE, VC and E) concentration (all operations). Blue colours are areas where sample concentration did not vary much with time; red colours are areas with greater temporal variation. (c), (d), (h) and (i) show permeability-weighted (FWA) transect port chlorinated ethene concentration compared with monitoring well concentration. In the case of (c) and (h) ports used are those directly upgradient of the screen interval of the monitoring wells (solid black circles in (b) and (g)); for (d) and (i) ports used are from the high-K zone at 5 m bgl (dashed black circles in (b) and (g)). (e) and (j) show chloride and sulphate results using the high-K (dashed circle) ports.

5.3.3 Evidence to suggest monitoring wells reflect concentrations moving through the cell

When comparing between sampling operations, temporal variance in chlorinated ethene concentration were not uniform in space (Figure 5.6 b, g). Particularly for T2a (and to a lesser extent T3a) areas of the ML transect associated with smaller changes in concentration with time (blue colours, Figure 5.6 b, g) were generally located in areas with lower hydraulic conductivity (Figure 5.6 a, f). By contrast, areas where changes in concentration with time were greater (reds and yellows) were generally associated with zones of higher hydraulic conductivity. If changes in ML concentration with time are indicative of upgradient changes in concentration then

transport away from the source zone appears to have been biased towards the high-K pathways in the river terrace gravels at 5 m bgl. If groundwater was moving more slowly through (or even bypassing) the lower-K regions of the transect (e.g. the low K zone on the bottom left-hand side of the cell across T2a, Figure 5.4a) then the relatively unchanging concentrations in these regions are explained.

SW70 and SW75 sample concentrations showed a relatively high temporal variance (Figure 5.6 b, g) comparable to that in the higher K regions of the cell and indicative of concentrations moving away from the source zone and through the cell.

The importance to groundwater transport away from the source zone (and spatial continuity) of this high-K zone at 5 m bgl in T2a was further underlined by the conservative tracer test results (contoured in Figure 5.7 to aid discussion). Fastest breakthrough time at T2a (< 0.25 d, Figure 5.7 b) and peak observed concentrations both (Figure 5.7 f, g, h, j) occurred in the high-K zone located on the right-hand side of the cell at *c.* 5 m bgl.

Analysis of tracer breakthrough at 25 m down the cell observed from a single snapshot taken after 6 days suggested maximum and mean cell velocities of 3 – 4 m/d and 2.1 m/d respectively (Rivett et al., 2014). Such velocities resulted in estimates of minimum and mean travel times between SW70 and the abstraction well of 4.25 - 5 d and 8.1 d, respectively. Travel times from SW75 to the abstraction well are approximately one quarter those from SW70 to the abstraction well.

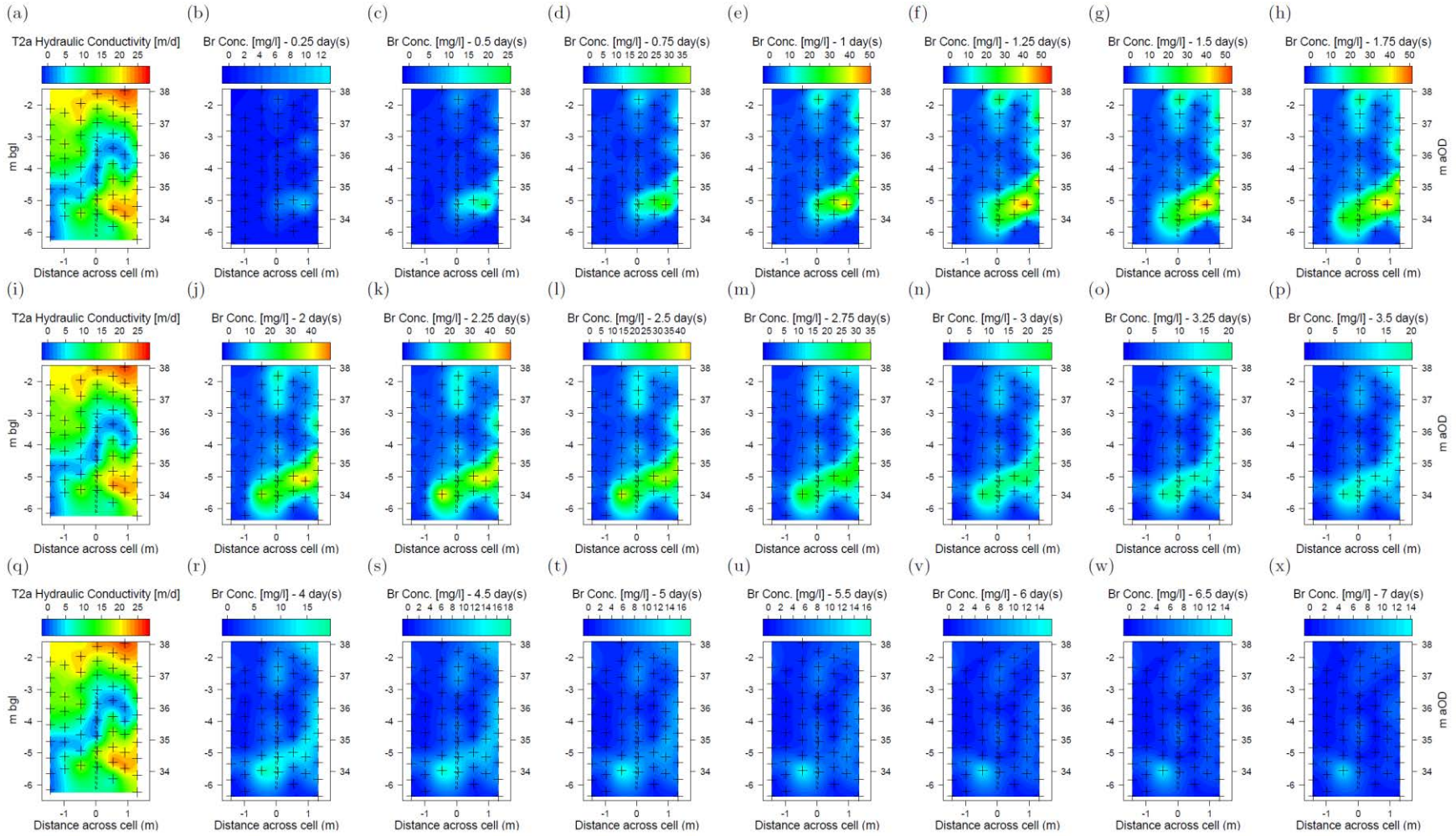

Figure 5.7: Bromide tracer breakthrough at T2a (0.25-7 days). Tracer was introduced 5 m upgradient (Figure 5.1). Breakthrough monitoring continued with no further significant breakthrough until 45 d

Despite such uncertain travel times (and pathways) between SW70/SW75 and the abstraction well, abstraction well concentrations (which are indicative of permeability-weighted average concentrations moving through the cell) were a good indicator of SW70 and SW75 concentration. Such is the case during the seven sampling operations considered in detail herein (Figure 5.8 a squares and circles) and across a wider range of sampling events (Figure 5.8 b) during baseline monitoring and active remediation in the cell. This result is particularly of note given the orders of magnitude variation in concentration at T2a and T3a transects and provides a further line of evidence that the monitoring well samples may be representative of concentration movement away from the source zone.

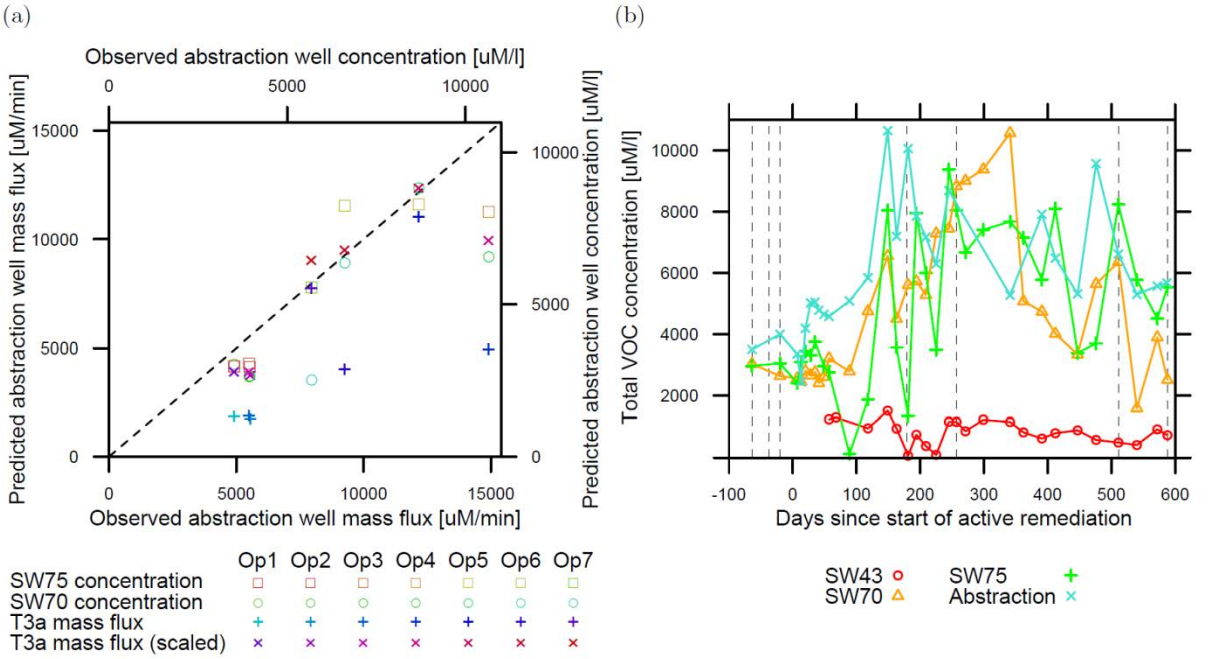

Figure 5.8: SW70, SW75 and T3a as predictors of observed total molar chlorinated ethene (TCE, cDCE, VC and E) concentration and mass flux at the abstraction well (a) SW70 and SW75 concentration vs. abstraction well concentration for all operations; T3a mass flux vs. abstraction well mass flux for all operations. T3a fluxes calculated using kriged hydraulic conductivity and chloroethene concentration distributions assuming: (1) flow through T3a is perpendicular to the transect; (2) flow proportional to hydraulic conductivity; (3) total flow through T3a is equivalent to abstraction rate (1.4 l/min); T3a mass flux data points (blue crosses) calculated using original hydraulic conductivity distribution (from Hvorslev analysis of falling head tests), T3a mass flux (scaled) data points (purple xs) calculated using numerical modelling calibrated T3a K distribution (Figure 5.11 b). (b) Total molar chlorinated ethene concentration in SW70, SW75, the abstraction well and SW43 (located immediately upgradient of the cell entrance) as a function of the time since start of active remediation. Dashed lines indicate the timing of the seven sampling operations (Op1 - Op7).

Data during the seven sampling operations were relatively limited due to intermittent ethene sampling, however in general molar fractions of TCE and its daughter products

remained constant or became further dechlorinated when comparing SW70, SW75 and the abstraction well (Figure 5.9). An exception occurred during operation 5 when non-detection of TCE in SW70 suggests either other pathways were contributing to the TCE detected at SW75 and the abstraction well or possibly some analytical/sampling uncertainties.

Increases in VC and Ee in SW75 and the abstraction well relative to SW70 during active remediation (Figure 5.9) suggest continued breakdown of TCE and cDCE as the dissolved phase plume travels down the cell. The column experiments of Mack et al. (2010) , carried out in support of SABRE field work, support reductive dechlorination in the dissolved plume. They found that biodegradation in the plume was an important mechanism for complete reduction of TCE and that such reduction caould be rapid in the presence of suitable electron donors.

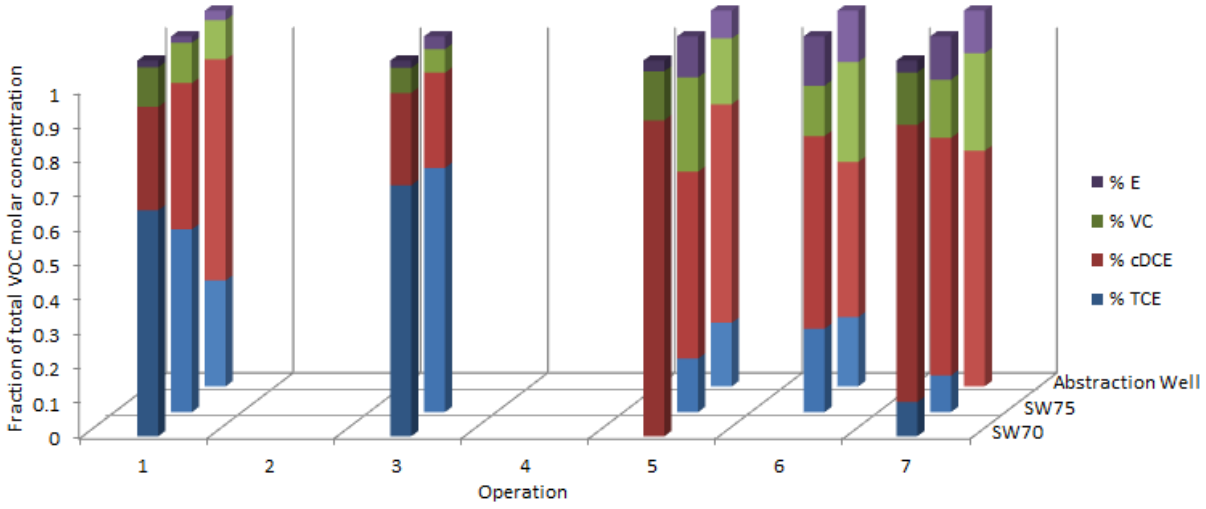

Figure 5.9: TCE, cDCE, VC and Ethene (E) as a fraction of total chlorinated ethene molar sample concentration; data shown are from SW70, SW75 and the abstraction well for all 7 sampling operations (samples which did not include analysis for ethene are excluded for the plot)

Increases in chloride concentration above background can provide a conservative indicator of TCE dechlorination (one chloride ion is produced in each dechlorination step from TCE -> cDCE -> VC -> E). Background chloride concentrations, estimated at the entry to the cell from sampling of SW43, ranged from 88 to 150 mg/l. However, even accounting for these background values, estimates of additional chloride inferred from observed molar

concentrations of cDCE, VC and Ee were not sufficient to fully account for the high chloride levels observed in SW70, SW75 and the abstraction well. However, anaerobic degradation rates of ethene are high in comparison to its more chlorinated parent products (Clement et al., 2000). Use of an additional constant to account for removal of ethene (fitted to be 0.5, such that 0.5 ethene moles are removed for every one mole remaining in the sample) provided an improved match between moles of chloride observed and moles of chloride predicted from daughter products present (Figure 5.10).

Observation of total chlorinated ethene concentrations (Figure 5.8), daughter product molar fractions (Figure 5.9) and chloride concentrations (Figure 5.10) confirm previous evidence that, by the very nature of the sample bias towards high-K zones, pumped samples from both monitoring wells were representative of pathways important to mass removal from the source zone and transport to the abstraction well.

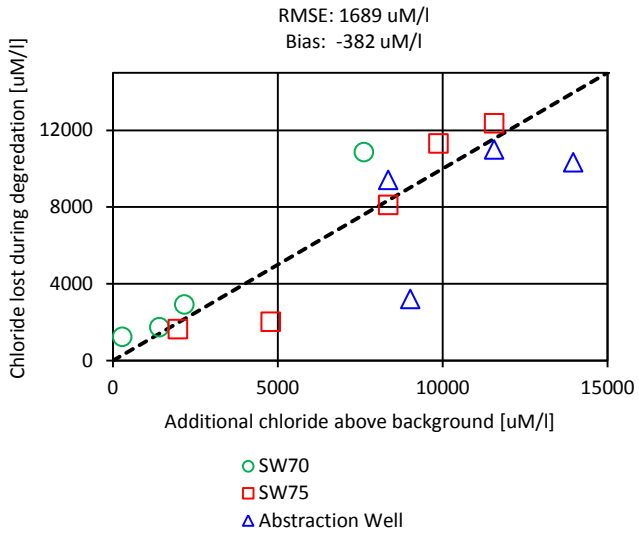

Figure 5.10: Additional chloride ions above background compared with estimated chloride ions produced from reduction of TCE

5.3.4 Numerical modelling as a means to understand monitoring well concentrations

The ML transect ports provided insight into the possible origin of the monitoring well samples (Figure 5.6). However, due to the physically and chemically heterogeneous environment well capture zone (and hence sample concentration) variation with time and

pumping rate are difficult to estimate. Numerical modelling allowed the capture zone dynamics to be further investigated. Using a cell permeability distribution interpolated/extrapolated (see Section 5.2.3.1) from T2a/T3a falling head permeability distributions, a best match to monitoring well sample concentrations was obtained after 30 minutes of pumping (Figure 5.11 a and b). However, the match obtained was imperfect. For SW70 (Figure 5.11 a), the match with observed TCE and VC concentrations was generally good but cDCE concentrations were overestimated. For SW75 (Figure 5.11 b), TCE concentrations were underestimated particularly in operations 4 to 7.

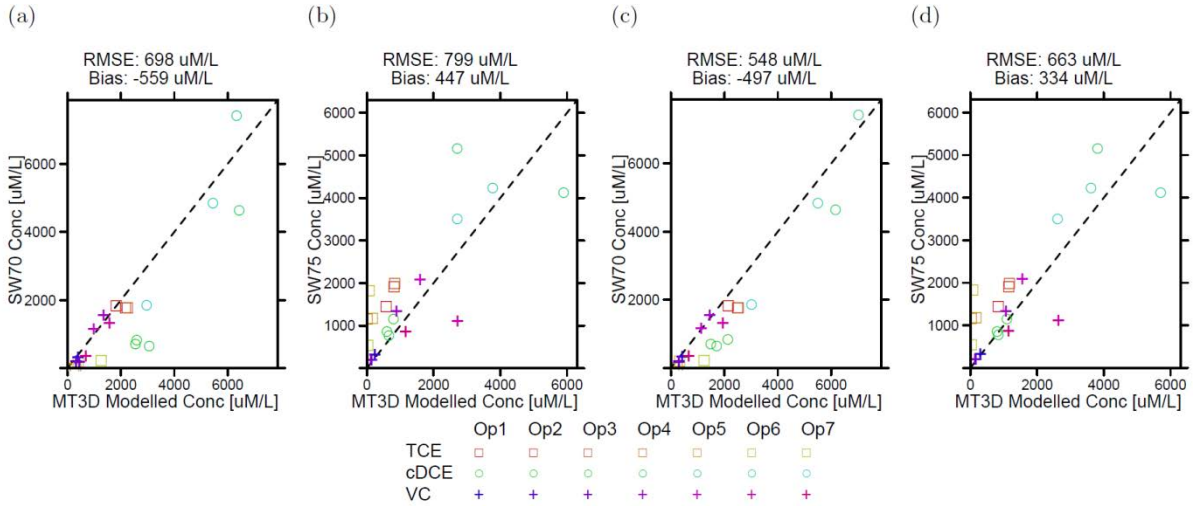

Figure 5.11: Simulated vs. observed SW monitoring well VOC sample concentration using: initial model K distribution (a and b) and scaled K distribution (c and d). Sampling rate is 1 L/min; sample taken after 30 minutes pumping. (RMSE and bias for best fit transect ports (Figure 5.6 b, g), excluding ethene, are 225 uM/l and 2 uM/l respectively for SW70; 644 uM/l and -212 uM/l respectively for SW75)

Model predictions using the starting permeability distribution were similar to those obtained by averaging upgradient port concentrations (Figure 5.6 c, e); insufficient weighting was given to the contribution to well inflows from the high-K zone at 5 m bgl in the cell. Model predictions Figure 5.11 c and d) were improved by weighting the transect hydraulic conductivity distribution adjacent to the screen interval towards this zone of preferential flow (Figure 5.12 a and b).

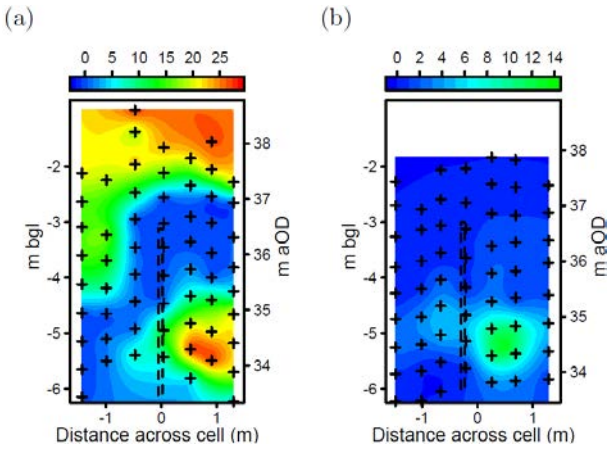

Figure 5.12: Calibrated T2a (a) and T3a (b) K distributions

Comparison of the simulated monitoring well capture zones (MODPATH) using the initial (Figure 5.13) and calibrated (Figure 5.14) hydraulic conductivity distributions demonstrated the difference in capture zone that resulted from this increased weighting towards the high-K zones in the lower half of the screen interval. The change in capture zone following K calibration was more significant in SW70 (Figure 5.14 a, b, c compared with Figure 5.13 a, b, c). The permeability distribution was such that the majority of the monitoring well sample was drawn from the lower half of the screen interval even after 60 minutes of pumping (Figure 5.14 c). After 15 minutes of pumping (removal of 2.5 screen volumes) in SW70 and SW75, the well capture zone had still not spread to encompass the entire screen interval (Figure 5.13 a, d; Figure 5.14 a, d). The time (in screen volumes purged) until a screen integrated sample is achieved depends on the relative volumes of water entering different parts of the screen and moving to the pump intake: this volume is a function of screen inflows (and therefore the permeability distribution).

Modelled SW monitoring well concentration was relatively insensitive to the model K-distribution in regions not immediately adjacent to the screened interval (both laterally and above the screen interval). Rather, it was the local permeability (and in particular the relative contrast in permeability immediately adjacent to the screen interval) that assumed most importance in determining the contribution to sample concentration from different parts of the

screen interval (Figure 5.13, Figure 5.14). The hydraulic conductivity values of the low-K zones adjacent to the screen interval in both SW70 and SW75 (Figure 5.12 a, b) were similar. However, the contribution to the pumped sample from the low K zone adjacent to SW70 is much less (Figure 5.14 a, b, c) than that from the low K zone adjacent to SW75 (Figure 5.14 d, e, f). In determining well inflows it is the relative difference in permeabilities that is important and not the absolute values.

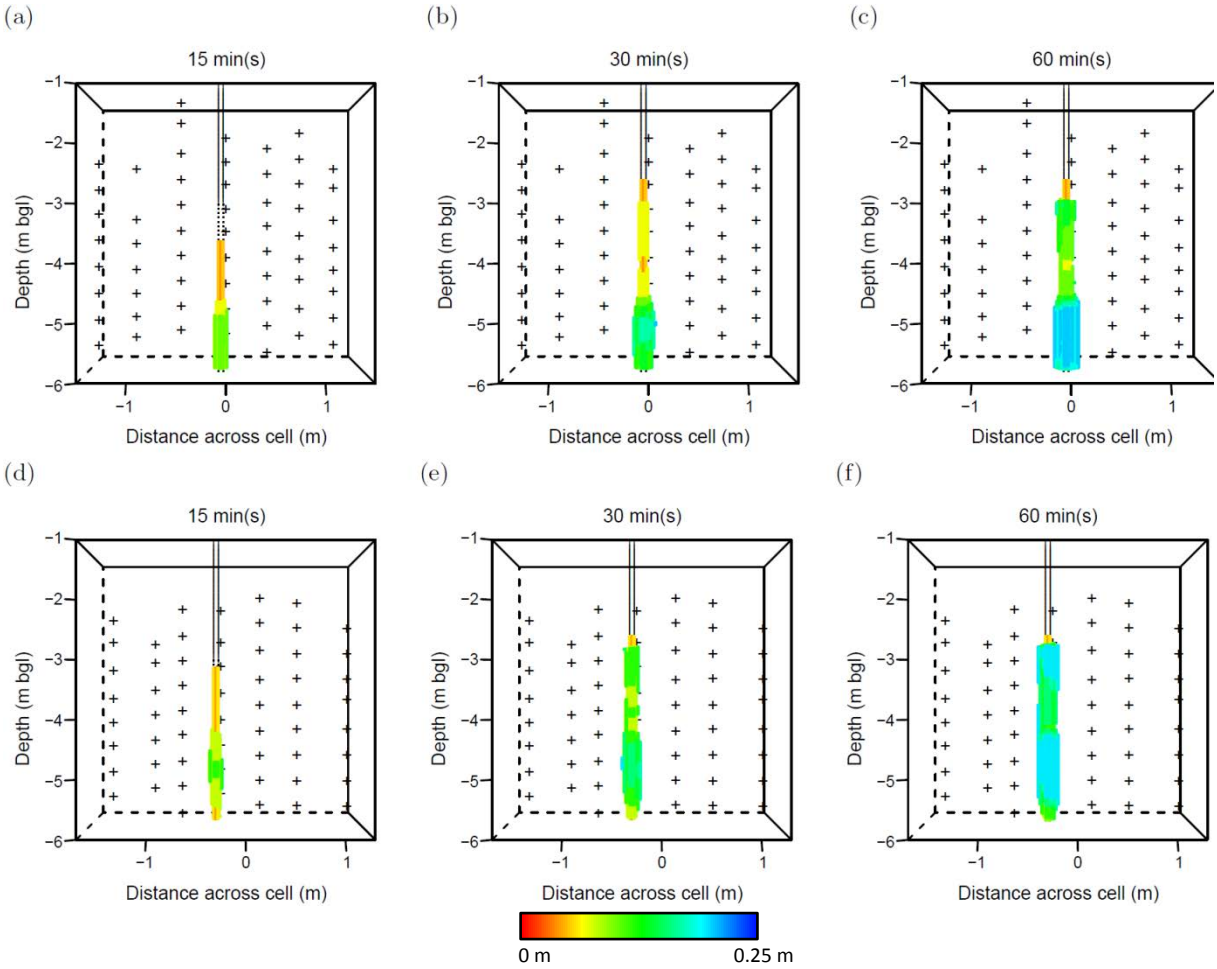

Figure 5.13: SW70 and SW75 simulated pumping capture zone for initial model K distribution. SW70 is top row (a - c), SW75 is bottom row (d – f) The pumping rate is 1 l/min. Capture zones shown are after 15, 30 and 60 minutes of pumping (2.5, 5 and 10 screen volumes). Particle colour indicates radial distance from well; crosses are upgradient ML port locations; dashed lines indicated the well screen, solid lines the well casing.

While monitoring well samples were very sensitive to the local permeability distribution, sampling results from such wells were insufficient to constrain hydraulic conductivity estimates at a distance from the monitoring wells. T2a tracer test results and mass flow estimates through T3a provided better metrics of whole transect flow and transport properties.

Observed peak tracer test breakthrough in the high-K zone at 5 m bgl in T2a was 1 - 2 days (Figure 5.7). Modelled advective breakthrough time (calculated from particle tracking using the initial model K distribution) was 7.9 days. Simulated values were close to the cell averages; much like the simulated monitoring well sample concentrations (Figure 5.11 a and b), insufficient weighting was given to the high-K zone. By comparison, weighting the model hydraulic conductivity towards the high-K zone in T2a (Figure 5.12 a) gave both a better match to observed SW70 monitoring well sample concentration (Figure 5.11 c) and a much improved advective travel time estimate in this region (2.7 d).

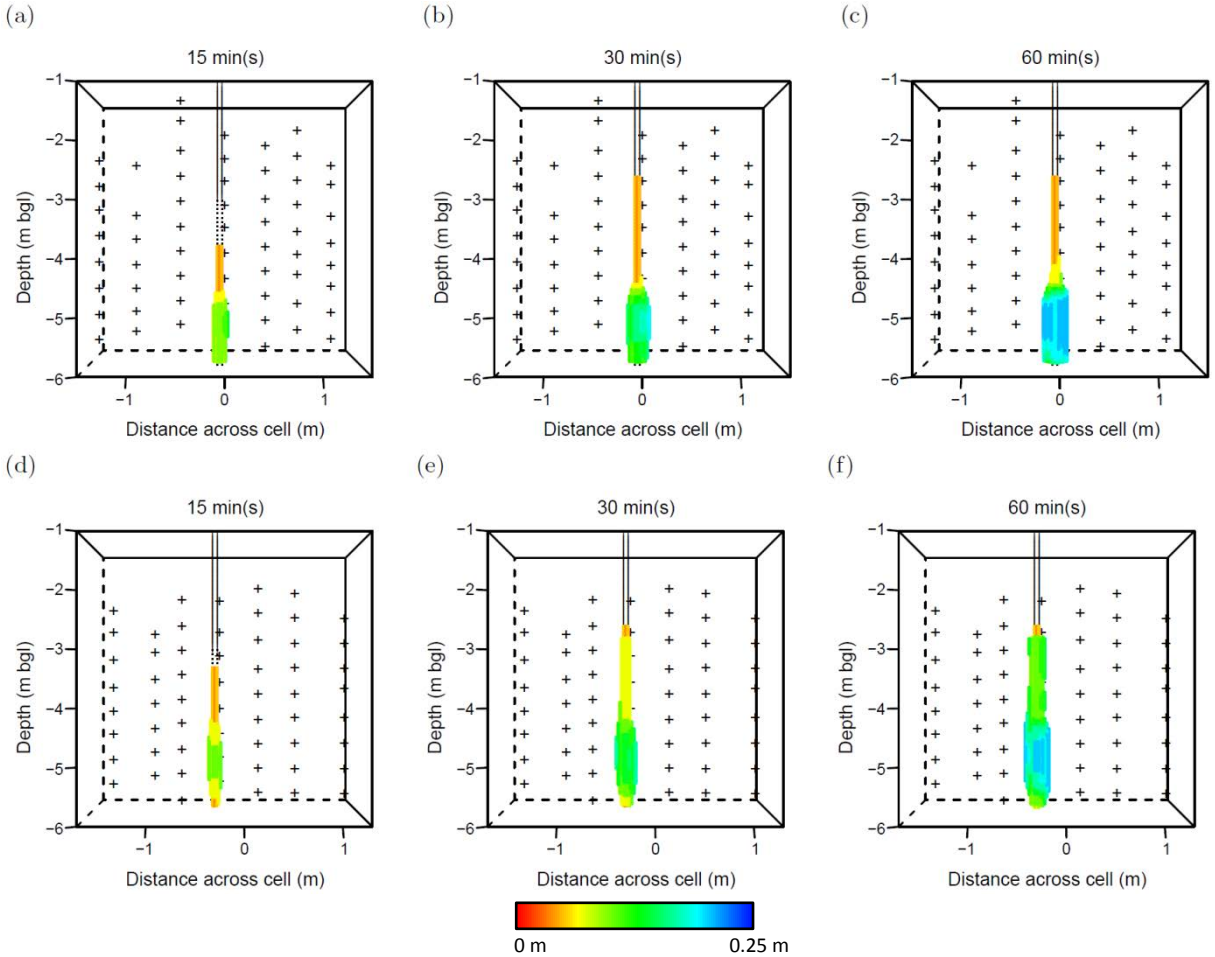

Figure 5.14: SW70 and SW75 simulated pumping capture zone for calibrated model K distribution. SW70 is top row (a – c), SW75 is bottom row (d – f). The pumping rate is 1 l/min. Capture zones shown are after 15, 30 and 60 minutes of pumping (2.5, 5 and 10 screen volumes). Particle colour indicates radial distance from well; crosses are upgradient ML port locations; dashed lines indicated the well screen, solid lines the well casing.

Using the initial T3a hydraulic conductivity distribution to provide a Darcy flux estimate for calculations of chlorinated ethene molar mass flux through T3a gave a poor match with

observed abstraction well mass flux rates (Figure 5.8 a, blue cross symbols). For all but two of the sampling operations (Op 5 and Op 7), chlorinated ethene molar mass flux was greatly underestimated. This poor mass flux estimates occur despite a sufficiently high sampling density at T3a (3.75 points/m^2) to minimize mass flux estimate uncertainty (Li et al., 2007; Béland-Pelletier et al., 2011; Cai et al., 2012). Initial T3a permeability distributions gave too much weight to abstraction well contributions from the upper half of the cell where lower chlorinated ethene concentrations were found. Due to their reduced water levels, Operations 5 and 7 did not include flow from this part of the cell and hence mass flux estimates were much better. To obtain a good match to abstraction well mass flux estimates across all operations (Figure 5.8 a, purple x symbols) it was necessary to almost entirely prevent flow to the abstraction well from the upper half of the cell at T3a (Figure 5.12b). The abstraction well is cased to approximately 3 m bgl; a laterally extensive low-K layer (as observed in T3a at 3 to 4 m bgl) might be sufficient to have prevented groundwater above the low-K layer from reaching the abstraction well; alternatively some other barrier to flow must have existed between the upper half of T3a and the abstraction well. The existence of such a barrier (and hydraulic separation from flows lower in the cell that originate from the source zone) during SABRE sampling is further supported by the consistently very low molar chlorinated ethene concentrations recorded above 4 m bgl in T3a (Figure 5.5) and by heads observed at T3a (Figure 5.15). Cross cell hydraulic heads recorded in T3a were consistently higher above 3.5 m bgl when compared with those recorded below this point. Existence of such a barrier to flow (and therefore dissolved plume bypass of the top half of the cell) is also supported by consideration of a snapshot of the dissolved plume taken from a transect orthogonal to the cell at day -49 (Rivett et al., 2014). Convergence of the chlorinated ethene dissolved plume towards the lower half of the cell by T3a was clear. Flow bypass of the top half of the cell

would account for the large (and not previously fully explained) concentration decreases seen in the top half of the cell at 20 m down cell when compared with upgradient concentrations.

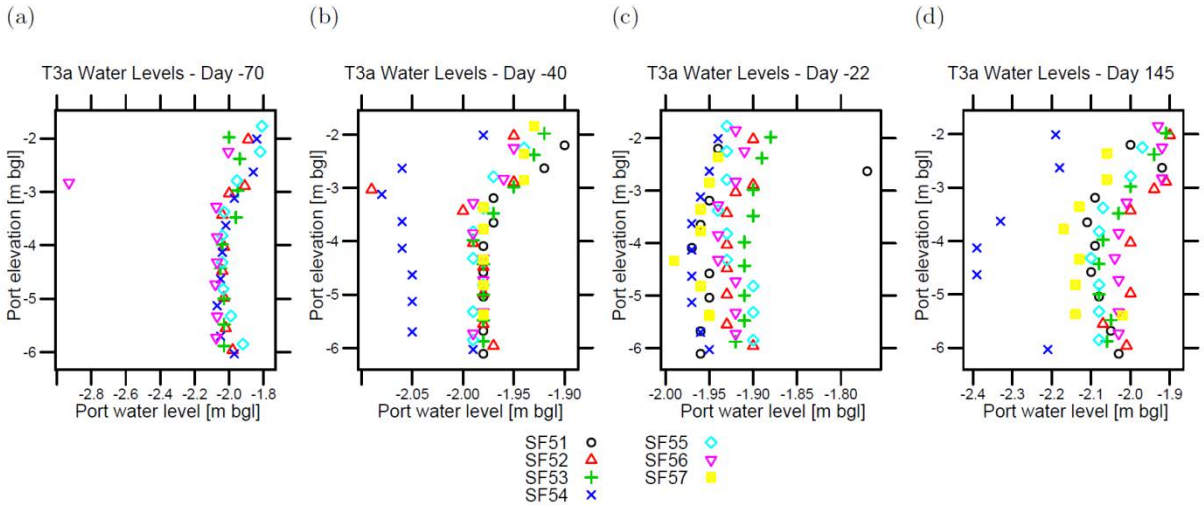

Figure 5.15: Variation in T3a water levels during SABRE cell operation. Day -70, -40 and -22 are during operations 1, 2 and 3, respectively (baseline sampling operations); day 145 is during operation 4.

Heads recorded below 3-4 m bgl in T3a generally showed little variation with depth (Figure 5.15). However, heads at SF54 (the multi-level directly upgradient of SW75) were typically lower than those in the adjacent multi-levels (Figure 5.15 b, c, d). During later operations (Figure 5.15 c and d, Operation 3 and 4) the lowest heads in SF54 were found adjacent to the higher permeability zone at 5 m bgl in T3a. Such heads suggests the presence of the screen interval of SW75 resulted in convergence of flow towards the screen during cell operation. Groundwater entering from all portions of the screen interval may have preferentially exited into the high gravel pathway at 5 m bgl.

5.3.4.1 Predictive modelling of alternate sampling strategies

At long times (> 3 screen volumes (SV) purging), numerical modelling suggested that monitoring well sample concentration is independent of the pumping rate and pump intake locations considered (Figure 5.16). Such pumping rate independence was to be expected given steady-state screen inflow rates depended on the variation in permeability local to the screen interval and were independent of pumping rate and pump intake location in SW70 and

SW75 (Figure 5.17 a and b). The exception was if drawdown was sufficient for cell water levels to enter the screen interval. During Operations 5 and 7, cell water levels were within the screen interval at SW75. For these two operations, the long-time screen inflows depended on the pumping-induced drawdown in the well and hence the pumping rate (Figure 5.17 c). Interestingly, while screen inflows varied with pumping rate during operations 5 and 7 in SW75, simulated SW75 monitoring well concentrations varied little (Figure 5.16 d, e, f). This lack of simulated sample concentration variation with pumping rate can be explained by: (1) the small contribution to total screen inflow from the top half of the screen (due to bias towards the high-K zone at 5 m bgl); (2) convergence of flow from higher up in the formation (as evidenced by the small peaks in the inflow profiles at the water level in Figure 5.17 c).

Early time (< 3 SV) simulated sample concentration was independent of pumping rate but did depend on the pump intake location (Figure 5.16). Differences in early time simulated sample concentrations as a function of pump intake location were only significant if a large concentration contrasts existed across the screen interval (e.g. Op 1 TCE: Figure 5.4 b and Figure 5.5 b, Figure 5.17 a and d). Where little or no concentration contrast existed with depth (e.g. T3a VC concentrations during Op1 – 3, Figure 5.5 r, s, t, Figure 5.17 f) variation in sample concentration with pump intake location was small or negligible.

The change of simulated sample concentration with time during early times (< 1 screen volume) was also a function of the variation in chlorinated ethene concentration with depth adjacent the screen interval. Greatest sample variation with time occurred when variation in chlorinated ethene concentration across the screen interval was high (e.g. during Ops 1 - 3 for SW70, Figure 5.4; Figure 5.16 a, b, c). Pump intake location can also be important in early-time sample variation. The greatest change in simulated sample concentration with time occurred when starting concentrations were very different from the permeability-weighted, long-time average (e.g. SW70 cDCE, Ops 1-3, Figure 5.4 j, k, l; Figure 5.17b).

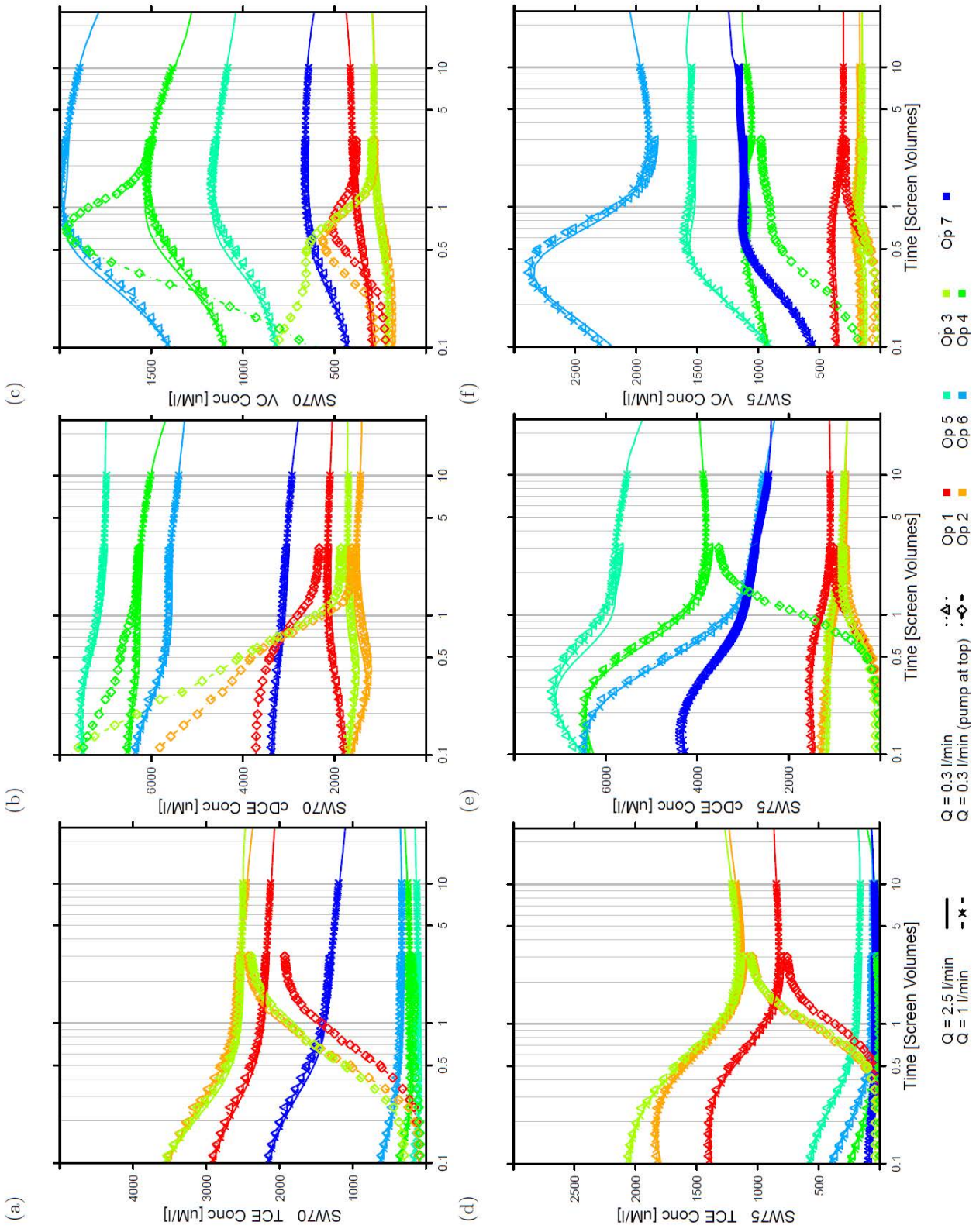

Figure 5.16: Simulated SW monitoring well sample concentration as a function of pumping rate, shown in screen volumes; one screen volume is 6 l. Pumping rates are 2.5 l/min (solid lines), 1 triangle data points). For the diamond data points the pump intake was located at the top of the located at the bottom of the screen interval. Pumping from the top of the screen interval is not in within the screen interval. Data point/line colour indicates the sampling operation. Calibrated

During predictive modelling, the initial well contaminant distribution was assumed representative of that found in the immediately upgradient multilevel; full vertical mixing across the well screen was not assumed. Different starting conditions would clearly have had an impact on early time sampling predictions. However, the analytical solution of Martin-Hayden (2000) suggests that the relationship between early time sampling variability and near-screen vertical stratification in contamination remains even if in-well starting conditions assume a fully mixed sample for example.

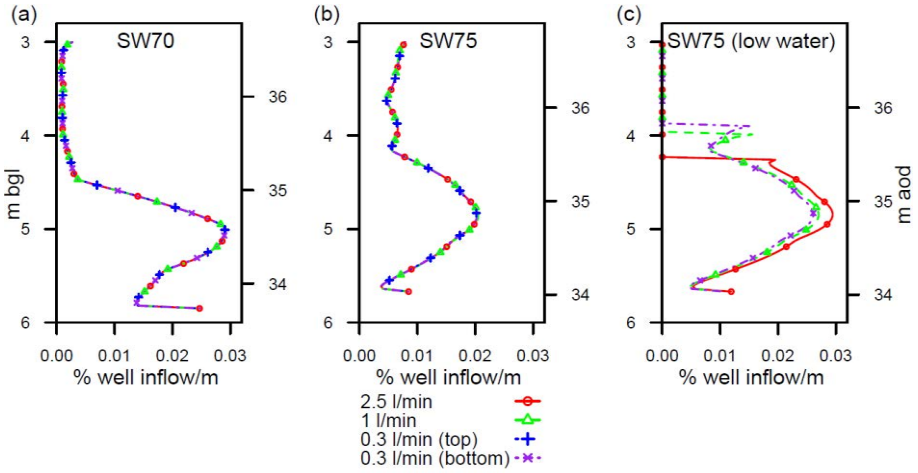

Figure 5.17: Monitoring well screen inflows per m as a function of pumping rate for: (a) SW70; (b) SW75; (c) SW75 with rest water level within the screen interval. Pumping rates and pump intake locations are as per those in Table 5.3.

The possibility of using early time variations in sample concentration as an indicator of contaminant variability has been previously suggested, for example from consideration of analytical solution results of Martin-Hayden (2000). However, practical observation of such changes may be difficult. Direct observation of changes in the contaminant of interest with time depends on taking multiple early-time samples (and that laboratory analysis requirements do not preclude the use of relatively small sample volumes). Alternatively, inline measurements may be possible if a more easily measurable analogue (e.g. electrical conductivity, dissolved oxygen) exists. However, equilibration of sampling equipment when purging first starts may make it difficult to reliably observe early-time variations in such field

parameters. The time to remove one screen volume may also have a bearing. For pumping rates of 0.3, 1 and 2.5 l/min, the time to remove 1 screen volume is 20, 6 and 2.4 minutes respectively. In addition to minimizing drawdown, lowering the pumping rate has the advantage of allowing a greater time in which to collect samples or allow field equipment equilibration. The disadvantage is that the overall sampling event will take longer.

After removal of 2 - 3 SV, early time variations in sample concentration (due to the influence of pump intake location or vertical contaminant distribution) have largely been resolved; sample concentrations were drawn from across the screen interval (Figure 5.14) and relative stability resulted. The requirement to remove 2-3 screen volumes to achieve stability was indicated also from the modelling of Martin-Hayden et al. (2014) (to account for partial mixing and transport times to the pump) and from numerical modelling in Chapter 3 (to account for the delayed arrival of casing water at the pump). However, in such a physically and chemically heterogeneous environment true stability may never be achieved. Sample concentrations were still subject to change with purging time even after two to three screen volumes had been removed (Figure 5.16). This long-term variation was the result of water of different concentration located at a distance in the aquifer arriving at the pump intake location. Dispersion meant changes with time became less pronounced but it is likely that a truly unchanging sample concentration would never have been achieved.

5.3.4.2 Model limitations

Uncertainty in falling-head permeability measurements or chemical analyses is relatively easily quantified by means of repeat measurements. However, a much greater contribution to model uncertainty is made by factors inherent to the assumptions and processes involved in data assimilation and model construction. For example, in heterogeneous dissolved phase plumes, small zones may be important for transport away from the source zone. In the field observations of Brooks et al. (2008) and (Guilbeault et al., 2005) 75 % of source zone mass

discharge was observed to occur across only 5-10% of dissolved plume cross sectional area. T2a and T3a sampling density are sufficient to minimize uncertainty (Li et al., 2007; Béland-Pelletier et al., 2011) . However, despite such high resolution sampling, the in depth statistical analyses of Béland-Pelletier et al. (2011) suggest sampling density is still the largest contributor to mass flux estimate uncertainty.

Extrapolation of the interpolated transect permeability and concentration distributions can only multiply these uncertainties. The modelling presented here is focused on the monitoring wells immediately downgradient of their respective transects. The assumption of continuity of concentration and hydraulic conductivity can perhaps be justified over the short distances considered (< 50 cm). This assumption is a result of the cell-constrained flow direction and the fact longitudinal dispersion is expected to be much greater than transverse dispersion (in the vertical and horizontal). However, such an assumption relies on plume-fringe effects, which can result in steep concentration gradients (Cieslak et al., 2015), not being important. Similarly, given the deposition environment, continuity of permeability is perhaps more likely in the horizontal than the vertical. However, if inferences were to be drawn from modelling away from the transects they can, at best, be taken as a general guide.

Confidence in model predictions can be improved by incorporation of varied data into model calibration. Data providing information on larger scale flow and transport (i.e. the tracer test or mass flux metrics such as abstraction well concentration) gave greater confidence in model calibrated results. Indeed, the holistic approach to data incorporation was also an improvement on previous attempts to predict in-cell conditions. For example, T3a permeability interpolation and the assumption of a uniform hydraulic gradient (as in the approaches of Cai et al. (2012)) was insufficient for estimating chlorinated ethene mass flux when downgradient barriers to flow exist.

Despite best efforts, it is certain that any model is non-unique. For example, transport times can be calibrated by adjusting permeability or porosity. Assumptions of uniform porosity, and indeed the lack of temporal variability in porosity and hydraulic conductivity (despite observations of possible clogging in the cell, Cai et al. (2012)) may be incorrect.

5.3.5 Reverse flow tests

From consideration of data from the historical SABRE monitoring well sampling rounds, supplementary lines of evidence from the tracer test and abstraction well concentration observations, and the numerical modelling presented herein it has been inferred that samples from SW70 and SW75 were very much biased towards the high-K zones at 5 m bgl. The bias towards these high-K zones at the bottom of the screen intervals was significantly more than might have been suggested from consideration of hydraulic conductivity testing in the ML transects alone. Reverse flow testing was undertaken as a means to further confirm such inferences regarding sample provenance in SW70 and SW75.

Main stem (the main pump intake) samples from SW70 during 2014 (Figure 5.18, closed circles) suggest that, compared with the end of SABRE project sampling, chlorinated ethene concentrations were much reduced with total molar chlorinated ethene concentration well below TCE solubility limit. The absence of TCE and much higher chloride concentrations observed compared with the end of SABRE project sampling suggest further biodegradation post SABRE.

Excluding VC, there was little variation in main stem pumped concentration with time: changes were relatively small both for both the other chlorinated ethenes present (cDCE, Figure 5.18 b; no TCE is detected, Figure 5.18 a) and the inorganics (chloride and sulphate, Figure 5.18 d and e). Even for VC, main stem samples (with the pump intake located at the bottom of the screen interval) had stabilised after 3 SV of purging (pale and dark green closed circles, Figure 5.18 c). While main-stem pumped samples may have shown little variability,

non-main stem samples (the interim depth samples) taken with the pump intake located at the bottom of the screen showed concentration distributions in the well were not uniform with depth (Figure 5.18, open circles). This was the case even for the baseline conditions before purging started (Figure 5.18, red open circles). For example, with the pump intake at the bottom of the screen interval, and even once main stem concentrations have stabilised, concentrations of cDCE (Figure 5.18 b) and VC (Figure 5.18 c) recorded in the screen interval above the pump intake were 5 to 6 times higher than those recorded at the main stem (Figure 5.18, dark and light green data points). By contrast, chloride concentrations (Figure 5.18 d, dark and light green data points) were higher (~900 mg/l) at the pump intake when compared with those recorded in the non-main stem samples above (~750 mg/l). Unlike the full mixing across the screen interval predicted from the laboratory experiments of Britt (2005) for example, the data suggest groundwater quality stratification was present in SW70. Such stratification may have been the result of small (or even negligible) flow through the well screen due to the non-operational cell.

Non-main stem samples from interval 1 (taken from within the casing) suggest chlorinated ethenes in the casing were higher than main-stem stabilised values (Figure 5.18 b, c); casing chloride concentrations were lower than main-stem stabilised values (Figure 5.18 f). However, drawdown in SW70 during pumping at 0.38 l/min was only 25 cm. There was insufficient drawdown to account for the high chlorinated ethene concentrations and low chloride concentrations observed in the well screen interval above 5 m bgl.

Main stem samples taken immediately on switching the pump intake location to the top of the screen interval (pale blue closed triangle, Figure 5.18) were broadly consistent with the previously observed non-main stem sample from that location. However, after purging a further 5 screen volumes, main stem (and non-main stem) sample concentrations (dark blue

triangles, Figure 5.18) were comparable with stabilised concentrations observed with the pump intake located at the bottom of the well.

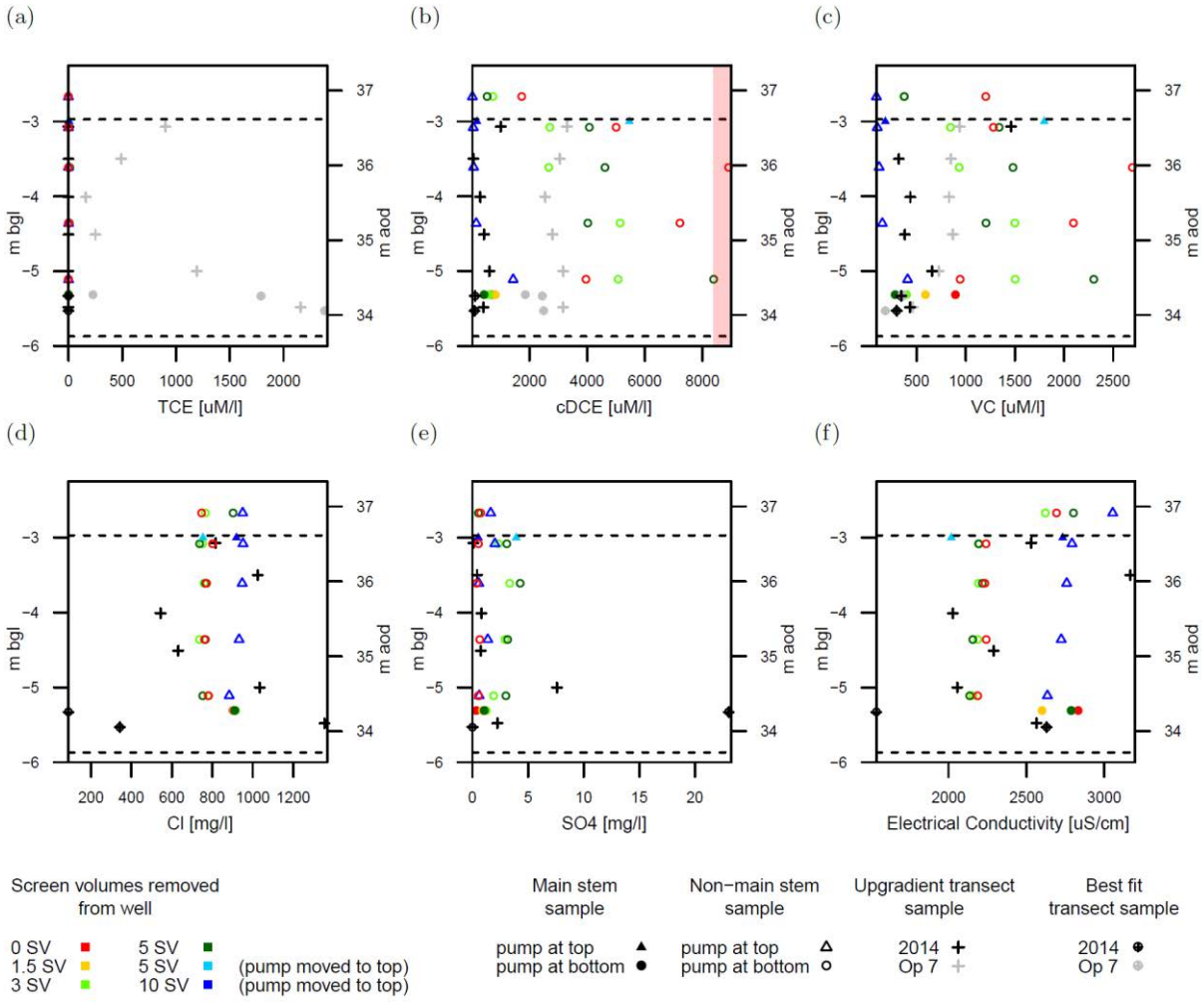

Figure 5.18: SW70 sampling results (April 2014): (a) TCE; (b) cDCE; (c) VC; (d) Cl; (e) SO_4; (f) EC. Coloured data points show the evolution in main stem (closed data points) and non-main samples (open data points) with purging time. Colour indicates the number of screen volumes removed. Circle and triangle data points are samples taken with the main stem pump intake located at the bottom of the screen interval and the top of the screen interval respectively. Greyscale cross and cross in circle data points are T2a samples; colour indicates transect sampling time (black is 2014, grey are values from the final SABRE sampling operation, Op 7); symbol indicates port location (cross data points are from T2a ports immediately upgradient of SW70 (black circles in Figure 5.6 b), cross in circle data points are from T2a ports in the high-K zone (dashed circles in Figure 5.6 b)). Pink shaded rectangle is TCE solubility limit.

The changes observed in screen interval concentration with pump intake location are evidence of flow bias in SW70. Indeed, significant flow bias must have existed to explain the lack of impact the high chlorinated ethene concentrations observed higher in the screen interval had on main stem sample chlorinated ethene concentrations. Well samples were very biased to inflows of low chlorinated ethene, high chloride groundwater at the bottom of the

screen interval. With the pump intake located at the bottom of the screen interval, high cDCE and VC concentration (but low volume) inflows located higher in the screen interval can be observed. With the pump intake located at the top of the screen interval, samples taken from throughout the screen interval were dominated by the high volume inflows at the bottom of the well. Such an inference was further supported by inline electrical conductivity values recorded during SW70 purging (Figure 5.19). On switching the pump intake location to the top of the screen interval after 5 well volumes an initial drop in electrical conductivity was observed, consistent with lower conductivity values observed higher up in the screen interval (Figure 5.18 f). Within 1 screen volume of further purging, main-stem sample concentrations had returned to those observed prior to changing the pump intake position. Any influence from the lower conductivity water observed higher in the screen interval was drowned out as the higher conductivity water entering the well from the bottom of the screen interval arrived at the pump intake.

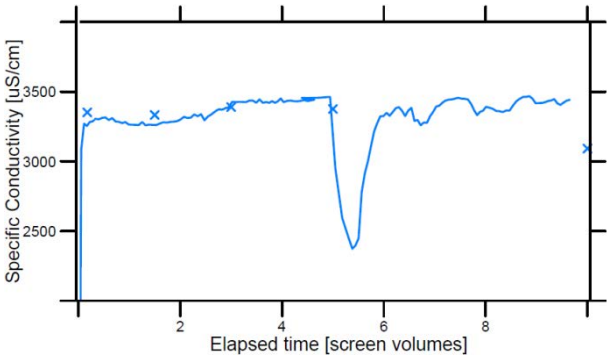

Figure 5.19: Main stem electrical conductivity with screen volumes removed. The solid line is inline electrical conductivity measured at the pump outlet; crosses are main stem sample electrical conductivity values taken at time intervals as specified in Table 2. The main stem pump intake location was switched from the bottom to the top of the screen interval of SW70 after 5 screen volumes of purging. The rise in conductivity immediately after starting pumping (0 SV) is due to equilibration of sampling equipment

5.3.5.1 Prediction of aquifer concentrations from reverse flow test analysis

RFT analysis to estimate aquifer permeability and concentration distributions was undertaken using combined cDCE, VC and chloride sampling data. Such analysis was able to give a good match to in-well concentrations observed with the pump intake located at the bottom and at the top of the screen interval Figure 5.20 a, b, c). RFT predicted inflows across the screen interval (Figure 5.20 d) were broadly consistent with those predicted from the hydraulic-conductivity-calibrated SABRE cell model (Figure 5.17 a). The RFT predicted aquifer concentrations distribution (+ symbols in Figure 5.20 a, b, c) were consistent with (although slightly lower than) those values recorded during the baseline sampling round undertaken prior to purging started (triangle symbols in Figure 5.20 a, b, c). However, it should be noted that, due to the very low contribution to pumped sample concentration from the upper third of the screen interval, the final RFT fitted solution is relatively insensitive to predicted aquifer concentrations in this region.

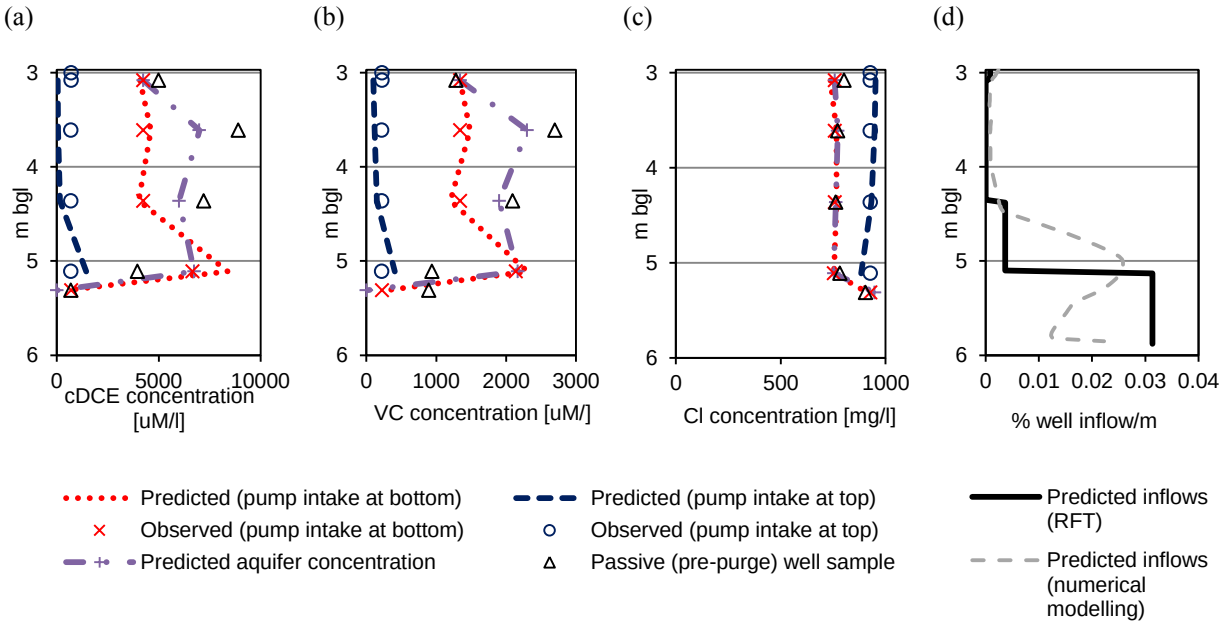

Figure 5.20: Reverse flow test prediction results. (a) cDCE results, (b) VC results, (c) chloride results, (d) reverse flow test predicted (and numerical modelling predicted) well inflows per metre depth in the screen interval. Final RFT RMSE values for cDCE, VC and Cl are 2288 uM/l, 369 uM/l and 62 mg/l respectively.

RFT predicted aquifer chloride concentration distribution was broadly supported by samples taken in the adjacent T2a transect (Figure 5.18 d, black data points). However, this

was not the case for the chlorinated ethenes (excepting TCE where concentrations were below detection limit across the board, Figure 5.18 a). Transect cDCE and VC concentrations (Figure 5.18 b and c) were generally similar in value to the integrated main stem sample; values recorded higher in the transect did not reflect the much higher values inferred from reverse flow test analysis (Figure 5.20 a, b). Transect sampling was undertaken using dedicated narrow diameter Teflon tubing. The tubing was installed to the depth of each port in the multilevel with at least 3 Teflon tubing volumes purged prior to sampling. However, sampling the multi-level transects was extremely difficult due to clogging; if the port intervals were clogged it is possible that the samples taken were representative of drawn down multi-level casing water and not groundwater from the aquifer adjacent to the ML ports. Alternatively, with low to no flow through the SW70 screen above 4 m bgl, water in this region may have been in chemical isolation from the transect 50 cm away. Higher chlorinated ethene concentrations may have been the result of stalled reductive dechlorination due to aerobic conditions local to the well. If aquifer concentrations immediately adjacent to SW70 were as predicted using RFT analysis then purging SW70 prior to sampling was not necessary. Passive sampling could adequately discriminate concentration with depth.

5.3.5.2 Notes on SW75

Neither TCE nor either of its daughter products was detected at SW75 (Figure 5.21). Chloride values were similar to background levels observed in SW43 at the inflow to the cell during SABRE operations (section 3.5). Little variation in inorganics concentration values or EC was observed with purging time (excepting baseline conditions), with depth in the screen interval or between the screen interval and the casing. As is the case with SW70, SW75 well concentrations were different from the adjacent multi-level transect. T3a chloride (and EC) values were higher than those observed in SW75.

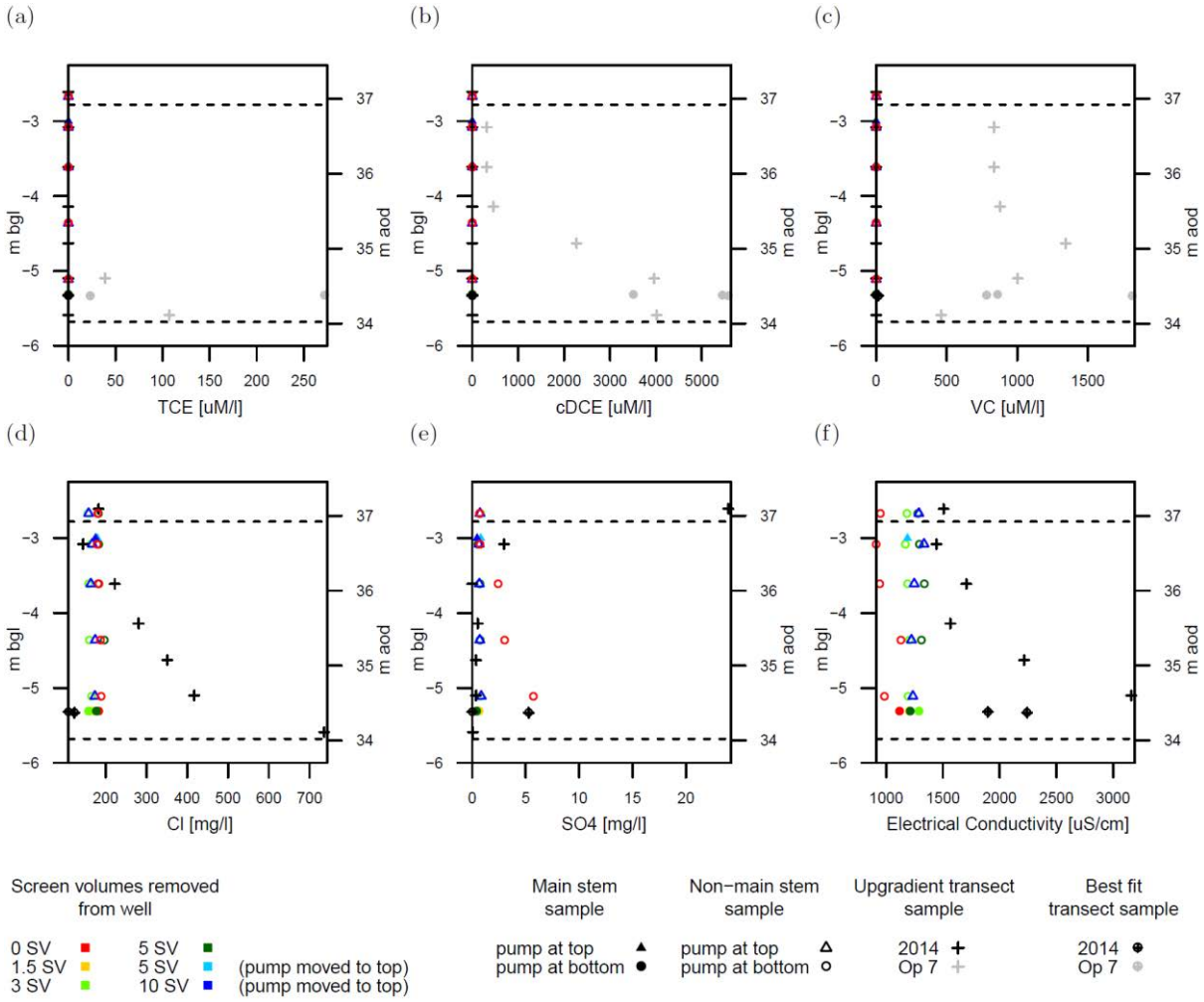

Figure 5.21: SW75 sampling results (April 2014): (a) TCE; (b) cDCE; (c) VC; (d) Cl; (e) SO_4; (f) EC. Coloured data points show the evolution in main stem (closed data points) and non-main samples (open data points) with purging time. Colour indicates the number of screen volumes removed. Circle and triangle data points are samples taken with the main stem pump intake located at the bottom of the screen interval and the top of the screen interval respectively. Greyscale cross and cross in circle data points are T3a samples; colour indicates transect sampling time (black is 2014, grey are values from the final SABRE sampling operation, Op 7); symbol indicates port location (cross data points are from T3a ports immediately upgradient of SW75 (black circles in Figure 5.6 b), cross in circle data points are from T3a ports in the high-K zone (dashed circles in Figure 5.6 b)).

The lack of chlorinated ethenes and near background chloride levels in SW75 suggests groundwater in SW75 was not representative of post-biodegradation cell water. Possible explanations for the water origin include upwelling from clay (upward head gradients have been observed previously, Dearden et al., 2013), possible leakage through the cell walls or recharge via the effluent trench located between the abstraction well and end of cell. In any case, there was insufficient variation in sample results to make reverse flow testing analysis possible.

5.3.5.3 RFT Conclusions

2014 RFT testing in SW70 corroborated previous inferences on groundwater quality sample provenance in the well. Samples origin in the screen interval is very much biased toward the bottom of the screen. As inferred previously, this is likely a result of the presence of the high-K zone here. RFT data also support the predictive numerical modelling; within 3 screen volumes of purging pumped sample concentrations had stabilised. SW75 results indicate a disadvantage of RFT as a means to assess well screen inflows with depth. Such assessment is not possible where there is little variation in groundwater quality with depth. However, in such a chemically homogenous setting sampling method, pump intake position and the relative contribution to groundwater quality sample from different parts of the screen assume less importance; the sample will be representative of the homogenous aquifer concentrations.

5.4 Conclusions

The study presented provides detailed field observations and numerical modelling to support the investigation into the origins of samples taken in 3 m monitoring wells in a chemically and physically heterogeneous environment within and immediately downgradient of a DNAPL source zone.

Numerical modelling and supporting field data confirmed that, at long times (> 3 – 5 screen volumes) monitoring well samples are independent of pumping rate and pump intake location. Samples are drawn from across the screen interval but weighted by vertical variations in permeability local to the screen. Hence, the monitoring well samples may not reflect maximum or minimum chlorinated ethene concentrations in the adjacent aquifer. At early times, purged sample variability depends on chemical stratification adjacent to the screen interval and the difference between initial concentrations in the well and long-time

permeability-weighted chemical concentrations. Even at late purging times, in such a chemically heterogeneous environment, true sample chemical stability may never be reached.

Where heterogeneities are significant, with K varying over orders of magnitude, mass flux from the high K zone will dominate and hence the concentration sampled will be most reflective of this transmissive zone. Such permeability-weighting is handy as the sampled monitoring well concentration is representative of the dominant flux through the aquifer. Hence monitoring wells can provide a reasonable indicator of dissolution of and transport away from a DNAPL source. Such information may be useful as an indication of remedial performance, for example. However, without considerable effort (e.g. RFT), such wells will not discern concentration heterogeneity in the aquifer. Samples from monitoring wells within or immediately downgradient of a DNAPL source zone may miss very high concentrations from a low-K highly contaminated pool zone where flow contribution are low and masked (diluted out) by the water quality in the more transmissive zones.

Understandably, data drawn from multi-level transect sampling provided significantly more insight into cross-cell contaminant distribution and possible DNAPL presence (Rivett et al., 2014). However, data drawn from permeability testing and water quality sampling from the multi-level transects alone were insufficient to estimate mass flux through the cell, to adequately predict tracer breakthrough times, or indeed accurately predict monitoring well concentrations. This is partly a function of the number of ML sampling points which despite being of sufficient density to minimise uncertainty may not pick up the extreme variability resulting in the very chemically and physically heterogeneous environment. Perhaps more importantly was the inability of spot permeability measurements to predict pathways important to transport through the cell. Monitoring wells should be seen as complementary to (rather than an alternative to) multi-levels.

Ultimately, the definition of an appropriate sample from a 3 m monitoring well depends on the sampling objectives. If there is little flow through the well screen, as is the case in 2014 sampling, multiple passive samples may be sufficient to discriminate formation concentrations with depth. However, under higher hydraulic gradients, bias from vertical flows that can be inferred from head gradients observed adjacent to SW75, may mean passive sampling is not able to adequately discriminate changes in formation concentration across the screen interval. At its simplest (and most repeatable), an appropriate sample from a 3 m monitoring well is a permeability-weighted sample drawn from across the screen interval. To obtain such a sample it is necessary to remove at least three screen volumes prior to sampling (assuming drawdown is minimised by low pumping rates). Even in low-flow sampling, monitoring to stability is insufficient; to achieve comparable samples at different points in time (for example for observing trends), more importance must be placed on recording the volume of water removed. Indeed, in a chemically heterogeneous aquifer such as the one considered here, chemical stability (which might never be achieved) perhaps assumes even less importance.

CHAPTER 6 CONCLUSIONS

6.1 Conclusions

Specific technical conclusions are made in the prior individual chapter conclusions. Here, overarching conclusions are drawn.

This thesis set out to critically examine groundwater quality sampling in long-screen monitoring wells. Appropriate ground water quality sampling is challenging in such wells due to uncertainty arising as a result of in-well mixing processes, permeability variation across the screen interval and vertical flows induced by naturally occurring vertical head gradients. Such factors may be manifest even in wells of relatively short (3 m) screen lengths. Rather than writing off the utility of sampling in such wells, four complementary studies at multiple scales of interest sought to answer the questions:

- What are appropriate samples from long-screen wells?
- What are such samples representative of?
- How best can such samples be obtained?
- How should data arising be most appropriately used?

Conclusions relating to each objective are presented below.

6.1.1 What are appropriate samples from long-screen wells?

Discussion in this thesis has demonstrated that there is no one measure of groundwater quality that is appropriate to all investigatory purposes. For example, in contaminated land investigation such as might be undertaken at the chlorinated solvent contaminated SABRE site (Chapter 5) the most appropriate sample may be one giving an indication of aquifer maximum concentrations at a point. By comparison, for Water Framework Directive type investigations in the East Yorkshire Chalk (Chapter 2) an appropriate sample may be one giving an average of water quality over a much larger extent of an aquifer. Hence, it can be

concluded that an appropriate groundwater quality sample from a long-screen (or indeed any) well is one suitable to the circumstances for which the sampling is being undertaken. Obtaining appropriate (rather than representative) groundwater quality samples should be the goal of any groundwater quality investigation.

6.1.2 What are samples from long-screen wells representative of?

Whatever the investigatory goal, there are three alternate sampling objectives in long-screen wells which all represent a different measure of groundwater quality:

(1) Permeability-weighted sampling. Here sample groundwater quality represents an integrated sample drawn from across the screen/open interval of the borehole but weighted by permeability variation over said screen/open interval.

(2) Depth-discrete sampling. Such a sample represents a point measurement of groundwater quality at the depth of the sampling device.

(3) Flow-stream sampling. Rather than attempting to overcome vertical flows (which the results demonstrate may be difficult or impossible) perhaps a new sampling objective (in addition to e.g. BSI (2009)) should be considered. In this approach, intra-well flow streams are specifically targeted with the sample representing the quality of groundwater flowing through the well under ambient conditions.

In a chemically heterogeneous aquifer, each of the sampling objectives discussed above may result in a different groundwater quality result being realised. Assuming appropriate method application (e.g. avoiding sampling casing water) such results, while they may be of different value, are all representative of some measure of groundwater quality in the adjacent aquifer. There is no such thing as a single representative sample from a well.

Whether what each of these sampling objectives represents is appropriate for particular investigatory need is often a question of scale: the scale of interest, the scale of heterogeneity and the scale of measurement. A permeability-weighted average sample from a 3 metre well

screen might be deemed a point measurement of groundwater quality in the Triassic Sherwood Sandstone or the East Yorkshire Chalk. However, at the chemically and physically heterogeneous environment permeability-weighted sample from such wells cannot be guaranteed to represent a point measurement of minimum or maximum concentrations in the adjacent aquifer. However, field evidence from the SABRE site shows that this is not universally true. Some of the permeability-weighted samples from the 3 m monitoring wells did provide an estimate of maximum or minimum concentrations in the adjacent aquifer. This was a result of such concentrations coinciding with zones of very high permeability.

6.1.3 How best can appropriate groundwater samples be obtained from long-screen wells?

There are three different sampling methods that can be used for obtaining groundwater quality samples from long-screen wells:

- Volume purge sampling
- Low-flow sampling
- Passive sampling

Each sampling methods is more or less appropriate for achieving the different sampling objectives discussed above.

If a permeability-weighted sample is the objective then pump and purge sampling methods are most appropriate. Despite literature reports to the contrary (e.g. Britt, 2005), a permeability-weighted sample cannot be guaranteed if passive sampling methodologies are used. If volume purging sampling methods are used (where significant drawdown is anticipated) none of the study findings conflict with existing recommendations (e.g. Gibb et al., 1981) that a minimum of three to five well volumes should be removed prior to sampling. If low-flow sampling is used (and with drawdown and disturbance hence minimised) results indicate a minimum of three screen volumes should be removed prior to sampling. Such

recommendations on purging volumes are irrespective of stability monitoring. If such guidance on purging volumes is followed then results indicate that the origin of the sample in the screen interval is independent of pumping rate and the pump intake location.

Numerical modelling found that pumping rates must be 10s of times the maximum ambient vertical flow rate in the borehole to overcome vertical flows and achieve a permeability-weighted sample. However, if significant vertical well flows exist (and hence aquifer cross contamination is occurring) then a permeability-weighted sample may still be biased towards these inflowing horizons. Such a finding supports the work of Mayo (2010) for example.

In some instances (e.g. the 3 m monitoring wells considered at the SABRE site in Chapter 5) it might be possible to obtain depth-discrete samples by taking multiple passive samples at depths in a long-screen well. However, even if vertical well flows are not present, uncertain mixing processes mean that such an outcome cannot be guaranteed. Indeed, the only way to guarantee high-resolution depth-specific sampling is to use very short wells with the logical endpoint being multi-level (point) samples. Given appropriate coverage of multi-level monitoring points such samples can provide an indication of aquifer concentration minima/maxima. However, findings here suggest that use of multi-level data can still lead to interpretation challenges. Multi-level concentration and permeability distributions may not accurately reflect mass flux through the aquifer even with relatively high monitoring point densities.

If flow-stream sampling is the objective then this study demonstrates that such sample can be obtained using passive sampling or pumping where the pumping rate is << 50 % of the ambient vertical flow rate in the well. Purging is not necessary to obtain such flow-stream samples. Even at long times, modelling and field data find that sample origin in the well screen/open interval depends on the pump intake/passive sampler location. Such samples can

be used to provide an indication of vertical variation in aquifer groundwater quality distribution. However, borehole flow logging carried out in this study suggests that accurate quantification of such variation may rely on repeat measurement of borehole flows.

6.1.4 How should data arising from groundwater quality sampling in long-screen wells be most appropriately used?

Appropriate application of data arising from long-screen wells may depend on a detailed conceptual model of the well-aquifer system under study. In particular, firm understanding of the flow system, chemical and physical heterogeneity may be important. In this study a number of alternative methods have been applied at various scales to assess aquifer chemical heterogeneity and characterise borehole flow system and physical heterogeneity. Such methods for assessing chemical heterogeneity as used here as well as literature alternatives discussed in previous chapters are summarised in **Error! Reference source not found.**. Techniques used in this study to characterise the flow system and physical heterogeneity and literature alternatives presented in individual chapter discussions are summarised in **Error! Not a valid bookmark self-reference.**.

Method (in order of expense and rigour)	Comments
Electrical conductivity or other chemical profiling	Danger of false negatives; qualitative; may not reflect contaminant of interest
Depth sampling	Danger of false negatives; in-well mixing uncertain; qualitative
Pumped sample chemical disequilibrium	Danger of false negatives; qualitative
Monitoring change in concentration with time during pumping	Danger of false negatives; qualitative; need to observe early time purging data (can be difficult if equipment equilibration slow and/or pumping rates are high)
Reverse flow testing	Need to ensure vertical flows aren't present (or are overcome by pumping); applicable in narrow diameter relatively short (e.g. 3 m) monitoring wells
Packer interval sampling	Time consuming; flow-bypass in gravel pack an issue in screened monitoring wells; packers may not be available for relatively short, narrow diameter monitoring wells

Table 6.1: Techniques to assess aquifer chemical heterogeneity

The existence of such chemical and physical characterisation methods is no magic bullet. Rigorous investigation requires significant resource input; interpretation of investigation method results may be non-trivial. Borehole flows may change (seasonally, tidally, with changes in nearby abstractions). In this study, differences in boreholes across a site (e.g. small variation in casing length; intersection or non-intersection with flowing fractures) resulted in quite different borehole flows. If qualitative knowledge of flows is required then repeated measurements (perhaps as a minimum under low and high water levels) are necessary on a per-borehole basis.

Method (in order of expense and rigour)	**Comments**
Use of geological logs to identify low permeability horizons; fracture location	Weak; qualitative; doesn't indicate direction
Desk study to assess groundwater setting (e.g. recharge/discharge zone; proximity to abstraction; significant vertical anisotropy etc.)	Weak, qualitative; may indicate likely direction of flow
Temperature logging	Qualitative; doesn't indicate direction
OTV/CCTV observations of particle movements	Qualitative; will give direction of flow
In-well tracer testing	Relatively inexpensive and low tech; most sensitive method for very low flow rates; tracer may require permission; relatively simple and quick model interpretation
Reverse flow testing	Assesses physical heterogeneity only (need to ensure vertical flows aren't present (or are overcome); applicable in narrow diameter, relatively short (3 m) monitoring wells
Geophysical flow logging (e.g. heat pulse, electro-magnetic, impeller flow measurements)	Can be slow; provides most direct measurement of flow; impeller and heat pulse have limited velocity ranges; not applicable at very low flow rates
Active Distributed Temperature Sensing	Not applicable at very low flow rates; quick to comprehensively characterise long boreholes; interpretation difficult
Packer interval testing	Slow, flow-bypass in gravel pack an issue in screened wells

Table 6.2: Techniques to assess borehole flows and physical heterogeneity

Without such comprehensive investigation as discussed above any data interpretation must accept that there is incomplete knowledge of the sample origin and that significant uncertainty exists as to what the sample is representative of. If wells are long relative to the scale of interest then it may be prudent to assume the worst (chemically heterogeneity, physical heterogeneity, a significant vertical head gradient leading to significant vertical flows in the sampling well). Such worst-case assumptions should be reflected in any model or interpretation of the system. Similar to modelling approaches considered herein, options

might include explicit modelling of the borehole column and sampling method in model calibration and assessing the sensitivity of model predictions to vertical head gradients.

However, while the studies presented here do not reflect every possible set of site conditions they demonstrate that, even without comprehensive system knowledge, samples from long-screen wells can still be highly informative. Sampling of maximum (or minimum) aquifer concentrations cannot be guaranteed (and from a regulatory perspective may make the use of such wells more difficult). By the very nature of long-screen well samples being biased to high permeability zones, sampling can provide a good measure of contaminant flux in the adjacent aquifer. Long-screen well samples can also provide a good indication of trends in groundwater quality in the adjacent aquifer. Such is demonstrated for two contrasting settings: (1) diffuse nitrate contamination in an agricultural region in the East Yorkshire Chalk; and (2) dissolved phase transport of chlorinated ethenes within and immediately downgradient of a heterogeneous source zone in a sand/gravel aquifer underlying a contaminated site. Ultimately, whatever the screen length and the sampling objective, consistency in method application is key for repeatable groundwater sampling.

From a practitioner perspective consistent application of terminology (Table 6.3) in literature and guidance might help in improving understanding of issues surrounding groundwater quality sampling in long-screen wells.

Terminology	**Definition**	**Comments**
Representative	Having typical characteristics of a wider group	There is no such thing as “a” representative sample; rather different groundwater quality samples may be representative of different things. Knowledge of what a sample is representative of may depend on (non-trivial) borehole investigations (e.g. flow logging).
Appropriate	Suitable to the circumstances	A groundwater quality sample fit for purpose. Acquiring such a fit for purpose sample should be the goal of any groundwater quality sampling event.
Sampling objective	The type of sample required: permeability-weighted, depth-discrete or flow-stream	Different sampling objectives return different metrics of groundwater quality. Sampling objective selection ultimately depends on why the sampling investigation is being undertaken (e.g. groundwater quality status assessment versus vertical distribution information for contaminated land investigation).
Sampling method	The method of sampling: volume purge; low-flow or passive (zero purge) sampling	Different methods may be more or less suitable for achieving different sampling objectives.

Table 6.3: Suggested groundwater quality sampling terminology definitions

One area not discussed during this study is the development of technologies that are designed to seal the open well screen allowing multi-level groundwater sampling and head measurements unperturbed by the borehole column (e.g. FLUTe liners, Cherry et al. (2007)). As the study presented here shows, even modest vertical gradients can be problematic in determining the origin of long-screen well samples. These technologies may allow the benefits of long-screen wells while preventing cross-contamination and minimising uncertainty in sample origin. Use of such technologies could be considered as an alternative to extensive borehole flow characterisation when sampling long-screen wells.

6.2 Recommendations for further work

The research undertaken in this thesis leads to a number of topics for which further research would be beneficial.

The numerical modelling in Chapter 3 considered fourteen different ambient vertical flow scenarios as the starting point to model ambient-flow biased sampling in long-screen wells. The well inflows and outflows generated from these vertical flow scenarios could be used as input to the single borehole tracer test model (Chapter 2) or A-DTS model (Chapter 4). This approach would allow the anticipated SBTT or A-DTS response to be simulated for these flow conditions. Such an exercise would produce a useful lookup guide for practitioners when interpreting data arising from these flow measurement methods.

Evidence from flow logging using Active Distributed Temperature Sensing (A-DTS, Chapter 4) supported inferences made from this modelling regarding the pumping rates required to overcome vertical flows in wells (Chapter 3). However, the implications resulting from the modelling in Chapter 3 would benefit from systematic investigation at the field scale. These investigations could seek to corroborate, in a variety of hydrogeological settings, (a) the transition from vertical-flow-biased to permeability-weighted sampling, and (b) the factors that are most important in influencing ambient vertical flows in long-screen boreholes.

This research could be combined into a lookup table listing hydrogeological characteristics (e.g. proximity to discharge zone, well screen length, geology) and providing guidance on the relative likelihood of vertical flows occurring in the sampling well and the chances of overcoming them if pumped sampling is used.

List of electronic appendices

Appendix No	Description	Details
1	Published outputs	Papers (1) McMillan, L. A., Rivett, M. O., Tellam, J. H., Dumble, P., Sharp, H. (2014). Influence of vertical flows in wells on groundwater sampling. Journal of Contaminant Hydrology 169: 50-61. (2) McMillan, L. A., Rivett, M. O., Tellam, J. H., Dumble, P. (2015). Groundwater quality sampling at contaminated sites: The long and the short of it. International Environmental Technology 25(2): 50-51. Conferences (1) McMillan, L. A., Rivett, M. O., Tellam, J. H. (2012). Rigorous sampling in long-screen wells, 39th IAH Annual Congress, Niagara, Canada, 16th -21st September 2012. (2) McMillan, L. A., Rivett, M. O., Tellam, J. H., Dumble, P., Sharp, H. (2013). Water quality sample origin in wells under ambient vertical flow conditions. European Geosciences Union General Assembly 2013, Vienna, Austria, 7th- 12th April 2013. (3) McMillan, L. A., Rivett, M. O., Tellam, J. H., Dumble, P., Sharp, H. (2013). Uncertainties in sample origin due to ambient vertical flows during low-flow sampling. 8th IAHS International Groundwater Quality Conference (GQ13), Gainesville, Florida, USA, 21st -26th April, 2013. (4) McMillan, L. A. (2013). Low-flow and passive sampling in long wells. RGS-IBG Postgraduate Mid-Term Conference 2013, Birmingham, UK, 25th – 27th March 2013
2	Chapter 2 data	Birmingham SBTT observations and models (2011 and 2012) Kilham SBTT observations and models (2012 and 2013) Kilham fieldwork logs Kilham water quality sampling data (2012 and 2013) VBA code for SBTT numerical model Numerical model vs. analytical solution (Ogata Banks) comparison Reynolds number calculations Laboratory CTD-diver sensitivity tests
3	Chapter 3 data	GWV model input files for vertical flow Scenarios 1 – 14 Particle tracing model output Flow scenario model output

		Comparison with Martin-Hayden analytical solution Spreadsheet of model discretisation details
4	Chapter 4 data	DTS observed data (ambient and pumping conditions) Fieldwork log Cable power calculations and Reynold number calculations Thermistor observed data and calibration Calibrated model output
5	Chapter 5 data	RFT fieldwork data and analysis - Method statement and risk assessment - Jones laboratory chemical analyses - Field notes - Photos - In-situ water quality monitoring (AquaTROLL) - Borehole conductivity profiles (CTD Diver) - Measured pumping rates during RFT test - RFT solver model Historical SABRE data - Abstraction well mass flux observations - ML transect falling head test K values - Op 1 – Op 7 T2a and T3a chlorinated ethene concentrations - SABRE sampling data for all wells SABRE Modelling - Discretisation details - Model Import files (K and chlorinated ethene distributions) - Model output files o Predictive modelling simulated pump concentration with time (four scenarios) o Simulated drawdown o Well inflows over screen interval (four scenarios) Calculation spreadsheets - Chloride at SW70, SW75 and abstraction well - ML port sampling density - SW chlorinated ethene well concentrations as a function of TCE solubility, fraction of TCE daughter products; TCE 10 % rule of thumb calculations Tracer test data - Tracer test observations and interpolated breakthrough at T2a files

List of References

Allen, D.J., Brewerton, L.J., Coleby, L.M., Gibbs, B.R. and Lewis, M.A., 1997. The physical properties of the major aquifers in England and Wales, British Geological Survey Technical Report WD/97/34, http://nora.nerc.ac.uk/13137/1/WD97034.pdf.

Allshorn, S.J.L., Bottrell, S.H., West, L.J. and Odling, N.E., 2007. Rapid karstic bypass flow in the unsaturated zone of the Yorkshire chalk aquifer and implications for contaminant transport. In: M. Parise and J. Gunn (Editors), Natural and anthropogenic hazards in karst areas: recognition, analysis and mitigation. Geological Society, London, Special Publications, pp. 111– 122, http://doi.org/10.1144/SP279.10

Annable, M. et al., 1998. Partitioning Tracers for Measuring Residual NAPL: Field-Scale Test Results. Journal of Environmental Engineering, 124(6): 498-503, http://doi.org/10.1061/(ASCE)0733-9372(1998)124:6(498).

Annable, M.D. et al., 2005. Field-scale evaluation of the passive flux meter for simultaneous measurement of groundwater and contaminant fluxes. Environmental Science & Technology, 39(18): 7194-7201, http://doi.org/10.1021/es050074g.

Appelo, C.A.J. and Postma, D., 2009. Geochemistry, groundwater and pollution, 2nd edition. A. A. Balkema Publishers, Leiden, the Netherlands.

ASTM, 2014. D6634M-14 Standard guide for selection of purging and sampling devices for groundwater monitoring wells, http://doi.org/10.1520/D6634_D6634M-14.

Avila, K. et al., 2011. The onset of turbulence in pipe flow. Science, 333(6039): 192-196, http://doi.org/10.1126/science.1203223.

Ayotte, J.D., Szabo, Z., Focazio, M.J. and Eberts, S.M., 2011. Effects of human-induced alteration of groundwater flow on concentrations of naturally-occurring trace elements at water-supply wells. Applied Geochemistry, 26(5): 747-762, http://doi.org/10.1016/j.apgeochem.2011.01.033.

Banks, E.W., Shanafield, M.A. and Cook, P.G., 2014. Induced temperature gradients to examine groundwater flowpaths in open boreholes. Ground Water, 52(6): 943-951, http://doi.org/10.1111/gwat.12157.

Barber, C. and Davis, G.B., 1987. Representative sampling of ground water from short-screened boreholes. Ground Water, 25(5): 581-587, http://doi.org/10.1111/j.1745-6584.1987.tb02888.x.

Barcelona, M.J., Gibb, J.P., Helfrich, J.A. and Garske, E.E., 1985. Practical guide for groundwater sampling, ISWS Contract Report 374, Illinois State Water Survey, Champaign, Illinois.

Barcelona, M.J., Varljen, M.D., Puls, R.W. and Kaminski, D., 2005. Ground water purging and sampling methods: history vs. hysteria. Ground Water Monitoring & Remediation, 25(1): 52-62, http://doi.org/10.1111/j.1745-6592.2005.0001.x.

Barcelona, M.J., Wermann, H.A. and Varljen, M.D., 1994. Reproducible well-purging procedures and VOC stabilization criteria for ground-water sampling. Ground Water, 32(1): 12-22, http://doi.org/10.1111/j.1745-6584.1994.tb00605.x.

Basu, N.B., Rao, P.S.C., Poyer, I.C., Annable, M.D. and Hatfield, K., 2006. Flux-based assessment at a manufacturing site contaminated with trichloroethylene. Journal of Contaminant Hydrology, 86: 105-127.

Basu, N.B. et al., 2008. Temporal evolution of DNAPL source and contaminant flux distribution: Impacts of source mass depletion. Journal of Contaminant Hydrology, 95(3-4): 93-109, http://doi.org/10.1016/j.jconhyd.2007.08.001.

Bauer, S. et al., 2004. Quantification of groundwater contamination in an urban area using integral pumping tests. Journal of Contaminant Hydrology, 75(3-4): 183-213, http://doi.org/10.1016/j.jconhyd.2004.06.002.

Bayer-Raich, M., Jarsjöb, J. and Teutscha, G., 2007. Comment on "Analysis of groundwater contamination using concentration-time series recorded during an integral pumping test: Bias introduced by strong concentration gradients within the plume" by Allelign Zeru and Gerhard Schäfer. Journal of Contaminant Hydrology, 90(3-4): 240-251, http://doi.org/10.1016/j.jconhyd.2006.10.001.

Bee, J., 2003. Investigating hydraulic properties in the Birmingham Triassic sandstone aquifer. Unpublished MSc Thesis, University of Birmingham.

Bejan, A., 2013. Convection Heat Transfer Fourth Edition. John Wiley & Sons.

Béland-Pelletier, C., Fraser, M., Barker, J. and Ptak, T., 2011. Estimating contaminant mass discharge: A field comparison of the multilevel point measurement and the integral pumping investigation approaches and their uncertainties. Journal of Contaminant Hydrology, 122(1-4): 63-75, http://doi.org/10.1016/j.jconhyd.2010.11.004.

Bliss, J.C. and Rushton, K.R., 1984. The reliability of packer tests for estimating the hydraulic conductivity of aquifers. Quarterly Journal of Engineering Geology and Hydrogeology, 17: 81-91, http://doi.org/10.1144/GSL.QJEG.1984.017.01.10.

Bouch, J.E. et al., 2006. Sedimentary and diagenetic environments of the Wildmoor Sandstone Formation (UK): Implications for groundwater and contaminant transport, and sand production. In: R.D. Barker and J.H.

Tellam (Editors), Fluid Flow and Solute Movement in Sandstones: The Onshore UK Permo-Triassic Red Bed Sequence. Geological Society Special Publications, pp. 129-158, http://doi.org/10.1144/GSL.SP.2006.263.01.07.

Brainerd, R.J. and Robbins, G.A., 2004. A tracer dilution method for fracture characterization in bedrock wells. Ground Water, 42(5): 774-780, http://doi.org/10.1111/j.1745-6584.2004.tb02731.x.

Brassington, F.C., 1992. Measurements of head variations within observation boreholes and their implications for groundwater monitoring. Water and Environment Journal, 6(3): 91-100, http://doi.org/10.1111/j.1747-6593.1992.tb00742.x.

Britt, S.L., 2005. Testing the in-well horizontal laminar flow assumption with a sand-tank well model. Ground Water Monitoring & Remediation, 25(3): 73-81, http://doi.org/10.1111/j.1745-6592.2005.00028.x.

Brooks, M.C. et al., 2008. Changes in contaminant mass discharge from DNAPL source mass depletion: Evaluation at two field sites. Journal of Contaminant Hydrology, 102(1-2): 140-153, http://doi.org/10.1016/j.jconhyd.2008.05.008.

BSI, 2009. Water quality - Sampling - Part 11: Guidance on sampling of groundwaters, BS ISO 5667-11:2009, British Standards Institution, 40 pp.

BSI, 2010. Water quality - Sampling - Part 22: Guidance on the design and installation of groundwater monitoring points, 36 pp.

BSI, 2012. Water quality - Sampling Part 3: Preservation and handling of water samples, BS EN ISO 5667-3:2012, British Standards Publication, 42 pp.

Buckley, D.K. and Talbot, J.C., 1994. Interpretation of geophysical logs of the Kilham area, Yorkshire Wolds, to support groundwater tracer studies, British Geological Survey Technical Report WD/94/10C.

Buss, S. et al., 2010. CL:AIRE SABRE Bulletin 1 - Project SABRE (Source Area BioRemediation) – an Overview, http://claire.co.uk/index.php?option=com_phocadownload&view=category&download=193:sabre-bulletin-01&id=13:sabre-bulletins.

Cai, Z., Wilson, R.D. and Lerner, D.N., 2012. Assessing TCE Source Bioremediation by Geostatistical Analysis of a Flux Fence. Groundwater, 50(6): 908–917, http://doi.org/10.1111/j.1745-6584.2012.00916.x.

Chambers, J. et al., 2010. Hydrogeophysical imaging of deposit heterogeneity and groundwater chemistry changes during DNAPL source zone bioremediation. Journal of Contaminant Hydrology, 118(1-2)): 43–61, http://doi.org/10.1016/j.jconhyd.2010.07.001.

Cherry, J.A., Parker, B.L. and Keller, C., 2007. A new depth-discrete multilevel monitoring approach for fractured rock. Ground Water Monitoring & Remediation, 27(2): 57-70, http://doi.org/10.1111/j.1745-6592.2007.00137.x.

Church, P.E. and Granato, G.E., 1996. Bias in ground-water data caused by well-bore flow in long-screen wells. Ground Water, 3(2): 262-273, http://doi.org/10.1111/j.1745-6584.1996.tb01886.x.

Cieslak, L., Thornton, S. and Rolfe, S., 2015. CL:AIRE ADVOCATE Bulletin 8 - The plume fringe: a zone of increased potential for

biodegradation in contaminant plumes.

Clement, T.P., Johnson, C.D., Sun, Y., Klecka, G.M. and Bartlett, C., 2000. Natural attenuation of chlorinated ethene compounds: model development and field-scale application at the Dover site. Journal of Contaminant Hydrology, 42: 113-140, http://doi.org/10.1016/S0169-7722(99)00098-4.

Dearden, R., Wealthall, G.P., Chambers, J.E. and Rivett, M.O., 2010. Forced gradient conservative tracer test in the SABRE research cell. British Geological Survey, Commissioned Report CR/09/054 (Nottingham, UK).

Dearden, R.A., Noy, D., Lelliott, M., Wilson, R. and Wealthall, G., 2013. Release of contaminants from a heterogeneously fractured low permeability unit underlying a DNAPL source zone. Journal of Contaminant Hydrology, 153: 141–155, http://doi.org/10.1016/j.jconhyd.2011.05.006.

Doughty, C. and Tsang, C., 2005. Signatures in flowing fluid electric conductivity logs. Journal of Hydrology, 310(1-4): 157-180, http://doi.org/10.1016/j.jhydrol.2004.12.003.

Douglas, J.F., Gasiorek, J.M., Swaffield, J.A. and Jack, L.B., 2011. Fluid mechanics (sixth edition). Prentice Hall.

Dumble, P., Fuller, M., Beck, P. and Sojka, P., 2006. Assessing contaminant migration pathways and vertical gradients in a low-permeability aquifer using multilevel borehole systems. Land Contamination and Reclamation, 14(3): 699-712.

EA, 2003. Guidance on monitoring of landfill leachate, groundwater and surface water, LFGTN02, Environment Agency, 287 pp, http://www.environment-agency.gov.uk/static/documents/Business/report_1_533191.pdf.

EA, 2011. Horizontal guidance H1 - Annex J 2 Guidance on the discharge of small quantities of substances for scientific purposes, Version 1.2, Environment Agency, 18 pp, https://www.gov.uk/government/uploads/system/uploads/attachment_data/file/298246/geho0212bult-e-e.pdf.

EA, 2013. Managing water abstraction, LIT 4892 / 746_12 Version 3, Environment Agency, Bristol, UK, 28 pp, https://www.gov.uk/government/uploads/system/uploads/attachment_data/file/297309/LIT_4892_20f775.pdf.

Elci, A., Flach, G.P. and Molz, F.J., 2003. Detrimental effects of natural vertical head gradients on chemical and water level measurements in observation wells: identification and control. Journal of Hydrology, 28: 70-81, http://doi.org/10.1016/S0022-1694(03)00201-4.

Elci, A., Molz, F.J.I. and Waldrop, W.R., 2001. Implications of observed and simulated ambient flow in monitoring wells. Ground Water, 39(6): 853-862, http://doi.org/10.1111/j.1745-6584.2001.tb02473.x.

FDEP, 2008. Monitoring Well Design and Construction Guidance Manual, Florida Department of Environmental Protection Bureau of Water Facilities Regulation, http://www.dep.state.fl.us/water/groundwater/docs/monitoring-well-manual-formatted-final.pdf.

Feenstra, S. and Cherry, J.A., 1988. Subsurface contamination by dense non-aqueous phase liquid (DNAPL) chemicals, International Ground Water Symposium, International Association of Hydrogeologists, Halifax, Nova Scotia, May 1-4, pp. 62-69.

Ferguson, H.A., 2006. Determining the hydraulic characteristics of the Wildmoor Sandstone formation and evaluating the condition of the study site. Unpublished MSc Thesis, University of Birmingham, UK.

Fretwell, B.A., Short, R.I. and Sutton, J.S., 2006. Guidance on the design and installation of groundwater quality monitoring points, Environment Agency Science Report SC020093, Environment Agency, 87 pp, https://www.gov.uk/government/uploads/system/uploads/attachment_data/file/290727/scho0106bkct-e-e.pdf.

Furlong, B.V. et al., 2011. Using regional groundwater flow models for prediction of regional wellwater quality distributions. Journal of Hydrology, 398(1–2): 1-16, http://doi.org/10.1016/j.jhydrol.2010.11.022.

Gale, I.N. and Rutter, H.K., 2006. The Chalk aquifer of Yorkshire. British Geological Survey Research Report RR/06/04, 60 pp.

GeoInsight, 2006. Hydrasleeve Manual. Date accessed: 24/04/15, https://www.hydrasleeve.com/images/stories/support/HydraSleeve_No-Purge_manual_updated.pdf.

Gibb, J.P., Schuller, R.M. and Griffin, R.A., 1981. Procedures for the collection of representative water quality data from monitoring wells, Champaign, Illinois: Illinois State Water Survey and Illinois State Geological Survey.

Gibs, J. et al., 1993. Effects of small-scale vertical variations in well-screen inflow rates and concentrations of organic compounds on the collection of representative ground-water-quality samples. Ground Water, 31(2): 201-208, Hard Copy Only.

Giddings, T., 1987. What is an adequate screen length for monitoring wells? Ground Water Monitoring & Remediation, 7(2): 96-103, http://doi.org/10.1111/j.1745-6592.1987.tb01049.x.

Gil-Rodríguez, M., Rodríguez-Sinobas, L., Benítez-Buelga, J. and Sánchez-Calvo, R., 2013. Application of active heat pulse method with fiber optic temperature sensing for estimation of wetting bulbs and water distribution in drip emitters. Agricultural Water Management, 120(0): 72-78, http://doi.org/10.1016/j.agwat.2012.10.012, http://www.sciencedirect.com/science/article/pii/S0378377412002594.

Grath, J., Ward, R. and Quevauviller, P., 2007. WFD CIS Guidance Document No. 15. Monitoring guidance for groundwater, European Commission , 50 pp.

Greswell, R.B., Durand, V., Aller, M.F., Riley, M.S. and Tellam, J.H., 2014. A method for conducting simultaneous convergent tracer tests in multilayered aquifers. Ground Water, 52(4): 525-534, http://doi.org/101111/gwat.12101.

Guilbeault, M.A., Parker, B.L. and Cherry, J.A., 2005. Mass and Flux Distributions from DNAPL Zones in Sandy Aquifers. Ground Water, 43(1): 70-86.

Gustavson, K.E. and Harkin, J.M., 2000. Comparison of sampling techniques and evaluation of semipermeable membrane devices (SPMDs) for monitoring polynuclear aromatic hydrocarbons (PAHs) in groundwater. Environmental Science & Technology, 34(20): 4445-4451, http://doi.org/10.1021/es0011010.

Hall, S.H., 1993. Single well tracer tests in aquifer characterization. Ground Water Monitoring & Remediation, 13(2): 118-124, http://doi.org/10.1111/j.1745-6592.1993.tb00443.x.

Harbaugh, A.W., Banta, E.R., Hill, M.C. and McDonald, M.G., 2000. Modflow-2000, the U.S. Geological Survey Modular Ground-Water Model - user guide to modularization concepts and the ground-water flow process, USGS Open-File Report 00-92, US Geological Survey, http://pubs.usgs.gov/of/2000/0092/report.pdf.

Hausner, M.B. et al., 2011. Calibrating single-ended fiber-optic raman spectra distributed temperature sensing data. Sensors, 11(11): 10859-10879, http://doi.org/10.3390/s111110859, http://www.mdpi.com/1424-8220/11/11/10859.

Humenick, M.J., Turk, L.J. and Colchin, M.P., 1980. Methodology for monitoring ground water at uranium solution mines. Groundwater, 18(3): 262-273, http://doi.org/10.1111/j.1745-6584.1980.tb03398.x.

Huntzinger, T.L. and Stullken, L.E., 1988. An experiment in representative groundwater sampling for water quality analysis, USGS Water-Resources Investigations Report 88-4178.

Hutchins, S.R. and Acree, S.D., 2000. Ground water sampling bias observed in shallow, conventional wells. Groundwater Monitoring & Remediation, 20(1): 86-93, http://doi.org/10.1111/j.1745-6592.2000.tb00255.x.

Hvorslev, M.J., 1951. Time lag and soil permeability in ground-water observations. In: U.C.o.E. Bulletin No. 36, Vicksburg, Mississippi, 50pp (Editor).

Jones, I. and Lerner, D.N., 1995. Level-determined sampling in an uncased borehole. Journal of Hydrology: 291-317, http://doi.org/10.1016/0022-1694(95)06015-B.

Joyce, E. et al., 2007. Fate and transport of phage and viruses in UK Permo-Triassic sandstone aquifers. Environment Agency UK and Wales, Science Report: SC030217/SR.

Kaleris, V., Hadjitheodorou, C. and Demetracopoulos, A.C., 1995. Numerical simulation of field methods for estimating hydraulic conductivity and concentration profiles. Journal of Hydrology, 171(3–4): 319-353, http://doi.org/10.1016/0022-1694(94)06012-T.

Kearl, P.M., Korte, N.E. and Cronk, T.A., 1992. Suggested modifications to ground water sampling procedures based on observations from the colloidal borescope. Ground Water Monitoring & Remediation, 12(2): 155-161, http://doi.org/10.1111/j.1745-6592.1992.tb00046.x.

Kearl, P.M., Korte, N.E., Stites, M. and Baker, J., 1994. Field comparison of micropurging vs. traditional ground water sampling. Ground Water Monitoring & Remediation, 14(4): 183-190, http://doi.org/10.1111/j.1745-6592.1994.tb00496.x.

Kerfoot, W.B., Beaulieu, B. and Kiely, L., 1991. Direct-reading borehole flowmeter results in field applications. Proceedings of the Fifth National Outdoor Action Conference on Aquifer Restoration, Ground Water Monitoring and Geophysical Methods. National Water Well Association, Dublin, Ohio, pp. 1073–1084, http://info.ngwa.org/GWOL/pdf/910153170.PDF.

Konikow, L.F. and Hornberger, G.Z., 2006. Modeling effects of multinode wells on solute transport. Ground Water, 44(5): 648-660, http://doi.org/10.1111/j.1745-6584.2006.00231.x.

Kozuskanich, J., Novakowski, K.S. and Anderson, B.C., 2012. Influence of piezometer construction of groundwater sampling in fractured rock. Ground Water, 50(2): 266-278, http://doi.org/10.1111/j.1745-6584.2011.00840.x.

Krause, S. and Blume, T., 2013. Impact of seasonal variability and monitoring mode on the adequacy of fiber-optic distributed temperature sensing at aquifer-river interfaces. Water Resour. Res., 49: 2408–2423, http://doi.org/10.1002/wrcr20232.

Krause, S., Blume, T. and Cassidy, N.J., 2012. Application of fibre-optic DTS to identify streambed controls on aquifer-river exchange fluxes in lowland rivers. Hydrol. Earth Syst. Sci., 16(6): 1775-1792, http://doi.org/DOI:10.5194/hess-16-1775-2012.

Kruseman, G.P. and De Ridder, N.A., 1990. Analysis and evaluation of pumping test data Second Edition (Completely Revised). International Institute for Land Reclamation and Improvement Publication 47, pp. 377 pp, http://www.samsamwater.com/library/Pub47.pdf.

Lacombe, S., Sudicky, E.A., Frape, S.K. and Unger, A.J.A., 1995. Influence of leaky boreholes on cross-formational groundwater flow and contaminant transport. Water Resources Research, 31(8): 1871-1882, http://doi.org/10.1029/95WR00661.

Lawrence, A.R., Foster, S.S.D. and Izzard, P.W., 1983. Nitrate pollution of Chalk groundwater in East Yorkshire - a decade on. Journal of the Institute of Water Engineering Science, 37(5): 410-420.

Le Borgne, T. et al., 2007. Comparison of alternative methodologies for identifying and characterizing preferential flow paths in heterogeneous aquifers. Journal of Hydrology, 345(3–4): 134-148, http://doi.org/10.1016/j.jhydrol.2007.07.007, http://www.sciencedirect.com/science/article/pii/S0022169407004283.

Leaf, A.T., Hart, D.J. and Bahr, J.M., 2012. Active thermal tracer tests for improved hydrostratigraphic characterization. Ground Water, 50: 726-735, http://doi.org/10.1111/j.1745-6584.2012.00913.x.

Lelliot, M.R., Cave, M.R. and Wealthall, G.P., 2008. A structured approach to the measurement of uncertainty in 3D geological models. Quarterly Journal of Engineering Geology and Hydrogeology, 42(1): 95-105, http://doi.org/10.1144/1470-9236/07-081.

Li, K.B., Goovaerts, P. and Abriola, L.M., 2007. A geostatistical approach for quantification of contaminant mass discharge uncertainty using multilevel sampler measurements. Water Resour. Res., 43(6), http://doi.org/10.1029/2006WR005427.

Libby, J.L. and Robbins, G.A., 2014. An unsteady state tracer method for characterizing fractures in bedrock wells. Ground Water, 51(1): 136-144, http://doi.org/10.1111/gwat.12045.

Liu, G., Knobbe, S. and Butler Jr., J.J., 2013. Resolving centimeter-scale flows in aquifers and their hydrostratigraphic controls. Geophysical Research Letters, 40(6): 1098-1103, http://doi.org/10.1002/grl.50282.

Ma, R., Zheng, C., Tonkin, M. and Zachara, J.M., 2011. Importance of considering intraborehole flow in solute transport modeling under highly dynamic flow conditions Journal of Contaminant Hydrology, 123(1-2): 11-19, http://doi.org/10.1016/j.jconhyd.2010.12.001.

Mack, E.E., Harkness, M.R. and Roberts, J., 2010. CL:AIRE SABRE Bulletin 3 - Results of laboratory column studies to determine the potential for bioremediation of chlorinated solvent DNAPL source areas.

Martin-Hayden, J.M., 2000a. Sample concentration response to laminar wellbore flow: implications to ground water data variability. Ground Water, 89(1): 12-19, http://doi.org/10.1111/j.1745-6584.2000.tb00197.x.

Martin-Hayden, J.M., 2000b. Controlled laboratory investigations of wellbore concentration response to pumping. Ground Water, 38(1): 121-128, http://doi.org/10.1111/j.1745-6584.2000.tb00209.x.

Martin-Hayden, J.M., Plummer, M. and Britt, S.L., 2014. Controls of wellbore flow regimes on pump effluent composition. Ground Water, 52(1): 96-104, http://doi.org/10.1111/gwat.12036.

Martin-Hayden, J.M. and Wolfe, N., 2000. A novel view of wellbore flow and partial mixing: digital image analyses. Ground Water Monitoring & Remediation, 20(4): 96-103, http://doi.org/10.1111/j.1745-6592.2000.tb00294.x.

Maurice, L., Barker, J.A., Atkinson, T.C., Williams, A.T. and Smart, P.L., 2011. A tracer methodology for identifying ambient flows in boreholes. Ground Water, 49(2): 227-238, http://doi.org/10.1111/j.1745-6584.2010.00708.x, http://dx.doi.org/10.1111/j.1745-6584.2010.00708.x.

Mayo, A.L., 2010. Ambient well-bore mixing, aquifer cross-contamination, pumping stress, and water quality from long-screened wells; What is sampled and what is not? Hydrogeology Journal, 18(4): 823-837, http://doi.org/10.1007/s10040-009-0568-2.

McCarthy, J. and Shevenell, L., 1998. Obtaining representative ground water samples in a fractured and karstic formation. Ground Water, 36(2): 251-260, http://doi.org/10.1111/j.1745-6584.1998.tb01090.x.

McDonald, J.P. and Smith, R.M., 2009. Concentration profiles in screened wells under static and pumped conditions. Ground Water Monitoring & Remediation, 29(2): 78-86, http://doi.org/10.1111/j.1745-6592.2009.01232.x, http://dx.doi.org/10.1111/j.1745-6592.2009.01232.x.

Metcalf, M.J. and Robbins, G.A., 2007. Comparison of water quality profiles from shallow monitoring wells and adjacent multilevel samplers. Ground Water Monitoring & Remediation, 27(1): 84-91, http://doi.org/10.1111/j.1745-6592.2006.00126.x.

Michalski, A. and Klepp, G.M., 1990. Characterization of Transmissive Fractures by Simple Tracing of In-Well Flow. Ground Water, 28(2): 191-198, http://doi.org/10.1111/j.1745-6584.1990.tb02246.x.

Molz, F.J., 1989. The impeller meter for measuring aquifer permeability variations: evaluation and comparison with other tests. Water Resour. Res., 25(7): 1677-1683, http://doi.org/10.1029/WR025i007p01677.

Molz, F.J., Boman, G.K., Young, S.C. and Waldrop, W.R., 1994. Borehole flowmeters - Field applications and data analysis. Journal of Hydrology, 163: 347-371, http://doi.org/10.1016/0022-1694(94)90148-1.

Newcomer, D.R., Bjornstad, B.N. and Vermeul, V.R., 2010. Vertical wellbore flow monitoring for assessing spatial and temporal flow relationships with a dynamic river boundary. Ground Water Monitoring & Remediation, 30(4): 123-135, http://doi.org/10.1111/j.1745-6592.2010.01304.x, http://dx.doi.org/10.1111/j.1745-6592.2010.01304.x.

Nielsen, D.M. and Nielsen, G., 2006. The essential handbook of ground-water sampling. CRC Press.

Ogata, A. and Banks, R.B., 1961. A solution of the differential equation of longitudinal dispersion in porous media. USGS Professional Paper 411-A, US Geological Survey, 7 pp.

Paillet, F.L., 1998. Flow modeling and permeability estimation using borehole flow logs in heterogeneous fractured formations Water Resour. Res., 34(5): 997-1010, http://doi.org/10.1029/98WR00268.

Paillet, F.L., Crowder, R. and Hess, A., 2000. High-resolution flowmeter logging applications with the heat-pulse flowmeter. Journal of Environmental & Engineering Geophysics, 1(1): 1-11, http://doi.org/10.4133/JEEG1.1.1.

Pankow, J., F. and Cherry, J.A., 1996. Dense chlorinated solvents and other DNAPLs in groundwater: history, behavior, and remediation. Waterloo Press, Portland, OR.

Parker, A.H., West, L.J., Odling, N.E. and Bown, R.T., 2010. A forward modeling approach for interpreting impeller flow logs. Ground Water, 48(1): 79-91, http://doi.org/10.1111/j.1745-6584.2009.00600.x, http://dx.doi.org/10.1111/j.1745-6584.2009.00600.x.

Parker, B.L., Cherry, J.A., Chapman, S.W. and Guilbeault, M.A., 2003. Review and Analysis of Chlorinated Solvent Dense Nonaqueous Phase Liquid Distributions in Five Sandy Aquifers. Vadose Zone J., 2: 116-137, http://doi.org/10.2136/vzj2003.1160, http://web.cecs.pdx.edu/~gjohnson/Parker%20et%20al%2003.pdf.

Pehme, P.E., Greenhouse, J.P. and Parker, B.L., 2007. The active line source temperature logging technique and its application in fractured rock hydrogeology. Journal of Environmental & Engineering Geophysics, 12(4): 307-322, http://doi.org/10.2113/JEEG12.4.307.

Pennino, J.D., 1988. There's no such thing as a representative ground water sample. Ground Water Monitoring Review, 8(3): 4-9, http://doi.org/10.1111/j.1745-6592.1988.tb01080.x.

Pitrak, M., Mares, S. and Kobr, M., 2007. A simple borehole dilution technique in measuring horizontal ground water flow. Ground Water, 45(1): 82-92, http://doi.org/ 10.1111/j.1745-6584.2006.00258.x.

Pollock, D.W., 1994. User's Guide for MODPATH/MODPATH-PLOT, Version 3: A particle tracking post-processing package for MODFLOW, the U.S. Geological Survey finite-difference ground-water flow model, USGS Open-File Report 94-464. U.S. Geological Survey, Reston, Virginia, http://water.usgs.gov/nrp/gwsoftware/modpath5/ofr94464.pdf.

Powell, R.M. and Puls, R.W., 1993. Passive sampling of groundwater monitoring wells without purging: multilevel well chemistry and tracer disappearance Journal of Contaminant Hydrology, 12, http://doi.org/10.1016/0169-7722(93)90015-K.

Price, M., Bird, M.J. and Foster, S.S.D., 1976. Chalk pore-size measurements and their significance. Water Services, October: 596-600.

Puls, R.W. and Barcelona, M.J., 1996. Low-flow (minimal drawdown) ground-water sampling procedures. EPA/540/S-95/504, http://http://www.epa.gov/superfund/remedytech/tsp/download/lwflw2a.pdf.

Puls, R.W., Eychaner, J.H. and Powell, R.M., 1990. Colloidal-facilitated transport of inorganic contaminants in groundwater, Part 1: Sampling Considerations. Environmental Research Brief EPA/600/M-90/023, R.S. Kerr Environmental Research Lab, Ada, OK.

Puls, R.W. and Paul, C.J., 1997. Multi-layer sampling in conventional monitoring wells for improved estimation of vertical contaminant distributions and mass. Journal of Contaminant Hydrology, 25(1-2): 85-111, http://doi.org/10.1016/S0169-7722(96)00026-5.

Read, T. et al., 2013. Characterizing groundwater flow and heat transport in fractured rock using fiber-optic distributed temperature sensing. Geophysical Research Letters, 40: 2055-2059, http://doi.org/10.1002/grl.50397.

Read, T. et al., 2014. Active-distributed temperature sensing to continuously quantify vertical flow in boreholes. Water Resour. Res., 50(5): 3706-3713, http://doi.org/10.1002/2014WR015273.

Reilly, T.E. and Gibs, J., 1993. Effects of physical and chemical heterogeneity on water-quality samples obtained from wells. Ground Water, 31(5): 805-813, http://doi.org/10.1111/j.1745-6584.1993.tb00854.x.

Reilly, T.E. and LeBlanc, D.R., 1998. Experimental evaluation of factors affecting temporal variability of water samples obtained from long-screened Wells. Ground Water, 36(4): 270-276, Hard Copy Only.

Riley, M.S., Tellam, J.H., Greswell, R.B., Durand, V. and Aller, M.F., 2011. Convergent tracer tests in multilayered aquifers: The importance of vertical flow in the injection borehole. Water Resour. Res., 47(7): W07501, http://doi.org/10.1029/2010WR009838.

Rivett, M.O., Dearden, R. and Wealthall, G., 2014. Architecture, persistence and dissolution of a 20 to 45 year old trichloroethene DNAPL source zone. Journal of Contaminant Hydrology, In Press, http://doi.org/10.1016/j.jconhyd.2014.09.008.

Rivett, M.O. and Feenstra, S., 2005. Dissolution of an Emplaced Source of DNAPL in a Natural Aquifer Setting. Environmental Science & Technology, 39(2): 447-455, http://doi.org/10.1021/es040016f.

Rivett, M.O., Feenstra, S. and Cherry, J.A., 2001. A controlled field experiment on groundwater contamination by a multicomponent DNAPL: creation of the emplaced-source and overview of dissolved plume development. Journal of Contaminant Hydrology, 49(1-2): 111-149, http://doi.org/10.1016/S0169-7722(00)00191-1.

Rivett, M.O., Lerner, D.N. and Lloyd, J.W., 1990. Temporal variations of chlorinated solvents in abstraction wells. Ground Water Monitoring & Remediation, 10(4): 127-133, http://doi.org/10.1111/j.1745-6592.1990.tb00029.x.

Rivett, M.O., Smith, J.W.N., Buss, S.R. and Morgan, P., 2007. Nitrate occurrence and attenuation in the major aquifers of England and Wales. Quarterly Journal of Engineering Geology and Hydrogeology, 40: 335-352, http://doi.org/10.1144/1470-9236/07-032.

Rivett, M.O., Turner, R.J., Glibbery, P. and Cuthbert, M.O., 2012. The legacy of chlorinated solvents in the Birmingham aquifer, UK: Observations spanning three decades and the challenge of future urban groundwater development. Journal of Contaminant Hydrology, 140-141: 107-123, http://doi.org/10.1016/j.jconhyd.2012.08.006.

Robbins, G.A. and Martin-Hayden, J.M., 1991. Mass balance evaluation of monitoring well purging: Part I. Theoretical models and implications for representative sampling. Journal of Contaminant Hydrology, 8: 203-224, http://doi.org/10.1016/0169-7722(91)90020-2.

Robin, M.L.J. and Gillham, R.W., 1987. Field evaluation of well purging procedures. Ground Water Monitoring & Remediation, 7(4): 85-93, http://doi.org/10.1111/j.1745-6592.1987.tb00967.x.

Rose, L., Krause, S. and Cassidy, N.J., 2013. Capabilities and limitations of tracing spatial temperature patterns by fiber-optic distributed temperature sensing. Water Resour. Res., 49: 1741–1745, http://doi.org/10.1002/wrcr.20144.

Savoie, J.G. and LeBlanc, D.R., 2012. Comparison of no-purge and pumped sampling methods for monitoring concentrations of ordnance related

compounds in groundwater, Camp Edwards, Massachusetts Military Reservation, Cape Cod, Massachusetts, 2009–2010. USGS Scientific Investigations Report 2012–5084, U.S. Geological Survey, Reston, Virginia, pp. 23pp, http://pubs.usgs.gov/sir/2012/5084.

Sayde, C. et al., 2010. Feasibility of soil moisture monitoring with heated fiber optics. Water Resour. Res., 46(6): W06201, http://doi.org/10.1029/2009WR007846, http://dx.doi.org/10.1029/2009WR007846.

Selker, J.S., 2008. Taking the temperature of ecological systems with fiber optics: fiber optic distributed temperature sensing for ecological characterization; Blue River, Oregon, 10–15 September 2007. Eos,

Transactions American Geophysical Union, 89(20): 187-187, http://doi.org/10.1029/2008EO200007, http://dx.doi.org/10.1029/2008EO200007.

Selker, J.S. et al., 2006a. Distributed fiber-optic temperature sensing for hydrologic systems. Water Resour. Res., 42(12): W12202, http://doi.org/10.1029/2006WR005326, http://dx.doi.org/10.1029/2006WR005326.

Selker, J.S., van de Giesen, N., Westhoff, M., Luxemburg, W. and Parlange, M.B., 2006b. Fiber optics opens window on stream dynamics. Geophysical Research Letters, 33(24): L24401, http://doi.org/10.1029/2006GL027979, http://dx.doi.org/10.1029/2006GL027979.

Schlumberger Water Services (SWS), 2014. CTD Diver Manual. Date accessed: 27/04/15, http://www.novametrixgm.com/pdfs/equipment/Diver_manuals/Diver_Product_Manual_en.pdf.

Shafer, J.M., Brantley, D.T. and Waddell, M.G., 2010. Variable-density flow and transport simulation of wellbore brine displacement. Groundwater, 48(1): 122-130, http://doi.org/10.1111/j.1745-6584.2009.00594.x.

Smedley, P.L., Neumann, I. and Farrell, R., 2004. Baseline Report Series - 10: The Chalk Aquifer of Yorkshire and North Humberside. British Geological Survey Commissioned Report CR/04/128N. Environment Agency National Groundwater & Contaminated Land Centre. Technical Report NC/99/74/10, http://www.bgs.ac.uk/downloads/start.cfm?id=754.

Sorensen, J.P.R., Butcher, A.S., Stuart, M.E. and Townsend, B.R., 2015. Nitrate fluctuations at the water table: implications for recharge processes and solute transport in the Chalk aquifer. Hydrological Processes, (In press), http://doi.org/10.1002/hyp.10447.

Stone, W.J., 1997. Low-flow ground water sampling - is it a cure-all? Ground Water Monitoring & Remediation, 17(2): 70–72, http://doi.org/10.1111/j.1745-6592.1997.tb01278.x.

Streetly, H.R., Hamilton, A.C.L., Betts, C., Tellam, J.H. and Herbert, A.W., 2002. Reconnaissance tracer tests in the Triassic sandstone. Quaterly Journal of Engineering Geology and Hydrogeology, 35: 167-178, http://doi.org/10.1144/1470-9236/2000-30.

Stuart, M.E., Chilton, P.J. and Butcher, A.S., 2008. Nitrate fluctuations in groundwater: review of potential mechanisms and application to case studies, Groundwater Science Programme Open Report OR/08/046. British Geological Survey, Keyworth, Nottingham, 57 pp, http://nora.nerc.ac.uk/7021/1/OR08046.pdf.

Sukop, M.C., 2000. Estimation of vertical concentration profiles from existing wells. Ground Water, 38(6): 836-841, http://doi.org/10.1111/j.1745-6584.2000.tb00681.x.

Tate, A.K., Robertson, A.S. and Gray, D.A., 1971. The hydrogeological investigation of fissure flow by borehole logging techniques. Quarterly Journal of Engineering Geology and Hydrogeology, 4(4): 381-383, http://doi.org/10.1144/GSL.QJEG.1971.004.04.21.

Taylor, R.G. et al., 2006. Vertical groundwater flow in Permo-Triassic sediments underlying two cities in the Trent River Basin (UK). Journal of Hydrology, 284: 92-113, http://doi.org/10.1016/S0022-1694(03)00276-2.

Tellam, J.H., 1992. Reversed Flow Test: a borehole logging method for estimating porewater quality and inflow rates along an uncased borehole profile. Ground Water Monitoring Review, 12(1): 146-153, http://doi.org/10.1111/j.1745-6592.1992.tb00045.x.

Tellam, J.H. and Barker, R.D., 2006. Towards prediction of saturated-zone pollutant movement in groundwaters in fractured permeable-matrix aquifer: the case of the UK Permo-Triassic sandstones. In: R.D. Barker and J.H. Tellam (Editors), Fluid Flow and Solute Movement in Sandstones: The Onshore UK Permo-Triassic Red Bed Sequence. Geological Society, pp. 1-48, http://doi.org/10.1144/GSL.SP.2006.263.01.01.

Thornton, S. and Wilson, R., 2008. CL:AIRE Technical Bulletin TB3 - Principles and practice for the collection of representative groundwater samples.

Tsang, C., Hufschmied, P. and Hale, F.V., 1990. Determination of fracture inflow parameters with a borehole fluid conductivity logging method Water Resour. Res., 26(4): 561-578, http://doi.org/10.1029/WR026i004p00561.

Tyler, S.W. et al., 2008. Spatially distributed temperatures at the base of two mountain snowpacks measured with fiber-optic sensors. J. Glaciol., 54(187): 673-679, http://doi.org/doi:10.3189/002214308786570827.

Tyler, S.W. et al., 2009. Environmental temperature sensing using Raman spectra DTS fiber-optic methods. Water Resour. Res., 45(4): W00D23, http://doi.org/10.1029/2008WR007052, http://dx.doi.org/10.1029/2008WR007052.

UKTAG, 2012. Paper 11b(i). Groundwater Chemical Classification for the purposes of the Water Framework Directive and the Groundwater Directive. UK Technical Advisory Group on the Water Framework Directive, 32 pp, http://http://www.wfduk.org/sites/default/files/Media/Environmental%20standards/Proposal%20for%20groundwater%20classification%20system_Final_100308.pdf.

USEPA, 1992. Estimating potential for occurrence of DNAPL at superfund sites, Publication 9355.4-07FS, US Environmental Protection Agency Office of Solid Waste and Emergency Response, Washington DC, http://www.epa.gov/superfund/health/conmedia/gwdocs/pdfs/estdnapl.pdf.

USEPA, 2010. Low Stress (Low Flow) purging and sampling procedure for the collection of groundwater samples from monitoring wells, EPASOP-GW 001, http://www.epa.gov/region1/lab/qa/pdfs/EQASOP-GW001.pdf.

van de Giesen, N. et al., 2012. Double-ended calibration of fiber-optic raman spectra distributed temperature sensing data. Sensors, 12(5): 5471-5485, http://doi.org/10.3390/s120505471, http://www.mdpi.com/1424-8220/12/5/5471.

Varljen, M.D., Barcelona, M.J., Obereiner, J. and Kaminski, D., 2006. Numerical simulations to assess the monitoring zone achieved during low-flow purging and sampling. Ground Water Monitoring & Remediation, 26(1): 44-52, http://doi.org/10.1111/j.1745-6592.2006.00029.x.

Vermeul, V.R., McKinley, J.P., Newcomer, D.R., Mackley, R.D. and Zachara, J.M., 2010. River-induced flow dynamics in long-screen wells and impact on aqueous samples. Ground Water, 49(4): 515-524, http://doi.org/doi: 10.1111/j.1745-6584.2010.00769.x.

Vermeul, V.R., McKinley, J.P., Newcomer, D.R., Mackley, R.D. and Zachara, J.M., 2011. River-induced flow dynamics in long-screen wells and impact on aqueous samples. Groundwater, 49(4): 515-524, http://doi.org/10.1111/j.1745-6584.2010.00769.x.

Verreydt, G., Bronders, J., Keer, I.V., Diels, L. and Vanderauwera, P., 2010. Passive samplers for monitoring VOCs in groundwater and the prospects related to mass flux measurements. Groundwater, 30(2): 114-126, http://doi.org/10.1111/j.1745-6592.2010.01281.x.

Voigt, D., van Geel, J.L.W.A. and Kerkhof, O., 2011. Spatio-temporal noise and drift in fiber optic distributed temperature sensing. Meas. Sci. Technol., 22: 085203, http://doi.org/10.1088/0957-0233/22/8/085203.

Vrana, B. et al., 2005. Passive sampling techniques for monitoring pollutants in water. Trac-Trends in Analytical Chemistry, 24(10): 845-868, http://doi.org/10.1016/j.trac.2005.06.006, <Go to ISI>://000233961000007.

Ward, R.S., Chada, D.S., Brewerton, L.J. and Aldrick, J., 1998. A tracer investigation of groundwater protection zones around Kilham PWS well, East Yorkshire. British Geological Survey Technical Report WE/98/19, 30 pp.

Ward, R.S. and Williams, A.T., 1995. A tracer test in the Chalk near Kilham, North Yorkshire. British Geological Survey Technical Report WD/95/7, 26 pp.

West, L.J. and Odling, N.E., 2007. Characterization of a multilayer aquifer using open well dilution tests. Groundwater, 45(1): 74-84, http://doi.org/10.1111/j.1745-6584.2006.00262.x.

Wiedemeier, T.H., 1999. Natural Attenuation of Fuels and Chlorinated Solvents in the Subsurface. John Wiley & Sons.

Williams, H.H. and Paillet, F.L., 2002. Using flowmeter pulse tests to define hydraulic connections in the subsurface: a fractured shale example. Journal of Hydrology, 265: 100-117, http://doi.org/10.1016/S0022-1694(02)00092-6.

Yeskis, D. and Zavala, B., 2002. Ground-water sampling guidelines for superfund and RCRA project managers, EPA 542-S-02-001, U.S. Environmental Protection Agency, http://www.epa.gov/superfund/remedytech/tsp/download/gw_sampling_guide.pdf.

Young, S.C. and Pearson, H.S., 1995. The electromagnetic borehole flow meter: description and application. Ground Water Monitoring & Remediation, 15(4): 138-147, http://doi.org/10.1111/j.1745-6592.1995.tb00561.x.

Zaidman, M.D., Middleton, R.T., West, L.J. and Binley, A.M., 1999. Geophysical investigation of unsaturated zone transport in the Chalk in Yorkshire. Quarterly Journal of Engineering Geology and Hydrogeology, 32(2): 185-198, http://doi.org/10.1144/GSL.QJEG.1999.032.P2.08.

Zeru, A. and Schäfer, G., 2005. Analysis of groundwater contamination using concentration–time series recorded during an integral pumping test: Bias introduced by strong concentration gradients within the plume. Journal of Contaminant Hydrology, 81(1-4), http://doi.org/10.1016/j.jconhyd.2005.08.005.

Zheng, C. and Wang, P., 1999. MT3DMS A modular three-dimensional multispecies transport model, Contract Report SERDP-99-1. U.S. Army Corps of Engineers, http://www.dtic.mil/cgi-bin/GetTRDoc?Location=U2&doc=GetTRDoc.pdf&AD=ADA373474.